12-2001

Development of a Model for Predicting the Vertical Profile of Ozone Based on Ground-Level Ozone Observations and Cloud Cover

Gi-Dong Kim
University of Tennessee - Knoxville

To the Graduate Council:

I am submitting herewith a dissertation written by Gi-Dong Kim entitled "Development of a Model for Predicting the Vertical Profile of Ozone Based on Ground-Level Ozone Observations and Cloud Cover." I have examined the final electronic copy of this dissertation for form and content and recommend that it be accepted in partial fulfillment of the requirements for the degree of Doctor of Philosophy, with a major in Civil Engineering.

Dr. Wayne T. Davis, Major Professor

We have read this dissertation and recommend its acceptance:

Dr. Terry L. Miller, Dr. Gregory D. Reed, Dr. Joshua S. Fu, Dr. Susan M. Smith

Accepted for the Council:

Carolyn R. Hodges

Vice Provost and Dean of the Graduate School

(Original signatures are on file with official student records.)

To the Graduate Council:

I am submitting herewith a dissertation written by Gi-Dong Kim entitled " Development of a Model for Predicting the Vertical Profile of Ozone Based on Ground-Level Ozone Observations and Cloud Cover." I have examined the final electronic copy of this dissertation for form and content and recommend that it be accepted in partial fulfillment of the requirements for the degree of Doctor of Philosophy, with a major in Civil Engineering.

Dr. Wayne T. Davis, Major Professor

We have read this dissertation
and recommend its acceptance:

Dr. Terry L. Miller

Dr. Gregory D. Reed

Dr. Joshua S. Fu

Dr. Susan M. Smith

Accepted for the Council:

Dr. Anne Mayhew

Vice Provost and Dean of
Graduate Studies

(Original signatures are on file in the Graduate Student Services office.)

Development of a Model for Predicting the Vertical Profile of Ozone Based on Ground-Level Ozone Observations and Cloud Cover

A Dissertation
Presented for the
Doctor of Philosophy Degree
The University of Tennessee, Knoxville

Gi-Dong Kim
December 2001

ACKNOWLEDGEMENTS

I would like to acknowledge with profound gratitude my major professor, Dr. Wayne T. Davis, who has given me invaluable advice and encouragement with great patience throughout the course of this work. I also wish to thank Dr. Terry L. Miller, Dr. Gregory D. Reed, Dr. Joshua S. Fu, and Dr. Susan M. Smith for serving on my committee and for the critical examination of my dissertation.

I would like to thank my parents for their constant and dedicated loving support. Their self-sacrificing love should be rewarded. Finally, I also extend my appreciation to my wife (Un-Kyong Ham), my two-year old son (William Kim), and my one-year old daughter (Julia Grace Kim).

ABSTRACT

Ozone formed in a chemical reaction is vertically dispersed and mixed with the ozone mass aloft by turbulent convection due to solar radiation. The mixing height, which depends on the stability of the atmosphere, varies by day/night time and by season of year and is characteristic of season and day and night time from year to year. Ground level ozone is generally the combined result of dynamics of the atmosphere resulted from the turbulent convection in the atmospheric boundary layer (ABL), production and destruction processes such as transport from upper air mass, subsequent transport to the ground, photochemical production and chemical destruction. Such processes are a function of the photochemical activity of chemical species (NO_x and VOC) present in the ABL and meteorological conditions that are recurrent phenomena in a year. The purpose of this study is to develop a model to predict high elevation ozone concentration for a particular time as a function of elevation based on ground level ozone observation with and without incorporating cloud cover that influences ozone concentration and the atmospheric stability, using a number of techniques. This study demonstrated that the overall regression model, which did not consider the effect of cloud cover, provided an approach that estimates the high elevation ozone concentrations based on the statistical results with 13.48 ppb prediction error and 0.66 index of agreement between the observed and predicted datasets. The “clear to partly cloudy” and “cloudy” day component regression models associated with cloud cover provided improvement over the overall regression model.

TABLE OF CONTENTS

CHAPTER **Page**

LIST OF TABLES

TABLE **Page**

(list of tables continued)

TABLE **Page**

(list of tables continued)

TABLE **Page**

LIST OF FIGURES

(list of figures continued)

FIGURE **Page**

(list of figures continued)

FIGURE **Page**

(list of figures continued)

FIGURE **Page**

(list of figures continued)

FIGURE **Page**

(list of figures continued)

FIGURE **Page**

(list of figures continued)

FIGURE **Page**

(list of figures continued)

FIGURE **Page**

(list of figures continued)

FIGURE **Page**

(list of figures continued)

FIGURE **Page**

(list of figures continued)

FIGURE **Page**

(list of figures continued)

FIGURE **Page**

CHAPTER 1

INTRODUCTION

Ozone occurs in two layers of the atmosphere: the troposphere and the stratosphere. The definition of the troposphere is the atmospheric zone from the layer surrounding the earth's surface up to 10 miles above earth's surface. The stratosphere is extended upward from 10 to 30 miles. Naturally created ozone in the stratosphere protects life on earth from the sun's harmful ultraviolet rays. However, ground-level ozone formed in a photochemical reaction with pollutants emitted from a variety of sources causes various environmental and health problems (Horvath and Mckee, 1994). These health problems include chest pains, coughing, nausea, throat irritation, and reduced lung capacity. In addition, ground-level ozone reduces crop production, damages trees and other plants, and degrades regional scale visibility (Heck et al., 1984;Hogsett et al., 1997).

Ozone is not directly emitted into the air by specific sources, but is a gas that forms in the atmosphere as a result of photochemical reactions involving nitrogen oxides ($NO_x = NO + NO_2$) and Volatile Organic Compound (VOC) precursors when 3 atoms of oxygen are combined (O_3) in the presence of sunlight. The ozone precursors are emitted by a variety of sources, including mobile sources (cars, trucks and other vehicles), stationary sources (boilers and medium to large manufacturing operations), and area sources (small businesses and activities of home owners and individuals).

Ozone formed in a chemical reaction is vertically dispersed and then mixed with the ozone mass aloft by thermal turbulence due to solar radiation. The degree of the

vertical dispersion is defined as mixing height. It is coupled with the vertical temperature profile that strongly influences the dilution of pollutants released into the Atmospheric Boundary Layer (ABL) (Shaw and Munn R.E, 1971). The ABL is defined as part of the troposphere which is directly influenced by the earth's surface and which responds to surface forces, having time scales of an hour or less (Beyrich et al., 1996;Randerson, 1984;Stull, 1988).

The vertical mixing depends on stability that is determined by cloudy cover at the time (Nicholson et al., 2001). The mixing height varies by day/night time and by season of year: it is larger in the afternoon than the morning and in the summer than the winter (Nevers, 1995). Typical values of the mixing height range from 200 to 1100 meters, from 600 to 4000 meters, from 200 to 900 meters and from 600 to 1400 meters in summer morning, summer afternoon, winter morning, and winter afternoon, respectively. Aneja et al. (2000) reported that the mean heights of the mixing layer at measurement sites were estimated to be about 202 m at 7:00 a.m., 1021 m at 1:00 p.m., and 1270 m at 7:00 p.m., in Raleigh, NC.

In early morning, the mixing height starts out near the surface and then grows during the day. For the mid-afternoon condition, there is vigorous vertical mixing in which the pollutants released at ground level are mixed almost uniformly up to the mixing height. The vigorous vertical mixing is due to the fact that the quantity of solar energy is greater at mid-afternoon than early morning and late afternoon, the period for a summer day being approximately twice as long as for a winter day (Nicholson et al., 2001;Wark et al., 1998). Ground level ozone is generally the combined result of dynamics of the atmosphere in the ABL, production and destruction processes such as

transport from upper air mass, subsequent transport to the ground, photochemical production and chemical destruction (Altshuller, 1986;Yap et al., 1988). Such processes are a function of the photochemical activity of chemical species (NOx, VOC, and reactive hydrocarbons) present in the ABL and meteorological conditions that are recurrent phenomena in a year.

Although air quality monitoring networks provide observations of the temporal variation of ozone and ozone precursors, they provide no information about several complicating factors involved in assessing the photochemical activity of the chemical species aloft on surface ozone concentrations (Berkowitz et al., 2000). In spite of the absence of information regarding the photochemical activity and assuming that certain meteorological conditions are characteristic of season and day and night time in a year, it may be possible to find a reasonable and predictable relationship between ground level ozone and high elevation ozone within the troposphere.

The purpose of this study is to explore the relationship between ground level ozone concentrations and high elevation ozone concentrations for the typical ozone season (April – October) for the four-year period (1995 – 1998) with and without incorporating meteorological parameters using a number of techniques. More specifically, this study develops an algorithm to predict high elevation ozone concentrations based on measured ground level ozone concentrations. In support of this purpose, the following objectives are identified:

- to identify a relationship between ground level and high elevation ozone concentrations for a particular time as a function of elevation;

- to compare high elevation ozone concentrations observed and predicted by a developed overall regression model;
- to evaluate the performance of the overall regression model in terms of the difference between the observed and the predicted concentration standard deviation (s_o-s_p), Mean Absolute Error (MAE), Mean Bias Error (MBE), Root Mean Square Error (RMSE), coefficient of determination (r^2), and index of agreement (d_1, α=1);
- to demonstrate the use of the overall regression model for predicting high elevation ozone concentrations based on ground level ozone observation;
- to demonstrate how accurately the overall regression model performs across different ozone years without considering meteorological parameters;
- to see if "clear," "cloudy," and "clear to partly cloudy" component regression models that include cloud cover as a meteorological variable show a significant improvement over the overall regression model, a statistical model that does not consider meteorological parameters; and
- to see if any improvement over the overall regression model can be developed.

One motivation of this research is that CALPUFF (U.S. EPA's air quality regulatory model), which is a multi-layer Lagrangian puff model that can simulate the effects of meteorological variations in space and in time on the transport, dispersion, transformation, and removal of multiple pollutant species, requires ground level hourly ozone concentrations as input in calculating the transformation rates of SO_2 and NO_x to sulfates and nitrates, respectively, as shown below (Scire et al., 1999):

$$k_1 = 36R^{0.55}[O_3]^{0.71}S^{-1.29} + k_{1(aq)}$$
$$k_2 = 1206[O_3]^{1.5}S^{-1.41}[NO_x]^{-0.33}$$
$$k_3 = 1261[O_3]^{1.45}S^{-1.34}[NO_x]^{-0.12}$$

where the aqueous phase component of the SO_2 conversion rate is parameterized as:

$$k_{1(aq)} = 3x10^{-8}RH^4$$

Here k_1 is the SO_2 to SO_4 transformation rate (percent/hour), k_2 is the NO_x to HNO_3 + RNO_3 transformation rate (percent/hour), k_3 is the NO_x to HNO_3 (only transformation rate (percent/hour), R is the total solar radiation intensity (kw/m^2), S is a stability index ranging from 2 to 6 (PGT class A and B=2, C=3, D=4, E=5, F=6), RH is the relative humidity in % and $[O_3]$ and $[NO_x]$ are concentrations of background ozone and NO_x in the plume in ppm (Scire et al., 1999).

The chemical transformation scheme (called the MESOPUFF II scheme) in CALPUFF is initiated as soon as a puff is released from an emission source. The puff picks up the ground level hourly ozone concentration as representative of the mixing layer through which a plume is traveling because the scheme was developed under the assumption that the ground level ozone concentration is fully mixed through an entire vertical layer during daytime (Scire et al., 1999). The ozone concentration of the mixing layer through which the plume travels is equivalent to the ground level ozone concentration.

However, it has been reported that mean ozone concentrations vary with elevation (Reiter et al., 1987;Ryan et al., 1998;Trotter, 1998). Thus CALPUFF, which essentially utilizes ground level hourly ozone data as an input, could underestimate or overestimate the amount of wet and dry acid deposition when simulating the above chemical transformation rate in cases where the ozone concentration is not constant throughout the ABL (i.e. not the same as the ground level ozone concentration). This concern as well as the general desire to understand the relationship of ground level and elevated ozone concentrations prompted this study. The developed algorithm could be utilized for a variety of purposes:

- as a means of estimating concentrations at higher elevations in complex terrain (in the absence of actual monitoring data),
- as input to models such as the Urban Airshed Model (UAM) to provide a three dimension ozone input when only ground-level ozone data were available, and
- as a means of converting ground level ozone concentrations to representative ozone concentrations of the mixing layer through which a plume emitted from an emission source travels, prior to running air quality models such as CALPUFF which requires ground level hourly ozone concentrations as an input in acid deposition calculations.

CHAPTER 2

LITERATURE REVIEW

This chapter focuses on a review and discussion of three main areas that fall within the scope of this study: the atmosphere, meteorology of air pollution, and tropospheric ozone. The first section includes the layers of atmosphere, solar radiation and mechanisms that affect atmospheric circulation, and vertical mixing. The second section covers temperature structure, the diurnal cycle of vertical temperature structure, atmospheric stability, and meteorological wind patterns associated with topographic features. The last section introduces meteorology and ozone relationships, source, formation, and transport of ozone, and diurnal variations and vertical profiles of ozone concentrations.

2.1 The Atmosphere

2.1.1 The Layers of the Atmosphere

The height of the atmospheric boundary layer (ABL) is a fundamental parameter characterizing the structure of the atmosphere; awareness of its value is of particular importance for various applications such as environmental monitoring and the prediction of air pollution or as a scaling parameter for the description of vertical profiles. Despite this importance, no overall accepted definition or criterion for it's practical determination has yet been formulated (Seinfeld and Pandis, 1997).

In the most general terms, the atmosphere is divided into lower and upper regions. The lower atmosphere is generally considered to extend to the top of the stratosphere at

an altitude of about 50 kilometers (km). Study of the lower atmosphere is known as *meteorology*. Study of the upper atmosphere is called *aeronomy*.

The Earth's atmosphere is characterized by variations of temperature and pressure with height. The variation of the average temperature profile with altitude is the basis for distinguishing the layers of the atmosphere. The regions of the atmosphere are displayed in Figure 2-1 and are as follows: (All figures can be found/are located in Appendix B).

Troposphere. Extends from the Earth's surface up to the tropopause that is at 10 to 15 km altitude depending on latitude and time of year. The troposphere is characterized by decreasing temperature with height and the potential for a rapid vertical mixing.

Stratosphere. Extends from the tropopause to the stratopause (~45 to 55 km altitude). Temperature increases with altitude, leading to a layer in which vertical mixing is slow.

Mesosphere. Extends from the stratopause to the mesopause (~80 to 90 km altitude). Temperature decreases with altitude to the mesopause, which is the coldest point in the atmosphere. The mesosphere is also characterized by rapid vertical mixing.

Thermosphere. The region above the mesopause, characterized by high temperatures as a result of absorption of short wavelength radiation by N_2 and O_2.

Ionosphere. The region of the upper mesosphere and lower thermosphere where ions are produced by photoionization.

Exosphere. The outermost region of the atmosphere (>500 km altitude), where gas molecules with sufficient energy can escape from the Earth's gravitational attraction.

The caldron of all weather, the troposphere contains almost all of the atmosphere's water vapor. Although the troposphere accounts for only a small fraction of the atmosphere's total height, it contains about 80% of its total mass. In the troposphere, the temperature decreases almost linearly with height, on the average. The troposphere can be divided into the *atmospheric boundary layer* (*or planetary boundary layer*), extending from the Earth's surface up to about 1 km, and the *free troposphere*, extending from about 1 km to the tropopause (Seinfeld and Pandis, 1997).

2.1.2 Solar Radiation and Mechanisms that Affect Atmospheric Circulation

In order to understand the mechanisms that affect atmospheric motion, it is necessary not only to investigate the magnitude of the solar radiation output measured at the top of the atmosphere, but also to understand how forms of energy transfer such as radiation, conduction, and convention work closely together in the Atmospheric Boundary Layer. The general circulation and the major wind systems are driven by differences in the density of air that develop because of variations in the amount of solar energy absorbed in different locations (Cole, 1980).

The angle of the sun's ray is not coincident with respect to the earth's surface in a perpendicular direction for different seasons, except for a relatively small area. The surface location of this area varies during the season because of the earth's motion. The earth rotates in the earth orbit's axis once every 24 hours with respect to the sun. The course rotation accounts for the alternation of night and day. To evaluate the role played by each of these factors in maintaining the earth-atmosphere heat balance, the rate of energy arrival should be determined per unit area measured at the top of the atmosphere.

This quantity is called the solar constant and is defined as the flux (rate of flow) of solar radiation received at the top of the earth's atmosphere, on a unit surface area perpendicular to the direction of propagation, at the mean earth-sun distance. There is a large heat imbalance between different parts of the earth and the atmosphere. This imbalance must be compensated for by a heat-transfer mechanism (Cole, 1980).

Figure 2-2 illustrates how solar radiation reaches the earth's surface. The intensity of solar radiation falling on a horizontal unit of the earth's surface depends on the distance from the outer reaches of the atmosphere to earth's surfaces called the path length. The path length is a function of the angle of the sun, with respect to latitude, time of day, and season. The amount of solar radiation is characteristic of time of day and season in a year; the length of the day varies with the latitude and season (Cole, 1980).

Another major factor influencing the amount of energy at the surface is the extent and thickness of cloud cover that reflects much of the solar energy, thus depleting the insolation. Variations in cloud cover are very important in the amount of the radiation since they determine the areas that receive radiation at the ground (Eagleman, 1980). The clouds reflect more than 80% of the sunlight and transmit most of the rest. On the average, about 50% of the energy that strikes cloud tops is reflected with the exact amount varying with the thickness and type of cloud (Eagleman, 1980).

Heat is transferred to the atmosphere from the earth's surface. Some energy is transferred by sensible heat as the sunlight absorbed by the earth's surface warms the lower meters of the atmosphere by a form of energy transfer called conduction. Deeper layers of the atmosphere are affected as the earth's surface warms the atmosphere through convection and turbulent mixing (Eagleman, 1980). Considerable heat is also

transferred upward in the form of latent heat. The atmospheric heating occurs as the absorption of solar radiation on a sunny day rapidly increases the temperature of the earth's surface, transferring it upward by conduction, convection, and radiation emitted from the ground (Eagleman, 1980). Molecular conduction from the ground to the atmosphere is very slow and affects only a very shallow atmospheric layer. Convection and turbulent mixing, along with radiation of energy from the ground to the atmosphere, are responsible for warming most of the lower atmosphere.

Vertical motions in the atmosphere result from convection from solar heating of the Earth's surface, convergence or divergence of horizontal flows, horizontal flow over topographic features at the Earth's surface (Randerson, 1984;Stull, 1988). Under sunny daytime conditions, the mixing height typically extends 1 to 2 km above the heated ground until a stable layer abruptly halts it. On clear nights, a stable stratified layer develops at the ground, extending upward several hundred meters to the top of the surface temperature inversion (Randerson, 1984).

The characteristics of ground-based inversions are summarized in Table 2-1. (All tables can be found/are located in Appendix A). Median depths of early morning ground-based inversions are lower in the spring (315 m) than the other seasons (414 m). Quartile deviations of early morning ground-based inversions range from 107 m in the summer to 153 m in the spring. Fall and winter quartile deviations are 113 and 149m, respectively. In the winter, deep ground-based inversions (greater than 500 m) occur more frequently than any other season. Deep winter inversions occur at anytime during the day; the 15:00 median is only 24% less than the early morning value of 414 m (Myrick et al., 1994). Figure 2-3 shows cumulative frequency distribution of inversion depth in the early

morning sounding as a function of a season. In general, only the lowest part of the nocturnal stable layer is turbulent, although weak and sporadic turbulence may extend to higher levels (Berman et al., 1997).

2.1.3 Vertical Mixing

Mixing height (MH) is one of the most relevant parameters to characterize the dispersion state of the atmospheric boundary layer (ABL). It is one of the most important parameters affecting the concentration and dispersion of atmospheric pollutants released near the ground (Maughan, 1979;Park et al., 1990;Pekour and Kallistratova, 1993). The mixing height has been defined by some researchers as the height of the layer adjacent to the ground over which pollutants or any constituents emitted within this layer or entrained into it become mixed by convection or mechanical turbulence within a time scale of about one hour or less (Beyrich et al., 1996;Randerson, 1984;Stull, 1988).

Figure 2- 4 shows the mixing height is function of season and time of day. As indicated in Table 2-2, median mixing heights are lowest, intermediate, and highest for spring, summer, and fall. The diurnal variability of winter mixing heights is relatively small compared to other seasons. The median mixing height at solar noon are lowest in winter (162 m) and highest in summer (683 m). The spring and fall values are 659 and 381 m, respectively, in Alberta, Canada (Myrick et al., 1994).

Vertical mixing involves turbulent diffusion, convection, and relief-driven upslope and downslope flows and develops in response to the forces acting on the air. The force of gravity affects any volume of air with a greater force on a volume that contains more mass. All the molecules within the atmosphere would be pulled down to

the earth's surface if there were no counteracting upward force. The upward force is a vertical pressure gradient force that exists because of the pressure decrease with altitude (Figure 2-5). When the vertical pressure gradient force balances the downward gravitational force, no new vertical air currents are initiated since the two vertical forces are in equilibrium. Since the gravitational pull on the molecules that comprise the air and the resulting decrease in pressure with altitude is very constant, the major cause of imbalances in the two vertical forces is variations in the density of the air. The molecules in the atmosphere obey the ideal gas law: warm air expands, becomes less dense, expands, and would be forced upward into surrounding areas while cold air contracts in volume, becomes denser, and would be forced downward (Cole, 1980).

2.2 Meteorology of Air Pollution

2.2.1 Temperature Structure

Atmospheric temperature structure is closely related to boundary layer structure. The vertical temperature gradient, lapse rate, is used to determine the stability of the atmosphere and the magnitude of atmospheric turbulence at a particular time. Throughout the troposphere, temperature changes from an average global surface temperature of 15^{o}C to –56^{o}C at 11 km giving an average lapse rate of 6.5^{o}C/km. Typically, a decrease of temperature is associated with an increase in elevation. This inverse relationship results from the earth's surface serving as the primary source of heat energy for heating the atmosphere (Eagleman, 1980;Randerson, 1984;Slade, 1968).

The negative of the temperature gradient in the atmosphere is referred to as a lapse rate. Of special significance are the adiabatic and normal or standard lapse rates.

The adiabatic lapse rate is the unique atmospheric lapse rate where an element of air is displaced from one level to another while maintaining the same temperature or density as the surrounding air. The adiabatic lapse rate is equal to approximately 1 ^{o}C/100 m (5.4 ^{o}F/1000 ft). The troposphere is characterized by the normal or standard lapse rate that is 0.66 ^{o}C/100 m (3.6 ^{o}F/1000 ft). If there is no change of temperature with height, the atmospheric layer is described as isothermal lapse rate. If temperature increases with elevation, the layer is referred to as an inversion. If the temperature decreases at a rate greater than the adiabatic rate, the lapse rate is termed superadiabatic and the atmosphere is unstable. Under superadiabatic conditions, vertical motions are accelerated because warmer masses of air are forced to rise whereas cooler air is forced downward. Conversely, if the atmospheric temperature decreases at a rate less than the adiabatic rate, the lapse rate is called subadiabatic and the atmosphere is stable. Figure 2-6 illustrates examples of low-level vertical temperature structure (Randerson, 1984;Slade, 1968;Stull, 1988;Wark et al., 1998).

2.2.2 The Diurnal Cycle of Vertical Temperature Structure

The typical diurnal cycle of a vertical temperature pattern is shown in Figure 2-7. The plots were constructed from data obtained during late summer and early fall at Oak Ridge, Tennessee. During the early morning, 0600 to 0700 EST, a surface-based temperature inversion is present. By 0800 EST, the heating effect of the rising sun has resulted in the initial destruction of the lowest section of the inversion. By 1000 EST, the inversion layer has completely dissipated. An unstable layer is present near the ground throughout the day. The nocturnal inversion begins to return around 1800 EST. As the

earth progressively cools throughout the night, the inversion becomes far more pronounced (Holland, 1953).

2.2.3 Atmospheric Stability

The degree of atmospheric stability must be known to understand dispersion, transport, transformation, and deposition of air pollutants. Atmospheric stability classes are typically categorized into three broad classes: unstable, neutral, and stable. The classes refer to the reaction of an air parcel displaced adiabatically in the vertical direction. Figure 2-8 illustrates environmental lapse rates associated with the three stability classes (Trotter, 1998).

An air parcel originates at an elevation represented by the small circle in Figure 2-8. The temperature of the air parcel is the same as that of the surrounding environment. If the density of the air parcel is less than that of the environment ($\rho_p < \rho_e$ or $T_p > T_e$), the parcel accelerates upward; the atmosphere is classified as unstable. If the density of the air parcel is greater than that of the environment ($\rho_p > \rho_e$ or $T_p < T_e$), the parcel accelerates downward and the atmosphere is viewed as stable. It the density of the air parcel is the same as that of the environment ($\rho_p = \rho_e$ or $T_p = T_e$), there is no force applied and the parcel continues at its original speed. Under these conditions, the atmosphere is said to be neutral (Trotter, 1998).

2.2.4 Meteorological Wind Patterns Associated with Topographic Features

The altitude and amplitude of hills and mountains determine the variations of air processes in regions of complex terrain. Meteorological systems associated with

topographic features result from influences on airflow produced by differing, juxtaposed topographic features such as mountains and valleys. These airflow patterns consist of cross-valley axis and along-valley axis circulations. Cross-valley-axis circulations result when a sloping surface is heated or cooled. Rising or sinking air parcels follow the terrain as depicted in Figure 2-9. As the morning sun warms and evaporates the upper surface of the cloud, the whole bank gradually thins out and begins to disperse. By midday the nocturnal inversion is broken down and convection currents cause strong thermals. It generates an upvalley or anabatic wind of rising motions during the afternoon as illustrated in Figure 2-9(A). These winds result from heating of mountain-valley slopes by the rising sun. When the rising air reaches ridge top, it separates and continues to rise until reaching the capping stable layer or entrainment zone (Hanwell, 1980).

Figure 2-9(B) depicts the nighttime situation where cool air drains down mountain-valley slopes and pools in the valley floor. In areas with comparatively steep slopes, these descending flows are referred to as katabatic winds (Hanwell, 1980;Randerson, 1984;Slade, 1968;Stull, 1988). Along-axis circulations are generally referred to as mountain-valley or slope-valley winds. On clear nights with light prevailing winds, the wind in a valley frequently assumes a configuration similar to that depicted in Figure 2-9(B). As the valley slopes cool by radiation, air adjacent to the slopes cools and becomes denser than air over the center of the valley floor. This denser air flows down the mountain-valley slopes toward the valley floor. However, since drainage flow occurs at locations throughout the valley, descending air will combine into a general flow toward the valley mouth. After the slope-valley circulation is established, it will normally extend

to ridge top height. This wind pattern is destroyed after sunrise by heating of the valley floor and slopes.

On clear days with light winds, an opposite effect, an up valley, up slope wind may develop. This flow results from heating of air adjacent to the sun-warmed valley floor and slopes. However, this condition is not as pronounced as the nighttime flow. At night, turbulence in the valley is suppressed by the nocturnal boundary layer. Thus, airflow patterns in the valley floor remain relatively undisturbed. During the day, heated land surfaces warm adjacent air and create atmospheric turbulence. As turbulence increases, air within the valley mixes with free airflow above the ridge tops. The development of daytime turbulent mixing constitutes a disruptive mechanism that hinders establishment of the up slope, up valley wind patterns. Although such patterns are known to exist, they are neither as common nor pronounced as the nighttime down-valley flows (Randerson, 1984;Slade, 1968;Stull, 1988).

2.3 Tropospheric Ozone

2.3.1 Sources, Formation and Transport of Ozone

As shown in Figure 2-10, tropospheric ozone is photochemically produced from reactions involving a variety of volatile organic compounds (VOCs), composed mainly of non-methane hydrocarbons (HC) in the presence of nitrogen oxide (NO_x) such as nitric oxide (NO) and nitrogen dioxide (NO_2) emitted from both mobile and stationary sources (Finlayson-Pitts and Pitts, 1993;Jacob et al., 1996). Meteorology plays an important role in ozone formation, destruction, and transport. The photochemical reactions are greatly influenced by atmospheric temperature, which is a function of solar radiation and cloud

cover as mentioned in section 2.1.2. Ozone formed in the photochemical reaction is vertically transported by thermal distribution due to solar radiation (Finlayson-Pitts and Pitts, 1993).

2.3.2 Meteorology and Ozone Relationships

It is well known that meteorological conditions are a crucial factor contributing to atmospheric photochemical reaction. An abundance of studies have attempted to elucidate ozone dependence on meteorology because of this strong association (Feister and Balzer, 1991;Robeson and Steyn, 1990;Shreffler and Evans, 1982;Wolff and Lioy, 1978).

Some researchers found that high ozone concentrations are associated with light winds, high-pressure weather systems that result in sunshine, high temperatures, clear sky, and stagnant air (NRC (National Research Council), 1991;Seaman and Michelson, 2000). These systems typically result in less convective mixing with a temperature inversion that helps contain precursor pollutants (NO_x and VOCs) in the troposphere. The tropospheric layer becomes a stable condition. Winds associated with high-pressure systems are typically light, thus increasing the chance that pollutants will accumulate in the atmospheric boundary layer. Warm cloudless conditions associated with these systems are favorable to photochemical production of ozone (Seaman and Michelson, 2000).

Other researchers have considered some 100 meteorological variables and found maximum surface temperature, relative humidity, mixing height, and opaque cloud cover, to be significant meteorological predictors for study of ozone production in the United

States (Cox and Chu, 1993;Cox and Chu, 1996). Aneja et al. (2000) reported that the meteorological variables such as temperature, pressure, and humidity play an important role on ozone concentrations in the atmospheric boundary layer.

Ozone is simultaneously destroyed via oxidation of an additional reactant (D), typically one of the NO_x. These relationships van be expressed conceptually as (Comrie, 1997)

$$NO_x + VOCs + UV \longrightarrow O_3 \qquad \text{(Equation 2-1a)}$$

$$O_3 + D \longrightarrow DO + O_2 \qquad \text{(Equation 2-1b)}$$

Each term in these reactions is related to the weather-dependency of ozone production in several respects:

- Precursor emissions processes (combustion, evaporation) are sensitive to temperature, vapor pressure, etc.
- Dispersion conditions (e.g., wind speed, atmospheric stability, mixing height) influence ambient concentrations of precursors and ozone.
- Reaction rates between the pollutants vary according to temperature and meteorological controls on UV availability (e.g., cloudiness and other forms of attenuation in the atmosphere) (Comrie, 1997).

The schematic diagram of Figure 2-11 summarizes the overall photochemical and chemical oxidation reaction for ozone formation that occurs in an atmosphere containing nitrogen oxides, reactive hydrocarbons, and oxygen. For example, nitric oxide (NO)

emitted from a variety of sources reacts with organic dioxides to produce nitrogen dioxide (NO_2). Nitrogen dioxide produces nitric oxide (NO) and atomic oxygen (O) in the presence of sunlight. The atomic oxygen reacts with oxygen yielding ozone. This ozone formation is explained by chain reactions involving the inter-conversion of nitric oxide (NO) and nitrogen dioxide (NO_2), the oxidation of hydrocarbons, and the generation of reactive intermediates, particularly the hydroxyl radical (HO^-).

The hydroxyl (OH) radical is the key reactive species in the chemistry of ozone formation. Photolysis of ozone is the major sources of the hydroxyl radical in the troposphere. An increase in O_3 will produce more OH, resulting in decreased lifetimes of many trace species, such as methane and the hydrochlorofluorocarbons (HCFC) (Finlayson-Pitts and Pitts, 1993).

The VOC-OH reaction initiates the oxidation sequence. There is a competition between VOCs and NO_x for the OH radical. At a high ratio of VOC to NO_x concentration, OH will react mainly with VOCs; at a low ratio, the NO_x reaction can predominate. The hydroxyl radical reacts with VOC and NO_2 at an equal rate when the VOC-to-NO_2 concentration ratio is a certain value; this value depends on the particular VOC or mix of VOCs present, as the OH rate constants of VOCs differ for each VOC species (Seinfeld and Pandis, 1997). The photochemical formation of ozone is strongly related to the intensity of the UV radiation. However, the dynamic chemical equilibrium is not solely mediated by solar radiation, as temperature also plays an important role in the chemical reaction speed (Schlink et al., 1999).

A brief overview of the chemistry of volatile organic compounds (VOC) and oxides of nitrogen (NO_x) that lead to ozone formation is included. Photodissociation of

NO_2 by sunlight is the only significant anthropogenic source of O_3 in photochemical smog:

$$NO_2 + hv(\lambda < 430\ nm) \longrightarrow NO + O \qquad \text{(Equation 2-2a)}$$

$$O + O_2 + M \longrightarrow O_3 + M \qquad \text{(Equation 2-2b)}$$

where the M in Equation 2-2b represents N_2 or O_2 or another third molecule that absorbs the excessive vibration energy and thereby stabilizes the O_3 molecule formed. The essential role played by VOC is the oxidation of NO to NO_2, the precursor of O_3 via reactions 2-2a and 2-2b. This role of VOC can be illustrated using the atmospheric photo-oxidation of methanol, a widely promoted "alternate fuel":

$$CH_3OH + OH \longrightarrow CH_2OH + H_2O \qquad \text{(Equation 2-3a)}$$

$$CH_3OH + OH \longrightarrow CH_3O + H_2O \qquad \text{(Equation 2-3b)}$$

$$CH_2OH + O_2 \longrightarrow H_2CO + HO_2 \qquad \text{(Equation 2-4)}$$

$$CH_3O + O_2 \longrightarrow H_2CO + HO_2 \qquad \text{(Equation 2-5)}$$

$$HO_2 + NO \longrightarrow NO_2 + OH \qquad \text{(Equation 2-6)}$$

$$OH + NO_2 \xrightarrow{M} HNO_3 \qquad \text{(Equation 2-7)}$$

In its overall features, this gas phase mechanism applies to VOC oxidation in the troposphere. Chain reaction initiation by OH occurs in reactions 2-3a and 2-3b to

generate free radicals that react with molecular O_2 to form formaldehyde and the hydroperoxyl radical (HO_2), reactions 2-4 and 2-5. This oxidation of formaldehyde occurs slowly in polluted atmospheres and more rapidly in the combustion/tailpipe system of vehicles using it as an alternate fuel; removal of HCHO by an effective oxidation catalyst is essential from both health and air quality considerations if methanol is to be widely used as an "alternate fuel" (Finlayson-Pitts and Pitts, 1986;Wayne, 1985).

HO_2 rapidly oxidizes NO to NO_2 in reaction 2-6, and in this critical chain reaction carrying step, regenerates OH radicals. The reaction 2-7 of OH with NO_2 to form nitric acid ($HONO_2$) is a major chain reaction termination step (Finlayson-Pitts and Pitts, 1986;Wayne, 1985). When photochemical ozone production ceases and vertical transport of ozone mass aloft is inhibited by a thermal inversion of the normal temperature profile at night, ozone loss occurs in non-photochemical reactions with nitric oxide (NO) and nitrogen dioxide (NO_2) in the following reactions (Finlayson-Pitts and Pitts, 1986;Seinfeld and Pandis, 1997;Wayne, 1985):

$$O_3 + NO \longrightarrow NO_2 + O_2 \qquad \text{(Equation 2-8)}$$

$$NO_2 + O_3 \longrightarrow NO_3 + O_2 \qquad \text{(Equation 2-9)}$$

In locations near large sources of NO and NO_2, the nighttime minimum in ozone can be quite pronounced because of the rapid reaction between ozone and NO and NO_2. In fact, in many urban areas the NO source is strong enough to cease the complete nighttime disappearance of ozone (Seinfeld and Pandis, 1997).

2.3.3 Diurnal Variations of Ozone Concentrations

During the summers of 1978 – 1980, a researcher collected ozone and precursor data at rural sites in South Dakota, Louisiana, and Virginia. The patterns display a period of ozone increase from sunrise until mid-afternoon. A period of ozone decrease occurs from late afternoon until sunrise. The mean diurnal ozone patterns at all three sites are shown in Figure 2-12(A). Figure 2-12(B) contains ozone profiles during episode and non-episode periods at the Louisiana site. Diurnal patterns are similar with periods of significant ozone increase occurring from 07:00 to 11:00, and periods of significant ozone decrease occurring from late afternoon until sunrise (Kelly et al., 1984).

However, episode ozone concentrations throughout the night and early morning are 10 – 15 ppb higher than non-episode concentrations. During the daytime, peak ozone concentrations for episodes are approximately 30 ppb higher than non-episodes. Interesting average patterns for mixing heights in Louisiana and Virginia are shown in Figure 2-13. He estimated the height of the nocturnal inversion at 50 ± 30 m. The inversion dissipates by approximately 07:00. By 10:00, the mixing height exceeds 1500 m at both the sites more than 95% of the time. He attempted to separate the effects of mixing from those of photochemistry by breaking the period of increasing ozone into smaller time segments whereby one mechanism should predominate over the other. The data at the three sites suggest that vertical mixing accounts for approximately half of the overall increase in ozone from morning to afternoon (Kelly et al., 1984).

In another research effort, the atmospheric sciences division at Georgia Institute of Technology analyzed hourly ozone measurements collected from 29 stations in the southeastern United States. The average hourly ozone profile, shown in Figure 2-14,

clearly confirms the diurnal pattern of high values during the daylight hours and low values during the night hours. The team of researchers illustrates that, in the morning hours, ozone increases because of the breakup of the nocturnal inversion layer as air is mixed downward from aloft. During morning hours, ozone also increases due to photochemical production. At night, ozone is suppressed by reaction with oxides of nitrogen and by surface deposition in a shallow inversion layer (Casado et al., 1994).

The U.S. Environmental Protection Agency studied the change in the seasonally averaged ozone levels. The study shows diurnal patterns of four-year data collected at a monitoring station located at Allentown, Pennsylvania. The study shows no statistically significant change in the shape of the average diurnal profile (averaged by ozone season) across the four-year ozone data sets because of the similarity of meteorological conditions (Figure 2-15). They report that the diurnal patterns are greatly influenced by meteorological variation and photochemical precursors in rural areas without changing the implementation of control strategies (Lefohn et al., 1993). The similarity of hour-specific chemical and meteorological processes is supported by the characteristic diurnal pattern exhibited by surface ozone (Lefohn et al., 1993).

2.3.4 Vertical Profiles of Ozone Concentrations

Trotter et al. (1996) collected vertical ozone data up to 600 m above the ground to characterize the vertical structure of ozone during July and August of 1995, using a Tethersonde Ozone Sounding Systems (Model OZ-3A-T) in Oak Ridge in the eastern Tennessee region. They also analyzed permanent monitoring station data collected at the Look Rock monitoring station operated by the National Park Service. They reported that

the ozone data observed from high elevation monitoring stations in the Great Smoky Mountain National Park displayed little or no diurnal variation whereas ozone observations at low elevations stations near Oak Ridge revealed significant diurnal variation.

Figure 2-16(A) contains four morning profiles to visualize data collected at 05:00, 07:00, 09:00, and 11:00 Local Standard Time (LST). Figure 2-16(B) contains four evening profiles designated as 16:00, 18:00, 20:00, and 22:00 LST. As shown in Figure 2-16(A), the ozone profiles in the early morning remain quite low until a stable nocturnal inversion breaks up in the late morning due to surface heating. The early morning profiles indicate a surface-based inversion which is approximately 100 meters in depth by 07:00 LST. As the nocturnal surface inversion layer begins to break up at 09:00 LST, the mixing height start to rise. Then the ozone concentrations at ground level begin to rise as ozone mass aloft becomes entrained in the atmospheric mixing and ozone begins to form photochemically near the ground. The ground level ozone concentration continuously rises. Eventually, it is uniformly mixed through the mixing layer. The 11:00 and 16:00 LST profiles are indicative of thorough mixing with a mixing height well above 600 m. By 18:00 LST, ozone concentrations at the surface begin to drop. The later evening profiles, 20:00 and 22:00 LST, reflect the continual development and growth of the nocturnal inversion (Trotter et al., 1996).

Nappo et al. demonstrated similar diurnal patterns measured at ground and high elevations up to 600 m (Nappo et al., 1989). Güsten et al. observed that a well-mixed vertical ozone profile begins at about 11:00 a.m., and the constant ozone profile remains until 4:30 p.m. in the afternoon. They reported that a stable nocturnal surface inversion

disappears in the late morning and shows re-establishment in the evening (Güsten et al., 1998).

Aneja et al. conducted vertical measurements of ozone on a 610 m high-elevation tower in use by the NC Department of Environment and Natural Resources located about 15 km southwest of Raleigh, NC. They collected ozone data measured at ground level, 76, 128, 259, and 433 m above Mean Sea Level (MSL) during the ozone season of the period from 1993 through 1997. They examined correlations between ozone concentrations observed at the ground level and high elevations as well as effects of meteorological conditions on ozone concentrations with respect to temperature, pressure, and humidity. They reported that the meteorological variables play an important role on ozone concentrations in the atmospheric boundary layer. The correlations between ozone concentrations at the various high elevations were fairly strong, while those between the ground and high elevations were weak. They noted that a correlation between the ozone concentration in the previous night's residual layer and the maximum ground level concentration on the following day might be utilized as a method to predict high elevation ozone concentrations based on an observation-based model derived from the data (Aneja et al., 2000).

CHAPTER 3

AVAILABLE DATA AND ANALYTICAL METHODS

This chapter focuses on 1) a description of the available data, essential assumptions, methods used in this study to develop an algorithm to predict high elevation ozone concentrations, and 2) the algorithm development, formulation, and evaluation and comparison of model results. The first section includes ozone and meteorological data, and a description of ozone monitoring stations located in North Carolina and East Tennessee from which data were obtained to conduct this study. The second section introduces requisite assumptions for this study. The third section illustrates a number of different methods utilized to develop a regression model to predict high elevation ozone concentrations based on ground level ozone observations. The last section covers not only the process of the model development but also analytical methods to evaluate the performance of the model.

3.1 Available Data

3.1.1 Ozone Data

This section presents ozone data used in this study and describes the ozone-monitoring stations where ozone data were collected in North Carolina and East Tennessee. The overall criterion used to select the sites was that ozone data had to be available at multiple elevations above the ground. The North Carolina sampling site is located approximately 15 km east-southeast of downtown Raleigh, NC at 35.683333 Latitude and –78.55 Longitude, approximately 300 meters west of US-70 (Expressway).

The base of the multi-elevation sampling tower is at 97.5 m elevation above Mean Sea Level (MSL). It is a "suburban" location setting with "agricultural" land use. Ozone monitoring is located at ground level, and at 76 m, 128 m, and 433 m above the ground on the Auburn Transmitter Tower, a 610-m multi-communications tower located near the town of Auburn, NC.

Ozone concentrations, measured using the ultraviolet (UV) photometric detection principle, were sampled at ground level, 259 m, and 433 m during the ozone-monitoring season in 1995. The sampling began May 16 for ground and 259 m, and on May 25 for 433 m, and continued until October 2. Ozone measurements were made at ground level, 76 m, 128 m, and 433 m during the ozone season in 1996, 1997, and 1998. Sampling was initiated at ground level on May 30 in 1996, and was initiated at 76 m on May 24, 128 m on May 23, and 433 m on May 17; sampling ended September 19. In 1997, sampling at all levels was initiated on May 15 and ended September 12, except for ground-level sampling, which ended October 31. In 1998, ozone monitoring at the ground level of the tower began on April 15, and continued through October 31, 1998. Monitoring at the upper levels began on May 8, with the exception of the uppermost level (433 m). Therefore, data analysis for North Carolina was conducted for four different elevations: 76m (173.5m MSL), 128m (225.5m MSL), 259m (356.5m MSL), and 433m (530.5m MSL). The operational dates are summarized in Table 3-1.

East Tennessee ozone data were collected from Look Rock, Cove Mountain, and Clingman's Dome monitoring stations located at elevations of 793m MSL, 1243m MSL and 2021m MSL, respectively by the National Park Service (NPS) as part of EPA's national air monitoring network. The Rutledge Pike Mascot monitoring station is located

near the valley floor. The other monitoring stations, shown in Figure 3-1, are essentially located at the ridge-top of these mountains.

Based on location descriptions of the monitoring stations in Figure 3-2, data measured at land surface above MSL are called ground-level ozone concentrations. East Tennessee ozone data measured at the top of mountains like Look Rock, Cove Mountain, and Clingman's Dome are called high elevation surface site ozone concentrations. North Carolina data measured from the multi-elevation sampling tower above the land surface are called ozone concentrations at high elevation above surface site. The actual ozone concentration may differ substantially between the NC and TN sites. However, the methods used in this study do not utilize the actual ozone concentration to develop functional relationships, but the ratio of the high elevation ozone concentration to the appropriate values of ground level concentration (i.e., today's maximum, previous day's maximum, or today's current hour). It was anticipated that the use of the ratio would provide a normalized ratio that would allow both data sets (NC and TN) to be combined.

The data used in this study were collected by the Knox County Department of Air Pollution Control (KCAPC) and the National Park Service (NPS) from monitoring stations in eastern Tennessee from 1995 to 1998. The ozone data measured at an elevation of 267m MSL is regarded as reference data for ground-level ozone data because the monitoring sites are located at an elevation of approximately 267m above MSL. Although the Rutledge Pike Mascot monitoring station, located at elevation of 299m MSL in Table 3-1, is a little higher than the MSL of the sampling site, it is regarded as ground level in this study. Therefore, data analysis for East Tennessee is examined at

three different altitudes: 526m (793m MSL), 976m (1243m MSL), and 1754m (2021m MSL).

Ozone monitoring stations located in rural areas in North Carolina and Tennessee, where agriculture and forests are dominant, were selected to avoid undue influence from nearby point sources, area sources, or local activity. Some of the ozone data were not recorded because of the period of calibration. The detailed information regarding the ozone monitoring stations and operational dates is summarized in Table 3-1.

3.1.2 Meteorological Data

In the analysis of ozone and meteorology, the relative locations of the ozone and meteorological monitors are different. Measurements from meteorological monitors not co-located with ozone monitors are frequently used since airports often provide high-quality meteorological surface observations (Thompson et al., 2001). Meteorological data used in this study were complied from standard airport observations by the National Climatic Data Center (NCDC). North Carolina's meteorological data were taken from the station located at the Raleigh Durham international airport. Tennessee's meteorological data were taken from the station located at the McGhee Tyson airport in Alcoa TN (near Knoxville TN).

The cloud cover meteorological variable, which significantly influences ozone concentrations, was extracted from the meteorological data for the same period as the full ozone-monitoring season (April – October of 1995 – 1998). The extracted cloud cover data were utilized to develop "clear," "cloudy," and "clear to partly cloudy" component regression models.

3.2 Assumptions

To develop an algorithm to predict high elevation ozone concentrations based on ground level ozone observations, this study assumes the following:

- Meteorological conditions are recurrent phenomena and characteristic of season and day/night time in a year;
- Vertical mixing height is maximized and the Atmospheric Boundary Layer (ABL) is fully mixed up to the highest elevation stations (1754m) when the maximum ground level ozone concentration occurs;
- The ozone data collected at high elevation surface sites such as Look Rock, Cove Mountain, and Clingman's Dome are representative of ozone concentrations that would have existed at high elevation above a surface site located at lower elevations (i.e., Knoxville and surrounding valley areas);
- The ozone data collected at these monitoring sites are representative of the day-to-day meteorologically related fluctuations in ozone that this study is intended to address.

3.3 Methods

Prior to developing a regression model to predict high elevation ozone concentrations based on ground level ozone concentrations, the relationship between ground level hourly ozone concentrations and high elevation hourly ozone concentrations was investigated. For purposes of this study, this approach is referred to as "Present Day's Ground Level Concentration" or the "do-nothing" method since it is the approach

used in the existing air quality models like CALPUFF. As mentioned in Chapter 1, many researchers reported ozone concentrations vary with elevation (Reiter et al., 1987;Ryan et al., 1998;Trotter, 1998). The motivation of this study was, in part, based on the unreasonable approach used in the existing air quality models where it is often assumed that ozone is constant with elevation and equal to the ground-level observation.

Two different algorithms were developed for prediction of high elevation ozone concentrations based on ground level ozone observations. One is an overall regression model that did not consider meteorological conditions. The other algorithm utilizes "clear," "cloudy," and "clear to partly cloudy" components in the regression models in order to account for meteorological conditions. For developing the overall regression model, the three methods ("Prediction based on Present Day's Maximum," "Prediction based on Previous Day's Maximum," and "Prediction based on Present Day's Hourly") discussed in the following three sections were first investigated. The relative performances of these methods were compared to each other in terms of statistical results produced by a linear regression. The best method was selected and development was continued in an effort to arrive at an overall regression model to predict high elevation ozone concentrations. "Prediction based on Cloud Cover/Present Day's Maximum" method in Section 3.3.4 is used for developing the "clear," "cloudy," and "clear to partly cloudy" component regression models. Overall processes used to develop the overall regression model and each component regression model are shown in Figure 3-3. In this study, data with errors or missing data for any ozone data and meteorological variable were removed from the analysis.

3.3.1 "Prediction based on Present Day's Maximum" Method

As mentioned in Section 3.2, the "Prediction based on Present Day's Maximum" method is based on the assumption that vertical mixing height is maximized and the Atmospheric Boundary Layer (ABL) is fully mixed up to the highest elevation stations when the maximum ground-level ozone concentration occurs. Ozone concentration becomes homogeneous throughout the vertical ABL under the assumption that the ground-level ozone concentration should be approximately equal to the ozone concentration observed at the highest elevation stations above the surface site at the same point in time. This has been shown in the past to be a reasonable assumption, based on limited vertical profile studies conducted by Trotter (Trotter, 1998).

The first proposed method ("Prediction based on Present Day's Maximum" method) assumes that there is a predictable relationship between a current day's ground-level maximum one-hour ozone concentrations (independent variable) and the current day's high elevation hourly ozone concentrations (dependent variable). The relationship between the current day's ground-level maximum one-hour ozone concentrations and the concentrations observed at a high elevation was determined for each discrete hour of the day, based on 1998 data. The relationships were evaluated with respect to statistical results produced by linear regression analysis.

3.3.2 "Prediction based on Previous Day's Maximum" Method

As Neu (1994) reported, up to 50 – 70% of the ozone concentration measured in the morning of the following day can be originated from the nocturnal residual ozone mass that remained aloft in the ABL (Neu et al., 1994). This illustrates that the previous

day's high elevation ozone concentration influences the current day's ozone concentration. Based on Neu's conclusion and the assumption that vertical mixing height is maximized and the ABL is fully mixed up to the highest elevation stations when the ground level maximum ozone concentrations occurs, it was hypothesized in this study that there might be a relationship between the previous day's ground-level maximum one-hour ozone concentrations and the current day's high elevation hourly ozone concentrations.

Thus, the "Prediction based on Previous Day's Maximum" method compares and evaluates the relationship between the previous day's ground-level maximum one-hour ozone concentrations (independent variable) and the current day's high elevation hourly ozone concentrations (dependent variable), using 1998 data. This method analyzes the ratio of ozone concentrations (current day's high elevation hourly ozone concentrations/previous day's ground-level maximum one-hour concentrations) for each hour of the day, for all of the data within the 1998 ozone season.

3.3.3 "Prediction based on Present Day's Hourly" Method

As solar energy is transferred to the atmosphere from the earth's surface in the early morning, the earth's surface warms the lower meters of the atmosphere by a form of energy transfer called conduction. As the convective boundary layer develops during daytime, a vertical mixing height gradually increases through convective turbulence in the ABL (Eagleman, 1980;Nicholson et al., 2001). Thus, a vertical mixing of ground level ozone and high elevation ozone concentration occurs and the ground level ozone concentration changes according to the degree of the vertical mixing.

The "Prediction based on Present Day's Hourly" method assumes that there is a predictable relationship between a current day's ground-level hourly ozone concentrations (independent variable) and the current day's high elevation hourly ozone concentrations (dependent variable). The "Prediction based on Present Day's Hourly" method evaluates the relationship between a current day's ground level hourly ozone concentrations and the current day's high elevation hourly ozone concentrations, using 1998 data. The method analyzes the ratio of ozone concentrations (current day's high elevation hourly ozone concentrations/current day's ground-level hourly ozone concentrations) for each hour of the day, for the data available in the 1998 ozone season.

3.3.4 "Prediction based on Cloud Cover/Present Day's Maximum" Method

The "Prediction based on Cloud Cover/Present Day's Maximum" method presented here includes an effort to incorporate the influence of meteorology on ambient ozone concentrations using cloud cover as a meteorological parameter. Cloud cover serves as a surrogate for all meteorological variables that affect ozone (Cox and Chu, 1993;Cox and Chu, 1996;NRC (National Research Council), 1991;Seaman and Michelson, 2000). It is a critical meteorological parameter used to characterize the atmospheric condition. This is because the degree of cloud cover affects radiation fluxes and atmospheric stability, which influences vertical mixing as well as the thermal inversion. An overcast meteorological condition limits the amount of vertical mixing even during daytime in the ABL; on the other hand, a vigorous vertical mixing occurs on a clear day (Cooper and Alley, 1994).

Prior to conducting analyses using the "Prediction based on Cloud Cover/Present Day's Maximum" method, each one of the first three methods was compared with respect to statistical results yielded by linear regression analysis. The best method, "Prediction based on Present Day's Maximum" method, was selected from the comparison and extended for developing each component regression model that includes the influence of meteorology on ozone concentrations. In the "Prediction based on Cloud Cover/Present Day's Maximum" method for developing each component regression model, ozone data were separated into three distinct categories: clear, cloudy, and clear to partly cloudy. To do so, the values of total sky cover were extracted from NCDC surface meteorological data. The values ranged from zero to ten and were reportedly hourly in the surface meteorological data format of the National Climatic Data Center. Values of daily average cloud cover were calculated for the 1998 full ozone season. In the case that a calculated value of daily average cloud cover falls in the range between greater than or equal to 0 and less than or equal to 3, the corresponding ozone data were considered as a "clear day." In the case where a value falls in the range between greater than or equal to 7 and less than or equal to 10, the corresponding ozone data were considered as a "cloudy day." Days with cloud cover falling between 3 and 7 were initially excluded from the analysis in an effort, to see if an improved relationship could be developed for the two extremes of clear and cloudy. Later, an analysis was conducted for the case where a value falls in the range between or equal to 0 and less than 7; the corresponding ozone data set was considered "clear to partly cloudy day."

An attempt to develop an algorithm to predict high elevation ozone concentration by hour of day was made for three cases (clear, cloudy, and clear to partly cloudy days)

separately with the same method as the overall regression model. They are called “clear,” “cloudy,” “clear to partly cloudy” component regression models. The performance of each component model was compared to those of the overall regression model in terms of statistical results for model evaluation. The comparison might give useful information to see if each component model, a statistical model that includes a meteorological parameter (cloud cover), shows a significant improvement over the overall regression model, a statistical model that does not consider meteorological parameter, and to see if any improvement over the simpler regression model can be developed.

3.4 Detailed Description of the Analyses Used in the Four Methods

This section illustrates the analyses used in each of the four methods. In the “Prediction based on Present Day’s Maximum” method, 214 values for current day’s ground level maximum one-hour ozone concentrations for the 214 days for the 1998 full ozone season (April – October) were extracted from the ozone database. The 214 values for the current day’s high elevation hourly ozone concentrations were extracted for each of the 24 hours of day and six different elevations separately. Thus, the 144 paired data sets were used to find relationships between the current day’s ground level maximum one-hour ozone concentrations and the current day’s high elevation hourly ozone concentrations for 24 hours of the day and six different elevations. Then, a linear regression was applied for each paired data set to find the relationship between the current day’s ground level maximum one-hour ozone concentrations and the current day’s high elevation hourly ozone concentrations. The linear regression analysis yielded

144 slopes, $m_{h,z}$, representing a relationship of a paired ozone data set. Figure 3-4(a) shows an example to find the relationship between a current day's ground level maximum ozone concentrations and the current day's 76 m elevation ozone concentrations measured at 13:00 EST. The "Prediction based on Previous Day's Maximum" and "Prediction based on Present Day's Hourly" methods followed the same approach as the "Prediction based on Present Day's Maximum" method. Slopes, $m_{h,z}$, yielded by the linear regression analysis for the three methods ("Prediction based on Present Day's Maximum," "Prediction based on Previous Day's Maximum," and "Prediction based on Present Day's Hourly") are as follows:

"Prediction based on Present Day's Maximum" method: $m_{h,z} = \frac{C_{h,z\,(\text{current day})}}{C_{\text{MAX-G (current day)}}}$

"Prediction based on Previous Day's Maximum" method: $m_{h,z} = \frac{C_{h,z\,(\text{current day})}}{C_{\text{MAX-G (previous day)}}}$

"Prediction based on Present Day's Hourly" method: $m_{h,z} = \frac{C_{h,z\,(\text{current day})}}{C_{\text{h-G (current day)}}}$

"Prediction based on Cloud Cover/Present Day's Maximum" method:
Made for three cases (clear, cloudy, and clear to partly cloudy days) separately with the same method as the best method, "Prediction based on Present Day's Maximum", selected from the comparison of the three methods ("Prediction based on Present Day's Maximum," "Prediction based on Previous Day's Maximum," and "Prediction based on Present Day's Hourly")

In the equations, $C_{h,z}$ indicates ozone concentrations measured at a specific hour (h) of day and a specific elevation (z), $C_{MAX\text{-}G}$ indicates ground level daily maximum one-hour

ozone concentrations (ppb), $C_{h\text{-}G}$ indicates ground level hourly ozone concentrations (ppb), and $m_{h,z}$ is the slope (or linear best fit gradient).

3.5 Formulation of "Overall" and "Clear," "Cloudy," and "Clear to Partly Cloudy" Component Regression Models

In order to develop equations to predict vertical ozone concentrations for a particular time as a function of elevation from ground level up to the well-mixed homogeneous layer, relationships between current day's ground level maximum ozone concentrations (independent variable) and the current day's ground level hourly ozone concentrations were also developed. The linear regression analyses yielded 24 slopes (or linear best fit gradients) for each hour of day for North Carolina and 24 slopes for East Tennessee. These were determined so that there would be a slope for each elevation (ground-level and the six elevated sites).

The values of the 192 slopes (144 slopes for 24 hours of the day and six different elevations plus 48 slopes for 24 hours of the day and two ground levels in North Carolina and East Tennessee) were used to find a relationship between elevation (independent variable) and the linear best-fit gradient ($m_{h,z,}$ dependent variable) to develop the overall regression model. Figure 3-5 shows an example plot of the linear best-fit gradient and elevation for 0:00 EST. In order to find optimized equations to describe the nonlinear curve of the data points in the plots, many nonlinear equations were evaluated to obtain a better r^2 value. Two nonlinear equations and a constant value were found to be adequate to describe the 24 relationships for each hour of day as follow:

For hours 0:00 – 9:00 EST and 18:00 – 23:00 EST

$$m_{h(p)} = A(1-e^{-B(Z-C)}) \quad \text{(Equation 3-1a)}$$

For hours 11:00 – 17:00 EST

$$m_{h(p)} = (a+be^{-cZ}) \quad \text{(Equation 3-1b)}$$

For 10:00 EST

$$m_{h(p)} = D \quad \text{(Equation 3-1c)}$$

Here Z is the elevation in meters ranging from 0 to 1800 meters; A, B, C, a, b, and c are coefficients determined to yield the best fit for each equation; and D is a constant. Having determined the equations describing $m_{h(p)}$ as a function of elevation Z, the predicted concentration ($C_{h(p)}$) at any elevation Z can then be determined using the appropriate equations to be

$$C_{h(p)} = m_{h(p)}C_{MAX\text{-}G,\ current\ day} \quad \text{(Equation 3-2)}$$

Substituting Equations 3-1a, 3-1b, and 3-1c into Equation 3-2, then the set of equations is

For hours 0:00 – 9:00 EST and 18:00 – 23:00 EST

$$C_{h(p)} = \{A(1-e^{-B(Z-C)})\}C_{MAX\text{-}G,\ current\ day} \quad \text{(Equation 3-3a)}$$

For hours 11:00 – 17:00 EST

$$C_{h(p)} = \{(a+be^{-cZ})\}C_{MAX\text{-}G,\ current\ day} \quad \text{(Equation 3-3b)}$$

For 10:00 EST

$$C_{h(p)} = \{D\}C_{MAX\text{-}G,\ current\ day} \quad \text{(Equation 3-3c)}$$

Note that $C_{MAX\text{-}G}$ refers to ground-level maximum one-hour ozone concentration.

The combined twenty-four equations (i.e., one for each hour of day) were formulated and comprise the overall regression model to predict high elevation ozone concentration based on the day's maximum ground level ozone concentrations. Elevation and ground level daily maximum ozone concentration were used as input into the overall regression model. The approach utilized in developing the overall regression model was also applied for the formulation of the "clear," "cloudy," and "clear to partly cloudy" component regression models.

3.6 Evaluation of Methods and Evaluation of Models' Performance with Respect to Statistical Results

Regression analyses were applied for relationships between ground level ozone concentrations and high elevation ozone concentrations, using the "Prediction based on Present Day's Maximum," "Prediction based on Previous Day's Maximum," "Prediction based on Present Day's Hourly," and "Prediction based on Cloud Cover/Present Day's Maximum" methods mentioned in sections 3.3.1 through 3.3.4, respectively. The performance of each method was evaluated in terms of the residuals between the standard deviations of ozone observations and predictions (s_o-s_p), Mean Absolute Error (MAE), Mean Bias Error (MBE), Root Mean Square Error (RMSE), coefficient of determination (r^2), and index of agreement (d_1, α=1). After comparing the performance of each method, the best one was selected based on the relative performances with respect to r^2 and d_1 and continued to develop an algorithm to prediction high elevation ozone concentration ozone concentrations for a particular time as a function of elevation as mentioned in Section 3.5.

The developed algorithm was called the "overall regression model." It was evaluated in an effort to measure success of the model and the degree to which the model-predicted ozone concentrations approach a linear function of the observed ozone concentrations. These were grouped into measures of difference (or error), and measures of agreement. The measures of difference used here are Mean Bias Error (MBE), Mean Absolute Error (MAE), and Root Mean Square Error (RMSE), which were calculated as follows (Comrie, 1997;Gardner and Dorling, 2000;Seaman, 2000;Spellman, 2000):

$$MBE = \frac{1}{N}\sum_{i=1}^{N}(P_i - O_i) \qquad \text{(Equation 3-4)}$$

$$MAE = \frac{1}{N}\sum_{i=1}^{N}|P_i - O_i| \qquad \text{(Equation 3-5)}$$

$$RMSE = \left[\frac{1}{N}\sum_{i=1}^{N}(P_i - O_i)^2\right]^{0.5} \qquad \text{(Equation 3-6)}$$

MBE (Equation 3-4) is based on the simple difference between predicted (P_i) and observed (O_i) values. Perfect accuracy would yield an MBE of 1.0. This measure indicates the degree that observed concentrations are over or underpredicted. Of more value is MAE (Equation 3-5), which is easy to interpret and defined as the mean absolute value of the difference between model predictions and observed values (the residuals), whereas RMSE (Equation 3-6) is the square root of all squared residuals.

The observed (s_o) and modeled (s_p) concentration standard deviations quantify the amount of the variance the model is capturing compared to the observed data. Although measures of correlation do not give any indication of model accuracy, they are also

commonly reported. The coefficient of determination (r^2) is an intuitively attractive statistic since it describes the proportion of the total variance in the observed data that can be explained by the model. It ranges from 0.0 to 1.0, with higher values indicating better agreement, and is given by

$$r^2 = \left\{ \frac{\sum_{i=1}^{N}(O_i - O)(P_i - P)}{\left[\sum_{i=1}^{N}(O_i - O)^2\right]^{0.5}\left[\sum_{i=1}^{N}(P_i - P)^2\right]^{0.5}} \right\}^2 \qquad \text{(Equation 3-7)}$$

where P_i and O_i are the modeled and observed concentrations. O and P mean observed and predicted value, respectively. However, the coefficient of determination is limited in that it standardizes for differences between the observed and predicted means and variances since it only evaluates linear relationships between the variables. A more useful measure of model performance is provided by the "index of agreement" (Equation 3-8), which is defined as (Willmott, 1981)

$$d_\alpha = 1 - \frac{\left[\sum_{i=1}^{N} | P_i - O_i |^\alpha\right]}{\left[\sum_{i=1}^{N} \left(| P_i - O | + | O_i - O | \right)^\alpha\right]} \qquad \text{(Equation 3-8)}$$

where P_i and O_i are the modeled and observed concentrations. The index of agreement has been widely used to evaluate the performance of air quality models (Comrie,

1997;Gardner and Dorling, 2000;Hurley et al., 2001;Kolehmainen et al., 2001;Kousa et al., 2001;Kukkonen et al., 2001a;Kukkonen et al., 2001b;Mendoza-Dominguez and Russell, 2001;Oettl et al., 2001;Power, 2001;Seaman, 2000;Spellman, 2000). This study utilized the index of agreement (d_1, α=1) to estimate the agreement between the measured and predicted hourly ozone concentrations. The value of d_1 is normalized and indicates the extent that predicted deviations differ from the observed deviations about the mean observed value, indicating the degree to which model predictions are error free. The value of d_1 shows how the predicted deviations about the mean observed value (O) differ from the observed deviations about O considering both sign and magnitude. Estimates of central tendency (means) are calculated for observed and predicted ozone concentrations (Willmott et al., 1985). In addition, an adequacy of the model is measured: the relationship between observed and predicted ozone concentrations is linear, or at least it is well approximated by a straight line; the error term (ε) has zero mean; and the errors are normally distributed.

The overall regression model developed with 1998 ozone data was applied and tested using ground-level ozone data observed for the period of four years from 1995 through 1998 collected at the NC and TN sites, to see how well these would be simulated. In order to compare and evaluate the performance of the overall regression model, a linear relationship of the best fit through the origin (0,0) was applied for observed and predicted ozone concentrations. The performance of the overall regression model was statistically conducted in terms of difference of dispersion (s_o-s_p), Mean Absolute Error (MAE), Mean Bias Error (MBE), Root Mean Square Error (RMSE), coefficient of determination (r^2), and index of agreement (d_1) based on the outputs produced by the

linear relationship of the best-fit line. The performances of the "clear," "cloudy," and "clear to partly cloudy" component regression models associated with meteorological conditions were compared to those of the overall regression model not considering meteorological conditions in terms of the statistical results, to see if there was a significant improvement over the overall regression model.

CHAPTER 4

RESULTS AND DISCUSSION

4.1 Characterization of Ground and High Elevation Ozone

4.1.1 Diurnal Ozone Variations

Prior to presenting the results of the analyses conducted using the "Prediction based on Present Day's Maximum," "Prediction based on Previous Day's Maximum," "Prediction based on Present Day's Hourly," and "Prediction based on Cloud Cover/Present Day's Maximum" methods which were described in Chapter 3.3, it is useful to describe typical ozone diurnal profiles obtained at the North Carolina and East Tennessee monitoring sites and to discuss the typical time of day that the ground level one-hour ozone concentration occurred. Diurnal ozone profiles at the ground and high elevations are shown in Figure 4-1 for a typical day in August 1998 for the North Carolina and Tennessee sites. As shown in the figure, the ground level one-hour ozone concentration slowly decreases down to approximately 10 ppb during early morning hours prior to sunrise. As the sun rises around 8:00 Eastern Standard Time (EST), the ozone concentration begins to increase due to increased vertical mixing of ozone from aloft and possible ozone formation. The ozone level increases throughout the day until mid-afternoon. The ozone level peaks during mid-afternoon between 12:00 and 16:00 EST (80 – 130 ppb). Then the ground level ozone rapidly decreases after sunset.

In the case of high elevation ozone data, there is a significant difference in the degree of diurnal variation in ozone concentrations. While a strong diurnal pattern, with an afternoon maximum and an early morning minimum, is dominant at ground level, this

variation is much weaker at elevated levels. Strong photochemical production and vertical mixing with ozone reservoirs aloft due to strong convection in the mid-afternoon period cause ground level ozone concentrations to reach peak values of 130 ppb in the mid-afternoon. Maximum ozone concentration at the ground may be indicative of the degree of vertical mixing which contributes significantly to the ground-level ozone concentration. In late afternoon, ozone production decreases with diminishing intensity of sunlight. At sunset, the ground level ozone concentration decreases to about half of the afternoon maximum value (70 ppb). As a Nocturnal Boundary Layer (NBL) begins to form in the evening, the ground level ozone concentrations near the surface continue to fall due to ozone destruction by non-photochemical reactions and ground scavenging. After sunrise, the cycle begins again as the mixing height begins to increase as the surface is heated and the nocturnal inversion is destroyed.

Although the diurnal pattern at the surface is obvious, it is less pronounced with increasing height and almost insignificant at the highest elevation site of 1754 m. Figure 4-1 shows that the amplitudes of the diurnal profiles at elevated levels were much less than those at ground level. The ozone above the surface-based inversion is effectively cut off from a sink due to the formation of the NBL. The ozone concentrations at elevated levels above the NBL are not subjected to surface scavenging, so ozone levels at these elevations remained relatively high throughout the nighttime period.

4.1.2 Frequency Distributions of Daily Maximum One-Hour Ground-Level Concentrations

Figures 4-2 (A) and (B) provide information regarding the frequency distributions of the hour of day when the maximum ground level one-hour ozone concentration occurred in the North Carolina and East Tennessee during the 1995 to 1998 ozone seasons for the NC and TN monitoring sites, respectively. As expected, most of the maximum ozone concentrations occurred during the period between noon and 4:00 p.m. For the NC data, this period accounted for 87.7%, 86.6%, 82.9%, and 86.4% in 1995, 1996, 1997, and 1998, respectively. The maximum ground level ozone concentration occurred more frequently at 3:00 p.m. (23.8%), 2:00 p.m. (23.2%), 3:00 (23.5%), and 3:00 p.m. (28.8%) than any other hour of day, in 1995, 1996, 1997, and 1998, respectively. For the TN data, the noon to 4:00 p.m. period accounted for 82.3%, 84.1%, 80%, and 83.1%, in 1995, 1996, 1997, and 1998, respectively. The ground level maximum ozone concentration occurred more frequently at 3:00 p.m. (23.4%), 3:00 p.m. (25.4%), 4:00 p.m. (21.9%), and 4:00 p.m. (25.8%) than any other hour of day, in 1995, 1996, 1997 and 1998, respectively. As shown in Figures 4-2 (A) and (B), the frequency analyses of occurrence of ground level daily maximum ozone concentrations observed at the TN monitoring sites showed a similarity to those of the NC monitoring sites for four years from 1995 through 1998. Interestingly, the maximum ground level ozone concentration occurred occasionally at unexpected time periods (for example, 1:00 EST, 2:00 EST). This could be explained by the occurrence of unexpected vertical mixing or an air mass moving into the area from outside of the region.

4.1.3 Relationship between Ground Level Hourly Ozone Concentrations and High Elevation Hourly Ozone Concentrations

Prior to developing a model to predict high elevation ozone concentrations based on ground level ozone concentrations, the relationship between ground level hourly ozone concentrations and high elevation hourly ozone concentrations was investigated. As mentioned in Chapter 1, CALPUFF and other similar air quality models have the capability of utilizing ground level hourly ozone concentrations as input in calculating the transformation rates of SO_2 and NOx to sulfates and nitrates, respectively. The chemical transformation scheme (called the MESOPUFF II scheme) in CALPUFF is initiated as soon as a puff is released from an emission source. The puff picks up the ground level ozone concentration as representative of the mixing layer through which a plume is traveling because the scheme was developed under the assumption that the ground level ozone concentration is fully mixed through an entire vertical layer during daytime (Scire, 1999). However, it has been reported (Reiter et al, 1987; Ryan, 1998; Trotter, 1998) that mean ozone concentrations vary with elevation. Dispersion models such as CALPUFF, which requires ozone concentrations as a required input, could underestimate or overestimate the amount of wet and dry acid deposition in the case that ground level ozone concentration is not constant throughout the ABL.

The "Present Day's Ground Level Concentration" method (the do-nothing approach) is the approach in which it is assumed that the ground level ozone concentration is an adequate measure of ozone throughout the ABL. Thus an analysis was conducted to determine the correlation between the ground level ozone concentrations and the high elevation ozone concentrations measured at the NC and TN monitoring sites.

Figure 4-3 shows scatter plots with linear least squares' fits to illustrate the relationship between the ozone concentrations at the six elevations and the corresponding ground level ozone concentrations at the NC and TN sites, using 1998 ozone data.

The figure shows the distinctly different scatter plots in the lower elevation NC ozone data and the higher elevation TN ozone data. The first two graphs in Figure 4-3 show that most of the data obtained at elevations of 76 m and 128 m lie on the diagonal curve, indicating that the elevated concentrations are essentially the same as the ground level concentrations. The remaining data that lie above the diagonal indicate that the ground level concentration is less than the corresponding ozone concentration at the higher elevation. This is due to the fact that ozone concentrations at these elevations are well mixed with the ozone at the ground during the daytime hours due to strong turbulent convection, particularly in mid-afternoon. At night however, the ground level ozone undergoes depletion due to the non-photochemical reaction with NO and NO_2 in the following reactions:

$$O_3 + NO \longrightarrow NO_2 + O_2$$

$$NO_2 + O_3 \longrightarrow NO_3 + O_2$$

and possibly with surfaces near the ground, whereas the ozone aloft is not depleted at the same rate thus remaining higher aloft. This effect becomes more pronounced at in the graph for 433m where an even greater number of the values are greater than the ground level values. This higher elevation is above the nocturnal mixing height and thus is less affected by the depletion that occurs at ground level. The Tennessee data, shown in the later three graphs in Figure 4-3, are all at higher elevations than the NC data and show a

further spreading of the data points about the diagonal line. While the data exhibit behavior that is similar to the NC data, a number of data points also lie below the diagonal line, indicating an increasing number of data points in which the ozone concentration at the ground is actually greater than the ozone concentration aloft. This is a clear indication that ozone formation at the ground does not mix completely with the ozone aloft at the higher elevations (526-1754 meters) in an instantaneous manner. The last graph (1754 m elevation data) clearly indicates a lack of ozone concentrations less than 30 ppb at the aloft site, probably a result of the lack of the presence of ozone depletion at the higher elevation and the lack of influence of ground level interaction. This is further supported by the observation that the minimum concentration observed at the elevated sites gradually shifts from near zero ppb at 76m to 30 ppb at the 1754 m site in a progressive way.

As expected, correlation between the ground and relatively low elevation ozone concentrations (76 m, 128 m elevation sites) are relatively good (r^2 = 0.62 and 0.52, respectively). On the contrary, relationships between the ground and upper levels (433 m, 526 m, 976 m, 1754 m elevation sites) progressively become weaker with increasing elevation. The linear regression analysis yielded r^2 values of 0.62, 0.52, 0.27, 0.13, 0.08, and 0.02 for the relationships between ground level and 76 m, 128 m, 433 m, 526 m, 976 m, and 1754 m high elevation sites, respectively. As shown in Figure 4-4, the r^2 value of the relationship between ground level ozone data and all six different elevation sites' ozone data is only 0.19.

The results illustrate that it is not reasonable to use ground level ozone concentrations to be representative of high elevation ozone concentration in the ABL

through which a plume is traveling, particularly in those cases where long-range transport is occurring and the plume from a source has been dispersed throughout the boundary layer. The "Present Day's Ground Level Concentration" relationship with r^2 of only 0.19 forms the baseline for comparison with the more refined methods ("Prediction based on Present Day's Maximum," "Prediction based on Previous Day's Maximum," "Prediction based on Present Day's Hourly," and "Prediction based on Cloud Cover/Present Day's Maximum"). The objective is to develop a more refined algorithm that would allow prediction of the ozone throughout the boundary layer with the input being the ground level hourly ozone concentrations for an area.

4.2 Comparison of Relative Performance of Methods Used to Develop Overall Regression Model

As mentioned in Chapter 3.3, the "Prediction based on Present Day's Maximum" method is to explore a predictable relationship between a current day's ground-level maximum one-hour ozone concentrations (independent variable) and the current day's high elevation hourly ozone concentrations (dependent variable). The "Prediction based on Previous Day's Maximum" method is to find a predictable relationship between the previous day's ground-level maximum one-hour ozone concentrations (independent variable) and the current day's high elevation hourly ozone concentrations (dependent variable). The "Prediction based on Present Day's Hourly" method is to find a predictable relationship between a current day's ground-level hourly ozone concentrations (independent variable) and the current day's high elevation hourly ozone concentrations (dependent variable).

The first task in developing an algorithm to predict high elevation ozone concentrations based on ground level ozone observations is to determine which method better represents relationships between high elevation ozone data and ground level ozone data. As discussed in Chapter 3.4, each method resulted in the development of 144 linear equations (one for each hour of day for each of the six elevations). This methodology was chosen because it enables the methods to compensate for the difference in meteorological data throughout the day and the variation in the strength of solar radiation that influences the thermal distribution that affects vertical mixing.

For comparison of the three methods ("Prediction based on Present Day's Maximum," "Prediction based on Previous Day's Maximum," and "Prediction based on Present Day's Hourly"), regressions to represent linear relationships between high elevation ozone concentrations and ground level ozone concentrations of each method were run on the ORIGIN6.1 software package. The results produced by the linear regression analysis for the "Prediction based on Present Day's Maximum" method are shown in Figure 4-5 for the 76 m monitoring site. The results for the other methods and for the other elevation sites are shown in Appendix C. The relative performance of these methods was compared in terms of statistical results produced by the linear regression, to select the method ("Prediction based on Present Day's Maximum," "Prediction based on Previous Day's Maximum," and "Prediction based on Present Day's Hourly") that would be used to develop a final regression model which would include the effect of elevation on ozone concentrations, based on ground level ozone observations.

In terms of r^2, as shown in Figures 4-6 to 4-8, the linear relationships yielded by these three methods exhibited pronounced variations in performance over the time of day

for all high elevation sites. For low elevation sites (76 m, 128 m, and 433 m), the "Prediction based on Present Day's Maximum" and "Prediction based on Present Day's Hourly" methods showed relatively low r^2 values in the early morning followed by a sharp increase in r^2 near sunrise. The r^2 values remained high during the daylight hours and decrease in late afternoon. The "Prediction based on Previous Day's Maximum" method at these same elevations showed relatively poor r^2 values throughout the entire day. For high-elevated sites (526 m, 976 m, 1754 m), the "Prediction based on Present Day's Maximum" method significantly outperformed the other methods during most of the day with r^2 values typically in the 0.55 – 0.65 range.

Figures 4-9 to 4-11 show that there is a clear ranking of the three methods, in terms of residuals between high elevation ozone concentrations and ground level ozone concentrations, with the linear regression. For most times of day in the six different high elevation sites, the residuals produced by the "Prediction based on Present Day's Maximum," "Prediction based on Previous Day's Maximum" methods were significantly less than those of the "Prediction based on Present Day's Hourly" method. However, the comparison of the "Prediction based on Present Day's Maximum" and "Prediction based on Previous Day's Maximum" methods was not clearly distinguishable.

As shown in Figure 4-12, the MBE values of the "Prediction based on Present Day's Maximum" and "Prediction based on Previous Day's Maximum" methods were not clearly distinguishable, however, both had much smaller MBE values than the "Prediction based on Present Day's Hourly" method. The "Prediction based on Present Day's Maximum" and "Prediction based on Previous Day's Maximum" methods exhibited little variability over the time of day for the six different high elevation sites. In

contrast, the "Prediction based on Present Day's Hourly" method produced large MBE values. In other words, the "Prediction based on Present Day's Hourly" method showed a poor relationship. Both MAE and RMSE are proportional to the absolute values of ground level ozone concentrations and high elevation ozone concentrations. MAE shown in Figure 4-13 paralleled the behavior of RMSE. As shown in Figures 4-13 and 4-14, the results of MAE and RMSE demonstrated that the "Prediction based on Present Day's Maximum" method generally outperformed the other two methods for the six different elevation sites.

Indices of agreement (d_1) exhibited similar results over the time of day for the six different elevation sites as shown in Figure 4-15. Comparing the performance of the three methods in terms of d_1 indicated that there is much less variability in the performance for the "Prediction based on Present Day's Maximum" method ($0.43 <= d_1 <= 0.88$) than for the "Prediction based on Previous Day's Maximum" method ($0.36 <= d_1 <= 0.66$) and the "Prediction based on Present Day's Hourly" method ($0.20 <= d_1 <= 0.92$). The index of agreement indicated that the "Prediction based on Present Day's Maximum" method performs best. Tables 4-1 to 4-3 provide information regarding the statistical results in detail.

Figure 4-16 shows scatter plots of predicted versus observed concentrations for the ground level and all six high elevation ozone data for each method for the 1998 data set for NC and TN data. Comparisons of the statistical results for the data shown in Figure 4-17 and Table 4-4 provide insight into the behavior of these methods. According to the statistical results shown in Table 4-4, the "Prediction based on Present Day's Maximum" method performed better than the "Prediction based on Previous Day's

Maximum" method that in turn was better than the "Prediction based on Present Day's Hourly" method, with r^2 of 0.59, 0.33, and 0.26 respectively. All these methods were an improvement over the do-nothing approach where r^2 was only 0.19.

4.3 Vertical Ozone Profile Predicted by the Overall Regression Model

As showed in Table 4-5, the "Prediction based on Present Day's Maximum" method yielded 192 linear best-fit gradients, $m_{h,z}$, for each hour of day and the six different elevation sites and two ground level sites (NC and TN). The scatter plots were applied for data of elevation (Z, independent variable) and the linear best-fit gradient ($m_{h,z}$, dependent variable) for each hour of day in Figure 4-18. A number of nonlinear equations were evaluated in an effort to find suitable relationships to describe elevation, Z, versus the linear best-fit gradient, $m_{h,z}$, for each hour of day. As shown in Table 4-6, two nonlinear equations and a constant value were found to be adequate to describe the 24 relationships for each hour of day as follow:

For hours 0:00 – 9:00 EST and 18:00 – 23:00 EST

$$m_{h(p)} = A(1-e^{-B(Z-C)}) \qquad \text{(Equation 4-1a)}$$

For hours 11:00 – 17:00 EST

$$m_{h(p)} = (a+be^{-cZ}) \qquad \text{(Equation 4-1b)}$$

For 10:00 EST

$$m_{h(p)} = D \qquad \text{(Equation 4-1c)}$$

Here Z is the elevation in meters ranging from 0 to 1800 meters; A, B, C, a, b, and c are coefficients determined to yield the best fit for each equation; and D is a constant. Having

determined the equations describing m_h as a function of elevation Z, the concentration (C_h) at any elevation Z can then be determined using the appropriate equations to be

$$C_{h(p)} = m_{h(p)}C_{MAX\text{-}G,\ current\ day} \qquad \text{(Equation 4-2)}$$

Substituting Equations 4-1a, 4-1b, and 4-1c into Equation 4-2, then the set of equations is

For hours 0:00 – 9:00 EST and 18:00 – 23:00 EST

$$C_{h(p)} = \{A(1-e^{-B(Z-C)})\}C_{MAX\text{-}G,\ current\ day} \qquad \text{(Equation 4-3a)}$$

For hours 11:00 – 17:00 EST

$$C_{h(p)} = \{(a+be^{-cZ})\}C_{MAX\text{-}G,\ current\ day} \qquad \text{(Equation 4-3b)}$$

For 10:00 EST

$$C_{h(p)} = \{D\}C_{MAX\text{-}G,\ current\ day} \qquad \text{(Equation 4-3c)}$$

Note that $C_{MAX\text{-}G}$ refers to ground-level maximum ozone concentration.

As shown in Figure 4-18, ground level ozone concentrations in the early morning remain quite low until a stable nocturnal inversion breaks up in the late morning due to surface heating. The early morning profiles indicated the presence of a surface-based inversion that is approximately 150 - 350 meters in depth by 7:00 EST. As the nocturnal surface inversion layer began to break up around 8:00 EST, the mixing height began to rise. The ground level ozone concentration continuously rose from around 8:00 EST until it reached its peak around 13:00 – 16:00 EST hours. This is because the ozone concentrations at ground level began to rise as the ozone mass from aloft was entrained in the atmospheric mixing and ozone began to form photochemically near the ground. The

10:00 EST profile is indicative of thorough mixing with a mixing height of at least 1800 m. Ground level ozone continued to increase until 16:00 EST and then began to drop. The ground level ozone concentration actually exceeded the concentration aloft by approximately 15 - 25% in the mid-afternoon from 12:00 to 16:00 EST, presumably due to the strong photochemical formation near the ground that was being mixed upward. The later evening profiles, 21:00 EST, reflected the continual development and growth of the nocturnal inversion (Güsten et al., 1998).

Figure 4-18 shows the vertical ozone profiles to vary over a pattern with ozone depletion at night and ozone formation in the mid-afternoon. This pattern probably resulted from daytime photochemical production or downward transport of ozone-rich air from above, combined with ozone loss by dry deposition and reaction with nitric oxide (NO) at night. Attempting to gain a quantitative understanding of the depletion and photochemical ozone formation based on the vertical ozone profiles predicted by the overall regression model, it was found that ozone levels decrease and increase more quickly at lower altitudes than at upper altitudes, suggesting the presence of enhanced ozone depletion and formation processes near the surface.

One of the interesting observations is that on the contrary to a pronounced fluctuation of ground level ozone concentrations, high elevation ozone concentrations were comparatively uniform with average values that are between 75 – 85% of the maximum ground level concentration. As shown in Figure 4-18, the mixing height, above which the ozone concentrations appeared to be homogeneous, varied in range from roughly 130 m to 1000 m depending on the time of day. In the late evening, the homogeneous ozone layer aloft occurred at a shallow ABL (approximately 130 m above

ground level) due to the formation of a stable nocturnal inversion near to ground. The deep homogeneous ozone layer sustained until sunrise because the vertical mixing was not sufficient to penetrate the nocturnal residual layer (NRL) created overnight. After sunrise around 8:00 EST, a significant down mixing of ozone occurred from the NRL due to vertical mixing. Thus, a relatively homogeneous ozone layer was created up to 1800 m from the ground by around 10:00 EST. The result showed a strong similarities to those found in many researchers (Güsten et al., 1998;Mckendry et al., 1997;Myrick et al., 1994). The homogeneous ozone layer typically extends up to 4000 m in the lower troposphere, although the measurements in this study only went to approximately 1800 m (Fast et al., 2000).

It is also interesting to note that while the ozone concentration is fairly homogeneous at 10:00 EST, it is only about 75% of the daily maximum concentration (i.e., $m_{h,z} \cong 0.70 – 0.80$). As the day progressed, the concentration at the ground exceeded the ozone aloft (as shown in Figure 4-18 at 12:00 – 16:00) such that by the time the ground level concentration reached a maximum (i.e., $m_{h,z} \cong 1.0$), the ozone aloft was only about 70 – 80 % of the maximum. This suggests strongly that the rate of ozone formation at the ground is large and that it does not instantaneously mix to the higher elevations (i.e., 1000 – 1800 m).

The other interesting thing is that ozone concentration continuously decreased even after sunset as shown in Figure 4-18. The probable explanation is that when photochemical ozone production ceases because of the absence of sunlight and vertical transport of ozone mass aloft is inhibited by an inversion of the normal temperature profile at night, ozone loss occurs in non-photochemical reactions with nitric oxide (NO)

and nitrogen dioxide (NO_2) in the following reactions (Finlayson-Pitts and Pitts, 1986;Nicholson et al., 2001;Seinfeld and Pandis, 1997;Wayne, 1985):

$$O_3 + NO \longrightarrow NO_2 + O_2$$

$$NO_2 + O_3 \longrightarrow NO_3 + O_2$$

4.4 Comparison and Evaluation of Overall Regression Model

4.4.1 Comparison of Observations and Predictions

After developing the overall regression model, ozone concentrations predicted by the model were compared with ozone observations in each hour of day for different elevations. The samples of the comparisons for the 76 m, 128 m, 433m, 526m, 976m, and 1754m elevation sites are shown in Figures 4-19 to 4-24, respectively. The predictive model reproduced the observed day-to-day variation well. Even though the model failed to predict consistently the extreme values of minimum and maximum, the model is likely to work well to catch the observation values. The reason that the model did not pick up extreme values is the regression models produce a best-fit or "average" prediction for a specified set of inputs, whereas observation data containing the extremes of the data distribution are taken at a particular meteorological condition which happened in each hour of day.

Interestingly, day-to-day ozone variations at 1:00 EST and 5:00 EST in the morning in Figure 4-19 show that there were peak values reaching up to 70 – 100 ppb. This is surprising since ozone destruction typically occurs in those time periods due to

non-photochemical reaction with nitric oxide (NO) and nitrogen dioxide (NO_2). However, it is probable that variations in the mixing height occurred unpredictably due to high temperature or unstable weather for the time period. Ozone transport from aloft might have caused the peak values. Such unexpected extreme ozone concentrations might make the comparison of the performances of the model against ozone observations worse. As clearly seen in Figures 4-20 to 4-24, there were generally good agreements between modeled and measured values for other elevation sites (128 m, 433 m, 526 m, 976 m, and 1754 m).

4.4.2 Statistical Results for the Evaluation of the Overall Regression Model

4.4.2.1 Mean Diurnal Variations - Estimates of Central Tendency (Means)

The first task in an evaluation of the results predicted by the overall regression model was to establish whether mean concentrations predicted in each hour of day agree well with observations. A scatter plot is a good tool in the attempt to solve this first task. Scatter plots can readily expose some tendencies: overestimating of the results, underestimating the results, significant deviations, etc. On the other hand, the scatter plots of mean predictions and observations do not say anything about the ability of the model to follow variations of the concentrations over the time of day. Therefore the scatter plots alone are not sufficient to describe the performance of the model, and more comparisons with measurements will be presented in the following section.

Estimates of means were calculated from observed and predicted data. Scatter plots, comparing the mean ozone concentrations predicted by the model in each hour of day for the full ozone season of 1998 with the corresponding observations, were

presented in Figure 4-25. The results shown in Figure 4-25 indicated that the mean values (on a full ozone season basis) of the high elevation ozone concentrations predicted by the model are close to the corresponding mean values of observations.

Figure 4-26 shows that the predicted mean values, which exactly match the observed mean values, fell on a straight line with an intercept (*a*) of 0.0 and slope (*b*) of 1.0. Thus, in addition to the graphical information on variability and range provided by a scatter plot, *b* quantifies useful information on systematic (linear) over-or-under-prediction by models (Robeson and Steyn, 1990;Willmott, 1981). Values of *b* ranged from 1.06 (at 11:00 EST for 526 m high elevation) to 0.80 (at 6:00 EST for 128 m high elevation). The model seems to work well in spite of a little variability of the central tendency.

Standard deviations were also calculated for the observed and predicted data. The standard deviation gives an indication of the spread of data distribution about the mean. Figures 4-27 and 4-28 provide column plots to visualize the residuals of the standard deviation of observations and predictions. The differences in the model performance are easily discernible over the time of day. The positive and negative values reflect the inability of the model to accurately reproduce the original variability in the data. The positive values mean the standard deviation of predictions is smaller than that of observations. As mentioned earlier, this is because an empirically derived model such as the overall regression model produces an average prediction for a specified data set, whereas observation data contain the full range of data including extreme outliners. Nonetheless, better models will more closely approximate the original variability.

As expected, the times of early morning and late evening had higher residual values and higher variability and likewise the times of mid-afternoon had lower residual values and lower variability. The residual absolute values ranged from 0.01 ppb (at 14:00 EST of 433 m elevation site) to 6.15 ppb (at 7:00 EST of 128 m elevation site).

4.4.2.2 Error Indices, Coefficient of Determination (r^2), and Index of Agreement (d_1)

The next task is to estimate error of the model in each hour of day for the different elevation sites. Figure 4-29 present a statistical assessment of the overall regression model for MAE that is simply the average absolute value of all deviations. MAE is not sensitive to outliers. The MAE ranged from 4.78 ppb (at 14:00 EST for 76 m elevation site) to 13.87 ppb (at 0:00 EST for 128 m elevation site). The values were smaller in mid-afternoon at the relatively low elevation sites (76 m, 128 m, 433 m) than in the early morning and late evening of the high elevation sites (526 m, 976 m, 1754 m).

MBE indicates the degree that predicted concentrations are over or underestimated. As shown in Figures 4-30 and 4-31, the values of the model repeatedly underestimated high elevation ozone concentrations of all the elevated sites except for 526 m elevation site slightly overpredicted. The underpredicted error ranged from 0.05 ppb (at 21:00 EST for 76 m elevation site) to 7.45 ppb (17:00 EST for 128 m elevation site); on the other hand, the overpredicted error was in the range between 1.50 ppb (0:00 EST) and 6.63 ppb (10:00 EST) for 526 m elevation site. This is because the ability of the overall regression model to capture the variance of ozone concentration differed markedly due to the varying statistical association between ground level daily maximum ozone concentrations and high elevation hourly ozone concentrations in each hour of day.

Both MAE (Figure 4-29) and RMSE (Figure 4-32) are proportional to the absolute values of the residuals of the observed and predicted ozone concentrations. RMSE is widely used and is more amenable to additional statistical analyses because MAE is not sensitive to outliers (Fox, 1981;Willmott, 1982). The results for RMSE followed a remarkably similar pattern to MAE, but with slightly higher values because of the outlier sensitivity. In general, the most accurate predictions were achieved in mid-afternoon from 13:00 EST to 16:00 EST of the relatively low elevation sites (76 m, 128 m, and 433 m) and there was a progressive decrease in accuracy to the early morning and late afternoon of the high elevation sites (526 m, 976 m, and 1754 m).

Although the coefficient of determination (r^2) does not give enough indication of model accuracy, they are commonly reported. This is because it indicates how much of the variability in the observed data is being reproduced by the model. The extent of agreement was further illustrated by r^2 and d_1. Figure 4-33 shows that the model exhibited similar levels of performance over the time of day for the relatively low elevation sites (76 m, 128 m, and 433 m) in terms of r^2. For example, in the 76 m elevation site, the r^2 value slowly decreased from midnight and then dropped to the minimum (0.14) at 6:00 EST. It began to increase and reached the maximum (0.90) at 15:00 EST. It again continuously decreased after 15:00 EST.

Interpretation of the correlation-based measures is straightforward; that is, the coefficient of determination (r^2) of the maximum (0.90) indicates that the model explains 90% of the variability in the observed data. The r^2 values for the 128 m and 433 m high elevation sites ranged from 0.25 (6:00 EST) to 0.90 (15:00 EST) and from 0.31 (3:00 EST) to 0.85 (15:00 EST), respectively. Contrary to the low elevation sites, the r^2 values

of the relatively high elevation sites were consistent over the time of day. The values ranged from 0.36 (9:00 EST) to 0.52 (19:00 EST), 0.45 (0:00 EST) to 0.59 (22:00 EST), and 0.33 (16:00 EST) to 0.46 (3:00 EST), for 526 m, 976 m, and 1754 m elevation sites, respectively.

A more useful measure of model performance is provided by the index of agreement value (Willmott, 1982). The indices of agreement shown in Figure 4-34 demonstrated similar results to those of r^2, indicating that the model performed best in the mid-afternoon from 13:00 EST to 16:00 EST and worst for the early morning of the relatively low elevation sites (76 m, 128 m, and 433 m). The indices of agreement had peak values of approximately 0.86 during mid-afternoon indicating that the overall predicted ozone concentrations were in good agreement with observations although the predicted data variability was somewhat smaller or larger than the observations. All statistical results are presented in Table 4-7 in detail. As shown in Figure 4-35, the performance of the model was compared separately for all high elevation sites. With respect to the r^2 values, the comparison summarizes that the model worked better in the relatively low elevation sites than at the high elevation sites.

4.4.3 Overall Regression Model's Performance for Other Years of Ozone Data

As mentioned in Chapter 2.3.2, meteorological conditions influence ozone concentrations. One of the assumptions in this study is that certain meteorological conditions are characteristic of season and day and night time and are recurrent phenomena from year to year. Thus, the model developed with 1998 ozone data was applied and tested to three other years of ground-level ozone data (1995, 1996, and 1997)

collected at the NC and TN sites to see how well these would be simulated. For comparison of the statistical results of the model performance, a linear regression method was applied for scatterplots of predicted and observed ozone concentrations for 1995 – 1998 as shown in Figure 4-36. The r^2 values produced by the linear regression method were 0.45, 0.50, 0.48, and 0.56 for 1995, 1996, 1997, and 1998 ozone data, respectively. The r^2 values for the first three years were slightly smaller than that for 1998, since the model was based on 1998 data.

The performance of the model was statistically evaluated for the full ozone season data for each year. MBE values shown in Figure 4-37 illustrate that the model generally underpredicted the observed data for other years. The extent of the underprediction varied from 1.78 ppb to 4.62 ppb for the other year. Comparing the performance of each year in terms of errors ($9.62 \leq$ MAE (ppb) ≤ 10.93, $12.39 \leq$ RMSE (ppb) ≤ 13.98)) also indicated that the model performed at a slightly lower level of accuracy. Table 4-8 illustrates comparison of relative performance of four-year data from 1995 to 1998 in terms of the statistical results produced by the overall regression model.

4.5 The "Overall" Regression Model versus the "Clear," "Cloudy," "Clear to Partly Cloudy" Component Regression Models

In an effort to improve the performance of the overall regression model, component models using only "clear," "cloudy," or "clear to partly cloudy" days were developed. If any of these component models yielded a significant improvement in model performance, then a more complex model would be developed incorporating cloud cover as an additional parameter. Figure 4-38 provides information regarding how many days

fell in “clear,” “cloudy,” and “clear to partly cloudy” categories, respectively. The figure demonstrates that the frequency of cloud cover was very different at the North Carolina and Tennessee sites used in this study. Based on data that fell in each category, an attempt to develop an algorithm to predict high elevation ozone concentration by hour of day was made for three cases (clear, cloudy, and clear to partly cloudy days) separately with the same method (“Prediction based on Present Day’s Maximum” method) as the overall regression model was developed.

The first step to develop the “clear” component regression model was that linear relationships were found between a current day’s ground-level maximum one-hour ozone concentrations (independent variable) and the current day’s high elevation hourly ozone concentrations (dependent variable) for each hour of day using only the reduced ozone data that fell in the “clear” category. Table 4-9 provides information regarding the linear best-fit gradients ($m_{h,z}$) yielded by the linear relationships. Then the non-linear curve fit was, as shown in Figure 4-39, applied for the relationship between elevation (independent variables) and the linear best-fit gradient ($m_{h,z,}$ dependent variable) to develop the “clear” component regression model. The statistical parameters produced by the non-linear curve fits are shown in Table 4-10. The same method was applied for the development of the “cloudy” and “clear to partly cloudy” component regression models. The statistical results produced by the development of the “cloudy” and “clear to partly cloudy” component models are available in Tables 4-11 to 4-14 and Figures 4-40 and 4-42. The performances of each component regression model associated with cloud cover were compared to those of the overall regression model not considering cloud cover, to see if there was a significant improvement over the overall regression model.

Table 4-15 shows that the calculated standard deviation values of the ozone observations during the 1998 full ozone season from April through October were 18.92 ppb, 18.77 ppb, 18.13 ppb, and 18.92 ppb for the overall ozone data set, clear days, cloudy days, and clear to partly cloudy days, respectively. The corresponding values of the ozone predictions were 18.77 ppb, 19.80 ppb, 17.23 ppb, and 18.52 ppb for the overall regression model, the "clear," "cloudy," and "clear to partly cloudy" component regression models, respectively. From the comparison of the MBE values shown in Table 4-15, the overall regression model tends to underpredict by approximately 1.43 ppb on the average in the case for which cloud cover was not considered. On the other hand, the component regression models predicted the observed ozone concentrations well. The RMSE values were 13.48 ppb, 14.34 ppb, 11.51 ppb, and 12.37 ppb for the overall regression model, the "clear," "cloudy," and "clear to partly cloudy" component regression models, respectively. The regression models in the "cloudy" and "clear to partly cloudy" components yielded less prediction errors than the overall regression model by approximately 15% and 8% on the average, respectively. The statistical results in Figure 4-43 and Table 4-15 show that the "cloudy" and "clear to partly cloudy" component models had slightly higher agreement between the observed and predicted datasets (0.69 for the "cloudy" days and 0.69 for the "clear to partly cloudy" days, respectively) than the overall regression model that had an index of agreement of 0.66.

A factor, which probably produces greater error values, should be considered when the model is utilized. The factor is that in one of the assumptions in this study the ozone data observed at the ground level, and high elevation sites in East Tennessee and the ground level and elevated sites located directly above ground level at the Raleigh NC

site will be minimally affected by horizontal variations in ozone that might be caused by up-the-valley and down-the-valley flow that might occur in a valley/ridge type of environment. These types of occurrences might affect statistical parameters such as prediction errors, coefficient of correlation, and index of agreement between ozone observations and predictions. The reason is that a valley/ridge type of topographic feature causes a more vigorous vertical motion due to a mountain induced advection circulation than a less hilly region. So an ozone-mixing layer fluctuates possibly more significantly from day to day in the valley/ridge region than in the less hilly region. From such facts, it is possible that the TN ozone datasets have a larger variability than the representative ozone concentrations that would have existed at high elevation sites located directly above a surface site that is the case for the NC site. Therefore, when the model in this study predicts the high elevation ozone concentrations for the TN ozone monitoring stations, it probably produces greater error values (MAE, MBE, and RMSE), less correlation (r^2), and lower agreement (d_1) between observations and predictions.

It is important to note that the model may have limitations in its use. The model was developed based on data collected in areas where local ozone production is probably moderate (NC and TN). The model may not predict ozone concentrations in the vertical in areas where local ozone production is really high (i.e., Houston TX) or where local ozone production is really low (i.e., over a barren area out in the middle of nowhere). This is because ozone concentration is determined by ozone formation, depletion, and vertical transport. Vertical transport is related to atmospheric physical mechanisms (e.g., wind, vertical temperature structure, stability, and sunlight). Ozone formation and depletion may also be significantly influenced by nearby point sources, area sources, or

other local activities, since ozone formation depends on production of nitrogen oxides (NO_x) and Volatile Organic Compounds (VOCs).

4.6 The Role of Cloud Cover on Ozone Concentration

As mentioned in Chapter 4.3, the complexity of the relationship between ground level ozone concentrations and high elevation ozone concentrations varies, depending on atmospheric physical mechanisms (e.g. wind, vertical temperature structure, stability, and sunlight), ozone formation reactions, and ozone depletion reactions in the ABL. One meteorological parameter that can affect all of these is the amount of cloud cover. In an effort to further understand how the mechanisms are affected by cloud cover for each hour of day (6:00 a.m., 10:00 a.m., 3:00 p.m., 6:00 p.m., and 8:00 p.m.) at different elevations, the two cases of "clear" and "cloudy" days were investigated. The results of the corresponding vertical ozone profiles are shown in Figures 4-39 and 4-40. As shown in Figure 4-41, typical vertical temperature profiles and conditions of atmospheric stability are different in the "clear day" case and the "cloudy day" case.

At 6:00 a.m. in the clear day, a vertical mixing is not strong enough to break out of a nocturnal inversion layer formed at the previous day's nighttime. As shown in Figure 4-39, ozone depletion occurs in non-photochemical reactions with nitric oxide (NO) and nitrogen dioxide (NO_2) at a shallow atmospheric boundary layer where the nocturnal inversion occurs. Vertical transport of ozone mass aloft is inhibited by a stable stability due to the thermal inversion. The vertical ozone profile above the nocturnal boundary layer shows a relatively constant ozone concentration because of a neutral stability in Figure 4-39. Thus, the vertical ozone profile shows low ozone concentration at the

ground level with a shallow boundary layer and a constant ozone concentration above the boundary layer.

By 10:00 a.m. in the clear day, the stable atmospheric condition at the shallow boundary layer is changed to an unstable atmospheric condition because of strong solar radiation that breaks up the nocturnal inversion layer. Ozone from aloft is transported downward by a vigorous vertical mixing resulting from turbulent convection. At the same time, ozone formation begins to occur near the surface due to photochemical reactions. As a result, a fairly homogeneous ozone profile is created in the atmospheric boundary layer.

By 3:00 p.m. on the clear day, the additional ozone production was added to the fairly homogeneous ozone-mixing layer that was previously formed. So, the ground level ozone concentration is actually greater than the high elevation ozone concentration, as shown in Figure 4-39. In other words, the ozone concentration gradually decreases from ground level to the highest elevation (1800 m) even though strong vertical mixing is occurring at the time. This suggests that ozone production created at the ground level does not instantaneously mix to the highest elevation.

By 6:00 p.m. on the clear day, the ozone production at the ground slows and the ozone profile appears uniform due to the vertical mixing in the ABL. The diluted ozone is reached up to the highest elevation (1800 m). As a result, the ozone concentration at the highest elevation at 6:00 p.m. is slightly greater than that at 3:00 p.m. Even though there is a moderate vertical mixing to sustain the homogeneous ozone-mixing layer in the ABL, the earth's surface temperature begins to drop down. Photochemical ozone production ceases and a thermal inversion begins to form, which inhibits vertical

transport of ozone mass aloft. Thus, the ground level ozone concentration becomes lower than that in the upper levels. By 8:00 p.m. on the clear day, ozone transport from aloft is cut off and ozone depletion is gradually accelerated as night progresses due to a change of atmospheric stability from unstable to stable condition resulting from the development of the nocturnal thermal inversion.

At 6:00 a.m. on the cloudy day, unlike the clear day where the ozone concentration decreases sharply within the shallow atmospheric boundary layer, the cloudy day's profile shows a gradual decrease from the highest elevation to ground level. This is because that a more neutral atmospheric condition dominates on the cloudy day. There is also minimal ozone formation at the ground. A moderate degree of ozone transport from aloft occurs in the neutral condition as shown in Figure 4-41. Ozone depletion and transport from aloft occur simultaneously.

By 10:00 a.m. on the cloudy day, unlike the clear day which shows a fairly homogeneous ozone-mixing layer, the ground level ozone concentration on the cloudy day is still lower than that of the upper levels. Neither ozone formation or vertical mixing are vigorous enough to create a homogeneous ozone vertical layer.

By 3:00 p.m. on the cloudy day, unlike the clear day where the ground level ozone concentration is greater than the high elevation ozone concentration, a uniform vertical profile is established. On the cloudy days, the clouds reflect 50 – 80% of the sunlight and transmit most of the rest (Eagleman, 1980). The degree of the reflection depends on the thickness of cloud cover. The transmitted sunlight warms the earth's surface. Heat is transferred to the atmosphere from the earth's surface to the atmosphere. A moderate vertical mixing occurs in the ABL. There is little photochemical reaction at

ground level because of the reduced sunlight. This may explain why it takes approximately three hours longer to establish a fairly homogeneous ozone layer than on the clear day.

By 6:00 p.m. on the cloudy day, the vertical ozone profile is relatively homogeneous except for the boundary layer immediately adjacent to the ground. This is due to the depletion of ozone by non-photochemical reactions with NO and NO_2. Ozone transport from aloft is significantly decreased due to relatively weak vertical mixing resulting from the decreased sunlight. After 8:00 p.m. on the cloudy day, the shallow boundary layer undergoes further ozone depletion and some minor vertical ozone mixing occurs. The ozone near the ground is slowly depleted as night progresses.

As mentioned in Section 3.3.4, the two extreme component models of "clear" and "cloudy" day cases were developed to see if an improved model could be developed over the overall regression model. The extreme component models did not contain a complete ozone dataset since the "partly cloudy" days were excluded. Later, the "clear to partly cloudy" component model including "partly cloudy" days was developed. The vertical ozone profile on the "clear to partly cloudy" days shown in Figure 4-42 was very similar to that of the "clear" days shown in Figure 4-39. So the discussion here will focus on the "clear to partly cloudy" and "cloudy" data that comprise all of the days in the data set. As shown in Figure 4-42, ground level ozone concentrations on clear to partly cloudy nights were reduced to approximately 20 – 35 percent of the maximum ground level ozone concentration. As mentioned in Chapter 2.2, cooling during the night changes the stability of atmosphere from the unstable daytime condition to a stable condition because of the formation of the nocturnal thermal inversion established at a shallow ABL

approximately 130 m above ground level. The stable atmosphere has little to no vertical mixing in the boundary where the inversion occurs. The ozone trapped by the inversion has been depleted during the nighttime since it cannot be replenished by the ozone mass aloft. As the day progresses, the nocturnal inversion layer begins to break up about 8:00 EST. Ozone from aloft is transported downward by turbulent convection due to solar radiation and the ozone concentration begins to increase because of a vertical mixing as the atmosphere becomes more unstable. In addition, ozone formation begins to occur due to photochemical reactions.

However, the vertical mixing is not instantaneous as shown in Figure 4-42. This is probably because the primary source of heat energy of heating the atmosphere is from the earth's surface as solar energy is transferred to the atmosphere. The earth's surface warms the lower meters of the atmosphere by a form of energy transfer called conduction. As the convective boundary layer develops during daytime, a vertical mixing height gradually increases from the earth surface through turbulent convection in the ABL. The vertical mixing, however, is not instantaneous, which may explain why ozone concentrations observed in the low boundary layer near the ground were higher than those observed at high elevation.

On the other hand, the vertical profiles of the cloudy days and nights shown in Figure 4-40 were significantly different from those of the clear to partly cloudy days and nights shown in Figure 4-42. A larger quantity of ozone goes through depletion by dry deposition and reaction with nitric oxide (NO) in the cloudy night than the clear night. This is because the cloudy night is dominated by a neutral atmospheric condition where moderate vertical mixing occurs. Thus, ozone aloft is transported to the ground through

the vertical mixing on a cloudy night. Unlike the clear to partly cloudy days that demonstrated higher ozone concentrations at ground level than those at high elevation due to the strong ozone formation in the mid-afternoon, the cloudy days showed a fairly homogeneous ozone layer that was sustained from noon to 16:00 EST suggesting that minimal new ozone was being formed due to the decreased sunlight.

CHAPTER 5

SUMMARY AND CONCLUSIONS

The purpose of this study was to develop a model to predict high elevation ozone concentrations based on appropriate ground level ozone concentrations and cloud cover. To support the goal, three different methods ("Prediction based on Present Day's Maximum," "Prediction based on Previous Day's Maximum," and "Prediction based on Present Day's Hourly" methods) were investigated to identify a relationship between ground level and high elevation concentrations for each hour of the day. While previous researchers (Aneja et al., 2000) have suggested that a correlation between the previous day's maximum ozone concentrations and the following day's ozone concentrations might be utilized as a method to predict high elevation ozone concentrations ("Prediction based on Previous Day's Maximum" method), the "Prediction based on Present Day's Maximum" method was found to be the best approach to use for predicting the relationship between ground level ozone concentrations and high elevation ozone concentrations.

To improve the methodology, the best method was utilized to develop a regression model with ("clear," "cloudy," and "clear to partly cloudy" component models) and without (overall regression model) considering cloud cover to predict high elevation ozone concentrations based on ground level ozone concentrations for each hour of day as a function of elevation. Observed high elevation ozone concentrations were compared to the values predicted by the regression model that did not consider cloud cover that influences ozone concentration. The performance of the overall regression

model was evaluated in terms of statistical results such as the residual difference between observed and predicted concentration standard deviation (s_o-s_p), MAE, MBE, RMSE, coefficient of determination (r^2), and index of agreement (d_1). Component regression models were also developed for "clear," "clear to partly cloudy," and "cloudy" days in an effort to improve on the overall predictions with the anticipation that cloud cover would serve as a suitable surrogate for other meteorological parameters such as wind, vertical temperature structure, stability, and sunlight.

Based on the findings of this study, the overall regression model (RMSE = 13.48, $r^2 = 0.56$, and $d_1 = 0.66$) developed with 1998 ozone data provided an approach that estimates the high elevation ozone concentrations based on the maximum ground level ozone observations for any given hour of any given day in the absence of meteorological information. When the overall regression model was applied and tested to three other years of ground-level ozone data (1995, 1996, and 1997), the performance was slightly deteriorated in terms of r^2 (coefficient of determination) and d_1 (index of agreement): $r^2 = 0.45$ and $d_1 = 0.59$ for 1995, $r^2 = 0.50$ and $d_1 = 0.63$ for 1996, $r^2 = 0.48$ and $d_1 = 0.62$ for 1997.

In the comparison of the performance of the overall regression model and component regression models based on the statistical results shown in Figure 4-43, the "cloudy" (RMSE = 11.51 ppb and $d_1 = 0.69$) and "clear to partly cloudy" component regression models (RMSE = 12.37 ppb and $d_1 = 0.69$) performed better than the overall regression model (RMSE = 13.48 ppb and $d_1 = 0.66$) in terms of the prediction error and the extent of the agreement between the observed and predicted datasets. From the comparison of the statistical results of the overall regression model and component

regression models, the cloud cover dependence of the model performance was clearly connected with the sensitivity of ozone concentrations affected by meteorological conditions. The "clear to partly cloudy" and "cloudy" component regression models predicted the observed concentrations well while the overall regression model tended to underpredict the observed concentrations. Therefore it is recommended that the "cloudy" and "clear to partly cloudy" component regression models be used to provide estimates of upper level ozone concentrations for cloudy days and clear to partly cloudy days based on the input of the day's maximum ground level concentration and cloud cover data. In the absence of information regarding cloud cover, the overall regression model could be utilized to predict high elevation ozone concentrations based on the maximum ground level ozone concentrations.

In conclusion, all of the developed models provided better predictions of ozone concentrations at low elevation sites than for the high elevation sites. The "clear to partly cloudy" and "cloudy" component regression models associated with cloud cover provided improvement over the overall regression model not considering cloud cover. The comparison of the vertical ozone profiles predicted by the "clear" and "cloudy" component models further substantiate that cloud cover affects the ozone concentrations and the ozone vertical profile. The developed algorithms could be utilized for a variety of purposes: 1) as a means of estimating concentrations at higher elevations in complex terrain (in the absence of actual monitoring data), 2) as input to models such as the Urban Airshed Model (UAM) to provide a three dimensional ozone input when only ground-level ozone data were available, and 3) as a means of converting ground level ozone concentrations to representative average ozone concentrations throughout the mixing

layer through which a plume from an emission source travels, prior to running air quality models such as CALPUFF which requires ground level hourly ozone concentrations as an input in acid deposition calculations.

For future research, it is recommended that the models based on atmospheric physical mechanisms should be expanded to include more specific meteorological variables such as temperature, humidity, pressure, and mixing height as input data to the models to possibly provide improved prediction of high elevation ozone concentrations. It is also recommended that the algorithms be compared to vertical profile datasets that are representative of high and low ozone formation regions to determine their applicability in settings which are very different from those used in this study.

REFERENCES

LIST OF REFERENCES

Altshuller, A. P. (1986). The Role of Nitrogen-Oxides in Nonurban Ozone Formation in the Planetary Boundary-Layer over N America, W Europe and Adjacent Areas of Ocean. Atmospheric Environment. 20[2]: 245-268.

Aneja, Viney P., Arya, S. P., Li, Yongxian, Murray, George C. and Manuszak, Thomas L. (2000). Climatology of Diurnal Trends and Vertical Distribution of Ozone in the Atmospheric Boundary Layer in Urban North Carolina. Journal of the Air & Waste Management Association. 50: 54-64.

Berkowitz, Carl M., Fast, Jerome D. and Easter, Richard C. (2000). Boundary Layer Vertical Exchange Processes and the Mass Budget of Ozone: Observations and Model Results. Journal of Geophysical Research. 105[D11]: 14789-14805.

Berman, Stephen, Ku, Jia-Yeong, Zhang, Jian and Rao, Trivikrama. (1997). Uncertainties in Estimating the Mixing Depth - Comparing Three Mixing-Depth Models with Profiler Measurements. Atmospheric Environment. 31[18]: 3023-3039.

Beyrich, F., Gryning, S. E., Joffre, S., Rasmussen, A., Seibert, P. and Tercier, P. (1996). On the Determination of Mixing Height - A Review. Proceeding of the 4th Workshop on Harmonization within Atmospheric Dispersion Modeling for Regulatory Purposes, Oostende. 155-162.

Casado, Luis S., Rouhani, Shahrokh, Cardelino, Carlos A. and Ferrier, Adrian J. (1994). Geostatistical Analysis and Visualization of Hourly Ozone Data. Atmospheric Environment. 28[12]: 2105-2118.

Cole, Franklyn. W. (1980). Introduction to Meteorology. Third Edition. John Wiley and Sons. New York.

Comrie, Andrew C. (1997). Comparing Neural Networks and Regression Models for Ozone Forecasting. Journal of the Air & Waste Management Association. 47: 653-663.

Cooper, C. D. and Alley, F. C. (1994). Air Pollution Control: A Design Approach. Second Edition. Waveland Press, Inc.

Cox, W. and Chu, S. (1993). Meteorologically Adjusted Ozone Trends in Urban Areas: A probabilistic Approach. Atmospheric Environment. 27B: 425-434.

Cox, W. and Chu, S. (1996). Assessment of Interannual Ozone Variation in Urban Areas from a Climatological Perspective. Atmospheric Environment. 30: 2615-2625.

Eagleman, Joe. R. (1980). Meteorology: The Atmosphere in Action. D. Van Nostrand Company. New York, NY.

Fast, J. D., Doran, J. C., Shaw, W. J., Coulter, R. L. and Martin, T. J. (2000). The Evolution of the Boundary Layer and Its Effect on Air Chemistry in the Phoenix Area. Journal of Geophysical Research-Atmospheres. 105[D18]: 22833-22848.

Feister, U. and Balzer, K. (1991). Surface Ozone and Meteorological Predictors on a Subregional Scale. Atmospheric Environment. 25A: 1781-1790.

Finlayson-Pitts, B. J. and Pitts, J. N. (1986). Fundamentals of Atmospheric Chemistry: Fundamentals and Experimental Techniques. Wiley. New York.

Finlayson-Pitts, B. J. and Pitts, J. N. (1993). Atmospheric Chemistry of Tropospheric Ozone Formation: Scientific and Regulatory Implications. Journal of the Air & Waste Management Association. 43: 1091-1100.

Finlayson-Pitts, B. J. and Pitts, J. N. (1999). Chemistry of the Upper and Lower Atmosphere: Theory, Experiments, and Applications. Academic Press.

Fox, D. G. (1981). Judging Air Quality Model Performance: A Summary of the AMS Workshop on Dispersion Model Performance. Bulletin of the American Meteorological Society. 62: 599-609.

Gardner, M. W. and Dorling, S. R. (2000). Statistical Surface Ozone Models: an Improved Methodology to Account for Non-Linear Behaviour. Atmospheric Environment. 34: 21-34.

Güsten, H., Heinrich, G. and Sprung, D. (1998). Nocturnal Depletion of Ozone in the Upper Rhine Valley. Atmospheric Environment. 32[7]: 1195-1202.

Hanwell, James D. (1980). Atmospheric Processes. George Allen & Unwin. London.

Heck, W. W., Cure, W. W., Rawlings, J. O., Zaragoza, A. S., Heagle, H. E., Heggestad, R. J. and Kohut, L. W. (1984). Assessing Impacts of Ozone on Agricultural Crops II, Crop Yield Functions and Alternative Exposure Statistics. Journal of the Air Pollution Control Association. 34: 810-817.

Hogsett, W. E., Weber, J. E., Tingey, D. T., Herstrom, A. A., Lee, E. H. and Laurence, J. A. (1997). An Approach for Characterizing Tropospheric Ozone Risk to Forests. Environmental Management. 21: 105-120.

Holland, J. Z. (1953). A Meteorological Survey of the Oak Ridge Area. Final Report Covering the Period 1948-1952. ORO-99. Office of Technical Information Service. Department of Commerce. Washington, D.C.

Horvath, S. M. and Mckee, D. J. (1994). Acute and Chronic Health Effects of Ozone, in Tropospheric Ozone: Human Health and Agricultural Impacts. Edited by D. J. Mckee, A. F. Lewis. New York.

Hurley, Peter J., Blockley, Adrian and Rayner, Ken. (2001). Verification of a Prognostic Meteorological and Air Pollution Model for Year-Long Predictions in the Kwinana Industrial Region of Western Australia. Atmospheric Environment. 35[10]: 1871-1880.

Jacob, D. J., Heikes, B. G., Fan, S. M., Logan, J. A., Mauzerall, D. L., Bradshaw, J. D., Singh, H. B., Gregory, G. L., Talbot, R. W., Blake, D. R. and Sachse, G. W. (1996). Origin of Ozone and NOx in the Tropical Troposphere: A Photochemical Analysis of Aircraft Observations over the South Atlantic Basin. Journal of Geophysical Research-Atmospheres. 101[D19]: 24235-24250.

Kelly, N. A., Wolff, G. T. and Ferman, M. A. (1984). Sources and Sinks of Ozone in Rural Areas. Atmospheric Environment. 18[7]: 1251-1266.

Kolehmainen, M., Martikainen, H and uuskanen, J. (2001). Neural Networks and Periodic Components Used in Air Quality Forecasting. Atmospheric Environment. 35[5]: 815-825.

Kousa, Anu, Karppinen, Ari, Aarnio, Päivi and Koskentalo, Tarja. (2001). Statistical and Diagnostic Evaluation of a New-Generation Urban Dispersion Modeling System against an Extensive Dataset in the Helsinki Area. Atmospheric Environment. 35[27]: 4617-4628.

Kukkonen, Jaakko, Härkönen, Jari, Karppinen, Ari, Pohjola, Mia, Pietarila, Harri and Koskentalo, Tarja. (2001a). A Semi-Empirical Model for Urban PM_{10} Concentrations, and Its Evaluation against Data from an Urban Measurement Network. Atmospheric Environment. 35[26]: 4433-4442.

Kukkonen, Jaakko, Härkönen, Jari, Walden, Jari, Karppinen, Ari and Lusa, Kaisa. (2001b). Evaluation of the CAR-FMI Model against Measurements near a Major Road. Atmospheric Environment. 35[5]: 949-960.

Lefohn, Allen S., Foley, Janell K. and Shadwick, Douglas S. (1993). Changes in Diurnal Patterns Related to Changes in Ozone Levels. Journal of the Air & Waste Management Association. 43: 1472-1478.

Linacre, Edward and Geerts, Bart. (1997). Climates and Weather Explained. Routledge Inc. New York, NY.

Manahan, Stanley E. (2000). Environmental Chemistry. Seventh Edition. Lewis Publishers.

Maughan, R. A. (1979). Frequency of Potential Contribution by Major Sources to Ground-Level Concentrations of SO2 in the Forth-Valley, Scotland: An Application of Acoustic Sounding. Atmospheric Environment. 13: 1697-1706.

Mckendry, I. G., Steyn, D. G., Lundgren, J., Hoff, R. M., Strapp, W., Anlauf, K., Froude, F., Martin, J. B., Banta, R. M. and Olivier, L. D. (1997). Elevated Ozone Layers and Vertical Down-Mixing over the Lower Fraser Valley, BC. Atmospheric Environment. 31[14]: 2135-2146.

Mendoza-Dominguez, Alberto and Russell, Armistead G. (2001). Estimation of Emission Adjustments from the Application of Four-Dimensional Data Assimilation to Photochemical Air Quality Modeling. Atmospheric Environment. 35[16]: 2879-2894.

Myrick, R. H., Sakiyama, S. K., Angle, R. P. and Sandhu, H. S. (1994). Seasonal Mixing Heights and Inversions at Edmonton, Alberta. Atmospheric Environment. 28[4]: 723-729.

Nappo, C. J., Herwehe, J. T. and Thompson, A. M. (1989). Observations of Ozone Profiles in the Developing Convective Boundary Layer. In: Ozone in the Atmosphere, R.D. Bajkov and P. Fabian, eds. A. Deepak Publishing.

Neu, U., Kunzle, T. and Wanner, H. (1994). On the Relation between Ozone Storage in the Residual Layer and Daily Variation in Near-Surface Ozone Concentration - A Case Study. Boundary Layer Meteorology. 69: 221-247.

Nevers, Noel D. (1995). Air Pollution Control Engineering. McGraw Hill, Inc.

Nicholson, J. P., Weston, K. J. and Fowler, D. (2001). Modeling Horizontal and Vertical Concentration Profiles of Ozone and Oxides of Nitrogen within High-Latitude Urban Areas. Atmospheric Environment. 35[11]: 2009-2022.

NRC (National Research Council). (1991). Rethinking the Ozone Problem in Urban and Regional Air Pollution. National Academy Press. Washington.

Oettl, Dietmar, Kukkonen, Jaakko, Almbauer, Raimund A., Sturm, Peter J., Pohjola, Mia and Härkönen. (2001). Evaluation of a Gaussian and a Lagrangian Model against a Roadside Data Set, with Emphasis on Low Wind Speed Conditions. Atmospheric Environment. 35[12]: 2123-2132.

Park, P. M., Smith, M. H. and Exton, H. J. (1990). The Effect of Mixing Height on Maritime Aerosol Concentrations over the North Atlantic Ocean. Quarterly Journal of the Royal Meteorological Society. 116: 461-476.

Pekour, M. S. and Kallistratova, M. A. (1993). Sodar Studies of the Boundary Layer over Moscow for Air Pollution Applications. Applied Physics. B57: 49-55.

Power, Helen C. (2001). Estimating Atmospheric Turbidity from Climate Data. Atmospheric Environment. 35[1]: 125-134.

Randerson, D. (1984). Atmospheric Science and Power Production. Technical Information Center, U.S. Dept. Energy, Washington, DC.

Reiter, R, Sladkovic, R and Kanter, H. J. (1987). Concentration of Trace Gases in the Lower Troposphere, Simultaneously Recorded at Neighboring Mountain Stations - Part II: Ozone. Meteorology and Atmospheric Physics. 37[1]: 27-47.

Robeson, S. M. and Steyn, D. G. (1990). Evaluation and Comparison of Statistical Forecast Models for Daily Maximum Ozone Concentrations. Atmospheric Environment. 24B: 303-312.

Ryan, W. F., Doddridge, B. G., Dickerson, R. R., Morales, R. M., Hallock, K. A., Roberts, P. T., Blumenthal, D. L. and Anderson, J. A. (1998). Pollutant Transport during a Regional O_3 Episode in the Mid- Atlantic States. Journal of the Air & Waste Management Association. 48[9]: 786-797.

Schlink, Uwe, Herbarth, Olf, Richter, Matthias, Rehwagen, Martina, Puliafito, Jose. L., Puliafito, Enrique, Puliafito, Carlos, Guerreiro, Pablo, Quéro, Jose. L. and Behler, Juan. C. (1999). Ozone-Monitoring in Mendoze, Argentina: Initial Results. Journal of the Air & Waste Management Association. 49: 82-87.

Scire, Joseph S., Strimaitis, David G. and Yamartino, Robert J. (1999). A User's Guide for the CALPUFF Dispersion Model (Version 5.0). Earth Tech, Inc. Concord, MA.

Seaman, Nelson L. (2000). Meteorological Modeling for Air-Quality Assessments. Atmospheric Environment. 34: 2231-2259.

Seaman, Nelson L. and Michelson, Sara A. (2000). Mesoscale Meteorological Structure of a High-Ozone Episode during the 1995 NARSTO-Northeast Study. Journal of Applied Meteorology. 39: 384-398.

Seinfeld, John H. and Pandis, Spyros N. (1997). Atmospheric Chemistry and Physics: From Air Pollution to Climate Change. A Wiley-Interscience publication. New York, NY.

Shaw, R. W. and Munn R.E. (1971). Introduction to the Scientific Study of Atmospheric Pollution (Edited by McCormax B. M). 53-96.

Shreffler, J. H. and Evans, R. B. (1982). The Surface Ozone Record from the Regional Air Pollution Study. Atmospheric Environment. 16: 1311-1321.

Slade, D. H. e. (1968). Meteorology and Atomic Energy 1968. Technical Information Center, U.S. Dept. Energy, Washington, DC.

Spellman, G. (2000). The Use of an Index-Based Regression Model for Precipitation Analysis on the Iberian Peninsula. Theoretical and Applied Climatology. 66: 229-239.

Stull, R. B. (1988). An Introduction to Boundary Layer Meteorology. Kluwer Academic Publishers. London.

Thompson, Mary L., Reynolds, Joel, Cox, Lawrence H., Guttorp, Peter and Sampson, Paul D. (2001). A Review of Statistical Methods for the Meteorological Adjustment of Tropospheric Ozone. Atmospheric Environment. 35[3]: 617-630.

Trotter, Mack S. (1998). Characterization of the Relationship of Mixing Height Development and Collapse to Surface-Level Ozone Concentrations. The University of Tennessee, Knoxville. Dissertation.

Trotter, Steven M., Pendergrass, William R., Davis, Wayne T. and Miller, Terry L. (1996). Measurement of Vertical Distribution of Ozone in Eastern Tennessee. Proceeding of the Journal of the Air & Waste Management Association.

Wark, K, Warner, C. F. and Davis, Wayne T. (1998). Air Pollution: Its Origin and Control. Addison Wesley Longman, Inc. Menlo Park, CA. Third Edition.

Wayne, R. P. (1985). Chemistry of Atmospheres. Clarendon Press. Oxford.

Willmott, C. J. (1981). On the Validation of Models. Physical Geography. 2: 184-194.

Willmott, C. J. (1982). Some Comments on the Evaluation of Model Performance. Bulletin of the American Meteorological Society. 63[11]: 1309-1313.

Willmott, C. J., Ackleson, S. G., Davis, R. E., Feddema, J. J., Klink, K. M., Legates, D. R., O'Donnell, J. and Rowe, C. M. (1985). Statistics for the Evaluation and Comparison of Models. Journal of Geophysical Research. 90[C5]: 8995-9005.

Wolff, G. T. and Lioy, P. J. (1978). An Empirical Model for Forecasting Maximum Daily Ozone Levels in the Northeastern United States. Atmospheric Environment. 11: 967-983.

Yap, D, Ning, D. T. and Dong, W. (1988). An Assessment of Source Contributions to the Ozone Concentrations in Southeastern Ontario 1979-1985. Atmospheric Environment. 22: 1161-1168.

APPENDICES

Appendix A

Tables Discussed in Body of Report

Table 2-1. Median and Frequency of Occurrence of Ground-Based Inversion Depth and Potential Temperature Gradient Adapted from Myrick et al., 1994

Time of day (MST)	Median GBI depth (m)	Median pot. Temp. gradient (°C/m)	Frequency of occurrence (%)
		Spring	
6:00	s	s	s
7:30	315	0.016	44
9:00	40	0.010	18
10:30	ni	ni	ni
12:00	54	0.017	8
13:30	43	0.012	7
15:00	54	0.011	10
		Summer	
6:00	414	0.021	70
7:30	63	0.010	16
9:00	18	0.010	3
10:30	ni	ni	ni
12:00	27	0.010	5
13:30	ni	ni	ni
15:00	s	s	s
		Fall	
6:00	s	s	s
7:30	414	0.026	88
9:00	414	0.019	57
10:30	229	0.013	13
12:00	49	0.014	10
13:30	83	0.012	27
15:00	67	0.011	16
		Winter	
6:00	s	s	s
7:30	s	s	s
9:00	414	0.030	71
10:30	381	0.032	47
12:00	373	0.028	47
13:30	365	0.018	29
15:00	315	0.021	54

MST – Mountain Standard Time
pot – potential
s – no sounding scheduled
ni – no inversion in small data set for this time

Table 2-2. Median and Frequency of Occurrence of Mixing Height
Adapted from Myrick et al., 1994

Time (MST)	Median (m)	Freq. of occ. (%)	Median (m)	Freq. of occ. (%)	Median (m)	Freq. of occ. (%)	Median (m)	Freq. of occ. (%)
	Spring		Summer		Fall		Winter	
6:00	s	s	72	30	s	s	s	s
7:30	216	56	128	84	153	12	s	s
9:00	315	82	414	97	108	43	282	29
10:30	706	100	513	100	216	87	167	53
12:00	659	92	683	95	381	90	162	53
13:30	706	93	686	100	398	73	216	71
15:00	769	90	s	s	579	84	222	46

occ – occurrence
s – no sounding scheduled

Table 3-1. Site Information of Stations for Ozone Data in North Carolina and East Tennessee

Site	County	Agency	Elevation (m)	Location	Land Use	Operational Dates
SPM, NC	Wake	DAQ	Ground Level	Suburban	Agricultural	05/16/95 - 10/02/95
						05/30/96 - 09/19/96
						05/15/97 - 10/31/97
						04/15/98 - 10/31/98
SPM, NC	Wake	DAQ	76	Suburban	Agricultural	05/24/96 - 09/19/96
						05/15/97 - 09/12/97
						05/08/98 - 09/30/98
SPM, NC	Wake	DAQ	128	Suburban	Agricultural	05/23/96 - 09/19/96
						05/15/97 - 09/12/97
						05/08/98 - 09/30/98
SPM, NC	Wake	DAQ	259	Suburban	Agricultural	05/16/95 - 10/02/95
SPM, NC	Wake	DAQ	433	Suburban	Agricultural	05/25/95 - 10/02/95
						05/17/96 - 09/19/96
						05/15/97 - 09/12/97
						05/28/98 - 09/30/98
Rutledge Pike Mascot, TN	Knox	KCAPC	Ground Level	Rural	Agriculture	04/01/95 - 10/31/98
Look Rock, TN	Blount	NPS	526	Rural	Forest	01/01/95 - 12/31/98[a]
Cove Mountain, TN	Sevier	NPS	976	Rural	Forest	03/01/95 - 12/31/95
						01/01/96 - 12/31/96
						01/01/97 - 12/31/97[a]
						02/01/98 - 12/31/98
Clingman's Dome, TN	Sevier	NPS	1754	Rural	Forest	04/01/95 - 10/31/95
						05/01/96 - 10/31/96
						04/01/97 - 10/31/97
						05/01/98 - 10/31/98

SPM = Special Purpose Monitoring
DAQ = Division of Air Quality in North Carolina state
KCAPC = Knox County Department of Air Pollution Control
NPS = National Park Service
a = November 1997 data missing

Table 4-1. Statistical Results of the Performance of "Prediction based on Present Day's Maximum" Method $m_{h,z}$ – linear best-fit gradient, 95% C.I. – standard error of $m_{h,z}$ at the 95% confidence interval, s_o and s_p – observed and predicted ozone concentration standard deviation (ppb), MAE – mean absolute error (ppb), MBE – mean bias error (ppb), RMSE – root mean squared error (ppb), r – correlation coefficient, r^2 – coefficient of determination, d_1 – index of agreement (α=1)

76M	0:00	1:00	2:00	3:00	4:00	5:00	6:00	7:00	8:00	9:00	10:00	11:00	12:00	13:00	14:00	15:00	16:00	17:00	18:00	19:00	20:00	21:00	22:00	23:00
$m_{h,z}$	0.63	0.59	0.56	0.53	-	0.47	0.42	0.41	0.48	0.62	0.76	0.85	0.91	0.94	0.96	0.98	0.97	0.94	0.91	0.87	0.82	0.77	0.73	0.68
95% C.I.	0.03	0.03	0.03	0.03	-	0.03	0.03	0.03	0.03	0.03	0.02	0.02	0.02	0.01	0.01	0.01	0.02	0.02	0.02	0.02	0.03	0.03	0.03	0.03
s_o	17.73	17.08	15.91	15.50	-	14.87	14.72	13.28	13.46	16.40	18.43	19.63	20.53	20.74	20.48	21.11	21.24	20.43	20.00	20.12	20.16	20.09	19.82	19.01
s_p	13.75	13.04	12.29	11.73	-	10.35	9.08	8.98	10.65	13.61	16.46	18.63	19.57	20.43	20.49	21.06	20.94	20.36	19.62	18.90	17.80	16.66	15.68	14.82
MAE	12.19	12.03	10.88	10.66	-	10.44	10.57	9.56	9.66	9.66	7.95	6.91	5.90	4.65	4.04	4.22	5.16	6.11	7.08	8.15	9.25	10.19	10.85	10.64
MBE	1.22	1.20	1.02	1.09	-	1.04	1.09	0.76	1.13	0.65	0.22	0.31	0.17	0.12	0.10	0.09	0.17	0.50	0.57	0.53	0.45	0.33	0.38	0.47
RMSE	15.42	15.07	13.66	13.73	-	13.64	13.81	11.92	12.19	12.43	10.18	8.77	7.81	5.88	5.17	5.55	7.18	8.54	9.44	10.66	11.97	12.88	13.85	13.99
r	0.55	0.53	0.56	0.52	-	0.46	0.42	0.48	0.51	0.67	0.84	0.90	0.93	0.96	0.97	0.97	0.94	0.91	0.89	0.85	0.81	0.77	0.72	0.68
r^2	0.30	0.28	0.31	0.27	-	0.22	0.18	0.24	0.26	0.45	0.70	0.80	0.86	0.92	0.94	0.93	0.89	0.83	0.79	0.73	0.65	0.59	0.52	0.47
d_1	0.51	0.49	0.51	0.51	-	0.47	0.43	0.47	0.50	0.60	0.72	0.78	0.82	0.86	0.88	0.88	0.85	0.81	0.78	0.74	0.70	0.66	0.62	0.60
128M																								
$m_{h,z}$	0.71	0.68	0.65	0.63	0.62	-	0.55	0.52	0.55	0.65	0.78	0.87	0.93	0.96	0.98	1.00	1.00	0.98	0.95	0.91	0.88	0.83	0.79	0.75
95% C.I.	0.04	0.04	0.03	0.03	0.03	-	0.03	0.03	0.03	0.03	0.02	0.02	0.02	0.01	0.01	0.01	0.01	0.02	0.02	0.02	0.02	0.03	0.03	0.03
s_o	19.40	18.84	18.48	18.02	17.92	-	17.37	16.76	14.81	16.06	18.30	19.57	20.36	20.39	20.52	20.84	20.92	19.98	19.73	19.60	19.62	19.67	19.66	19.39
s_p	15.44	14.79	14.11	13.58	13.44	-	11.79	11.39	11.93	13.94	16.89	18.72	20.24	20.79	21.07	21.48	21.40	20.98	20.42	19.63	18.91	17.91	17.02	16.18
MAE	13.54	13.05	11.80	11.65	12.22	-	11.90	11.33	10.19	9.88	7.71	7.25	5.91	4.79	3.94	4.09	4.95	5.80	7.03	7.54	7.80	9.33	10.71	10.39
MBE	1.59	1.46	1.15	1.11	1.20	-	0.90	0.81	1.20	0.92	0.41	0.42	0.43	0.38	0.32	0.35	0.45	0.73	0.81	0.72	0.57	0.65	0.80	0.69
RMSE	16.98	16.35	14.87	14.75	15.35	-	15.29	14.55	12.80	12.45	9.84	9.11	7.28	6.08	4.96	5.15	6.85	8.06	9.35	9.92	9.95	12.12	13.72	13.86
r	0.53	0.54	0.58	0.57	0.54	-	0.50	0.52	0.55	0.67	0.85	0.89	0.94	0.96	0.97	0.97	0.95	0.92	0.89	0.87	0.87	0.80	0.73	0.71
r^2	0.28	0.29	0.34	0.32	0.29	-	0.25	0.27	0.30	0.45	0.72	0.79	0.87	0.92	0.94	0.94	0.90	0.85	0.80	0.76	0.75	0.63	0.53	0.51
d_1	0.51	0.50	0.53	0.53	0.51	-	0.49	0.49	0.52	0.59	0.73	0.76	0.82	0.86	0.88	0.88	0.86	0.83	0.78	0.76	0.75	0.69	0.64	0.63
433M																								
$m_{h,z}$	0.79	0.78	0.77	0.76	0.75	0.74	-	0.70	0.71	0.70	0.73	0.79	0.84	0.88	0.90	0.92	0.95	0.95	0.93	0.92	0.90	0.87	0.84	0.81
95% C.I.	0.04	0.04	0.04	0.04	0.04	0.04	-	0.03	0.03	0.03	0.03	0.02	0.02	0.02	0.01	0.01	0.02	0.02	0.02	0.03	0.02	0.03	0.03	0.03
s_o	18.98	17.83	17.91	17.97	18.28	18.34	-	17.71	17.90	17.42	17.21	16.96	17.63	18.17	18.03	18.39	19.01	19.09	18.44	18.44	18.58	19.03	18.54	19.05
s_p	16.69	16.35	16.17	16.10	15.76	15.90	-	15.11	15.01	14.82	15.20	16.57	17.77	18.45	18.79	19.42	19.87	19.95	19.69	19.25	19.05	18.29	17.63	17.11
MAE	12.74	11.91	12.43	12.65	12.43	11.95	-	10.34	9.96	9.35	8.53	7.30	5.93	5.23	4.48	4.40	4.84	5.41	6.87	7.81	7.83	8.71	9.75	10.63
MBE	1.56	1.55	1.58	1.60	1.39	1.42	-	0.91	0.78	0.59	0.51	0.62	0.48	0.42	0.47	0.54	0.62	0.71	1.01	1.09	0.88	0.69	0.99	0.89
RMSE	16.32	15.18	15.52	15.70	15.51	15.52	-	13.40	13.25	12.05	10.99	9.31	7.39	6.61	5.86	5.89	7.34	8.15	9.57	10.83	10.04	10.81	12.53	13.32
r	0.59	0.61	0.59	0.58	0.60	0.60	-	0.68	0.69	0.73	0.78	0.85	0.91	0.94	0.95	0.95	0.93	0.91	0.88	0.84	0.86	0.83	0.76	0.73
r^2	0.35	0.38	0.35	0.34	0.36	0.36	-	0.46	0.48	0.54	0.60	0.72	0.83	0.87	0.90	0.91	0.87	0.84	0.77	0.70	0.74	0.70	0.58	0.54
d_1	0.55	0.56	0.54	0.53	0.54	0.56	-	0.60	0.62	0.64	0.67	0.73	0.79	0.83	0.85	0.86	0.85	0.83	0.78	0.74	0.74	0.71	0.66	0.63

Table 4-1. (Continued) Statistical Results of the Performance of "Prediction based on Present Day's Maximum" Method
$m_{h,z}$ – linear best-fit gradient, 95% C.I. – standard error of $m_{h,z}$ at the 95% confidence interval, s_o and s_p – observed and predicted ozone concentration standard deviation (ppb), MAE – mean absolute error (ppb), MBE – mean bias error (ppb), RMSE – root mean squared error (ppb), r – correlation coefficient, r^2 – coefficient of determination, d_1 – index of agreement (α=1)

526M	0:00	1:00	2:00	3:00	4:00	5:00	6:00	7:00	8:00	9:00	10:00	11:00	12:00	13:00	14:00	15:00	16:00	17:00	18:00	19:00	20:00	21:00	22:00	23:00
$m_{h,z}$	0.74	0.73	0.73	0.72	0.70	0.71	0.69	0.65	0.62	0.61	0.62	0.67	0.72	0.76	0.78	0.80	0.80	0.81	0.81	0.82	0.80	0.78	0.77	0.75
95% C.I.	0.02	0.02	0.02	0.02	0.02	0.02	0.02	0.02	0.02	0.02	0.02	0.02	0.02	0.02	0.02	0.03	0.03	0.03	0.03	0.02	0.02	0.02	0.02	0.02
s_o	17.40	17.91	17.95	18.05	17.65	17.57	17.43	16.39	15.09	14.32	13.89	15.61	16.49	17.08	18.23	18.91	19.13	19.43	19.25	19.57	18.71	18.45	18.03	17.75
s_p	16.72	16.52	16.37	16.34	15.90	15.92	15.46	14.63	13.97	13.33	13.90	15.31	16.33	16.97	17.73	18.09	18.19	18.08	18.30	18.45	17.99	17.51	17.32	16.96
MAE	10.93	11.02	10.66	10.72	10.65	10.35	9.95	9.98	9.67	9.95	9.82	9.49	10.33	10.91	11.52	12.06	12.06	11.92	11.77	11.08	10.71	10.89	10.77	10.87
MBE	1.55	1.41	1.25	1.22	1.17	1.10	0.96	1.07	1.24	1.36	1.56	1.29	1.36	1.44	1.54	1.58	1.56	1.43	1.51	1.27	1.33	1.36	1.31	1.29
RMSE	14.20	14.44	13.96	13.99	13.69	13.25	12.90	12.77	12.34	12.42	12.24	11.98	12.57	13.17	14.29	15.04	15.15	15.13	14.98	14.26	13.85	14.05	13.48	13.36
r	0.66	0.65	0.68	0.68	0.67	0.69	0.70	0.67	0.65	0.60	0.62	0.70	0.71	0.70	0.69	0.67	0.68	0.68	0.69	0.72	0.72	0.70	0.71	0.71
r^2	0.43	0.43	0.46	0.46	0.45	0.48	0.49	0.45	0.42	0.36	0.38	0.49	0.50	0.50	0.47	0.45	0.46	0.46	0.47	0.52	0.52	0.49	0.51	0.50
d_1	0.60	0.60	0.61	0.61	0.61	0.61	0.62	0.60	0.58	0.55	0.56	0.62	0.61	0.60	0.60	0.59	0.60	0.60	0.61	0.64	0.64	0.62	0.62	0.61
976M																								
$m_{h,z}$	0.79	0.79	0.79	0.80	0.78	0.79	0.77	0.77	0.75	0.73	0.72	0.74	0.76	0.78	0.79	0.80	0.80	0.82	0.84	0.85	0.84	0.82	0.82	0.80
95% C.I.	0.02	0.02	0.02	0.02	0.02	0.02	0.02	0.02	0.02	0.02	0.02	0.02	0.02	0.02	0.02	0.02	0.02	0.02	0.02	0.02	0.02	0.02	0.02	0.02
s_o	16.71	17.12	17.06	17.14	17.25	17.48	17.02	16.37	15.31	14.51	14.82	14.92	15.20	16.01	15.73	15.67	15.67	16.26	17.24	17.73	17.06	16.58	16.80	16.79
s_p	17.88	17.83	17.63	17.88	17.39	17.67	16.70	16.72	16.06	16.02	16.21	16.59	17.02	17.50	17.84	18.10	18.09	18.47	18.84	19.05	18.51	18.33	18.40	18.01
MAE	11.14	10.61	10.32	9.67	10.06	9.56	9.63	9.65	10.09	9.66	9.88	9.50	9.83	10.14	10.81	11.14	11.06	11.03	11.17	10.11	10.06	9.54	9.39	9.46
MBE	1.96	1.74	1.56	1.44	1.41	1.27	1.15	1.36	1.58	1.74	1.77	1.73	1.82	1.77	2.00	2.15	2.16	2.06	1.97	1.69	1.67	1.66	1.62	1.52
RMSE	14.19	13.82	13.17	12.37	12.90	12.14	12.14	12.20	12.61	12.35	12.53	12.05	12.48	12.83	13.28	13.69	13.76	13.67	14.13	13.19	12.83	12.27	12.21	12.07
r	0.67	0.69	0.72	0.75	0.73	0.76	0.74	0.73	0.68	0.68	0.68	0.72	0.71	0.72	0.70	0.69	0.68	0.70	0.70	0.75	0.75	0.76	0.77	0.77
r^2	0.45	0.48	0.51	0.57	0.53	0.58	0.55	0.54	0.47	0.47	0.47	0.52	0.51	0.51	0.49	0.47	0.47	0.50	0.49	0.56	0.56	0.58	0.59	0.59
d_1	0.60	0.62	0.63	0.65	0.64	0.66	0.65	0.64	0.60	0.61	0.60	0.62	0.62	0.62	0.60	0.59	0.60	0.61	0.62	0.66	0.65	0.66	0.66	0.66
1754M																								
$m_{h,z}$	0.80	0.80	0.80	0.80	0.80	0.80	0.79	0.77	0.76	0.74	0.73	0.72	0.72	0.72	0.73	0.75	0.77	0.78	0.80	0.81	0.81	0.80	0.81	0.81
95% C.I.	0.03	0.03	0.03	0.03	0.03	0.03	0.03	0.03	0.03	0.03	0.02	0.02	0.02	0.02	0.02	0.03	0.03	0.03	0.03	0.03	0.03	0.03	0.03	0.03
s_o	14.83	15.05	15.19	15.19	15.35	15.11	14.89	14.45	14.32	13.76	13.03	12.11	12.18	12.26	12.31	13.48	14.00	14.38	14.57	15.18	14.57	14.45	14.67	14.76
s_p	18.20	18.16	18.21	18.26	18.64	18.04	17.88	17.57	17.38	17.11	16.61	16.15	16.12	16.39	16.55	16.74	17.11	17.38	17.73	18.17	18.09	18.05	18.15	18.17
MAE	11.80	11.16	10.87	10.57	11.27	11.07	11.09	11.54	11.28	10.96	10.41	10.52	10.51	10.89	11.23	11.36	11.90	12.09	12.31	12.10	11.62	11.35	11.43	11.44
MBE	2.63	2.47	2.35	2.27	2.48	2.34	2.42	2.58	2.58	2.57	2.42	2.51	2.50	2.60	2.66	2.46	2.55	2.52	2.54	2.46	2.48	2.43	2.48	2.39
RMSE	15.18	14.74	14.32	13.89	14.42	14.29	14.53	14.99	14.88	14.48	13.56	13.47	13.46	13.71	14.02	14.20	14.82	14.93	14.99	14.96	14.49	14.19	14.51	14.19
r	0.61	0.63	0.66	0.68	0.67	0.65	0.63	0.59	0.59	0.59	0.62	0.59	0.59	0.59	0.58	0.59	0.58	0.58	0.60	0.62	0.64	0.65	0.64	0.66
r^2	0.37	0.40	0.43	0.46	0.44	0.42	0.40	0.35	0.35	0.35	0.38	0.35	0.35	0.35	0.34	0.35	0.33	0.34	0.36	0.39	0.41	0.42	0.41	0.43
d_1	0.55	0.58	0.59	0.61	0.59	0.58	0.57	0.55	0.55	0.55	0.56	0.54	0.54	0.53	0.52	0.53	0.52	0.52	0.53	0.55	0.56	0.57	0.57	0.57

Table 4-2. Statistical Results of the Performance of "Prediction based on Previous Day's Maximum" Method $m_{h,z}$ – linear best-fit gradient, 95% C.I. – standard error of $m_{h,z}$ at the 95% confidence interval, s_o and s_p – observed and predicted ozone concentration standard deviation (ppb), MAE – mean absolute error (ppb), MBE – mean bias error (ppb), RMSE – root mean squared error (ppb), r – correlation coefficient, r^2 – coefficient of determination, d_1 – index of agreement (α=1)

76M		1:00	2:00	3:00	4:00	5:00	6:00	7:00	8:00	9:00	10:00	11:00	12:00	13:00	14:00	15:00	16:00	17:00	18:00	19:00	20:00	21:00	22:00	23:00
$m_{h,z}$	0.63	0.60	0.56	0.53	-	0.47	0.43	0.41	0.48	0.61	0.74	0.82	0.86	0.90	0.92	0.93	0.93	0.90	0.87	0.82	0.77	0.74	0.69	0.65
95% C.I.	0.03	0.03	0.03	0.03	-	0.03	0.03	0.03	0.03	0.03	0.04	0.04	0.04	0.05	0.05	0.05	0.05	0.05	0.05	0.05	0.05	0.05	0.05	0.05
s_o	17.73	17.08	15.91	15.50	-	14.87	14.91	13.29	13.46	16.39	18.49	19.73	20.56	20.96	20.50	21.08	21.20	20.33	19.88	20.07	20.11	19.98	19.75	19.00
s_p	13.70	13.01	12.13	11.54	-	10.09	9.21	8.92	10.40	13.26	16.14	17.87	18.72	19.39	19.93	20.04	19.92	19.44	18.73	17.74	16.67	15.92	14.97	13.95
MAE	10.06	10.49	10.43	10.60	-	10.09	10.70	9.18	10.07	11.36	12.84	14.23	14.84	16.19	16.41	17.32	17.64	17.45	17.14	17.76	17.89	17.20	17.29	16.74
MBE	0.58	0.72	0.83	1.01	-	0.82	0.76	0.74	1.18	1.35	1.86	2.17	2.43	2.97	3.10	3.39	3.48	3.42	3.27	3.32	3.13	2.94	2.94	2.81
RMSE	13.43	13.65	13.22	13.67	-	13.27	13.61	11.93	12.54	14.69	16.89	18.34	19.70	21.51	21.26	22.74	23.17	22.34	21.67	22.36	22.20	21.72	21.75	20.99
r	0.66	0.62	0.59	0.52	-	0.49	0.45	0.48	0.48	0.53	0.54	0.53	0.51	0.44	0.46	0.40	0.38	0.38	0.39	0.32	0.30	0.30	0.25	0.23
r^2	0.44	0.38	0.34	0.28	-	0.24	0.20	0.23	0.23	0.28	0.29	0.29	0.26	0.20	0.21	0.16	0.15	0.15	0.15	0.10	0.09	0.09	0.06	0.05
d_1	0.59	0.56	0.53	0.50	-	0.48	0.43	0.49	0.48	0.52	0.54	0.53	0.53	0.50	0.50	0.48	0.47	0.46	0.45	0.42	0.40	0.41	0.38	0.36
128M																								
$m_{h,z}$	0.72	0.68	0.66	0.64	0.63	-	0.55	0.52	0.55	0.64	0.77	0.85	0.90	0.93	0.95	0.96	0.96	0.94	0.92	0.88	0.84	0.80	0.76	0.72
95% C.I.	0.03	0.03	0.03	0.03	0.03	-	0.03	0.03	0.03	0.03	0.04	0.04	0.04	0.05	0.05	0.05	0.05	0.05	0.05	0.05	0.05	0.05	0.05	0.05
s_o	18.96	18.43	18.09	17.65	17.56	-	17.09	16.76	14.45	16.06	18.30	19.57	20.36	20.39	20.52	20.84	20.92	19.98	19.73	19.60	19.62	19.67	19.66	19.39
s_p	15.48	14.83	14.28	13.71	13.56	-	11.98	11.40	11.97	14.12	16.69	18.29	19.54	20.04	20.35	20.65	20.58	20.25	19.80	18.86	17.99	17.22	16.43	15.57
MAE	10.76	11.35	11.12	11.59	11.51	-	11.86	10.88	9.92	11.13	12.20	14.22	15.19	16.08	16.63	17.20	17.25	17.11	16.75	17.29	17.45	17.19	17.31	16.94
MBE	0.81	0.93	0.98	1.15	0.98	-	0.97	0.78	1.18	1.55	1.80	2.21	2.76	3.15	3.28	3.48	3.56	3.52	3.31	3.50	3.33	3.27	3.15	3.03
RMSE	14.34	14.61	14.79	15.22	14.68	-	15.10	14.54	12.71	14.41	16.18	18.12	20.08	21.25	21.74	22.56	22.91	22.06	21.28	22.13	21.92	22.00	21.88	21.52
r	0.67	0.63	0.61	0.56	0.58	-	0.51	0.52	0.55	0.56	0.58	0.55	0.50	0.46	0.45	0.42	0.41	0.41	0.43	0.35	0.34	0.31	0.29	0.27
r^2	0.45	0.40	0.37	0.31	0.34	-	0.26	0.27	0.31	0.31	0.34	0.30	0.25	0.21	0.20	0.18	0.16	0.17	0.19	0.13	0.12	0.10	0.08	0.07
d_1	0.61	0.57	0.57	0.54	0.54	-	0.49	0.51	0.54	0.54	0.57	0.53	0.53	0.51	0.50	0.49	0.49	0.48	0.48	0.44	0.43	0.42	0.40	0.39
433M																								
$m_{h,z}$	0.80	0.78	0.78	0.77	0.76	0.74	-	0.69	0.70	0.70	0.72	0.77	0.81	0.84	0.86	0.89	0.91	0.91	0.90	0.88	0.86	0.83	0.81	0.78
95% C.I.	0.03	0.03	0.03	0.03	0.03	0.03	-	0.03	0.04	0.03	0.04	0.04	0.04	0.05	0.05	0.05	0.05	0.05	0.05	0.05	0.05	0.05	0.05	0.05
s_o	18.96	17.87	17.93	17.95	18.24	18.34	-	17.71	17.90	17.37	17.17	17.00	17.88	18.12	18.02	18.36	19.06	19.03	18.37	18.40	18.80	19.28	18.53	19.06
s_p	16.96	16.68	16.44	16.36	15.92	15.78	-	14.74	14.83	14.78	15.43	16.69	17.25	17.84	18.22	18.79	19.26	19.31	19.06	18.69	18.28	17.50	17.09	16.55
MAE	10.26	9.42	9.34	9.90	10.06	10.54	-	11.01	11.29	10.51	11.31	12.13	13.43	14.46	14.68	14.89	15.17	15.55	15.89	16.38	16.52	17.02	16.70	17.20
MBE	1.01	1.19	1.04	1.09	1.06	1.14	-	1.13	1.15	1.03	1.47	2.09	2.50	2.92	3.11	3.23	3.30	3.39	3.50	3.50	3.35	3.34	3.35	3.30
RMSE	13.86	13.42	13.09	13.43	14.09	14.61	-	14.59	14.82	13.83	14.73	15.95	18.09	19.52	19.96	20.44	21.13	21.41	21.21	21.40	21.44	22.03	21.51	21.96
r	0.71	0.70	0.72	0.70	0.67	0.64	-	0.61	0.61	0.64	0.60	0.56	0.48	0.42	0.41	0.41	0.41	0.39	0.38	0.35	0.35	0.30	0.29	0.26
r^2	0.50	0.49	0.51	0.49	0.45	0.42	-	0.37	0.37	0.41	0.36	0.31	0.23	0.18	0.17	0.17	0.17	0.15	0.14	0.12	0.12	0.09	0.08	0.07
d_1	0.64	0.66	0.66	0.64	0.63	0.61	-	0.57	0.57	0.59	0.56	0.55	0.53	0.51	0.50	0.51	0.51	0.50	0.47	0.45	0.45	0.42	0.41	0.40

Table 4-2. (Continued) Statistical Results of the Performance of "Prediction based on Previous Day's Maximum" Method
$m_{h,z}$ – linear best-fit gradient, 95% C.I. – standard error of $m_{h,z}$ at the 95% confidence interval, s_o and s_p – observed and predicted ozone concentration standard deviation (ppb), MAE – mean absolute error (ppb), MBE – mean bias error (ppb), RMSE – root mean squared error (ppb), r – correlation coefficient, r^2 – coefficient of determination, d_1 – index of agreement (α=1)

526M	0:00	1:00	2:00	3:00	4:00	5:00	6:00	7:00	8:00	9:00	10:00	11:00	12:00	13:00	14:00	15:00	16:00	17:00	18:00	19:00	20:00	21:00	22:00	23:00
$m_{h,z}$	0.75	0.74	0.73	0.72	0.71	0.71	0.68	0.65	0.62	0.60	0.61	0.66	0.71	0.74	0.77	0.78	0.79	0.79	0.78	0.79	0.78	0.75	0.75	0.73
95% C.I.	0.02	0.02	0.02	0.02	0.02	0.02	0.02	0.02	0.02	0.02	0.02	0.03	0.03	0.03	0.03	0.03	0.03	0.04	0.04	0.04	0.03	0.03	0.03	0.03
s_o	17.40	17.91	17.96	18.09	17.70	17.61	17.47	16.43	15.12	14.34	13.91	15.65	16.53	17.12	18.27	18.95	19.17	19.47	19.30	19.61	18.76	18.49	18.07	17.79
s_p	16.85	16.66	16.44	16.48	16.13	15.94	15.39	14.50	13.80	13.47	13.84	15.03	15.96	16.67	17.32	17.67	17.62	17.79	17.77	17.93	17.48	16.99	16.82	16.48
MAE	10.19	10.11	10.54	10.64	10.67	10.90	11.10	10.92	11.00	11.51	11.05	11.78	13.29	13.85	14.84	15.70	16.19	16.75	16.76	16.66	16.28	16.47	16.19	15.86
MBE	1.22	1.04	1.04	1.06	1.15	1.20	1.18	1.32	1.55	1.83	1.93	1.94	2.32	2.47	2.64	2.79	2.89	2.99	2.99	2.95	3.06	3.09	2.99	2.91
RMSE	12.65	12.73	13.04	13.20	13.37	13.70	13.90	13.87	13.73	13.95	13.68	14.85	16.67	17.40	18.72	19.73	20.36	20.78	20.64	20.77	20.50	20.51	19.88	19.48
r	0.73	0.73	0.72	0.71	0.69	0.67	0.65	0.61	0.56	0.51	0.52	0.54	0.48	0.48	0.46	0.43	0.40	0.39	0.40	0.40	0.38	0.35	0.37	0.37
r^2	0.53	0.54	0.52	0.51	0.48	0.45	0.42	0.37	0.31	0.26	0.27	0.29	0.23	0.23	0.21	0.19	0.16	0.16	0.16	0.16	0.14	0.12	0.13	0.14
d_1	0.63	0.63	0.62	0.62	0.61	0.60	0.58	0.56	0.52	0.48	0.50	0.52	0.50	0.49	0.48	0.47	0.45	0.44	0.44	0.45	0.44	0.42	0.42	0.43
976M																								
$m_{h,z}$	0.80	0.80	0.80	0.80	0.78	0.78	0.75	0.75	0.74	0.72	0.71	0.72	0.74	0.77	0.78	0.79	0.79	0.80	0.82	0.83	0.81	0.80	0.80	0.79
95% C.I.	0.02	0.02	0.02	0.02	0.02	0.02	0.03	0.03	0.03	0.03	0.03	0.03	0.03	0.03	0.03	0.03	0.03	0.03	0.03	0.03	0.03	0.03	0.03	0.03
s_o	16.69	17.11	17.04	17.13	17.29	17.51	17.06	16.41	15.35	14.54	14.86	14.95	15.23	16.05	15.77	15.71	15.71	16.30	17.28	17.78	17.10	16.62	16.84	16.83
s_p	18.10	18.17	18.10	17.86	17.61	17.62	17.16	17.08	16.49	16.28	16.32	16.38	16.73	17.37	17.66	17.92	17.88	18.22	18.63	18.75	18.40	18.02	17.98	17.26
MAE	9.88	10.07	10.59	10.74	11.17	10.88	11.51	12.02	12.37	12.19	12.36	11.45	12.02	13.24	13.69	13.99	14.85	15.30	15.89	15.79	15.78	15.17	15.07	14.73
MBE	1.62	1.53	1.65	1.68	1.68	1.54	1.79	2.10	2.38	2.45	2.48	2.31	2.41	2.61	2.94	3.14	3.34	3.37	3.44	3.22	3.29	3.16	3.12	2.90
RMSE	12.35	12.35	12.93	13.49	13.89	13.55	14.43	14.98	15.38	14.99	15.26	14.80	15.37	16.46	17.27	17.77	18.50	18.98	19.89	19.59	19.35	18.70	18.77	18.46
r	0.76	0.76	0.74	0.71	0.69	0.71	0.65	0.61	0.55	0.54	0.54	0.57	0.55	0.53	0.49	0.47	0.42	0.42	0.41	0.44	0.42	0.44	0.44	0.43
r^2	0.57	0.58	0.54	0.50	0.47	0.50	0.42	0.37	0.30	0.30	0.29	0.32	0.31	0.28	0.24	0.22	0.18	0.18	0.17	0.19	0.18	0.19	0.19	0.18
d_1	0.64	0.64	0.62	0.62	0.60	0.62	0.58	0.55	0.52	0.51	0.50	0.55	0.53	0.51	0.49	0.49	0.46	0.46	0.46	0.47	0.45	0.46	0.46	0.46
1754M																								
$m_{h,z}$	0.80	0.80	0.80	0.81	0.79	0.79	0.78	0.77	0.76	0.74	0.72	0.72	0.71	0.71	0.73	0.75	0.76	0.77	0.78	0.80	0.79	0.79	0.80	0.80
95% C.I.	0.03	0.03	0.03	0.03	0.03	0.03	0.03	0.03	0.03	0.03	0.03	0.03	0.03	0.03	0.03	0.03	0.03	0.03	0.03	0.03	0.03	0.03	0.03	0.03
s_o	14.83	15.05	15.19	15.19	15.35	15.11	14.89	14.45	14.32	13.76	13.03	12.11	12.18	12.26	12.31	13.48	14.00	14.38	14.57	15.18	14.57	14.45	14.67	14.76
s_p	18.21	18.15	18.15	18.08	18.31	17.94	17.75	17.45	17.21	16.67	16.41	16.12	16.09	16.27	16.52	16.69	17.05	17.18	17.58	17.98	17.91	17.93	17.99	17.99
MAE	11.83	11.56	11.55	11.74	12.67	12.65	12.99	13.02	13.01	12.58	12.81	12.27	12.17	12.31	12.61	13.00	13.74	14.24	14.79	15.05	14.54	14.15	14.55	14.65
MBE	2.48	2.38	2.36	2.37	2.67	2.66	2.85	3.02	2.99	2.83	3.01	3.05	3.00	3.06	3.12	3.02	3.23	3.34	3.54	3.52	3.47	3.37	3.39	3.39
RMSE	14.51	14.36	14.44	14.58	15.65	15.73	16.39	16.79	16.67	15.96	16.09	15.62	15.45	15.62	15.86	16.42	17.43	18.19	18.88	19.14	18.50	18.04	18.26	18.32
r	0.64	0.65	0.65	0.64	0.59	0.57	0.52	0.48	0.47	0.48	0.44	0.44	0.45	0.45	0.45	0.44	0.41	0.37	0.35	0.37	0.39	0.42	0.41	0.41
r^2	0.41	0.42	0.42	0.41	0.35	0.33	0.27	0.23	0.22	0.23	0.20	0.19	0.20	0.20	0.20	0.20	0.16	0.14	0.12	0.13	0.15	0.17	0.17	0.17
d_1	0.55	0.57	0.57	0.56	0.53	0.52	0.50	0.49	0.48	0.48	0.46	0.46	0.46	0.46	0.46	0.47	0.45	0.44	0.43	0.44	0.45	0.46	0.45	0.45

Table 4-3. Statistical Results of the Performance of "Prediction based on Present Day's Hourly" Method $m_{h,z}$ – linear best-fit gradient, 95% C.I. – standard error of $m_{h,z}$ at the 95% confidence interval, s_o and s_p – observed and predicted ozone concentration standard deviation (ppb), MAE – mean absolute error (ppb), MBE – mean bias error (ppb), RMSE – root mean squared error (ppb), r – correlation coefficient, r^2 – coefficient of determination, d_1 – index of agreement (α=1)

76M	0:00	1:00	2:00	3:00	4:00	5:00	6:00	7:00	8:00	9:00	10:00	11:00	12:00	13:00	14:00	15:00	16:00	17:00	18:00	19:00	20:00	21:00	22:00	23:00
$m_{h,z}$	1.61	1.61	1.63	-	-	1.76	1.60	1.29	1.10	1.05	1.04	1.03	1.03	1.02	1.01	1.03	1.07	1.16	1.32	1.48	1.53	1.58	1.60	1.60
95% C.I.	0.16	0.16	0.15	-	-	0.19	0.16	0.09	0.02	0.01	0.01	0.01	0.01	0.01	0.01	0.01	0.01	0.03	0.06	0.09	0.11	0.13	0.14	0.14
s_o	18.09	17.42	16.23	-	-	15.10	15.09	13.50	13.75	16.39	18.49	19.73	20.56	20.96	20.50	21.08	21.20	20.33	19.88	20.07	20.11	19.98	19.75	19.00
s_p	22.46	21.96	20.43	-	-	16.45	15.34	14.57	14.69	16.94	18.62	20.51	21.22	21.75	21.66	22.93	23.49	23.45	24.63	26.44	26.55	25.64	24.67	23.63
MAE	18.36	18.26	16.49	-	-	14.16	11.21	7.44	3.22	2.55	2.48	2.52	2.65	3.27	3.14	3.81	4.28	7.92	14.04	16.97	18.92	19.56	19.12	18.48
MBE	9.57	9.36	8.16	-	-	6.96	5.61	3.27	0.94	0.46	0.41	0.46	0.49	0.55	0.47	0.76	0.94	1.69	3.96	6.47	8.34	9.04	8.96	8.94
RMSE	24.91	23.34	21.13	-	-	19.53	16.73	11.85	4.36	3.66	3.80	3.40	4.14	5.23	4.23	5.40	5.83	9.90	17.41	22.05	25.14	26.21	25.64	24.77
r	0.36	0.41	0.44	-	-	0.30	0.41	0.66	0.96	0.98	0.98	0.99	0.98	0.97	0.98	0.97	0.97	0.91	0.73	0.62	0.51	0.44	0.43	0.43
r^2	0.13	0.17	0.19	-	-	0.09	0.17	0.43	0.92	0.96	0.96	0.97	0.96	0.94	0.96	0.95	0.94	0.83	0.53	0.38	0.26	0.19	0.19	0.18
d_1	0.45	0.43	0.45	-	-	0.44	0.53	0.67	0.86	0.90	0.92	0.92	0.92	0.90	0.91	0.89	0.88	0.77	0.61	0.55	0.51	0.49	0.48	0.48
128M																								
$m_{h,z}$	1.77	1.77	1.84	-	2.04	-	1.99	1.58	1.22	1.09	1.07	1.06	1.05	1.04	1.04	1.05	1.09	1.20	1.38	1.56	1.64	1.70	1.72	1.74
95% C.I.	0.18	0.18	0.19	-	0.26	-	0.21	0.14	0.05	0.01	0.01	0.01	0.01	0.01	0.01	0.01	0.02	0.03	0.06	0.09	0.12	0.13	0.15	0.16
s_o	19.40	18.84	18.48	-	17.92	-	17.37	16.76	14.81	16.06	18.30	19.57	20.36	20.39	20.52	20.84	20.92	19.98	19.73	19.60	19.62	19.67	19.66	19.39
s_p	25.00	24.13	23.23	-	21.29	-	18.87	17.70	16.30	17.49	19.29	20.92	21.60	22.28	22.72	23.41	24.04	24.17	25.67	27.80	28.29	27.48	26.73	25.76
MAE	22.15	21.95	21.10	-	22.28	-	16.25	12.89	6.33	2.88	2.94	2.62	2.69	3.10	3.07	3.95	4.66	8.77	14.95	18.30	20.54	21.24	22.46	21.94
MBE	11.37	10.93	10.74	-	11.52	-	7.52	5.60	1.90	0.71	0.65	0.60	0.67	0.83	0.78	1.01	1.26	2.13	4.46	7.20	9.29	9.92	11.00	10.96
RMSE	28.87	27.45	27.00	-	28.19	-	21.59	18.95	9.20	3.74	4.05	3.53	4.31	5.16	4.27	6.05	6.69	10.94	18.27	23.08	26.49	27.67	29.19	28.64
r	0.30	0.32	0.30	-	0.12	-	0.34	0.44	0.83	0.98	0.98	0.99	0.98	0.98	0.99	0.97	0.97	0.90	0.72	0.62	0.51	0.44	0.35	0.34
r^2	0.09	0.10	0.09	-	0.01	-	0.11	0.19	0.70	0.96	0.96	0.98	0.97	0.95	0.97	0.94	0.93	0.81	0.53	0.39	0.26	0.19	0.12	0.12
d_1	0.41	0.44	0.40	-	0.34	-	0.45	0.54	0.74	0.89	0.90	0.92	0.92	0.91	0.91	0.89	0.87	0.75	0.59	0.53	0.49	0.46	0.42	0.43
433M																								
$m_{h,z}$	2.03	2.12	2.24	-	2.51	2.73	-	2.04	1.50	1.15	1.01	0.96	0.95	0.95	0.95	0.97	1.03	1.15	1.35	1.57	1.71	1.77	1.84	1.91
95% C.I.	0.22	0.24	0.26	-	0.35	0.34	-	0.21	0.11	0.06	0.03	0.02	0.01	0.01	0.02	0.02	0.02	0.04	0.07	0.10	0.13	0.16	0.18	0.19
s_o	19.62	18.56	18.59	-	18.86	18.93	-	18.25	18.44	17.37	17.17	17.00	17.88	18.12	18.02	18.36	19.06	19.03	18.37	18.40	18.80	19.28	18.53	19.06
s_p	27.73	27.43	26.85	-	26.16	25.31	-	23.07	20.07	18.22	17.20	18.06	18.71	19.75	20.48	21.52	22.64	23.45	25.46	27.91	28.99	28.04	28.28	28.14
MAE	25.46	25.69	25.62	-	27.16	25.38	-	21.03	15.22	11.48	6.15	3.74	3.57	3.85	4.32	5.66	7.39	11.40	16.33	18.87	21.84	23.41	24.56	25.02
MBE	12.97	13.70	13.75	-	14.98	12.76	-	9.58	4.78	2.49	0.76	0.64	0.62	0.76	1.00	1.39	1.73	2.67	5.16	7.69	9.86	11.17	12.80	12.74
RMSE	31.51	31.35	31.92	-	33.27	30.53	-	26.48	20.07	15.47	9.08	5.52	5.35	5.83	6.18	8.03	9.45	13.61	19.59	23.62	27.28	30.18	31.64	31.18
r	0.29	0.28	0.22	-	0.13	0.21	-	0.29	0.48	0.64	0.86	0.95	0.96	0.96	0.96	0.93	0.92	0.82	0.67	0.60	0.50	0.34	0.29	0.32
r^2	0.08	0.08	0.05	-	0.02	0.04	-	0.09	0.23	0.41	0.74	0.91	0.92	0.92	0.92	0.87	0.84	0.68	0.45	0.36	0.25	0.12	0.08	0.10
d_1	0.36	0.34	0.34	-	0.31	0.32	-	0.39	0.51	0.60	0.78	0.87	0.88	0.88	0.86	0.82	0.78	0.66	0.53	0.50	0.45	0.41	0.37	0.38

Table 4-3. (Continued) Statistical Results of the Performance of "Prediction based on Present Day's Hourly" Method $m_{h,z}$ – linear best-fit gradient, 95% C.I. – standard error of $m_{h,z}$ at the 95% confidence interval, s_o and s_p – observed and predicted ozone concentration standard deviation (ppb), MAE – mean absolute error (ppb), MBE – mean bias error (ppb), RMSE – root mean squared error (ppb), r – correlation coefficient, r^2 – coefficient of determination, d_1 – index of agreement (α=1)

526M	0:00	1:00	2:00	3:00	4:00	5:00	6:00	7:00	8:00	9:00	10:00	11:00	12:00	13:00	14:00	15:00	16:00	17:00	18:00	19:00	20:00	21:00	22:00	23:00
$m_{h,z}$	1.94	2.00	2.07	2.18	2.33	2.31	2.32	2.00	1.46	1.12	0.92	0.85	0.82	0.82	0.83	0.85	0.87	0.93	1.06	1.26	1.42	1.56	1.77	1.89
95% C.I.	0.15	0.17	0.19	0.23	0.27	0.31	0.33	0.21	0.10	0.06	0.04	0.03	0.03	0.03	0.03	0.03	0.03	0.03	0.03	0.04	0.06	0.09	0.11	0.13
s_o	17.40	17.91	18.30	20.31	20.71	17.91	17.43	16.70	15.71	15.79	15.51	18.74	20.81	21.64	22.47	20.87	20.73	21.36	20.84	19.99	18.71	18.45	18.03	17.75
s_p	25.05	25.14	25.60	26.35	25.94	26.34	25.32	23.66	20.12	17.46	16.91	18.04	18.80	19.01	19.17	19.03	18.64	18.85	18.79	20.12	21.97	23.68	23.72	23.89
MAE	25.51	26.88	28.81	30.83	31.94	36.08	35.76	27.07	18.45	13.92	10.98	10.07	10.45	11.29	12.30	11.80	11.12	11.12	12.03	13.16	15.88	19.83	22.50	23.16
MBE	11.67	13.00	15.07	17.33	18.74	23.77	23.91	15.35	7.66	4.46	3.21	2.48	2.27	2.23	2.18	1.82	1.46	1.51	1.77	2.36	4.27	7.00	8.51	9.32
RMSE	30.04	31.90	33.92	35.96	36.93	40.96	40.62	32.15	22.86	17.59	14.65	13.20	13.10	13.81	15.08	14.84	14.05	14.13	15.15	16.27	19.59	24.15	26.75	27.51
r	0.19	0.12	0.06	0.03	-0.03	-0.12	-0.15	0.03	0.28	0.44	0.59	0.71	0.74	0.72	0.68	0.70	0.73	0.73	0.68	0.67	0.57	0.42	0.29	0.26
r^2	0.04	0.01	0.00	0.00	0.00	0.01	0.02	0.00	0.08	0.20	0.34	0.51	0.55	0.52	0.47	0.49	0.53	0.53	0.47	0.45	0.32	0.18	0.08	0.07
d_1	0.31	0.30	0.27	0.24	0.23	0.22	0.22	0.28	0.38	0.47	0.56	0.63	0.64	0.61	0.59	0.60	0.63	0.63	0.60	0.59	0.51	0.42	0.35	0.34
976M																								
$m_{h,z}$	2.11	2.22	2.28	2.37	2.60	2.67	2.62	2.37	1.75	1.35	1.07	0.93	0.86	0.85	0.84	0.86	0.87	0.94	1.10	1.32	1.48	1.65	1.90	2.03
95% C.I.	0.16	0.19	0.22	0.25	0.30	0.36	0.38	0.25	0.12	0.07	0.05	0.03	0.03	0.03	0.03	0.03	0.02	0.03	0.04	0.04	0.06	0.09	0.12	0.14
s_o	16.71	17.12	17.06	17.14	17.25	17.48	17.02	16.37	15.31	14.51	14.82	14.92	15.20	16.01	15.73	15.67	15.67	16.26	17.24	17.73	17.06	16.58	16.80	16.79
s_p	27.29	27.44	28.36	29.02	28.81	29.44	28.44	28.17	24.16	21.04	19.49	19.66	19.58	19.37	19.24	19.00	18.63	19.17	19.51	20.69	22.95	24.92	25.58	25.69
MAE	27.41	29.32	31.30	34.21	35.53	39.09	39.68	31.69	21.83	16.06	13.20	11.09	10.31	10.52	11.39	11.32	10.56	10.54	11.72	12.92	16.41	20.38	23.42	24.01
MBE	12.99	14.71	17.06	19.85	21.39	25.83	26.84	18.37	9.48	5.62	4.11	3.38	2.86	2.54	2.65	2.49	2.22	2.33	2.44	2.97	5.03	7.81	9.56	10.24
RMSE	31.62	34.22	36.50	39.22	40.46	44.10	44.35	36.64	26.10	19.90	17.18	14.74	13.52	13.69	14.26	14.00	13.22	13.49	14.89	16.29	19.97	24.52	27.68	28.31
r	0.21	0.10	0.06	-0.01	-0.05	-0.10	-0.15	0.06	0.31	0.48	0.56	0.69	0.74	0.73	0.70	0.70	0.72	0.73	0.68	0.66	0.57	0.43	0.31	0.29
r^2	0.05	0.01	0.00	0.00	0.00	0.01	0.02	0.00	0.10	0.23	0.31	0.47	0.55	0.53	0.48	0.49	0.52	0.53	0.47	0.44	0.32	0.19	0.09	0.08
d_1	0.29	0.27	0.24	0.22	0.22	0.21	0.20	0.25	0.35	0.45	0.53	0.60	0.64	0.63	0.60	0.60	0.62	0.63	0.60	0.58	0.49	0.40	0.34	0.33
1754M																								
$m_{h,z}$	2.21	2.34	2.54	2.72	3.06	3.07	3.25	2.67	1.86	1.42	1.09	0.91	0.82	0.78	0.78	0.80	0.83	0.90	1.06	1.28	1.47	1.69	1.97	2.15
95% C.I.	0.17	0.20	0.23	0.28	0.34	0.40	0.44	0.27	0.14	0.08	0.05	0.04	0.03	0.03	0.03	0.03	0.03	0.03	0.04	0.04	0.06	0.10	0.12	0.14
s_o	14.83	15.05	15.19	15.19	15.35	15.11	14.89	14.45	14.32	13.76	13.03	12.11	12.18	12.26	12.31	13.48	14.00	14.38	14.57	15.18	14.57	14.45	14.67	14.76
s_p	28.92	29.04	29.95	30.78	31.35	32.49	31.89	30.39	26.20	21.78	20.39	19.34	18.63	18.26	17.75	17.46	17.23	17.76	18.46	20.23	23.03	25.70	26.08	27.03
MAE	27.42	28.74	30.65	32.77	34.51	38.98	39.51	31.64	23.60	16.31	13.81	12.00	11.55	11.88	12.21	11.90	12.02	11.84	11.82	12.42	15.99	19.89	22.51	23.31
MBE	13.66	14.76	16.84	19.22	21.09	26.74	27.32	19.04	11.05	5.94	4.87	4.13	3.60	3.46	3.22	2.82	2.59	2.71	2.89	3.23	5.51	8.43	9.50	10.44
RMSE	31.74	33.37	35.76	38.15	39.80	44.20	44.78	37.08	28.28	20.44	17.95	15.91	14.80	14.87	14.85	14.81	14.73	14.80	15.04	15.49	19.65	24.49	26.72	27.79
r	0.28	0.20	0.15	0.10	0.08	0.05	-0.02	0.14	0.29	0.47	0.54	0.61	0.64	0.61	0.59	0.58	0.58	0.60	0.62	0.67	0.58	0.46	0.36	0.36
r^2	0.08	0.04	0.02	0.01	0.01	0.00	0.00	0.02	0.08	0.22	0.29	0.37	0.41	0.38	0.34	0.34	0.34	0.36	0.38	0.45	0.33	0.21	0.13	0.13
d_1	0.29	0.28	0.25	0.24	0.23	0.22	0.20	0.25	0.32	0.44	0.50	0.53	0.53	0.52	0.50	0.52	0.52	0.54	0.55	0.56	0.47	0.40	0.34	0.34

Table 4-4. Comparison of Relative Performance in Terms of the Statistical Results Produced by the "Prediction based on Present Day's Maximum," "Prediction based on Previous Day's Maximum," and "Prediction based on Present Day's Hourly" Methods s_o and s_p – observed and predicted ozone concentration standard deviation (ppb), MAE – mean absolute error (ppb), MBE – mean bias error (ppb), RMSE – root mean squared error (ppb), r – correlation coefficient, r^2 – coefficient of determination, d_1 – index of agreement (α=1)

Statistical Parameters	Prediction based on Present Day's Maximum Method	Prediction based on Previous Day's Maximum Method	Prediction based on Present Day's Hourly Method
s_o	18.92	18.94	19.22
s_p	18.89	18.40	25.58
MAE	9.25	11.79	17.06
MBE	7.60E-14	-7.19E-13	-4.11E-13
RMSE	12.03	15.04	22.03
r	0.77	0.58	0.51
r^2	0.59	0.33	0.26
d_1	0.70	0.61	0.53

Table 4-5. Statistical Parameters Used to Develop the Overall Regression Model Based on "Prediction based on Present Day's Maximum" Method $m_{h,z}$ - linear best-fit gradient, 95% C.I. – standard error of $m_{h,z}$ at the 95% confidence interval, r^2 – coefficient of determination

0 M (NC)	0:00	1:00	2:00	3:00	4:00	5:00	6:00	7:00	8:00	9:00	10:00	11:00	12:00	13:00	14:00	15:00	16:00	17:00	18:00	19:00	20:00	21:00	22:00	23:00
$m_{h,z}$	0.31	0.30	0.27	-	0.22	0.21	0.22	0.28	0.43	0.59	0.72	0.82	0.88	0.92	0.94	0.94	0.90	0.80	0.65	0.53	0.46	0.41	0.38	0.35
95% C.I.	0.02	0.02	0.01	-	0.01	0.01	0.01	0.01	0.01	0.01	0.01	0.01	0.01	0.01	0.01	0.01	0.01	0.01	0.01	0.02	0.02	0.02	0.02	0.02
r^2	0.07	0.05	0.04	-	0.01	0.02	0.03	0.09	0.24	0.50	0.71	0.81	0.88	0.93	0.95	0.93	0.86	0.71	0.50	0.37	0.29	0.20	0.19	0.17
0 M (TN)																								
$m_{h,z}$	0.30	0.27	0.24	0.21	0.18	0.16	0.15	0.22	0.36	0.49	0.64	0.77	0.87	0.92	0.94	0.94	0.92	0.86	0.75	0.62	0.53	0.44	0.37	0.33
95% C.I.	0.01	0.01	0.01	0.01	0.01	0.01	0.01	0.01	0.01	0.01	0.01	0.01	0.01	0.01	0.01	0.01	0.01	0.01	0.01	0.01	0.01	0.01	0.01	0.01
r^2	0.02	0.00	0.00	0.01	0.02	0.03	0.04	0.00	0.14	0.32	0.53	0.70	0.85	0.91	0.94	0.93	0.88	0.80	0.69	0.51	0.38	0.25	0.14	0.12
76 M																								
$m_{h,z}$	0.63	0.59	0.56	0.53	-	0.47	0.42	0.41	0.48	0.62	0.76	0.85	0.91	0.94	0.96	0.98	0.97	0.94	0.91	0.87	0.82	0.77	0.73	0.68
95% C.I.	0.03	0.03	0.03	0.03	-	0.03	0.03	0.03	0.03	0.03	0.02	0.02	0.02	0.01	0.01	0.01	0.02	0.02	0.02	0.02	0.03	0.03	0.03	0.03
r^2	0.30	0.28	0.31	0.27	-	0.22	0.18	0.24	0.26	0.45	0.70	0.80	0.86	0.92	0.94	0.93	0.89	0.83	0.79	0.73	0.65	0.59	0.52	0.47
128 M																								
$m_{h,z}$	0.71	0.68	0.65	0.63	0.62	-	0.55	0.52	0.55	0.65	0.78	0.87	0.93	0.96	0.98	1.00	1.00	0.98	0.95	0.91	0.88	0.83	0.79	0.75
95% C.I.	0.04	0.04	0.03	0.03	0.03	-	0.03	0.03	0.03	0.03	0.02	0.02	0.02	0.01	0.01	0.01	0.01	0.02	0.02	0.02	0.02	0.03	0.03	0.03
r^2	0.28	0.29	0.34	0.32	0.29	-	0.25	0.27	0.30	0.45	0.72	0.79	0.87	0.92	0.94	0.94	0.90	0.85	0.80	0.76	0.75	0.63	0.53	0.51
433 M																								
$m_{h,z}$	0.79	0.78	0.77	0.76	0.75	0.74	-	0.70	0.71	0.70	0.73	0.79	0.84	0.88	0.90	0.92	0.95	0.95	0.93	0.92	0.90	0.87	0.84	0.81
95% C.I.	0.04	0.04	0.04	0.04	0.04	0.04	-	0.03	0.03	0.03	0.03	0.02	0.02	0.02	0.01	0.01	0.02	0.02	0.02	0.03	0.02	0.03	0.03	0.03
r^2	0.35	0.38	0.35	0.34	0.36	0.36	-	0.46	0.48	0.54	0.60	0.72	0.83	0.87	0.90	0.91	0.87	0.84	0.77	0.70	0.74	0.70	0.58	0.54
526 M																								
$m_{h,z}$	0.74	0.73	0.73	0.72	0.70	0.71	0.69	0.65	0.62	0.61	0.62	0.67	0.72	0.76	0.78	0.80	0.80	0.81	0.81	0.82	0.80	0.78	0.77	0.75
95% C.I.	0.02	0.02	0.02	0.02	0.02	0.02	0.02	0.02	0.02	0.02	0.02	0.02	0.02	0.02	0.02	0.03	0.03	0.03	0.03	0.02	0.02	0.02	0.02	0.02
r^2	0.43	0.43	0.46	0.46	0.45	0.48	0.49	0.45	0.42	0.36	0.38	0.49	0.50	0.50	0.47	0.45	0.46	0.46	0.47	0.52	0.52	0.49	0.51	0.50
976 M																								
$m_{h,z}$	0.79	0.79	0.79	0.80	0.78	0.79	0.77	0.77	0.75	0.73	0.72	0.74	0.76	0.78	0.79	0.80	0.80	0.82	0.84	0.85	0.84	0.82	0.82	0.80
95% C.I.	0.02	0.02	0.02	0.02	0.02	0.02	0.02	0.02	0.02	0.02	0.02	0.02	0.02	0.02	0.02	0.02	0.02	0.02	0.02	0.02	0.02	0.02	0.02	0.02
r^2	0.45	0.48	0.51	0.57	0.53	0.58	0.55	0.54	0.47	0.47	0.47	0.52	0.51	0.51	0.49	0.47	0.47	0.50	0.49	0.56	0.56	0.58	0.59	0.59
1754 M																								
$m_{h,z}$	0.80	0.80	0.80	0.80	0.80	0.80	0.79	0.77	0.76	0.74	0.73	0.72	0.72	0.72	0.73	0.75	0.77	0.78	0.80	0.81	0.81	0.80	0.81	0.81
95% C.I.	0.03	0.03	0.03	0.03	0.03	0.03	0.03	0.03	0.03	0.03	0.02	0.02	0.02	0.02	0.02	0.03	0.03	0.03	0.03	0.03	0.03	0.03	0.03	0.03
r^2	0.37	0.40	0.43	0.46	0.44	0.42	0.40	0.35	0.35	0.35	0.38	0.35	0.35	0.35	0.34	0.35	0.33	0.34	0.36	0.39	0.41	0.42	0.41	0.43

Table 4-6. Performance of Non-Linear Curve Fit for Linear Best-Fit Gradient and Elevation to Develop the Overall Regression Model
Parameters (A, B, and C) are for $m_{h(p)} = A(1-e^{-B(Z-C)})$.
Parameters (a, b, and c) are for $m_{h(p)} = a+be^{-cZ}$.

Hour	A	B	C	a	b	c	Constant	r^2
0:00	0.7827	0.0146	-33.7264					0.99
1:00	0.7761	0.0129	-35.3513					0.99
2:00	0.7730	0.0114	-35.3367					0.99
3:00	0.7735	0.0108	-30.2923					0.99
4:00	0.7605	0.0108	-29.0632					0.99
5:00	0.7646	0.0085	-33.1094					0.99
6:00	0.7549	0.0073	-38.6030					0.98
7:00	0.7502	0.0051	-80.8598					0.97
8:00	0.7508	0.0034	-224.3914					0.94
9:00	0.7391	0.0023	-633.1671					0.68
10:00							0.7275	-
11:00				0.7138	0.1148	0.0020		0.52
12:00				0.7099	0.1952	0.0016		0.78
13:00				0.7111	0.2343	0.0014		0.86
14:00				0.7236	0.2419	0.0014		0.87
15:00				0.7397	0.2343	0.0013		0.83
16:00				0.7515	0.2044	0.0011		0.72
17:00				0.7629	0.1367	0.0006		0.34
18:00	0.8721	0.0245	-69.0662					0.58
19:00	0.8619	0.0313	-35.4715					0.88
20:00	0.8400	0.0313	-28.3022					0.94
21:00	0.8216	0.0293	-25.0225					0.98
22:00	0.8072	0.0228	-27.0998					0.99
23:00	0.7919	0.0186	-29.7385					0.99

Table 4-7. Statistical Results of the Performance of the Overall Regression Model $m_{h,z}$ – linear best-fit gradient, 95% C.I. – standard error of $m_{h,z}$ at the 95% confidence interval, s_o and s_p – observed and predicted ozone concentration standard deviation (ppb), MAE – mean absolute error (ppb), MBE – mean bias error (ppb), RMSE – root mean squared error (ppb), r^2 – coefficient of determination, d_1 – index of agreement (α=1)

76M	0:00	1:00	2:00	3:00	4:00	5:00	6:00	7:00	8:00	9:00	10:00	11:00	12:00	13:00	14:00	15:00	16:00	17:00	18:00	19:00	20:00	21:00	22:00	23:00
$m_{h,z}$	0.90	0.89	0.90	0.89	-	0.85	0.84	0.87	0.89	0.88	0.93	0.93	0.95	0.97	0.97	0.97	0.95	0.93	0.91	0.94	0.96	0.96	0.94	0.93
95% C.I.	0.02	0.03	0.02	0.03	-	0.03	0.03	0.03	0.03	0.02	0.02	0.01	0.01	0.01	0.01	0.01	0.01	0.01	0.01	0.01	0.02	0.02	0.02	0.02
s_o	18.09	17.42	16.23	15.79	-	15.10	15.09	13.50	13.75	16.39	18.49	19.73	20.56	20.96	20.50	21.08	21.20	20.33	19.88	20.07	20.11	19.98	19.75	19.00
s_p	13.57	12.81	12.06	11.45	-	9.99	9.19	9.01	10.42	12.88	15.63	17.45	19.03	19.87	20.23	20.47	20.07	18.96	18.20	18.13	17.53	16.74	15.69	14.78
MAE	12.49	12.30	11.15	10.91	-	10.61	11.06	9.90	9.91	10.18	8.34	7.77	6.59	5.50	4.78	4.95	6.19	7.79	8.51	8.50	9.23	10.29	11.04	10.65
MBE	-0.91	-1.08	-0.98	-1.25	-	-1.42	-0.67	-0.53	-1.05	-3.21	-2.70	-3.25	-2.43	-1.69	-1.67	-2.15	-2.79	-4.46	-5.12	-2.75	-1.00	-0.05	-0.38	-0.37
RMSE	15.96	15.56	14.15	14.16	-	13.96	14.36	12.48	12.60	12.89	11.43	10.77	9.64	8.57	7.47	7.13	8.60	10.21	11.05	10.87	11.94	13.17	14.22	13.95
r^2	0.30	0.28	0.31	0.27	-	0.20	0.14	0.21	0.26	0.43	0.64	0.73	0.79	0.84	0.88	0.90	0.85	0.80	0.76	0.73	0.65	0.57	0.49	0.47
d_1	0.50	0.49	0.50	0.50	-	0.46	0.42	0.46	0.49	0.57	0.70	0.75	0.79	0.83	0.86	0.85	0.82	0.76	0.73	0.72	0.70	0.66	0.61	0.60
128M																								
$m_{h,z}$	0.91	0.91	0.90	0.90	0.89	-	0.84	0.82	0.88	0.88	0.90	0.90	0.91	0.93	0.93	0.93	0.92	0.89	0.89	0.92	0.93	0.93	0.93	0.93
95% C.I.	0.02	0.02	0.02	0.02	0.03	-	0.03	0.03	0.02	0.02	0.01	0.01	0.01	0.01	0.01	0.01	0.01	0.01	0.01	0.01	0.01	0.01	0.02	0.02
s_o	19.40	18.84	18.48	18.02	17.92	-	17.37	16.76	14.81	16.06	18.30	19.57	20.36	20.39	20.52	20.84	20.92	19.98	19.73	19.60	19.62	19.67	19.66	19.39
s_p	15.39	14.78	14.17	13.60	13.32	-	11.53	10.61	11.38	13.10	15.67	17.24	18.73	19.48	19.91	20.18	19.85	19.10	18.59	18.41	17.91	17.45	16.84	16.11
MAE	13.87	13.35	12.65	12.44	12.80	-	12.20	11.86	10.71	10.52	8.54	8.92	7.86	6.52	5.93	6.31	7.54	9.53	9.60	8.82	9.24	9.87	11.08	10.66
MBE	-1.07	-0.83	-1.30	-1.10	-1.47	-	-2.54	-3.34	-2.48	-4.26	-4.86	-5.68	-5.32	-4.84	-4.74	-5.09	-5.69	-7.45	-7.34	-5.08	-3.67	-2.54	-1.83	-1.24
RMSE	17.60	16.96	16.53	16.23	16.47	-	15.77	15.20	13.37	13.09	11.68	11.81	10.71	8.99	8.27	8.27	9.79	11.43	12.11	11.19	12.11	12.93	14.53	14.29
r^2	0.28	0.29	0.29	0.28	0.25	-	0.25	0.26	0.30	0.43	0.66	0.72	0.79	0.86	0.89	0.90	0.86	0.81	0.77	0.75	0.66	0.60	0.49	0.48
d_1	0.50	0.50	0.51	0.51	0.49	-	0.47	0.46	0.50	0.56	0.69	0.70	0.75	0.80	0.82	0.81	0.78	0.71	0.70	0.72	0.70	0.67	0.62	0.63
433M																								
$m_{h,z}$	0.91	0.93	0.93	0.93	0.93	0.94	-	0.93	0.89	0.91	0.95	0.93	0.94	0.94	0.94	0.93	0.91	0.90	0.91	0.91	0.91	0.92	0.92	0.92
95% C.I.	0.02	0.02	0.02	0.02	0.02	0.02	-	0.02	0.02	0.02	0.02	0.02	0.01	0.01	0.01	0.01	0.01	0.01	0.01	0.01	0.01	0.02	0.02	0.02
s_o	19.62	18.56	18.59	18.61	18.86	18.93	-	18.25	18.44	17.37	17.17	17.00	17.88	18.12	18.02	18.36	19.06	19.03	18.37	18.40	18.80	19.28	18.53	19.06
s_p	16.64	16.22	16.12	16.14	16.07	15.82	-	14.82	14.27	14.18	15.29	16.01	17.04	17.63	18.02	18.41	18.46	18.22	18.32	18.11	17.70	17.31	17.01	16.64
MAE	13.54	12.73	13.19	13.36	13.12	12.38	-	10.72	10.67	9.77	8.83	8.06	7.05	6.17	5.75	5.92	7.56	8.86	8.73	9.29	9.36	9.65	10.51	11.13
MBE	-2.05	-1.51	-1.24	-1.07	-0.75	-0.49	-	-0.95	-2.99	-3.04	-1.28	-3.22	-3.16	-3.50	-3.70	-4.50	-6.04	-7.14	-5.90	-5.45	-5.55	-4.12	-3.76	-2.98
RMSE	17.83	16.96	17.16	17.21	16.92	16.45	-	14.36	14.42	12.76	11.64	10.86	9.70	8.37	8.27	8.55	10.74	11.31	11.50	12.51	12.71	12.97	13.60	14.27
r^2	0.32	0.33	0.32	0.31	0.33	0.36	-	0.46	0.48	0.50	0.56	0.65	0.74	0.83	0.84	0.85	0.79	0.79	0.73	0.66	0.65	0.61	0.54	0.49
d_1	0.53	0.54	0.52	0.51	0.53	0.55	-	0.59	0.59	0.62	0.65	0.70	0.75	0.79	0.81	0.80	0.76	0.71	0.71	0.69	0.69	0.67	0.63	0.61

Table 4-7. (Continued) Statistical Results of the Performance of the Overall Regression Model $m_{h,z}$ – linear best-fit gradient, 95% C.I. – standard error of $m_{h,z}$ at the 95% confidence interval, s_o and s_p – observed and predicted ozone concentration standard deviation (ppb), MAE – mean absolute error (ppb), MBE – mean bias error (ppb), RMSE – root mean squared error (ppb), r^2 – coefficient of determination, d_1 – index of agreement (α=1)

526M	0:00	1:00	2:00	3:00	4:00	5:00	6:00	7:00	8:00	9:00	10:00	11:00	12:00	13:00	14:00	15:00		17:00	18:00	19:00	20:00	21:00	22:00	23:00
$m_{h,z}$	1.00	1.00	1.01	1.01	1.02	1.02	1.02	1.04	1.05	1.06	1.11	1.07	1.05	1.04	1.03	1.02	1.02	1.01	1.03	1.01	1.00	1.01	1.00	1.00
95% C.I.	0.02	0.02	0.02	0.02	0.02	0.02	0.02	0.02	0.02	0.02	0.02	0.02	0.02	0.02	0.02	0.02	0.02	0.02	0.02	0.02	0.01	0.02	0.02	0.02
s_o	17.40	17.91	17.95	18.05	17.65	17.57	17.43	16.39	15.09	14.32	13.89	15.61	16.49	17.08	18.23	18.91	19.13	19.43	19.25	19.57	18.71	18.45	18.03	17.75
s_p	17.62	17.47	17.38	17.38	17.08	17.07	16.72	16.15	15.53	15.27	16.17	16.98	17.88	18.54	18.96	19.39	19.50	19.39	19.38	19.41	18.92	18.50	18.18	17.83
MAE	11.08	11.20	10.89	10.88	11.00	10.72	10.58	11.02	10.81	11.27	11.69	10.74	11.19	11.29	11.69	12.35	12.29	11.98	11.68	10.98	10.72	10.96	10.80	10.81
MBE	1.50	1.77	2.28	2.47	3.06	2.80	3.32	4.05	4.14	4.72	6.63	4.96	4.34	3.75	3.31	3.09	3.23	2.52	3.54	2.12	1.81	2.02	1.59	1.66
RMSE	14.52	14.78	14.41	14.47	14.35	13.83	13.62	13.82	13.52	13.91	14.90	13.61	13.88	14.20	15.13	15.77	15.91	15.64	15.84	14.66	14.20	14.45	13.78	13.68
r^2	0.43	0.43	0.46	0.46	0.45	0.48	0.49	0.45	0.42	0.36	0.38	0.49	0.50	0.50	0.47	0.45	0.46	0.46	0.47	0.52	0.52	0.49	0.51	0.50
d_1	0.60	0.60	0.61	0.61	0.61	0.61	0.61	0.58	0.56	0.52	0.52	0.59	0.60	0.60	0.61	0.59	0.60	0.61	0.63	0.65	0.64	0.63	0.62	0.62
976M																								
$m_{h,z}$	0.94	0.93	0.94	0.94	0.93	0.94	0.95	0.94	0.94	0.94	0.96	0.95	0.95	0.95	0.95	0.96	0.98	0.98	1.00	0.98	0.97	0.96	0.95	0.95
95% C.I.	0.01	0.01	0.01	0.01	0.01	0.01	0.01	0.01	0.01	0.01	0.02	0.01	0.01	0.01	0.01	0.01	0.01	0.01	0.01	0.01	0.01	0.01	0.01	0.01
s_o	16.71	17.12	17.06	17.14	17.25	17.48	17.02	16.37	15.31	14.51	14.82	14.92	15.20	16.01	15.73	15.67	15.67	16.26	17.24	17.73	17.06	16.58	16.80	16.79
s_p	17.63	17.48	17.41	17.42	17.13	17.22	16.99	16.82	16.62	16.23	16.38	16.44	16.91	17.36	17.74	18.22	18.50	18.84	19.64	19.41	18.92	18.50	18.18	17.83
MAE	11.18	10.76	10.53	9.84	10.18	9.65	9.68	9.77	10.15	9.72	9.89	9.53	9.86	10.22	10.89	11.09	10.88	10.88	10.87	10.05	10.03	9.54	9.59	9.58
MBE	-2.87	-3.04	-2.98	-3.16	-3.08	-2.84	-2.13	-2.85	-2.49	-2.81	-1.29	-2.11	-2.17	-2.50	-2.52	-1.81	-0.83	-0.84	0.58	-0.67	-1.38	-1.74	-2.63	-2.24
RMSE	14.19	13.85	13.22	12.47	12.98	12.22	12.15	12.27	12.62	12.37	12.51	12.03	12.45	12.82	13.26	13.66	13.80	13.69	14.35	13.20	12.80	12.24	12.23	12.06
r^2	0.45	0.48	0.51	0.57	0.53	0.58	0.55	0.54	0.47	0.47	0.47	0.52	0.51	0.51	0.49	0.47	0.47	0.50	0.49	0.56	0.56	0.58	0.59	0.59
d_1	0.60	0.61	0.62	0.65	0.63	0.66	0.64	0.63	0.60	0.60	0.60	0.62	0.62	0.62	0.60	0.60	0.61	0.62	0.63	0.66	0.65	0.66	0.66	0.65
1754M																								
$m_{h,z}$	0.93	0.92	0.92	0.92	0.91	0.92	0.91	0.92	0.93	0.94	0.94	0.95	0.96	0.96	0.96	0.97	0.97	0.98	1.04	1.01	1.00	0.98	0.95	0.94
95% C.I.	0.02	0.02	0.01	0.01	0.02	0.02	0.02	0.02	0.02	0.02	0.02	0.02	0.02	0.02	0.02	0.02	0.02	0.02	0.02	0.02	0.02	0.02	0.02	0.01
s_o	14.83	15.05	15.19	15.19	15.35	15.11	14.89	14.45	14.32	13.76	13.03	12.11	12.18	12.26	12.31	13.48	14.00	14.38	14.57	15.18	14.57	14.45	14.67	14.76
s_p	17.65	17.50	17.43	17.44	17.15	17.24	17.02	16.91	16.91	16.59	16.41	16.17	16.27	16.49	16.82	17.27	17.62	18.22	19.67	19.44	18.94	18.53	18.20	17.86
MAE	11.96	11.41	11.26	11.05	11.76	11.52	11.55	11.76	11.35	11.04	10.47	10.57	10.49	10.83	11.19	11.31	11.84	11.88	12.35	11.92	11.42	11.27	11.44	11.65
MBE	-4.16	-4.39	-4.74	-4.63	-5.36	-4.78	-5.09	-4.37	-3.35	-3.29	-2.93	-2.87	-2.26	-1.77	-1.73	-1.45	-1.42	-0.33	3.41	1.73	0.26	-1.07	-2.54	-3.73
RMSE	15.23	14.83	14.49	14.06	14.69	14.48	14.75	15.06	14.86	14.46	13.53	13.44	13.42	13.70	14.02	14.20	14.83	15.06	16.18	15.54	14.73	14.23	14.47	14.22
r^2	0.37	0.40	0.43	0.46	0.44	0.42	0.40	0.35	0.35	0.35	0.38	0.35	0.35	0.35	0.34	0.35	0.33	0.34	0.36	0.39	0.41	0.42	0.41	0.43
d_1	0.55	0.57	0.58	0.59	0.57	0.56	0.56	0.54	0.55	0.55	0.56	0.54	0.54	0.53	0.52	0.54	0.53	0.54	0.54	0.57	0.57	0.57	0.57	0.56

Table 4-8. Comparison of Relative Performance in Terms of the Statistical Results Produced by the Overall Regression Model When the Model Developed with 1998 Ozone Data Was Applied to Four-Year Ozone Data (1995 – 1998)

Year	s_o (ppb)	s_p (ppb)	$s_o - s_p$ (ppb)	MBE (ppb)	MAE (ppb)	RMSE (ppb)	r^2	d_1
1995	16.34	16.26	0.08	-4.62	10.93	13.98	0.45	0.59
1996	15.63	16.22	-0.60	-2.22	9.62	12.39	0.50	0.63
1997	16.54	16.93	-0.39	-1.78	10.20	13.29	0.48	0.62
1998	18.92	18.77	0.16	-1.43	10.36	13.48	0.56	0.66

Table 4-9. Statistical Parameters Used to Develop the "Clear" Component Regression Model Based on "Prediction based on Cloud Cover/Present Day's Maximum" Method $m_{h,z}$ - linear best-fit gradient, 95% C.I. – standard error of $m_{h,z}$ at the 95% confidence interval, r^2 – coefficient of determination

0 M (NC)	0:00	1:00	2:00	3:00	4:00	5:00	6:00	7:00	8:00	9:00	10:00	11:00	12:00	13:00	14:00	15:00	16:00	17:00	18:00	19:00	20:00	21:00	22:00	23:00
$m_{h,z}$	0.27	0.25	0.21	-	0.15	0.14	0.13	0.24	0.39	0.56	0.70	0.83	0.91	0.95	0.97	0.97	0.94	0.80	0.62	0.52	0.44	0.38	0.35	0.34
95% C.I.	0.03	0.03	0.03	-	0.02	0.02	0.02	0.02	0.03	0.02	0.02	0.02	0.02	0.01	0.01	0.01	0.01	0.02	0.03	0.04	0.04	0.04	0.04	0.03
r^2	0.01	0.01	0.05	-	0.01	0.02	0.01	0.11	0.25	0.71	0.83	0.87	0.88	0.95	0.97	0.98	0.92	0.73	0.47	0.37	0.32	0.25	0.27	0.36
0 M (TN)																								
$m_{h,z}$	0.26	0.23	0.19	0.17	0.13	0.10	0.09	0.16	0.33	0.47	0.63	0.77	0.87	0.92	0.94	0.94	0.92	0.86	0.73	0.60	0.51	0.42	0.33	0.30
95% C.I.	0.01	0.01	0.01	0.01	0.01	0.01	0.01	0.01	0.01	0.01	0.02	0.01	0.01	0.01	0.01	0.01	0.01	0.01	0.01	0.01	0.01	0.01	0.01	0.01
r^2	0.12	0.09	0.03	0.02	0.01	0.00	0.00	0.15	0.30	0.39	0.52	0.71	0.87	0.91	0.94	0.93	0.89	0.80	0.70	0.55	0.43	0.41	0.37	0.27
76 M																								
$m_{h,z}$	0.58	0.56	0.54	0.53	-	0.50	0.43	0.41	0.43	0.60	0.73	0.83	0.91	0.94	0.94	0.96	0.98	0.96	0.93	0.91	0.87	0.82	0.81	0.75
95% C.I.	0.04	0.04	0.04	0.03	-	0.03	0.03	0.04	0.03	0.03	0.03	0.02	0.02	0.01	0.01	0.01	0.01	0.01	0.02	0.03	0.03	0.03	0.04	0.04
r^2	0.40	0.37	0.43	0.37	-	0.34	0.35	0.27	0.13	0.46	0.66	0.80	0.89	0.93	0.93	0.95	0.95	0.94	0.83	0.71	0.59	0.60	0.58	0.50
128 M																								
$m_{h,z}$	0.66	0.65	0.62	0.61	0.62	-	0.58	0.57	0.54	0.64	0.78	0.87	0.93	0.95	0.96	0.98	1.00	0.98	0.94	0.93	0.90	0.86	0.82	0.78
95% C.I.	0.04	0.04	0.04	0.03	0.03	-	0.03	0.03	0.03	0.03	0.03	0.02	0.02	0.01	0.01	0.01	0.01	0.01	0.02	0.02	0.03	0.03	0.04	0.04
r^2	0.47	0.46	0.48	0.41	0.45	-	0.55	0.57	0.53	0.66	0.78	0.85	0.87	0.93	0.95	0.96	0.96	0.96	0.88	0.84	0.72	0.68	0.51	0.39
433 M																								
$m_{h,z}$	0.78	0.74	0.71	0.72	0.73	0.73	-	0.72	0.72	0.71	0.76	0.81	0.86	0.88	0.89	0.91	0.95	0.96	0.94	0.94	0.92	0.90	0.90	0.88
95% C.I.	0.03	0.03	0.03	0.04	0.03	0.03	-	0.03	0.03	0.03	0.03	0.02	0.02	0.01	0.01	0.01	0.01	0.01	0.02	0.02	0.03	0.03	0.04	0.03
r^2	0.68	0.64	0.54	0.48	0.61	0.62	-	0.75	0.71	0.70	0.79	0.88	0.90	0.92	0.95	0.97	0.96	0.92	0.84	0.83	0.76	0.74	0.62	0.63
526 M																								
$m_{h,z}$	0.74	0.73	0.73	0.73	0.71	0.72	0.71	0.67	0.64	0.62	0.62	0.67	0.72	0.76	0.78	0.81	0.81	0.81	0.82	0.83	0.80	0.78	0.77	0.75
95% C.I.	0.02	0.02	0.02	0.02	0.02	0.02	0.01	0.01	0.01	0.01	0.01	0.02	0.02	0.02	0.02	0.02	0.02	0.02	0.02	0.02	0.02	0.02	0.02	0.02
r^2	0.53	0.55	0.55	0.56	0.54	0.57	0.60	0.54	0.52	0.50	0.44	0.50	0.42	0.37	0.34	0.29	0.32	0.33	0.37	0.43	0.42	0.38	0.41	0.41
976 M																								
$m_{h,z}$	0.76	0.77	0.77	0.77	0.76	0.77	0.75	0.75	0.73	0.72	0.70	0.72	0.73	0.76	0.77	0.78	0.77	0.79	0.81	0.83	0.80	0.79	0.79	0.78
95% C.I.	0.02	0.02	0.02	0.01	0.02	0.01	0.02	0.01	0.02	0.01	0.02	0.02	0.02	0.02	0.02	0.02	0.02	0.02	0.02	0.02	0.02	0.02	0.02	0.02
r^2	0.53	0.54	0.55	0.63	0.55	0.64	0.59	0.63	0.50	0.54	0.52	0.55	0.49	0.43	0.39	0.36	0.32	0.35	0.34	0.45	0.47	0.51	0.49	0.52
1754 M																								
$m_{h,z}$	0.79	0.79	0.79	0.80	0.78	0.78	0.79	0.77	0.75	0.74	0.73	0.71	0.70	0.70	0.71	0.74	0.75	0.76	0.77	0.79	0.78	0.78	0.79	0.79
95% C.I.	0.02	0.02	0.02	0.02	0.02	0.02	0.02	0.02	0.02	0.02	0.02	0.02	0.02	0.02	0.02	0.02	0.02	0.02	0.02	0.02	0.02	0.02	0.02	0.02
r^2	0.53	0.56	0.58	0.61	0.61	0.56	0.54	0.46	0.46	0.42	0.47	0.45	0.46	0.45	0.41	0.36	0.29	0.29	0.31	0.39	0.44	0.44	0.43	0.43

Table 4-10. Performance of Non-Linear Curve Fit for Linear Best-Fit Gradient and Elevation to Develop the "Clear" Component Regression Model
Parameters (A, B, and C) are for $m_{h(p)} = A(1-e^{-B(Z-C)})$.
Parameters (a, b, and c) are for $m_{h(p)} = a+be^{-cZ}$.

Hour	A	B	C	a	b	c	Constant	r^2
0:00	0.77094	0.01225	-34.5299					0.99
1:00	0.76411	0.01209	-30.8328					0.99
2:00	0.76072	0.01145	-27.5183					0.99
3:00	0.76591	0.01117	-22.7437					0.98
4:00	0.75451	0.01179	-17.6617					0.99
5:00	0.75772	0.01154	-14.5334					0.99
6:00	0.76131	0.00943	-16.0876					0.99
7:00	0.74498	0.00726	-42.3804					0.98
8:00	0.74632	0.00394	-163.7838					0.96
9:00	0.72255	0.00424	-309.7023					0.82
10:00							0.7170	-
11:00				0.70072	0.12447	0.00172		0.55
12:00				0.68945	0.22644	0.00152		0.83
13:00				0.68636	0.27087	0.00138		0.91
14:00				0.70353	0.26598	0.00142		0.93
15:00				0.72424	0.25317	0.00137		0.91
16:00				0.73080	0.24030	0.00117		0.79
17:00				0.74244	0.16505	0.00071		0.39
18:00	0.85616	0.19301	-6.7679					0.55
19:00	0.85784	0.26406	-4.0277					0.83
20:00	0.83811	0.25514	-3.2778					0.90
21:00	0.81694	0.24773	-2.7166					0.95
22:00	0.81079	0.26149	-2.0898					0.97
23:00	0.79765	0.02937	-17.2420					0.97

Table 4-11. Statistical Parameters Used to Develop the "Cloudy" Component Regression Model Based on "Prediction based on Cloud Cover/Present Day's Maximum" Method $m_{h,z}$ - linear best-fit gradient, 95% C.I. – standard error of $m_{h,z}$ at the 95% confidence interval, r^2 – coefficient of determination

0 M (NC)	0:00	1:00	2:00	3:00	4:00	5:00	6:00	7:00	8:00	9:00	10:00	11:00	12:00	13:00	14:00	15:00	16:00	17:00	18:00	19:00	20:00	21:00	22:00	23:00
$m_{h,z}$	0.27	0.23	0.21	-	0.16	0.15	0.16	0.25	0.40	0.56	0.70	0.81	0.88	0.93	0.94	0.93	0.88	0.79	0.64	0.52	0.45	0.40	0.35	0.31
95% C.I.	0.02	0.02	0.02	-	0.02	0.02	0.02	0.02	0.03	0.03	0.02	0.02	0.01	0.01	0.01	0.01	0.02	0.02	0.02	0.03	0.03	0.03	0.02	0.02
r^2	0.09	0.05	0.04	-	0.03	0.03	0.02	0.05	0.12	0.35	0.58	0.76	0.89	0.94	0.95	0.91	0.86	0.74	0.50	0.34	0.28	0.24	0.21	0.15
0 M (TN)																								
$m_{h,z}$	0.47	0.49	0.48	0.45	0.41	0.39	0.36	0.39	0.50	0.56	0.65	0.72	0.78	0.81	0.85	0.88	0.90	0.87	0.78	0.68	0.56	0.51	0.49	0.45
95% C.I.	0.05	0.05	0.05	0.05	0.05	0.04	0.04	0.04	0.04	0.04	0.03	0.03	0.03	0.03	0.02	0.02	0.02	0.02	0.02	0.03	0.03	0.04	0.04	0.04
r^2	0.00	0.01	0.01	0.01	0.00	0.00	0.00	0.00	0.11	0.18	0.34	0.41	0.51	0.51	0.67	0.71	0.68	0.69	0.57	0.33	0.12	0.04	0.01	0.00
76 M																								
$m_{h,z}$	0.60	0.57	0.55	0.52	-	0.44	0.41	0.39	0.48	0.61	0.75	0.84	0.92	0.95	0.97	0.99	0.98	0.96	0.89	0.84	0.79	0.75	0.69	0.64
95% C.I.	0.02	0.03	0.03	0.03	-	0.02	0.03	0.02	0.03	0.03	0.02	0.02	0.02	0.01	0.01	0.01	0.01	0.01	0.02	0.02	0.02	0.02	0.02	0.02
r^2	0.36	0.35	0.34	0.28	-	0.19	0.14	0.17	0.16	0.38	0.72	0.77	0.85	0.91	0.93	0.93	0.93	0.89	0.82	0.77	0.66	0.60	0.62	0.62
128 M																								
$m_{h,z}$	0.69	0.66	0.65	0.63	0.61	-	0.52	0.49	0.52	0.64	0.77	0.86	0.94	0.98	1.00	1.02	1.01	0.99	0.95	0.91	0.86	0.82	0.78	0.74
95% C.I.	0.03	0.03	0.03	0.03	0.04	-	0.03	0.03	0.03	0.03	0.02	0.02	0.01	0.01	0.01	0.01	0.01	0.01	0.02	0.02	0.02	0.02	0.02	0.02
r^2	0.21	0.22	0.21	0.20	0.12	-	0.08	0.11	0.11	0.28	0.59	0.73	0.86	0.92	0.95	0.94	0.93	0.89	0.84	0.79	0.68	0.60	0.59	0.61
433 M																								
$m_{h,z}$	0.78	0.79	0.80	0.79	0.76	0.76	-	0.70	0.70	0.68	0.71	0.77	0.84	0.89	0.91	0.94	0.96	0.96	0.94	0.91	0.90	0.85	0.83	0.79
95% C.I.	0.03	0.03	0.03	0.03	0.03	0.03	-	0.03	0.03	0.02	0.02	0.02	0.02	0.01	0.01	0.01	0.01	0.01	0.02	0.02	0.02	0.02	0.02	0.02
r^2	0.22	0.32	0.31	0.32	0.29	0.36	-	0.43	0.40	0.45	0.49	0.66	0.80	0.88	0.90	0.92	0.87	0.88	0.79	0.71	0.74	0.67	0.66	0.55
526 M																								
$m_{h,z}$	0.91	0.87	0.82	0.82	0.82	0.79	0.74	0.73	0.71	0.69	0.72	0.74	0.77	0.80	0.84	0.85	0.86	0.86	0.86	0.87	0.86	0.83	0.83	0.81
95% C.I.	0.05	0.05	0.05	0.05	0.05	0.05	0.05	0.05	0.05	0.05	0.05	0.04	0.04	0.03	0.03	0.03	0.03	0.03	0.03	0.03	0.03	0.03	0.03	0.03
r^2	0.04	0.02	0.04	0.05	0.01	0.06	0.03	0.03	0.00	0.00	0.02	0.04	0.14	0.32	0.43	0.37	0.43	0.35	0.36	0.54	0.51	0.56	0.54	0.47
976 M																								
$m_{h,z}$	1.04	0.99	0.95	0.95	0.93	0.93	0.90	0.91	0.89	0.89	0.87	0.90	0.89	0.88	0.93	0.95	0.94	0.95	0.95	0.94	0.95	0.94	0.93	0.91
95% C.I.	0.03	0.03	0.03	0.03	0.04	0.03	0.04	0.04	0.04	0.04	0.04	0.04	0.04	0.04	0.03	0.03	0.03	0.02	0.03	0.03	0.03	0.02	0.02	0.02
r^2	0.53	0.34	0.43	0.40	0.34	0.46	0.41	0.30	0.23	0.14	0.18	0.21	0.10	0.22	0.31	0.29	0.33	0.49	0.43	0.47	0.47	0.51	0.57	0.53
1754 M																								
$m_{h,z}$	1.04	1.05	1.04	1.02	1.04	1.00	0.99	0.99	0.96	0.95	0.96	0.96	0.95	0.96	0.95	0.96	0.97	0.97	0.99	0.98	0.98	0.97	0.96	0.96
95% C.I.	0.04	0.04	0.03	0.03	0.03	0.03	0.03	0.03	0.03	0.03	0.03	0.03	0.03	0.03	0.03	0.03	0.04	0.04	0.03	0.03	0.03	0.03	0.03	0.03
r^2	0.02	0.19	0.31	0.35	0.33	0.25	0.31	0.26	0.16	0.21	0.25	0.14	0.11	0.12	0.11	0.12	0.08	0.10	0.24	0.30	0.27	0.12	0.12	0.14

Table 4-12. Performance of Non-Linear Curve Fit for Linear Best-Fit Gradient and Elevation to Develop the "Cloudy" Component Regression Model
Parameters (A, B, and C) are for $m_{h(p)} = A(1-e^{-B(Z-C)})$.

Hour	A	B	C	Constant	r^2
0:00	1.03410	0.00323	-154.0397		0.93
1:00	1.03592	0.00282	-170.8132		0.92
2:00	1.01651	0.00275	-171.9942		0.92
3:00	1.02445	0.00208	-285.3263		0.99
4:00	1.01917	0.00263	-137.2405		0.93
5:00	1.00417	0.00247	-132.4517		0.96
6:00	0.98624	0.00230	-146.4764		0.96
7:00	1.00737	0.00188	-202.0384		0.98
8:00	0.97861	0.00154	-381.3834		0.97
9:00	0.98070	0.00112	-775.0110		0.95
10:00	0.98201	0.00077	-1562.3570		0.82
11:00	0.98265	0.00059	-2672.5930		0.58
12:00				0.8721	-
13:00				0.8787	-
14:00				0.9061	-
15:00				0.9192	-
16:00				0.9203	-
17:00	0.94886	0.45783	-4.5037		0.63
18:00	0.93881	0.37903	-3.7286		0.78
19:00	0.91997	0.32633	-3.2507		0.84
20:00	0.90353	0.20617	-3.9380		0.87
21:00	0.91231	0.01314	-52.1956		0.93
22:00	0.90719	0.00996	-63.3384		0.93
23:00	0.89467	0.00842	-66.3829		0.92

Table 4-13. Statistical Parameters Used to Develop the "Clear to Partly Cloudy" Component Regression Model Based on "Prediction based on Cloud Cover/Present Day's Maximum" Method $m_{h,z}$ - linear best-fit gradient, 95% C.I. – standard error of $m_{h,z}$ at the 95% confidence interval, r^2 – coefficient of determination

0 M (NC)	0:00	1:00		3:00	4:00	5:00	6:00	7:00	8:00	9:00	10:00	11:00	12:00	13:00	14:00	15:00	16:00	17:00	18:00	19:00	20:00	21:00	22:00	23:00
$m_{h,z}$	0.31	0.30	0.27	-	0.22	0.21	0.22	0.28	0.43	0.59	0.72	0.82	0.88	0.92	0.94	0.94	0.90	0.80	0.65	0.53	0.46	0.41	0.38	0.35
95% C.I.	0.02	0.02	0.01	-	0.01	0.01	0.01	0.01	0.01	0.01	0.01	0.01	0.01	0.01	0.01	0.01	0.01	0.01	0.01	0.02	0.02	0.02	0.02	0.02
r^2	0.07	0.05	0.04	-	0.01	0.02	0.03	0.09	0.24	0.50	0.71	0.81	0.88	0.93	0.95	0.93	0.86	0.71	0.50	0.37	0.29	0.20	0.19	0.17
0 M (TN)																								
$m_{h,z}$	0.28	0.26	0.22	0.20	0.17	0.14	0.13	0.20	0.35	0.49	0.64	0.77	0.87	0.92	0.94	0.94	0.92	0.86	0.74	0.62	0.52	0.43	0.36	0.32
95% C.I.	0.01	0.01	0.01	0.01	0.01	0.01	0.01	0.01	0.01	0.01	0.01	0.01	0.01	0.01	0.01	0.01	0.01	0.01	0.01	0.01	0.01	0.01	0.01	0.01
r^2	0.04	0.01	0.00	0.00	0.00	0.01	0.02	0.01	0.18	0.34	0.53	0.68	0.84	0.91	0.93	0.93	0.87	0.78	0.67	0.50	0.40	0.32	0.19	0.17
76 M																								
$m_{h,z}$	0.64	0.60	0.56	0.54	-	0.49	0.44	0.43	0.49	0.64	0.77	0.86	0.91	0.93	0.94	0.97	0.97	0.94	0.92	0.88	0.84	0.79	0.75	0.70
95% C.I.	0.02	0.02	0.02	0.02	-	0.02	0.02	0.02	0.02	0.02	0.02	0.01	0.01	0.01	0.01	0.01	0.01	0.01	0.01	0.02	0.02	0.02	0.02	0.02
r^2	0.27	0.25	0.29	0.25	-	0.24	0.19	0.21	0.23	0.41	0.65	0.78	0.83	0.85	0.91	0.92	0.85	0.77	0.72	0.66	0.60	0.51	0.38	0.32
128 M																								
$m_{h,z}$	0.71	0.68	0.65	0.64	0.63	-	0.57	0.55	0.56	0.67	0.80	0.88	0.93	0.95	0.97	0.99	0.99	0.98	0.96	0.93	0.89	0.85	0.81	0.76
95% C.I.	0.02	0.02	0.02	0.02	0.02	-	0.02	0.02	0.02	0.02	0.01	0.01	0.01	0.01	0.01	0.01	0.01	0.01	0.01	0.01	0.01	0.02	0.02	0.02
r^2	0.25	0.26	0.29	0.26	0.33	-	0.36	0.33	0.34	0.43	0.73	0.76	0.80	0.89	0.93	0.93	0.86	0.81	0.73	0.70	0.67	0.57	0.40	0.35
433 M																								
$m_{h,z}$	0.79	0.76	0.75	0.75	0.74	0.73	-	0.70	0.71	0.72	0.75	0.80	0.84	0.87	0.89	0.91	0.94	0.94	0.93	0.92	0.90	0.87	0.84	0.83
95% C.I.	0.02	0.02	0.02	0.02	0.02	0.02	-	0.02	0.02	0.02	0.02	0.01	0.01	0.01	0.01	0.01	0.01	0.01	0.02	0.02	0.02	0.02	0.02	0.02
r^2	0.40	0.38	0.37	0.33	0.37	0.39	-	0.49	0.54	0.56	0.65	0.74	0.78	0.86	0.89	0.89	0.84	0.78	0.72	0.65	0.62	0.60	0.49	0.48
526 M																								
$m_{h,z}$	0.73	0.72	0.72	0.72	0.70	0.70	0.68	0.64	0.62	0.60	0.61	0.67	0.72	0.75	0.78	0.80	0.80	0.81	0.80	0.81	0.80	0.77	0.77	0.75
95% C.I.	0.01	0.01	0.01	0.01	0.01	0.01	0.01	0.01	0.01	0.01	0.01	0.01	0.01	0.01	0.01	0.01	0.01	0.01	0.01	0.01	0.01	0.01	0.01	0.01
r^2	0.45	0.44	0.45	0.45	0.47	0.47	0.48	0.44	0.41	0.36	0.37	0.47	0.45	0.41	0.39	0.37	0.37	0.38	0.39	0.44	0.44	0.40	0.43	0.42
976 M																								
$m_{h,z}$	0.78	0.78	0.78	0.78	0.77	0.77	0.76	0.76	0.74	0.72	0.71	0.72	0.75	0.77	0.78	0.79	0.79	0.81	0.83	0.84	0.83	0.81	0.81	0.79
95% C.I.	0.01	0.01	0.01	0.01	0.01	0.01	0.01	0.01	0.01	0.01	0.01	0.01	0.01	0.01	0.01	0.01	0.01	0.01	0.01	0.01	0.01	0.01	0.01	0.01
r^2	0.47	0.49	0.50	0.57	0.52	0.58	0.55	0.54	0.46	0.48	0.47	0.52	0.49	0.47	0.44	0.42	0.40	0.42	0.42	0.49	0.50	0.52	0.52	0.53
1754 M																								
$m_{h,z}$	0.79	0.78	0.79	0.79	0.78	0.78	0.78	0.76	0.75	0.73	0.72	0.71	0.70	0.71	0.72	0.74	0.75	0.77	0.79	0.80	0.79	0.79	0.80	0.80
95% C.I.	0.01	0.01	0.01	0.01	0.01	0.01	0.01	0.01	0.01	0.01	0.01	0.01	0.01	0.01	0.01	0.01	0.01	0.01	0.01	0.01	0.01	0.01	0.01	0.01
r^2	0.40	0.42	0.44	0.47	0.46	0.43	0.40	0.35	0.35	0.36	0.39	0.37	0.37	0.35	0.33	0.33	0.31	0.31	0.32	0.35	0.37	0.39	0.39	0.42

Table 4-14. Performance of Non-Linear Curve Fit for Linear Best-Fit Gradient and Elevation to Develop the "Clear to Partly Cloudy" Component Regression Model
Parameters (A, B, and C) are for $m_{h(p)} = A(1-e^{-B(Z-C)})$.
Parameters (a, b, and c) are for $m_{h(p)} = a+be^{-cZ}$.

Hour	A	B	C	a	b	c	Constant	r^2
0:00	0.77446	0.01620	-30.2226					0.99
1:00	0.76718	0.01378	-32.5093					0.99
2:00	0.76598	0.01209	-32.5956					0.99
3:00	0.76693	0.01173	-25.7254					0.99
4:00	0.75591	0.01138	-26.4487					0.98
5:00	0.75744	0.00963	-27.8423					0.99
6:00	0.75150	0.00837	-31.8339					0.98
7:00	0.73808	0.00630	-64.2428					0.97
8:00	0.73598	0.00408	-188.5564					0.94
9:00	0.70113	0.01191	-122.6802					0.69
10:00							0.7148	-
11:00				0.69777	0.13710	0.00170		0.54
12:00				0.69519	0.21028	0.00154		0.81
13:00				0.69661	0.24554	0.00137		0.88
14:00				0.71043	0.25037	0.00135		0.90
15:00				0.72768	0.24309	0.00127		0.86
16:00				0.73881	0.21661	0.00111		0.75
17:00				0.75132	0.14744	0.00066		0.38
18:00	0.85897	0.24162	-6.8075					0.53
19:00	0.85443	0.28884	-3.8388					0.85
20:00	0.83341	0.29057	-3.0272					0.93
21:00	0.81093	0.19814	-3.6748					0.97
22:00	0.79542	0.12762	-4.8578					0.98
23:00	0.79366	0.02099	-26.0360					0.99

Table 4-15. Comparison of the Performances of "Overall," "Clear," "Cloudy," and "Clear to Partly Cloudy" Component Regression Models

Name of Model	s_o	s_p	$s_o - s_p$	MBE	MAE	RMSE	r^2	d_1
Overall	18.92	18.77	0.16	-1.43	10.36	13.48	0.56	0.66
Clear	18.77	19.80	-1.03	-1.63E-13	11.29	14.34	0.48	0.64
Cloudy	18.13	17.23	0.90	2.54E-13	8.64	11.51	0.55	0.69
Clear to Partly Cloudy	18.92	18.52	0.40	4.26E-13	9.37	12.37	0.55	0.69

Appendix B

Figures Discussed in Body of Report

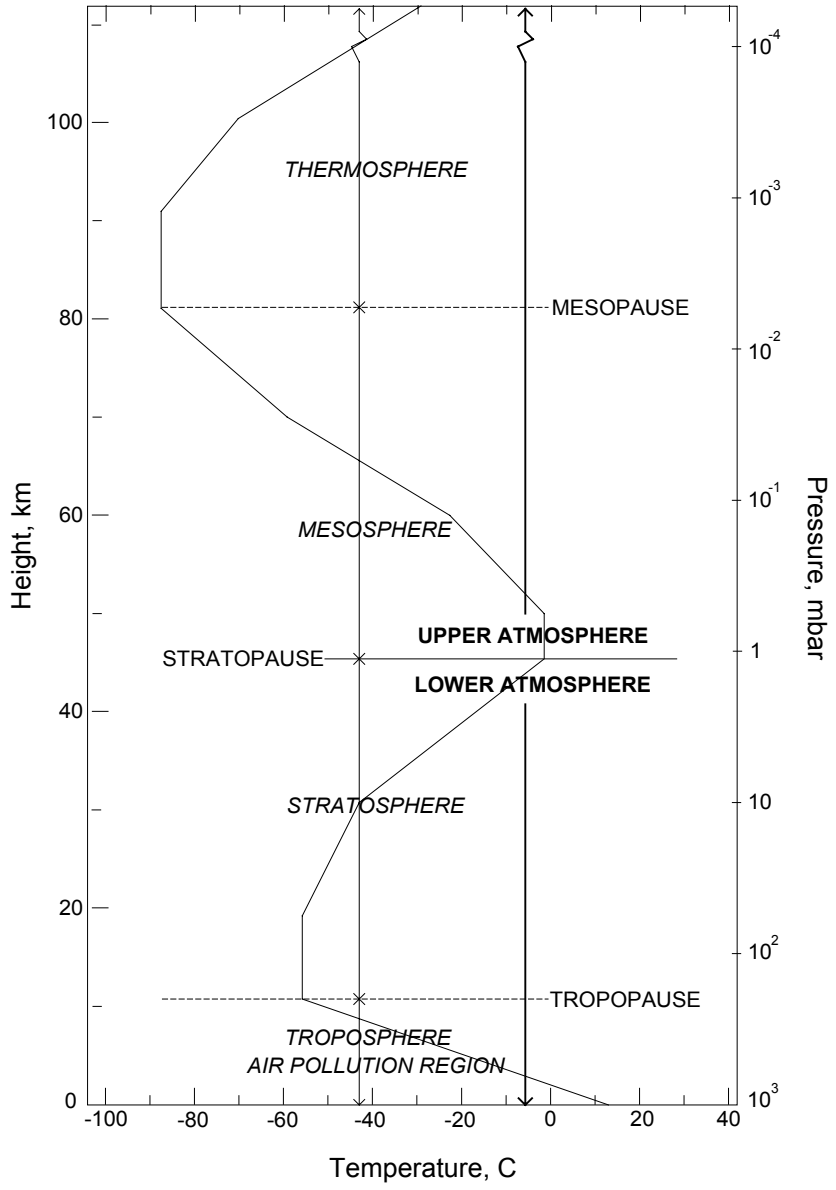

Figure 2-1. Layers of the Atmosphere
Adapted from Seinfeld et al., 1997

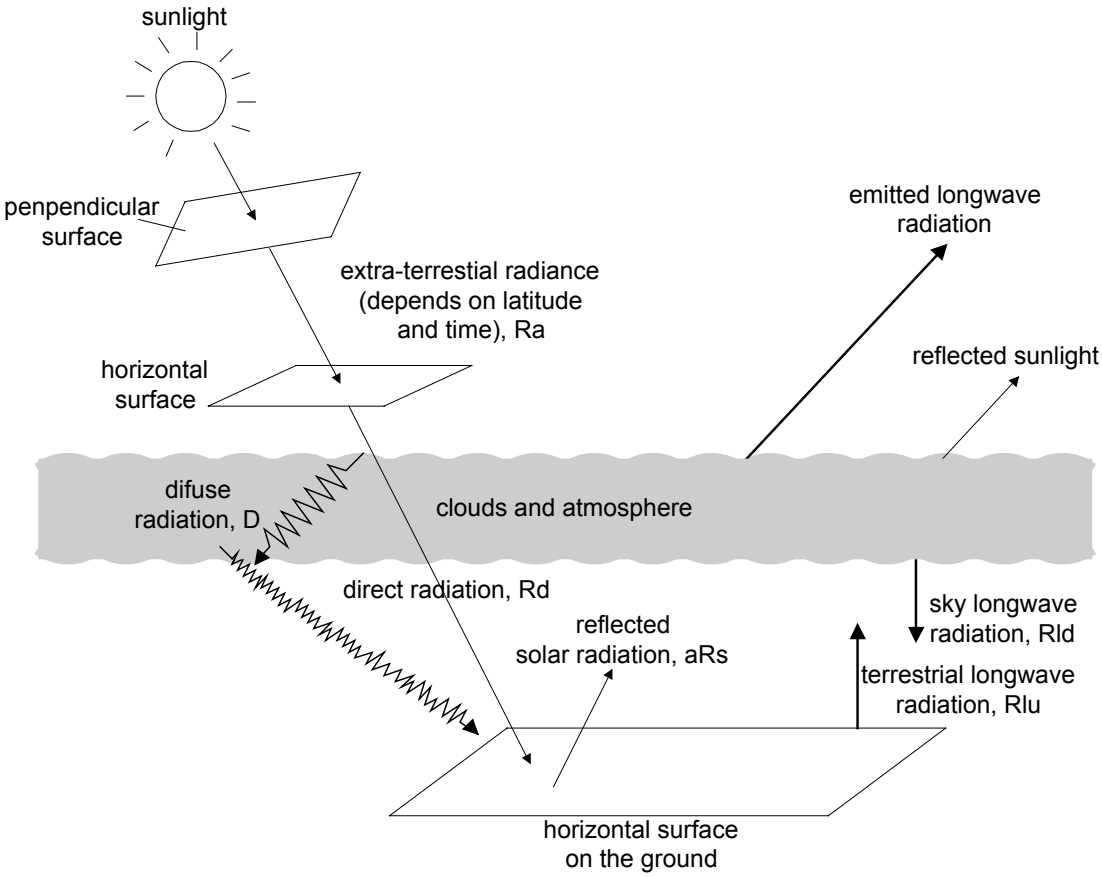

Figure 2-2. Solar Radiation Fluxes
Adapted from Linacre et al., 1997

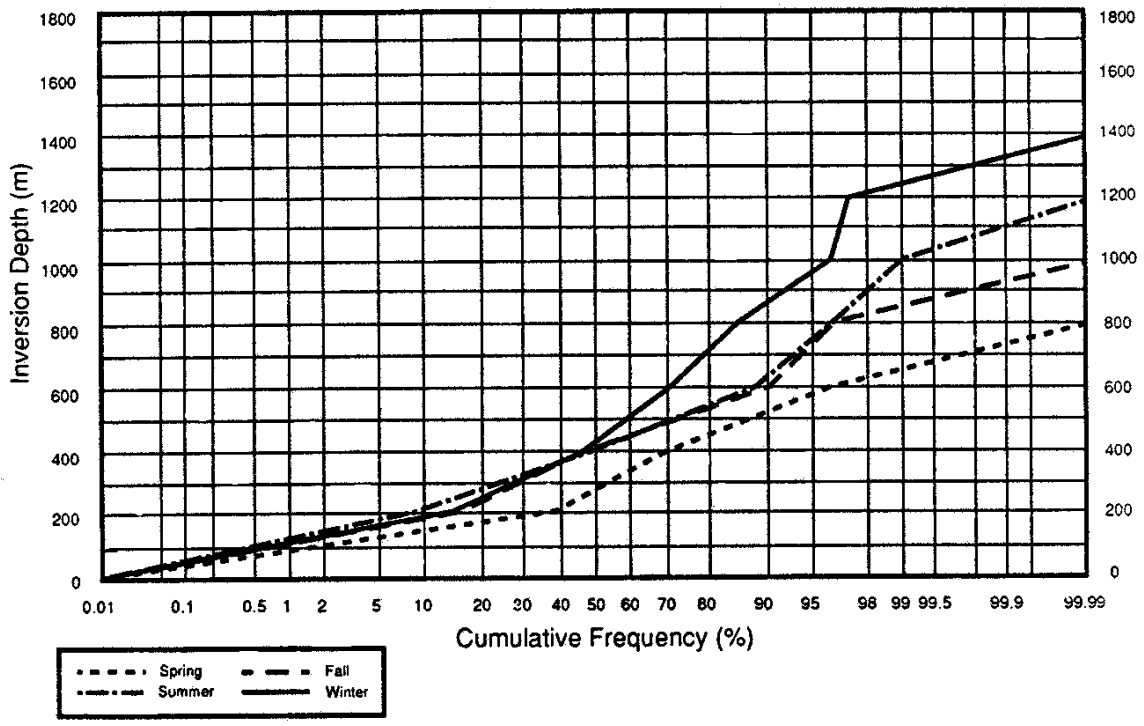

Figure 2-3. Cumulative Frequency Distribution of Inversion Depth in the Early Morning Sounding as a Function of Season
Adapted from Myrick et al., 1994

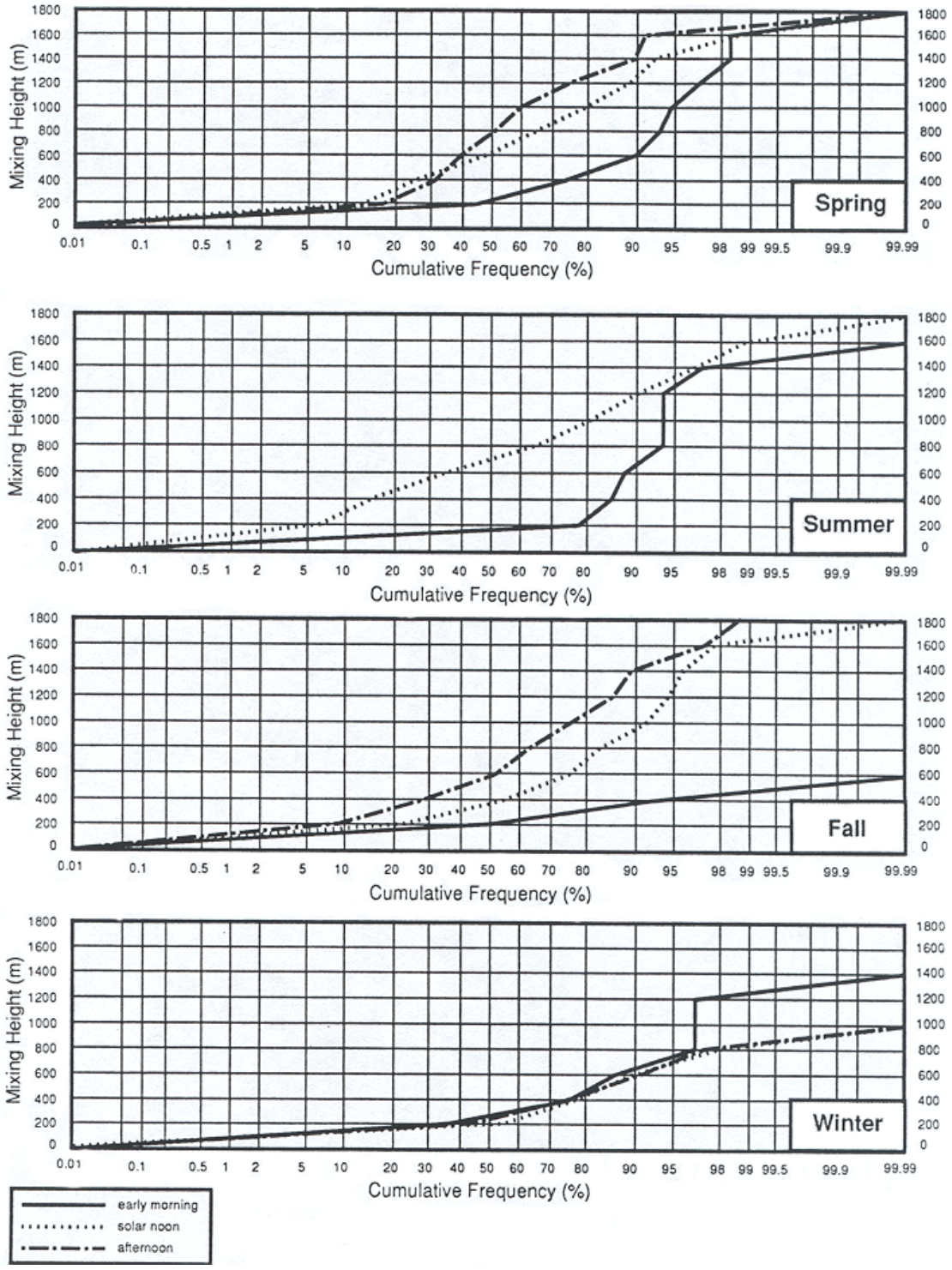

Figure 2-4. Cumulative Frequency Distribution of Mixing Height as a Function of Season and Time of Day Adapted from Myrick et al., 1994

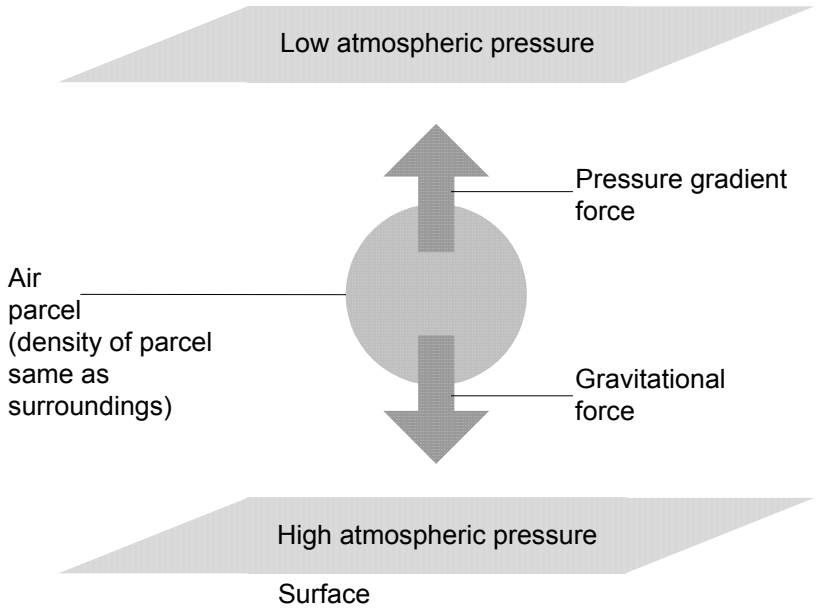

Figure 2-5. Vertical Motion that Occurs in the Atmosphere When the Vertical Forces, Pressure Gradient Force and Gravitational Force are Unbalanced
Adapted from Eagleman, 1980

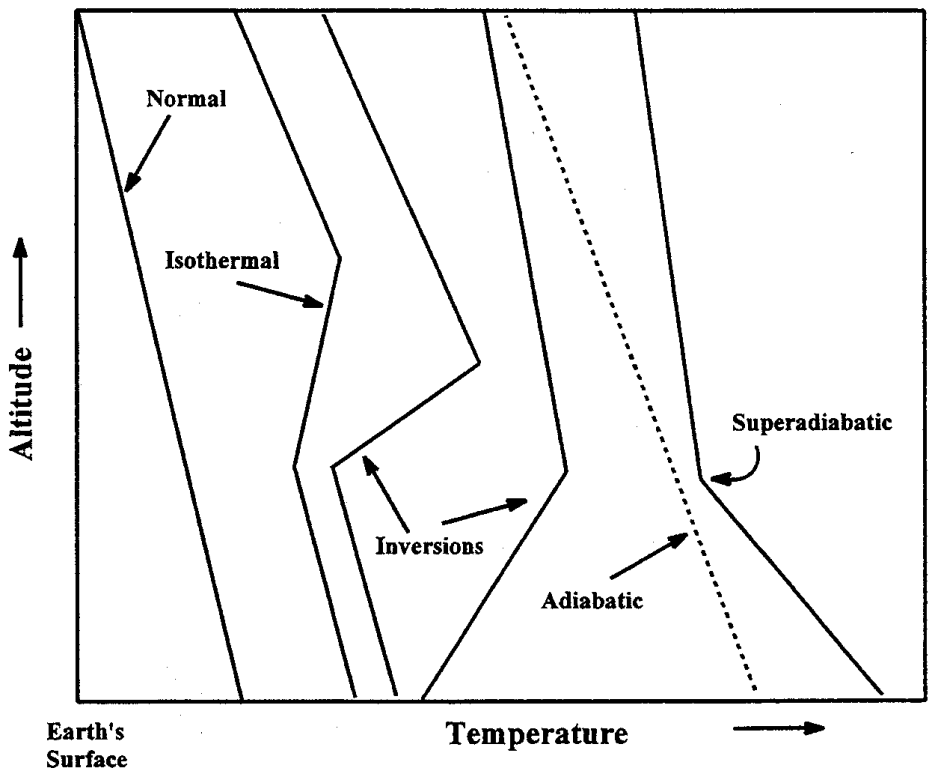

Figure 2-6. Vertical Temperature Structure
Adapted from Slade, 1968

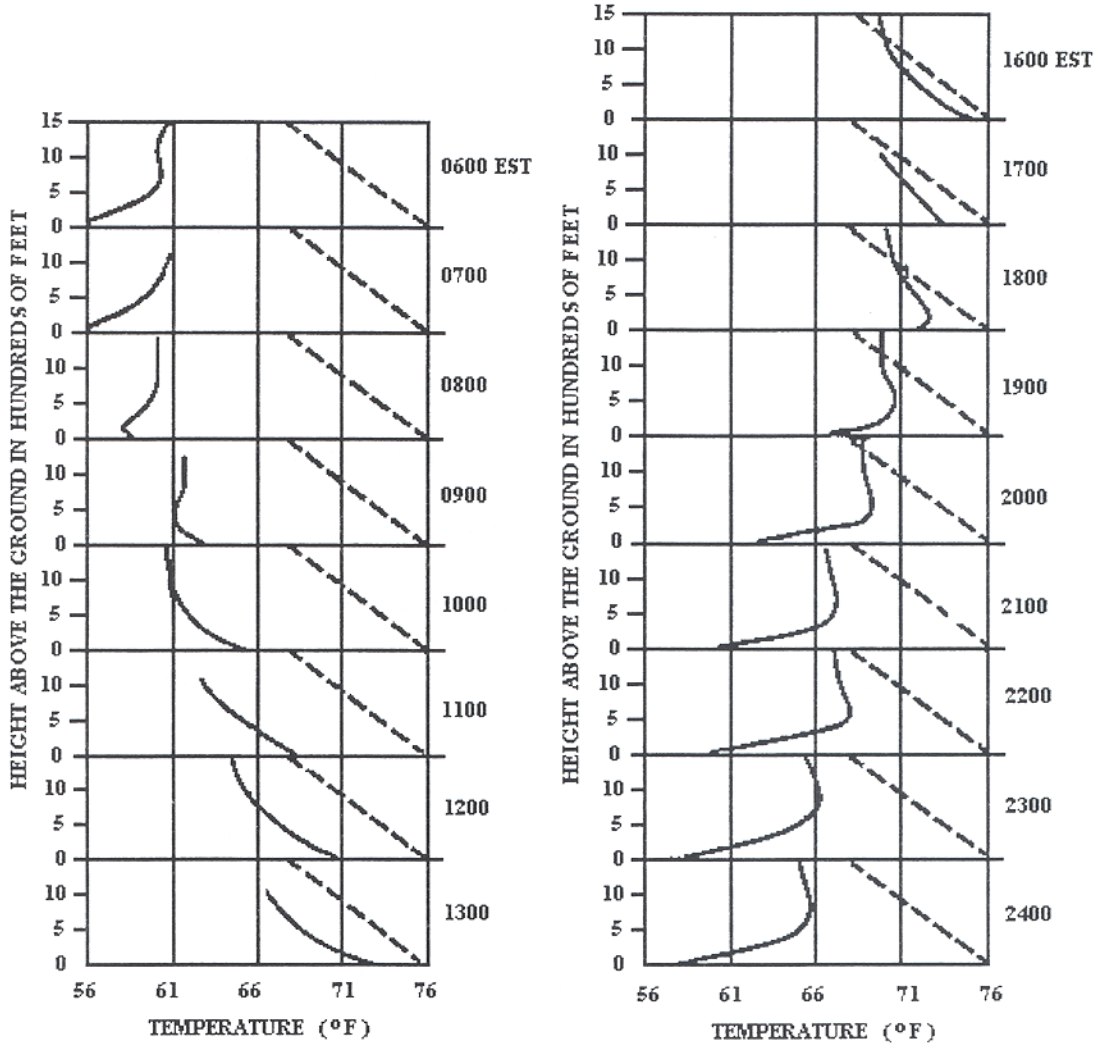

Figure 2-7. A Vertical Diurnal Variation of the Vertical Temperature Structure at Oak Ridge National Laboratory During the Period September – October 1950
Data was obtained from tethered-balloon sounding system. The dashed lines represent the adiabatic lapse rate. Adapted from Holland, 1953

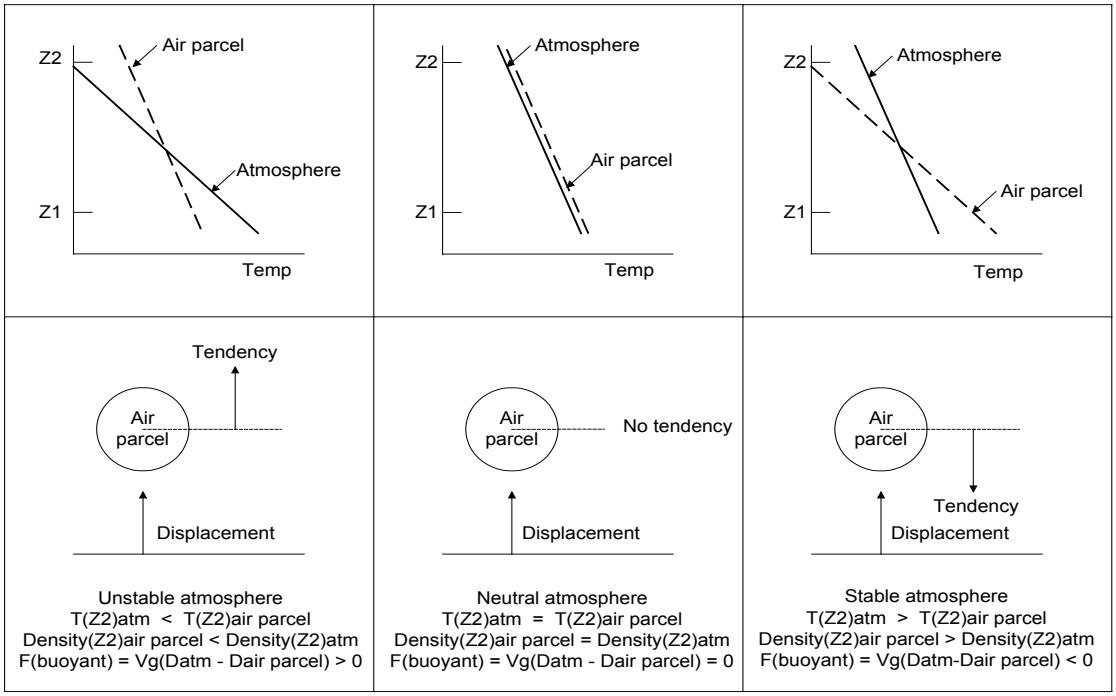

Figure 2-8. Adiabatic and Environmental Temperature Profiles
Solid lines represent unstable, neutral, and stable environmental temperature profiles. Dashed lines indicate adiabatic. Adapted from Cole, 1980

(A)

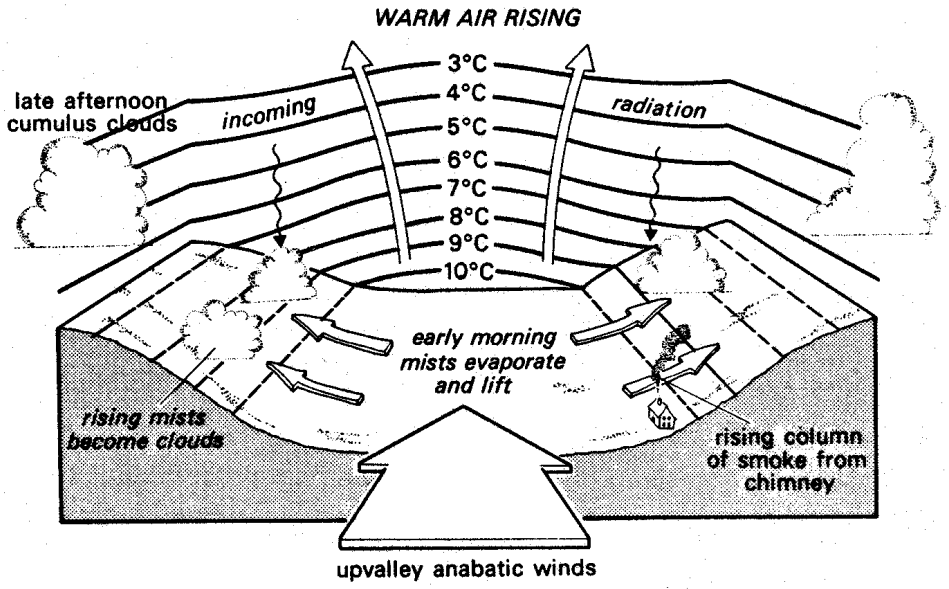

(B)

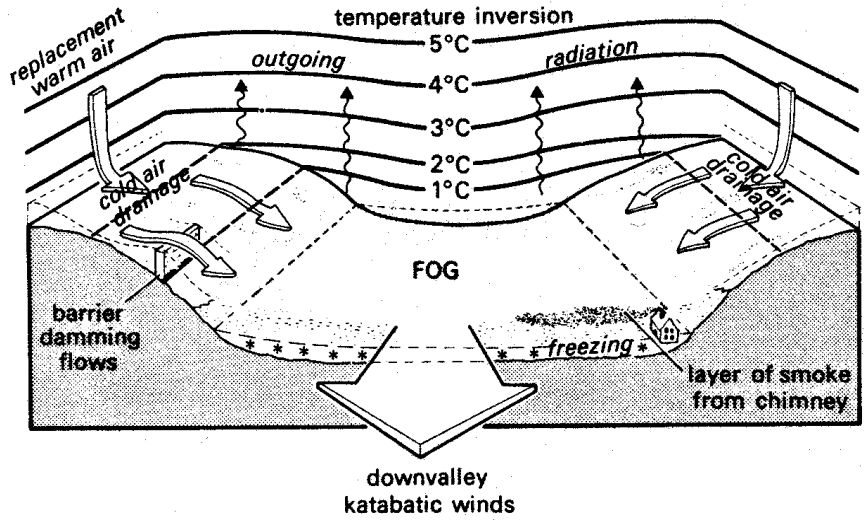

Figure 2-9. Meteorological Wind Patterns Associated with Topographic Features (A) Daytime Warming and Thermals in a Valley and (B) Nighttime Cooling and a Temperature Inversion in a Valley Adapted from Hanwell, 1980

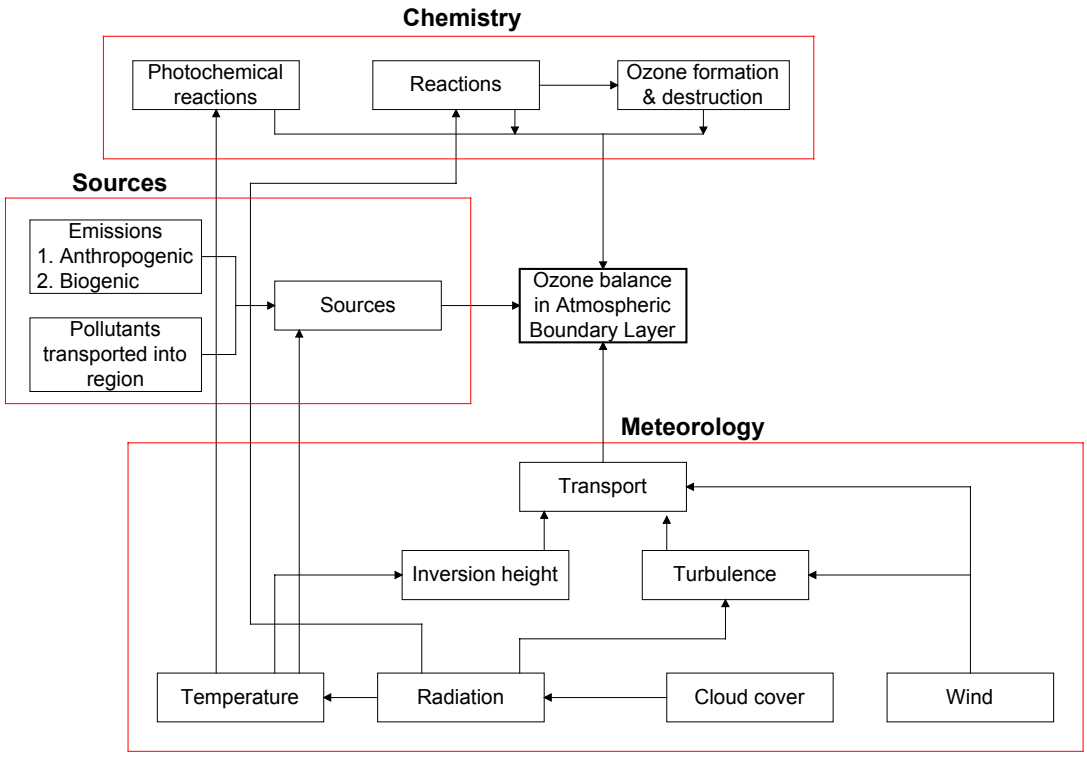

Figure 2-10. Interrelation between Sources of Ozone Precursors, Ozone Formation and Vertical Transport Adapted from Finlayson et al., 1999

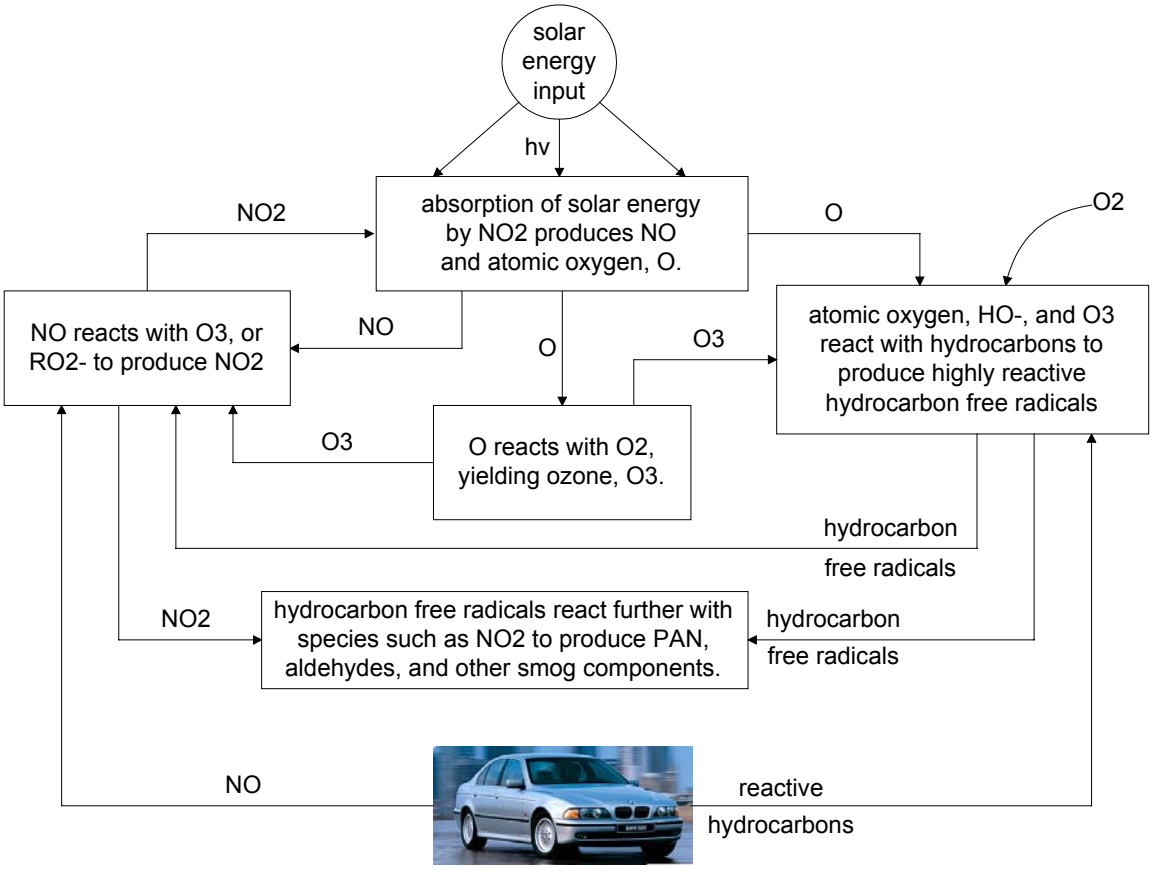

Figure 2-11. General Scheme for the Formation of Photochemical Ozone
Adapted from Manahan, 2000

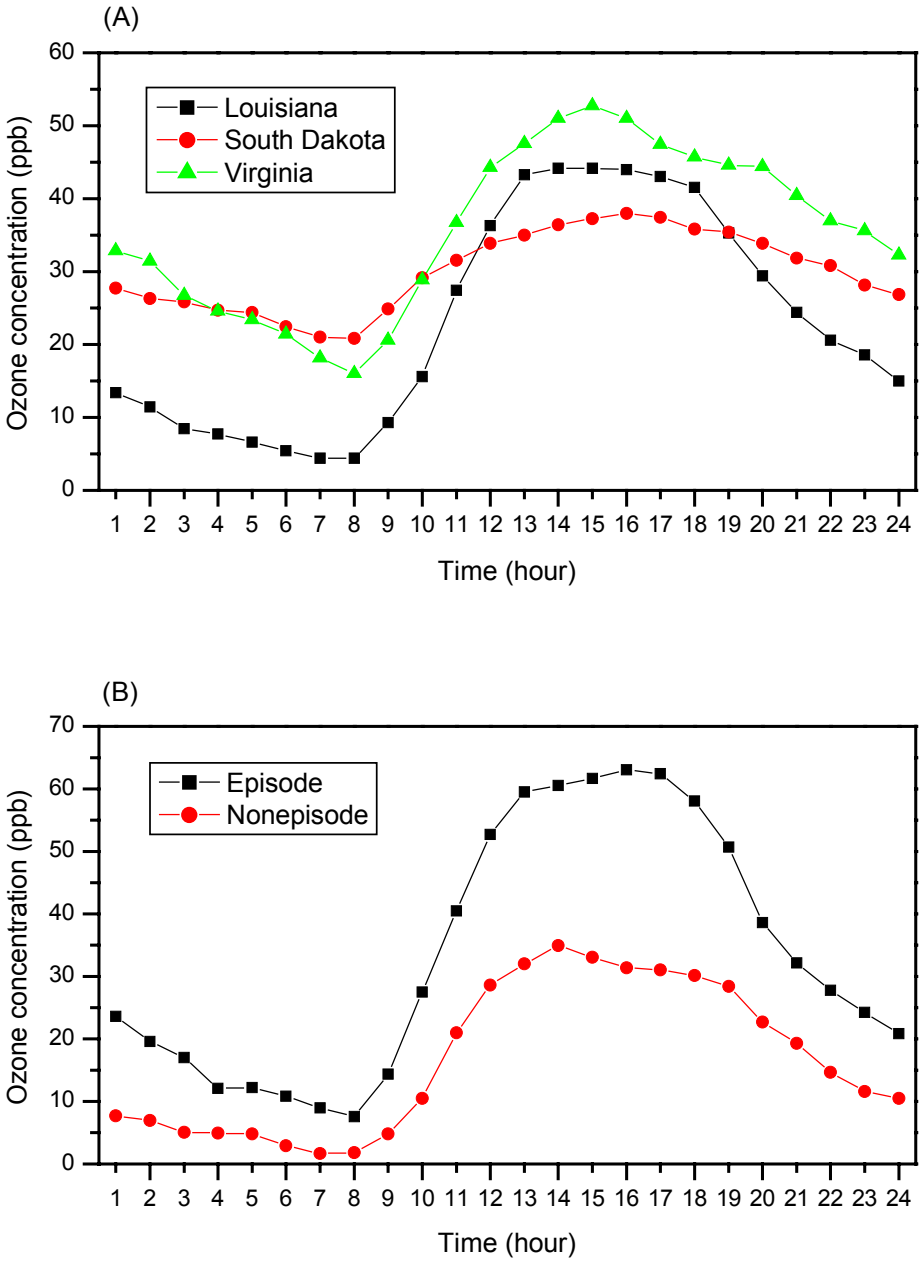

Figure 2-12. Mean Diurnal Ozone Patterns (A) Mean Diurnal Ozone Patterns for Three Rural Sites in Louisiana, South Dakota, and Virginia (B) Ozone Diurnal Profiles for a Rural Site in Louisiana during Episodic and Non-episodic Conditions
Hour of the day refers to Local Standard Time (LST) for each site. Episodic conditions were described as periods of high pollution based on maximum ozone concentrations. Adapted from Kelly et al., 1984

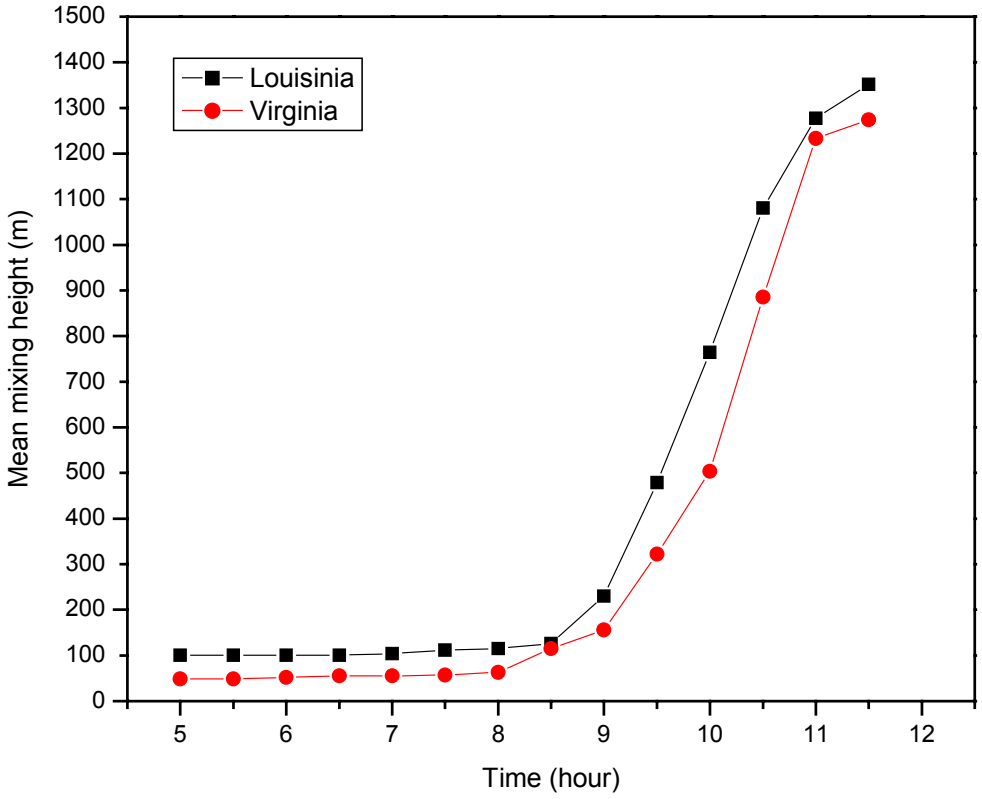

Figure 2- 13. Average Pattern for Mixing Height from 05:00 to 11:30
The mixing height was determined using an Aerovironment Model 310 monostatic acoustic sounder. Adapted from Kelly et al., 1984

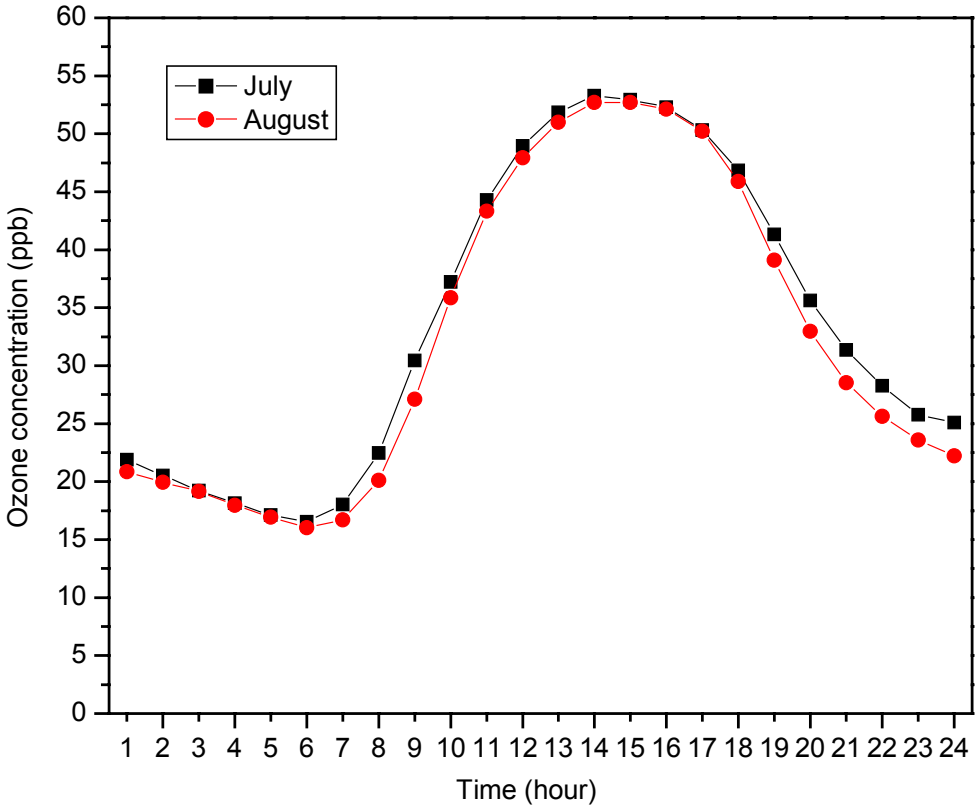

Figure 2-14. The July, August 1991 Station-Averaged Ozone Diurnal Patterns in the Southeastern United States
Adapted from Casado et al., 1994

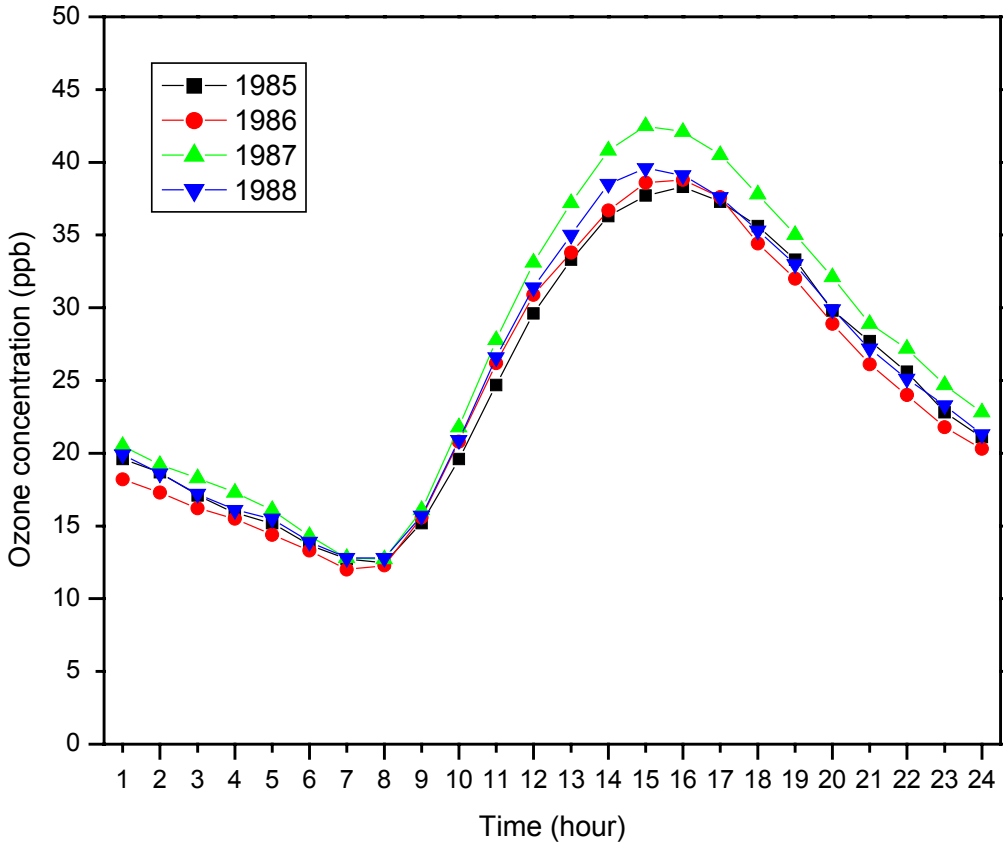

Figure 2-15. The Annually Averaged (January – December) Composite O_3 Diurnal Curve for the Allentown, PA Site for the Period 1985 – 1988
Adapted from Lefohn et al., 1993

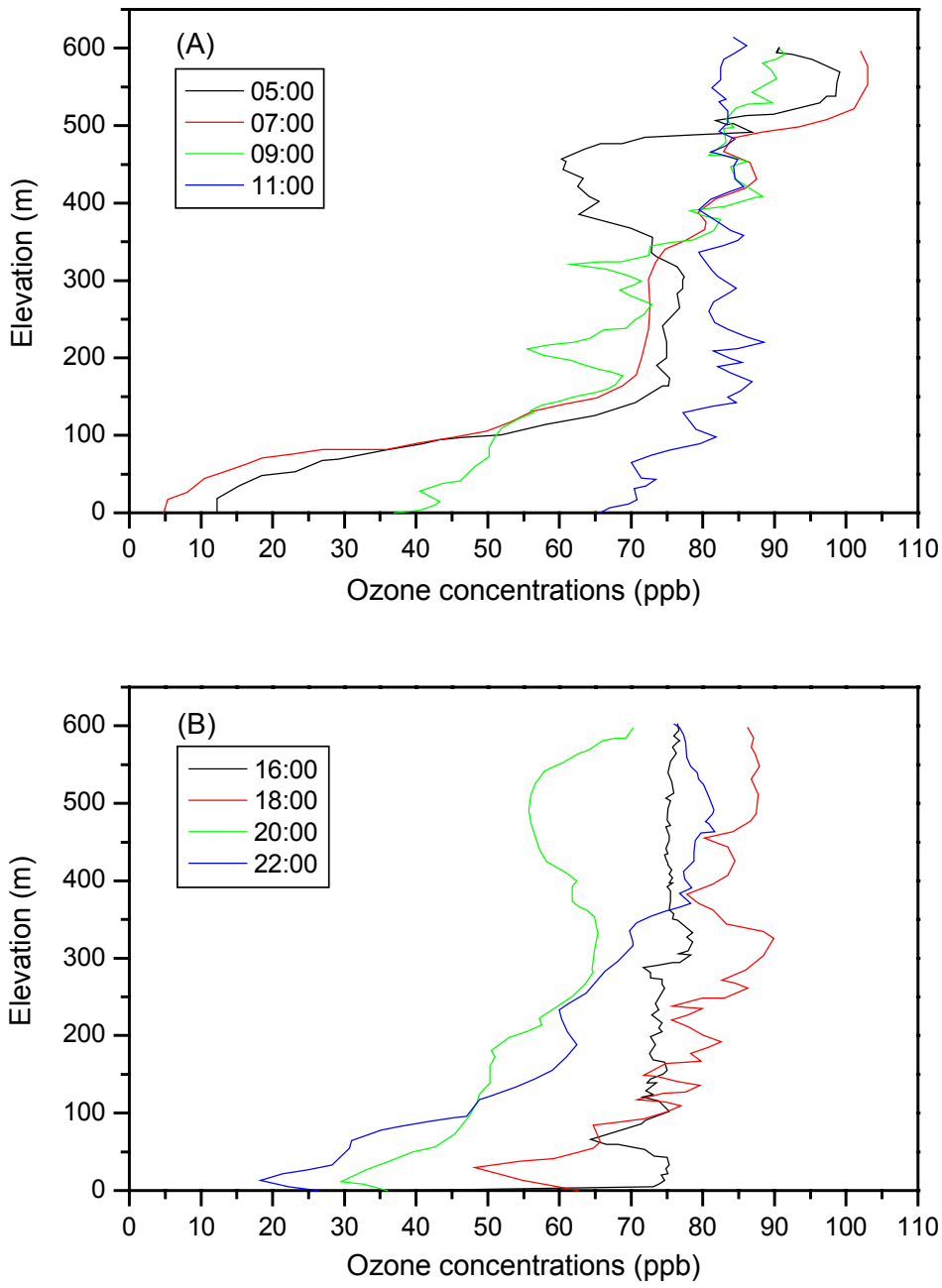

Figure 2-16. Vertical Profile of Ozone Concentrations Collected on August 30, 1995 in East Tennessee (A) Four Monitoring Profiles Obtained at 05:11-05:40, 07:02-07:29, 09:00-09:28, and 11:01-11:28 Local Standard Time (Referred to as 05:00, 07:00, 09:00 and 11:00, Respectively) (B) Four Evening Profiles Obtained at 16:05-16:33, 18:00-18:22, 20:02-20:22, and 21:57-22:23 Local Standard Time (Referred to as 16:00, 18:00, 20:00, and 22:00, respectively) Adapted from Trotter et al., 1996

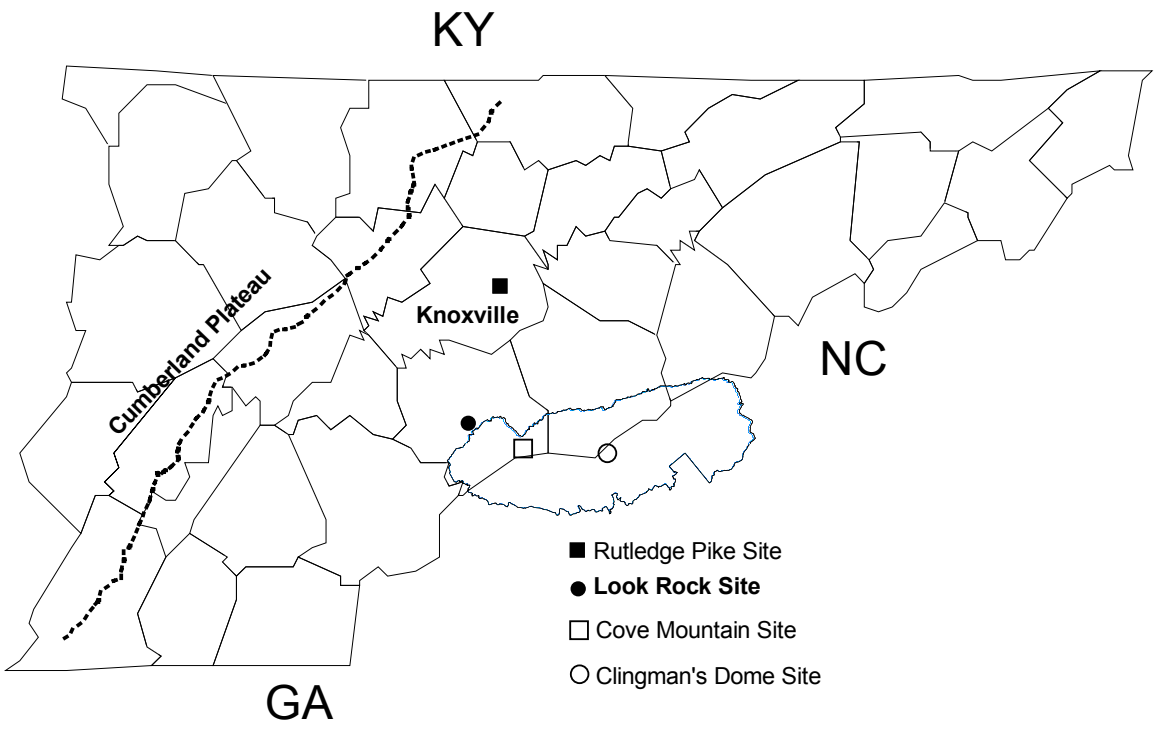

Figure 3-1. Location of Ozone Monitoring Stations in East Tennessee

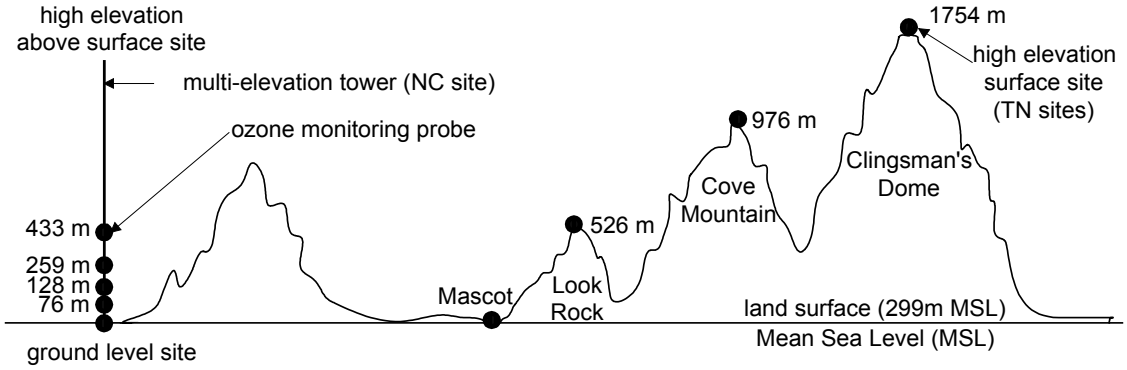

Figure 3-2. Description of Ozone Monitoring Stations in East Tennessee

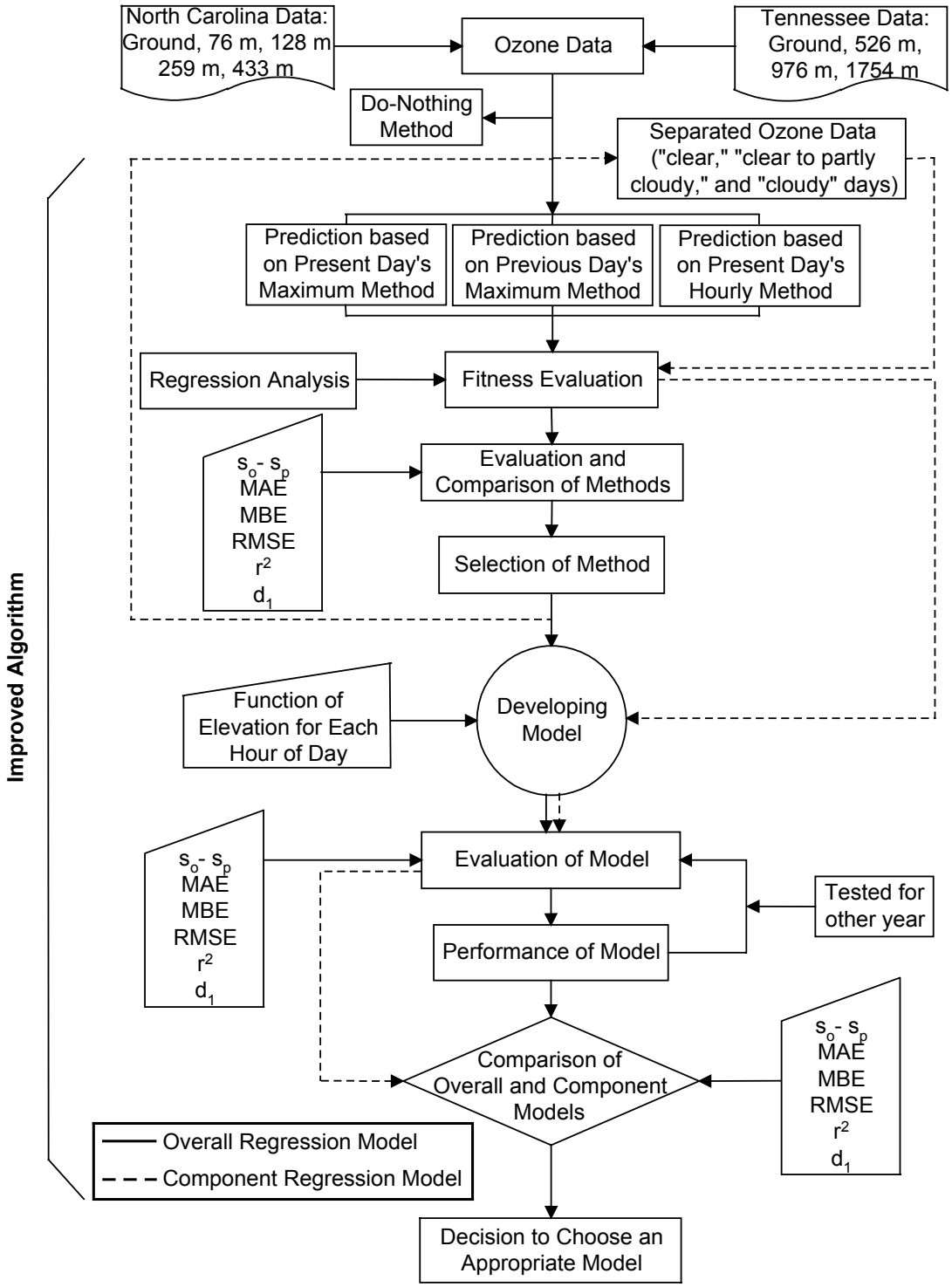

Figure 3-3. Flow Chart for Development of a Model

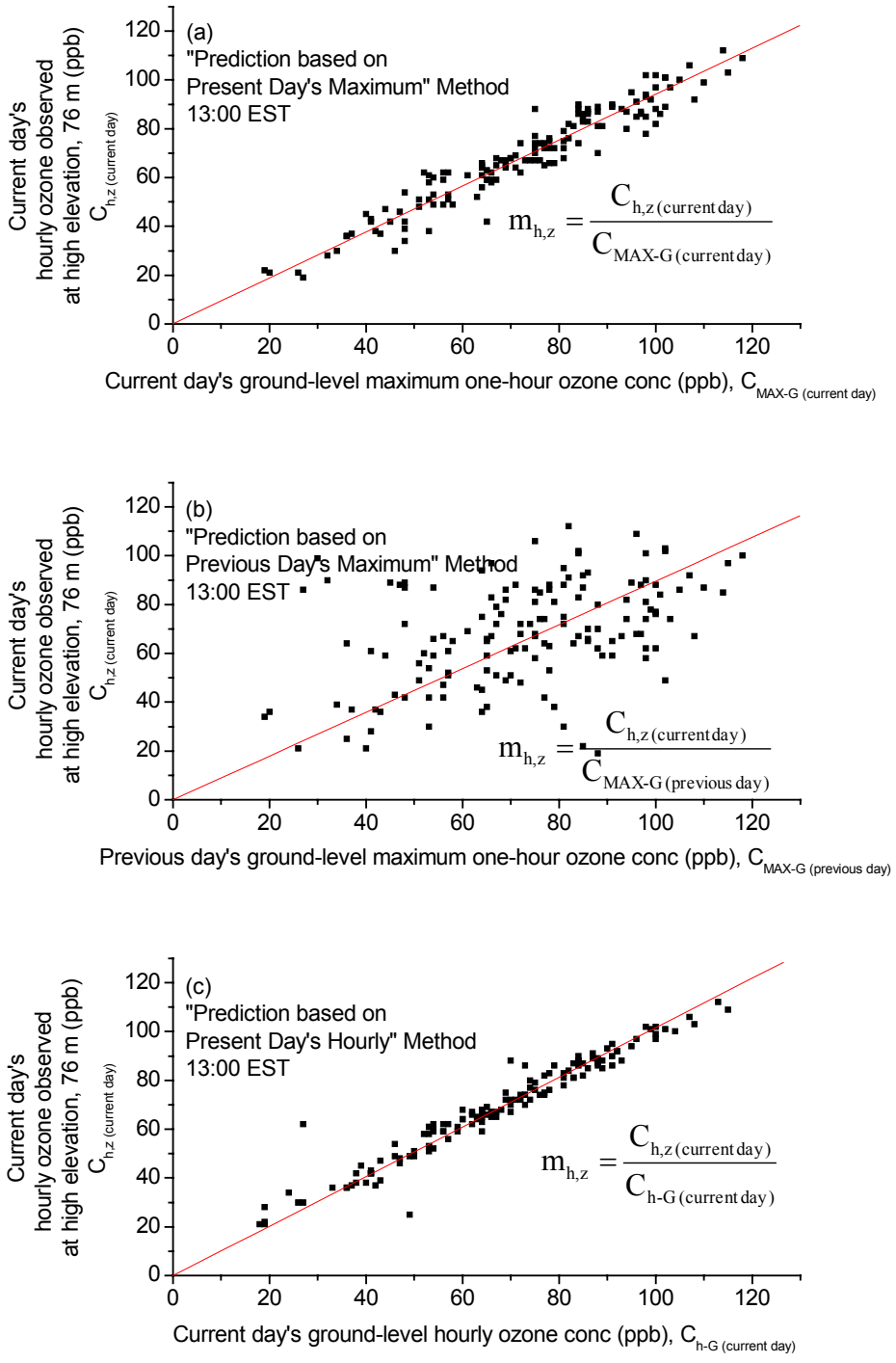

Figure 3-4. Linear Relationships for the "Prediction based on Present Day's Maximum," "Prediction based on Previous Day's Maximum," and "Prediction based on Present Day's Hourly" Methods

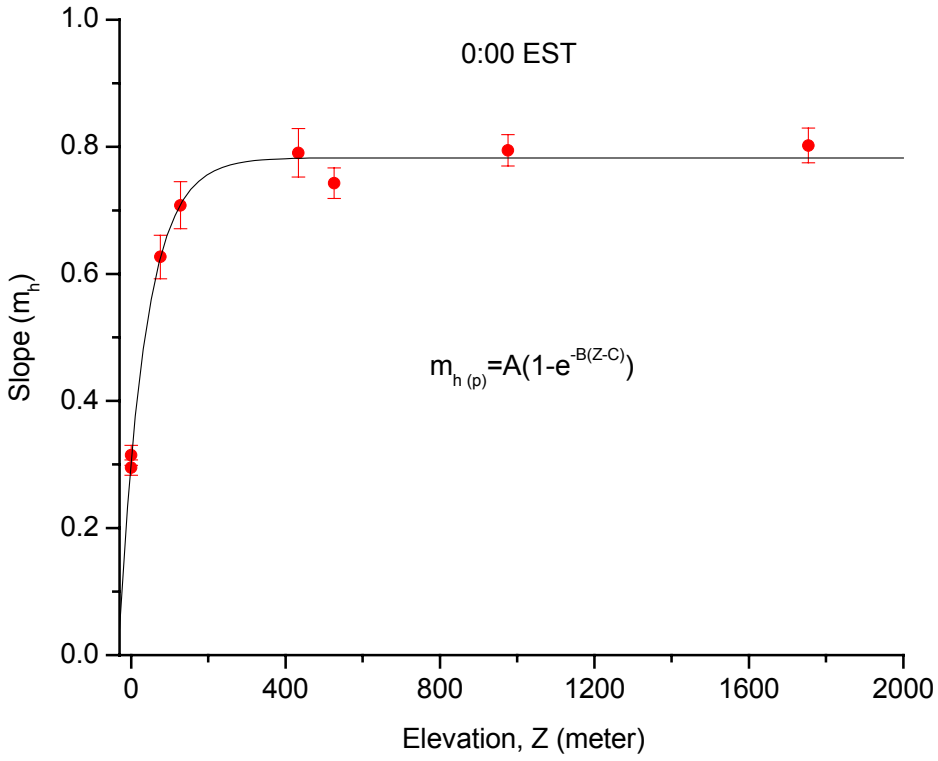

Figure 3-5. Illustration of Non-linear Curve Fitting for Model Development

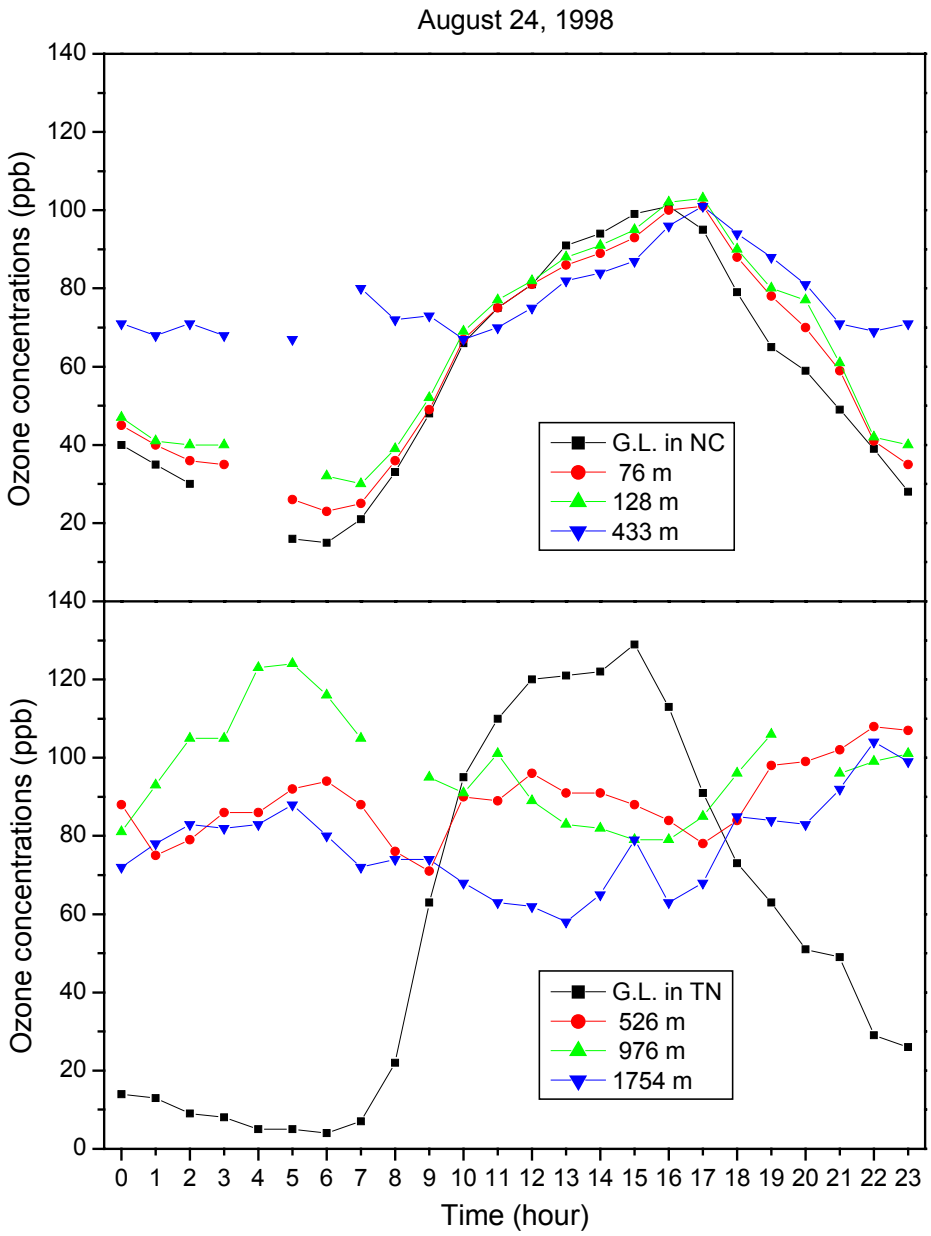

Figure 4-1. Daily Ozone Variation Observed at Ground Level (North Carolina), 76 m, 128 m, 433 m, Ground Level (East Tennessee), 526 m, 976 m, and 1754 m on August 24, 1998 in North Carolina and East Tennessee

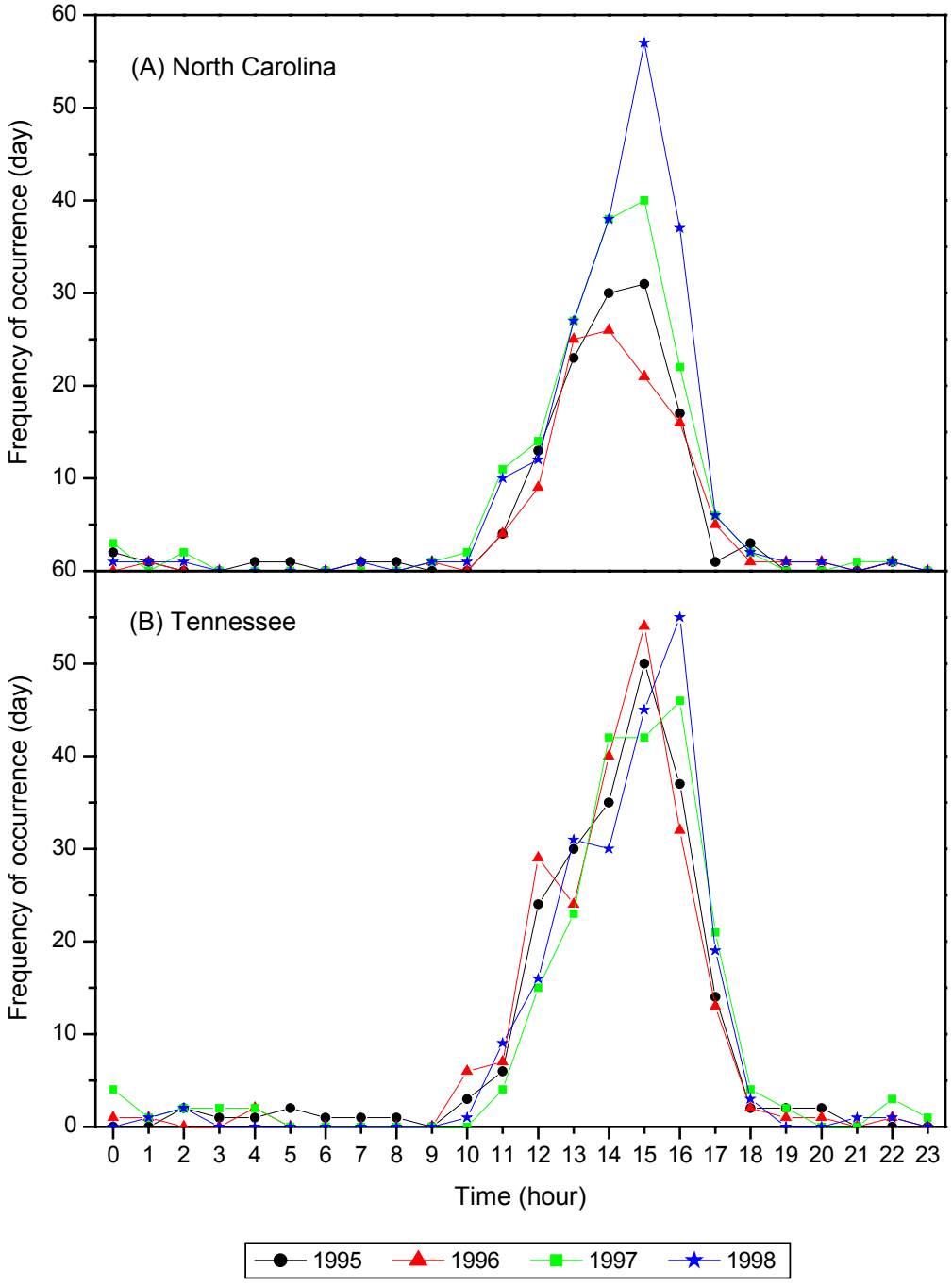

Figure 4-2. Frequency of Occurrence of Ground Level Daily Maximum Ozone Concentrations Observed during the Full Ozone-Monitoring Season (April – October) from 1995 through 1998 in (A) North Carolina and (B) East Tennessee

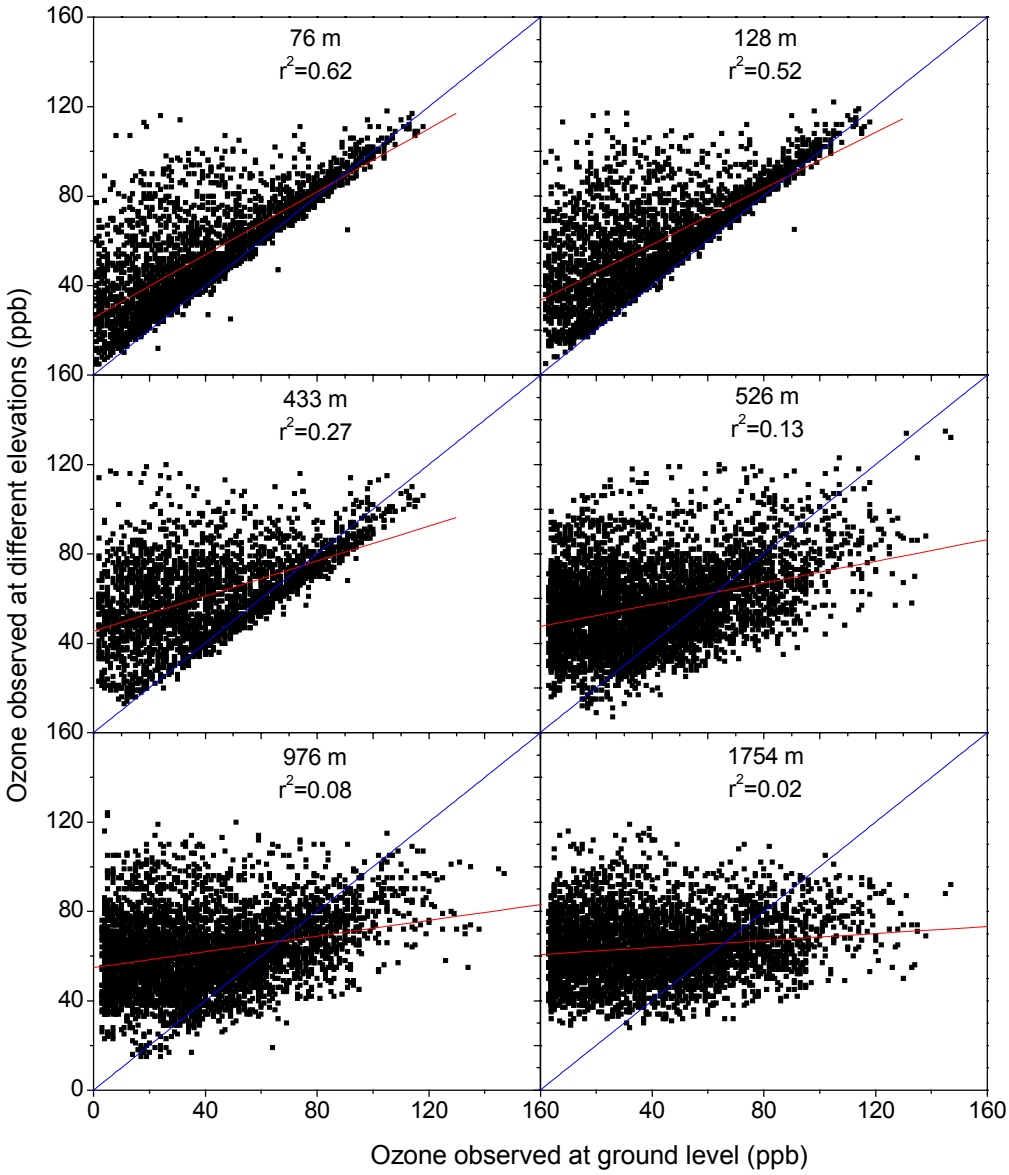

Figure 4-3. Correlation of All Hours Ozone Concentrations between Ground Level and High Elevations (76 m, 128 m, 259 m, 433 m, 526 m, 976 m, and 1754 m)
Full ozone season data (April – October) of 1998 were used. The diagonal in each plot indicates that ozone observed at different elevations is equal to the ozone observed at ground level.

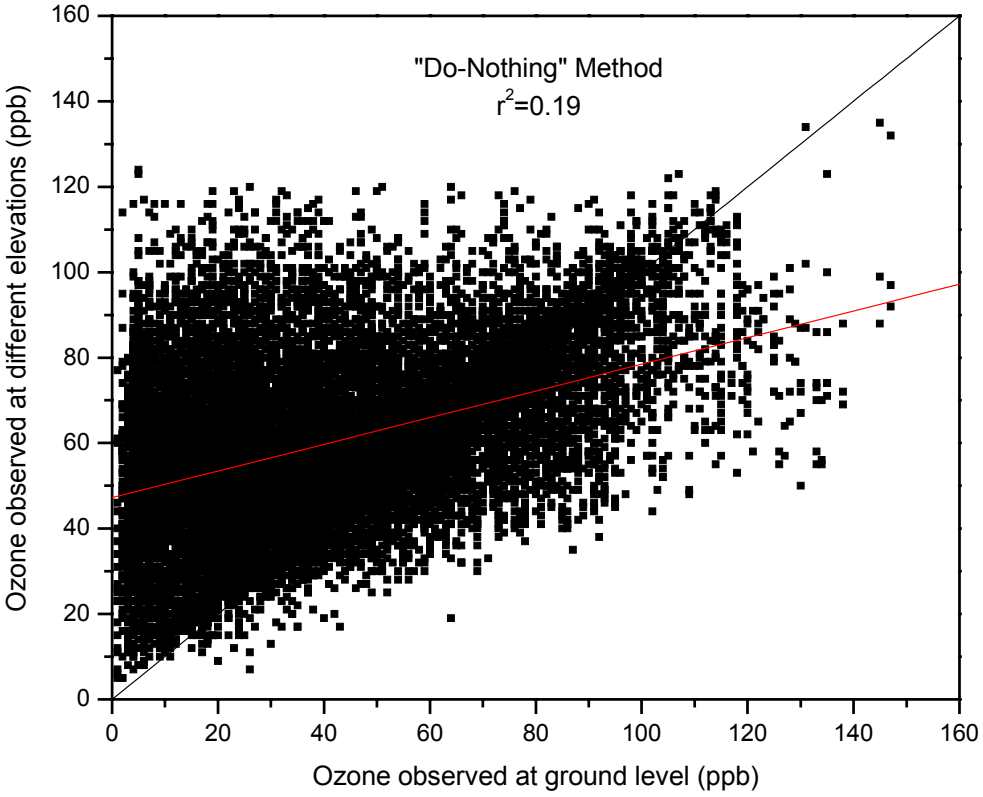

Figure 4-4. Scatter Plot of Ground-Level Ozone Observations against High Elevation Ozone Observations Measured at Six Elevated Sites (76 m, 128 m, 259 m, 433 m, 526 m, 976 m, and 1754 m) Full ozone season data (April – October) of 1998 were used. The two diagonals in the plot indicate the best-fit regression line through the data and the line of perfect correspondence between ground level and high elevation ozone observations.

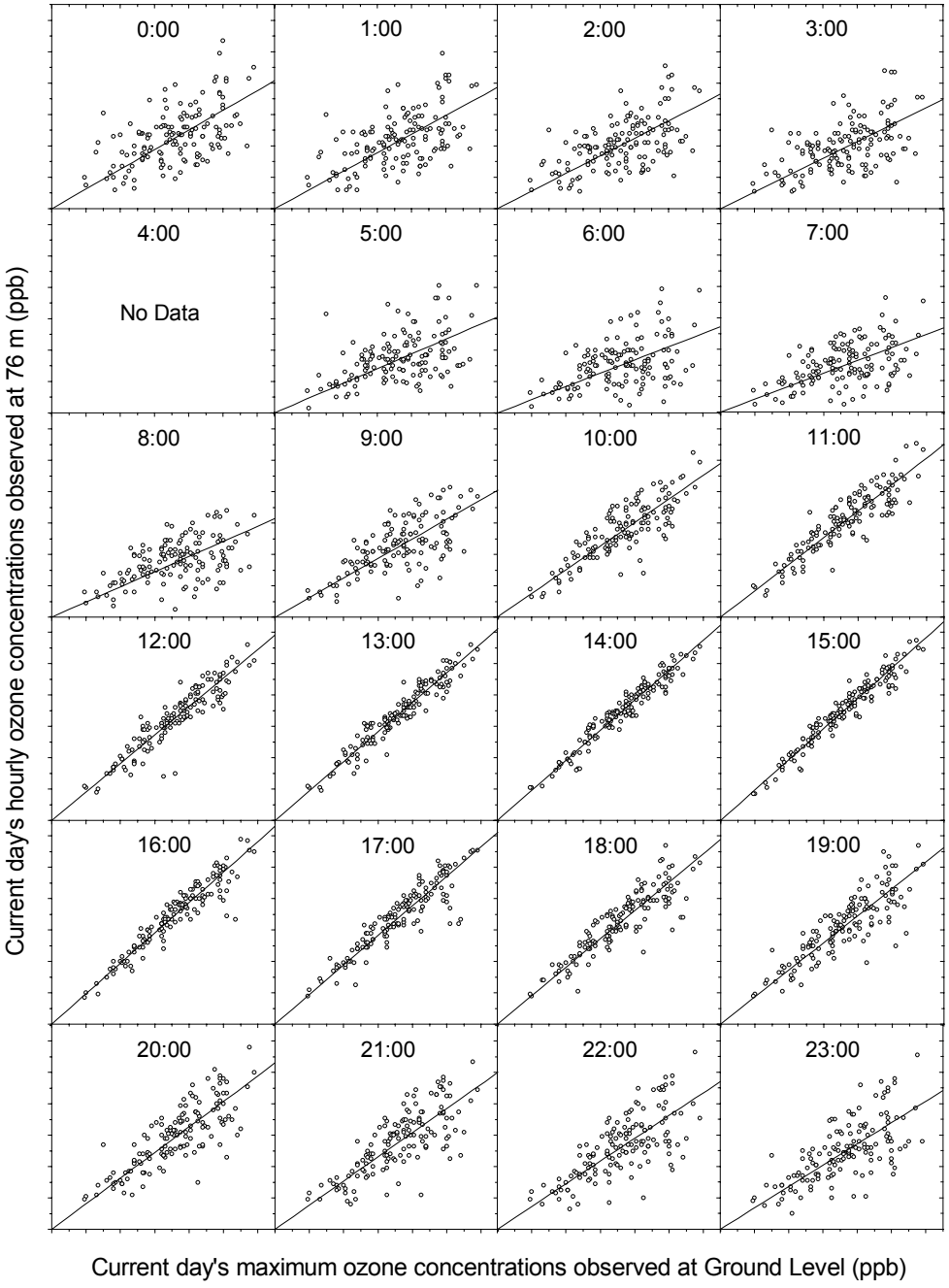

Figure 4-5. Scatter Plots of Current Day's Maximum Ozone Concentrations Observed at Ground Level against Current Day's Hourly Ozone Concentrations Observed at 76 m based on "Prediction based on Present Day's Maximum" Method
Full ozone season data (April – October) of 1998 were used. The scale on all axes is from 0 to 130 ppb in 10 ppb increment. The diagonal in each plot indicates the best-fit regression line through the origin.

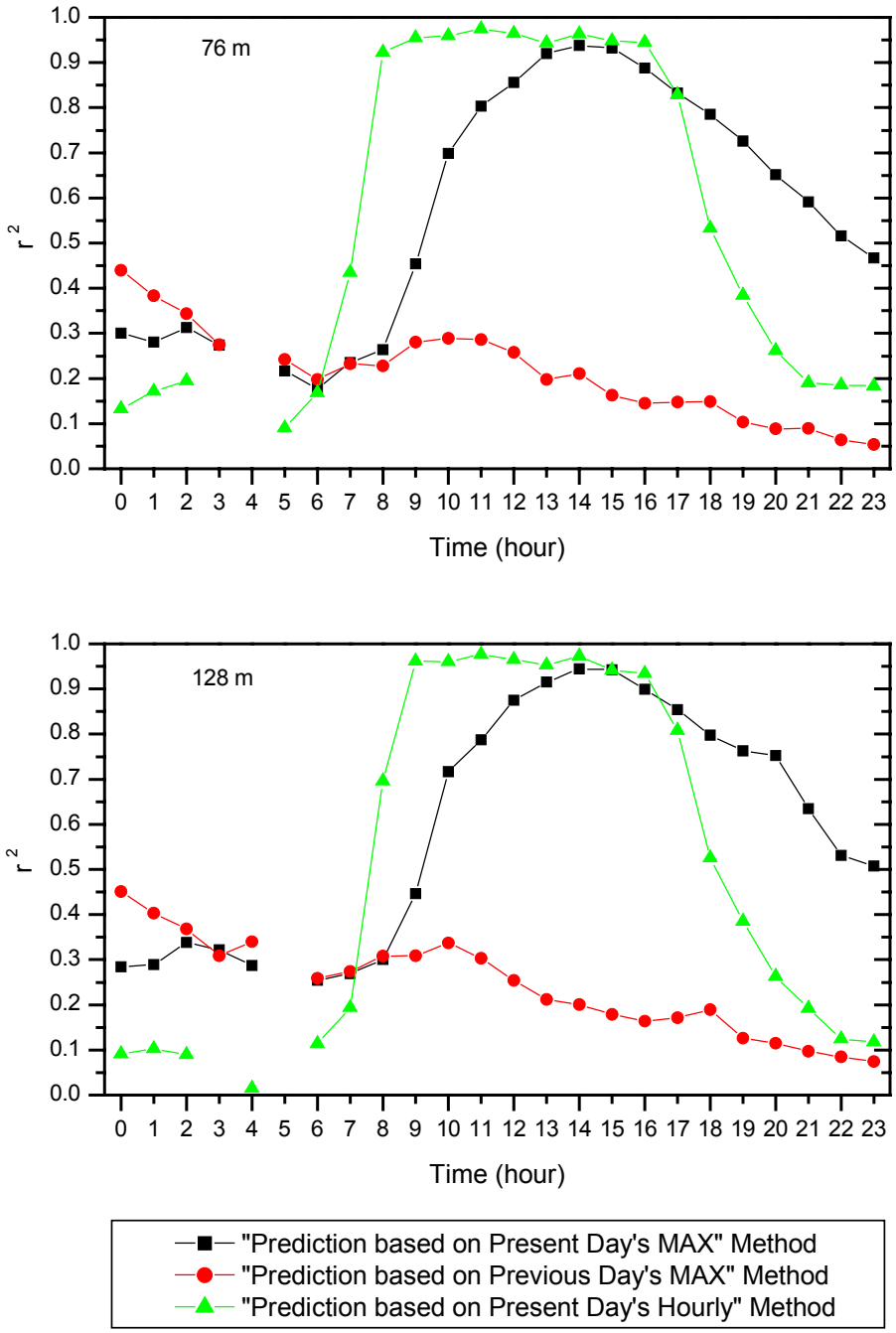

Figure 4-6. Comparison of r^2 (Coefficient of Determination) for High Elevations (76 m and 128 m), Using "Prediction based on Present Day's Maximum," "Prediction based on Previous Day's Maximum," and "Prediction based on Present Day's Hourly" Methods Full ozone season data (April – October) of 1998 were used.

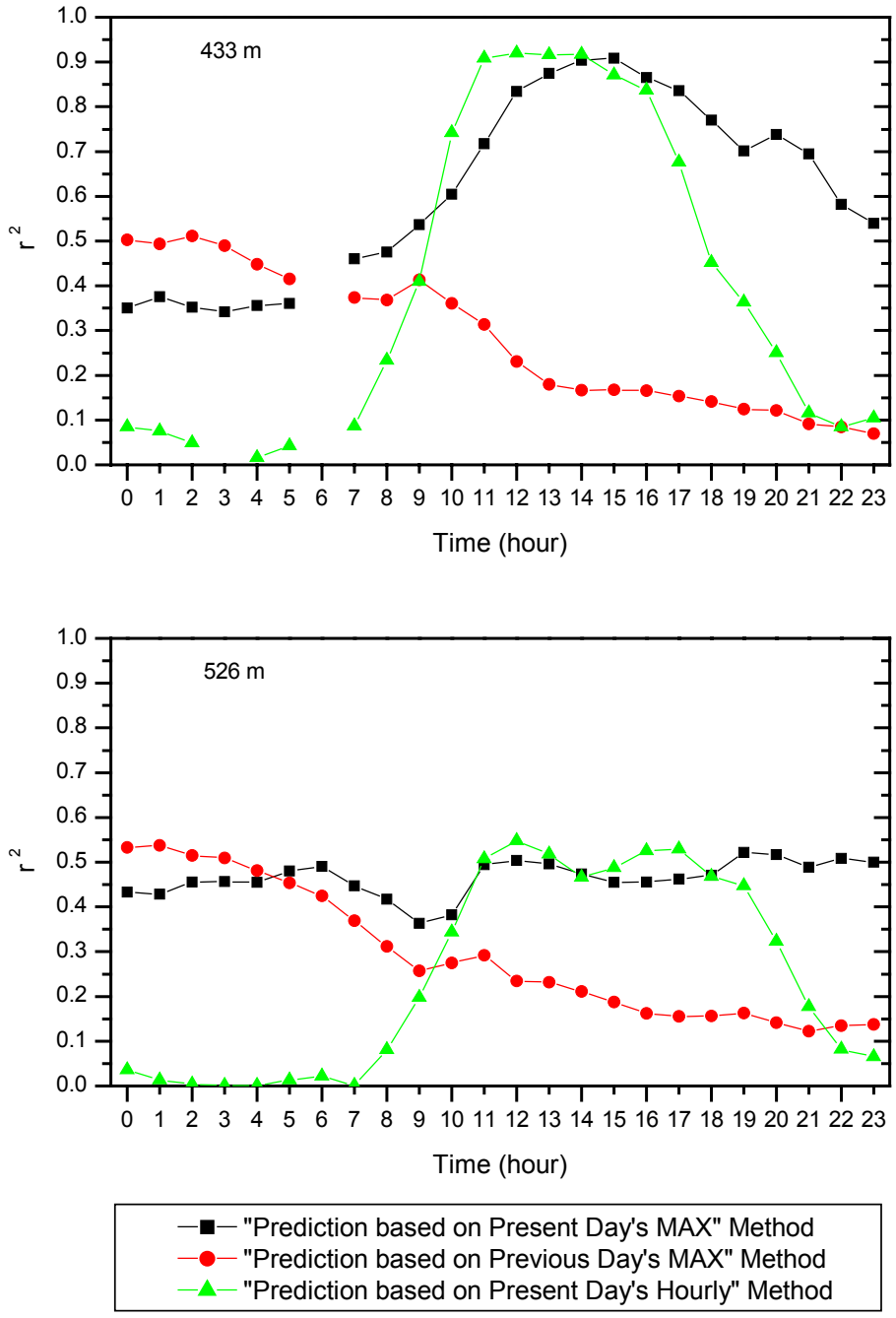

Figure 4-7. Comparison of r^2 (Coefficient of Determination) for High Elevations (433 m and 526 m), Using "Prediction based on Present Day's Maximum," "Prediction based on Previous Day's Maximum," and "Prediction based on Present Day's Hourly" Methods Full ozone season data (April – October) of 1998 were used.

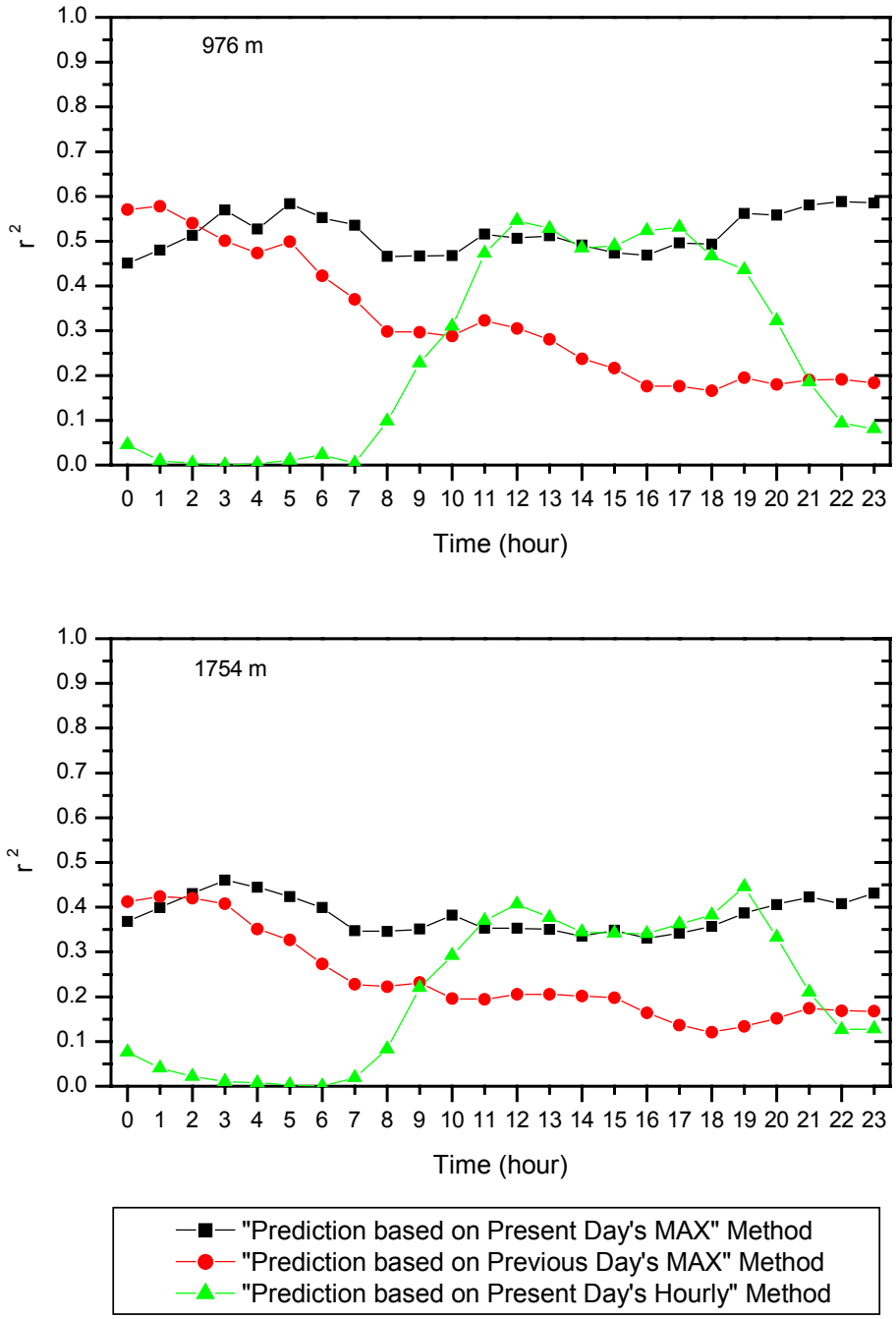

Figure 4-8. Comparison of r^2 (Coefficient of Determination) for High Elevations (976 m and 1754 m), Using "Prediction based on Present Day's Maximum," "Prediction based on Previous Day's Maximum," and "Prediction based on Present Day's Hourly" Methods Full ozone season data (April – October) of 1998 were used.

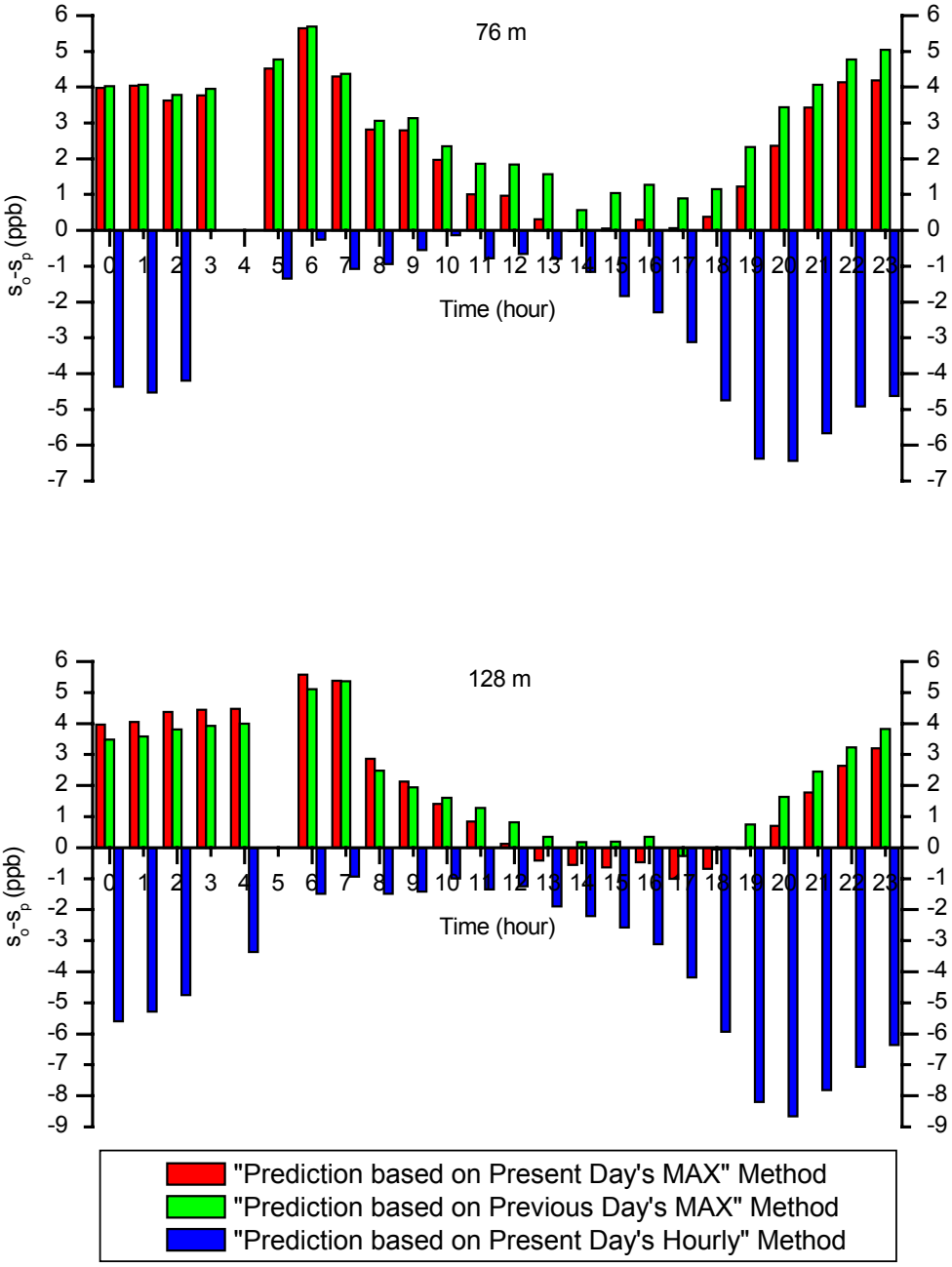

Figure 4-9. Comparison of Relative Performance of Each Method in terms of Residuals between the Standard Deviations of Ozone Observations and Predictions for High Elevations (76 m and 128 m)
Full ozone season data (April – October) of 1998 were used.

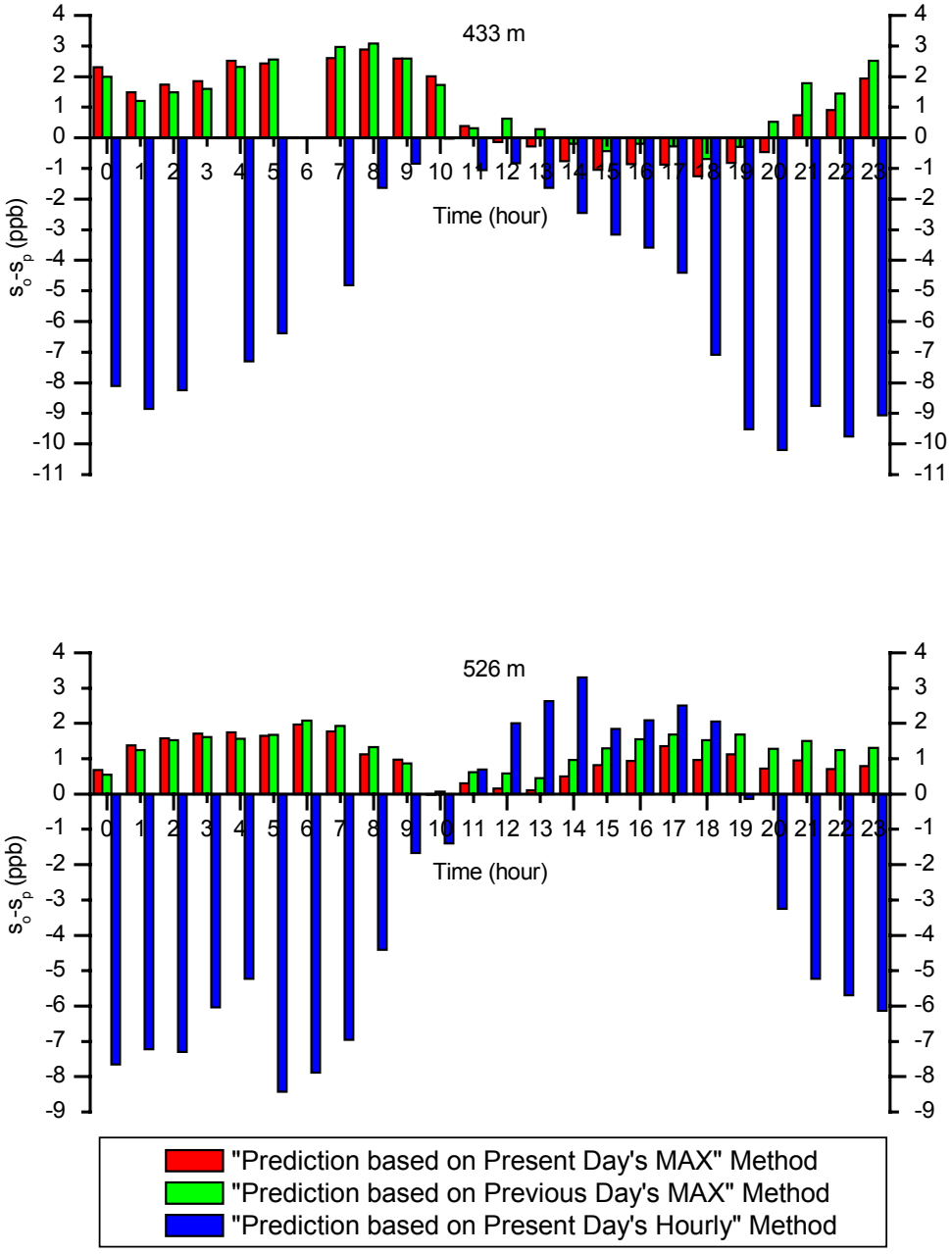

Figure 4-10. Comparison of Relative Performance of Each Method in terms of Residuals between the Standard Deviations of Ozone Observations and Predictions for High Elevations (433 m and 526 m)
Full ozone season data (April – October) of 1998 were used.

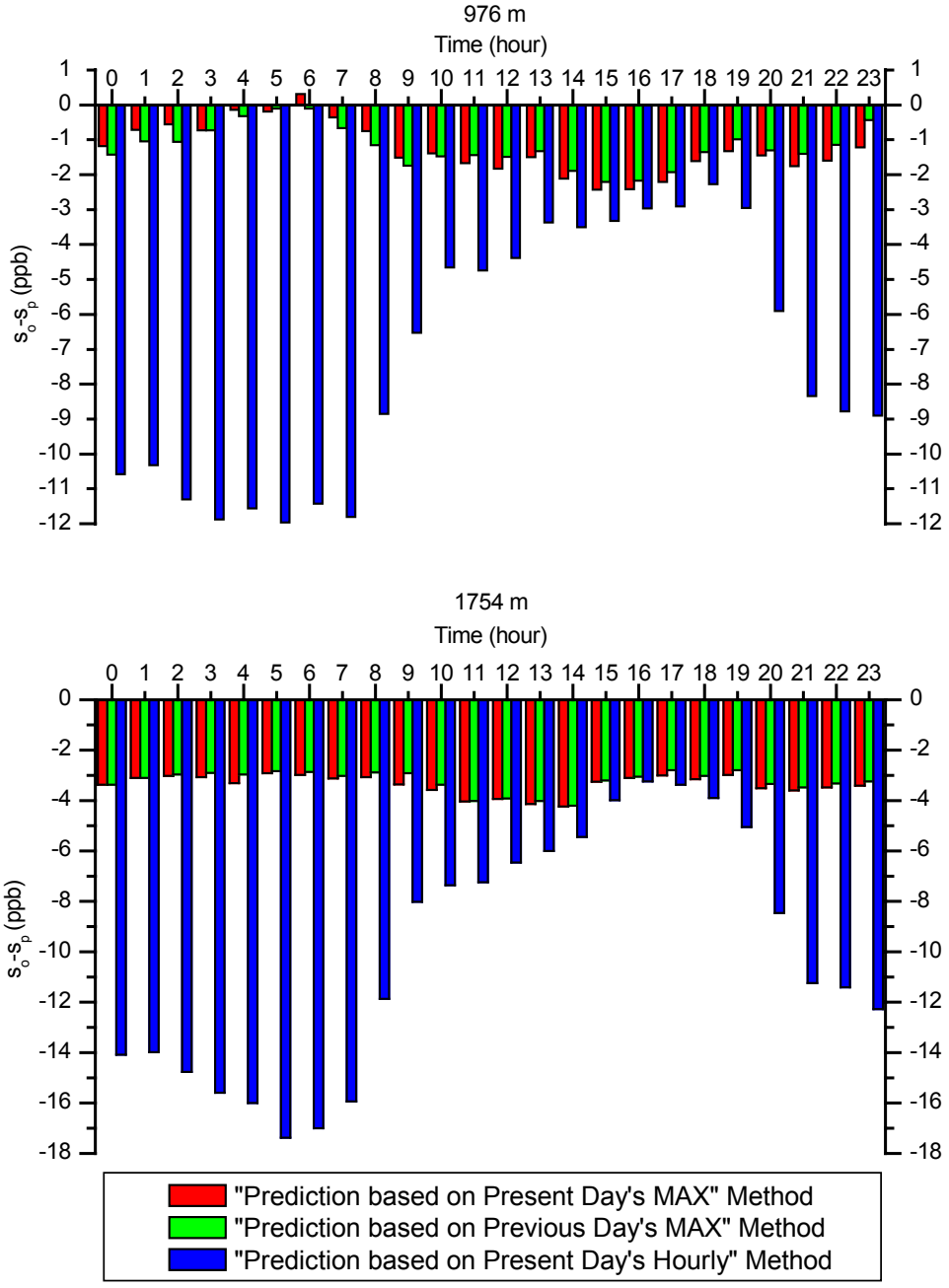

Figure 4-11. Comparison of Relative Performance of Each Method in terms of Residuals between the Standard Deviations of Ozone Observations and Predictions for High Elevations (976 m and 1754 m)
Full ozone season data (April – October) of 1998 were used.

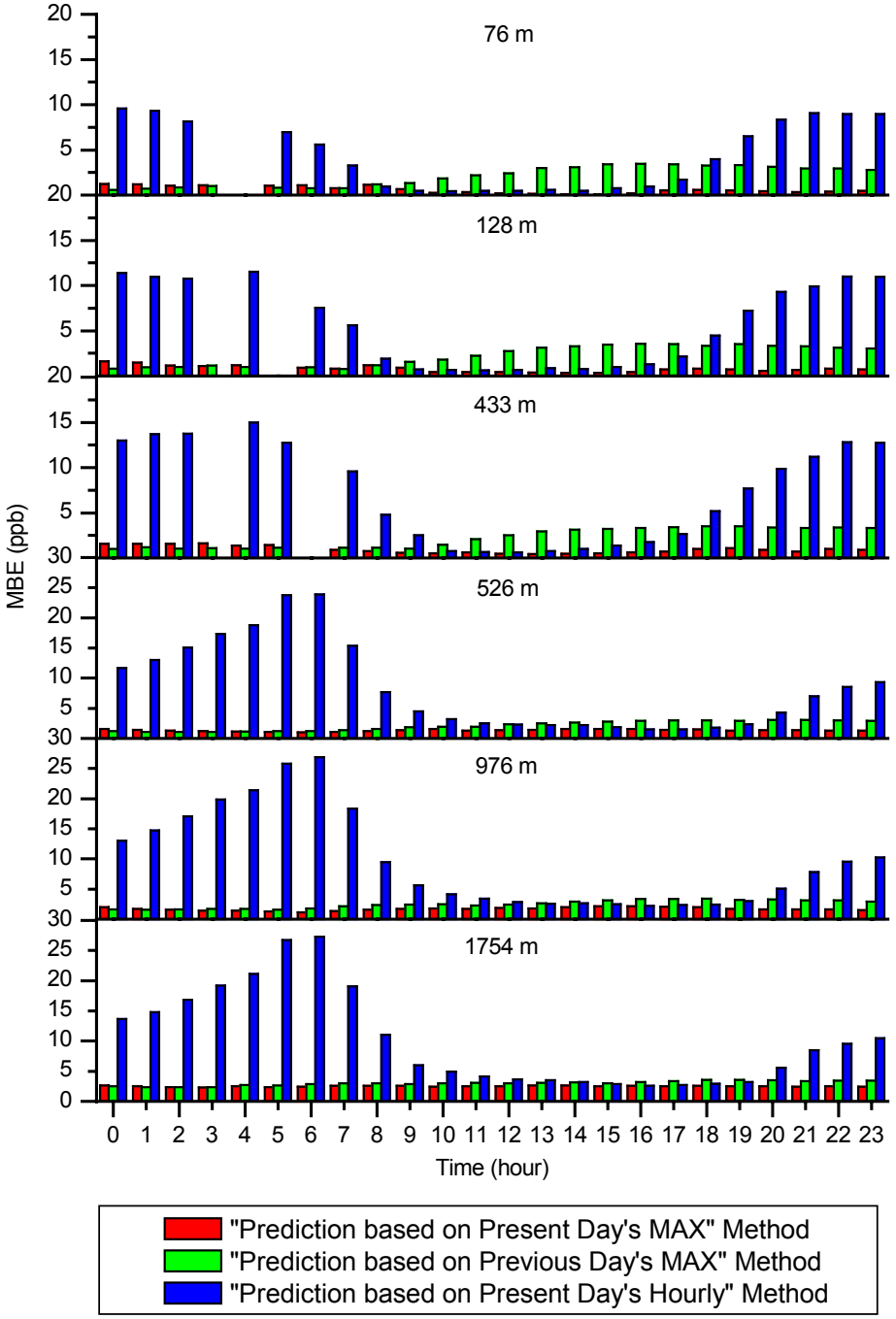

Figure 4-12. Relative Performance in Terms of Mean Bias Error for High Elevations (76 m, 128 m, 433 m, 526 m, 976 m, and 1754 m)
Full ozone season data (April – October) of 1998 were used.

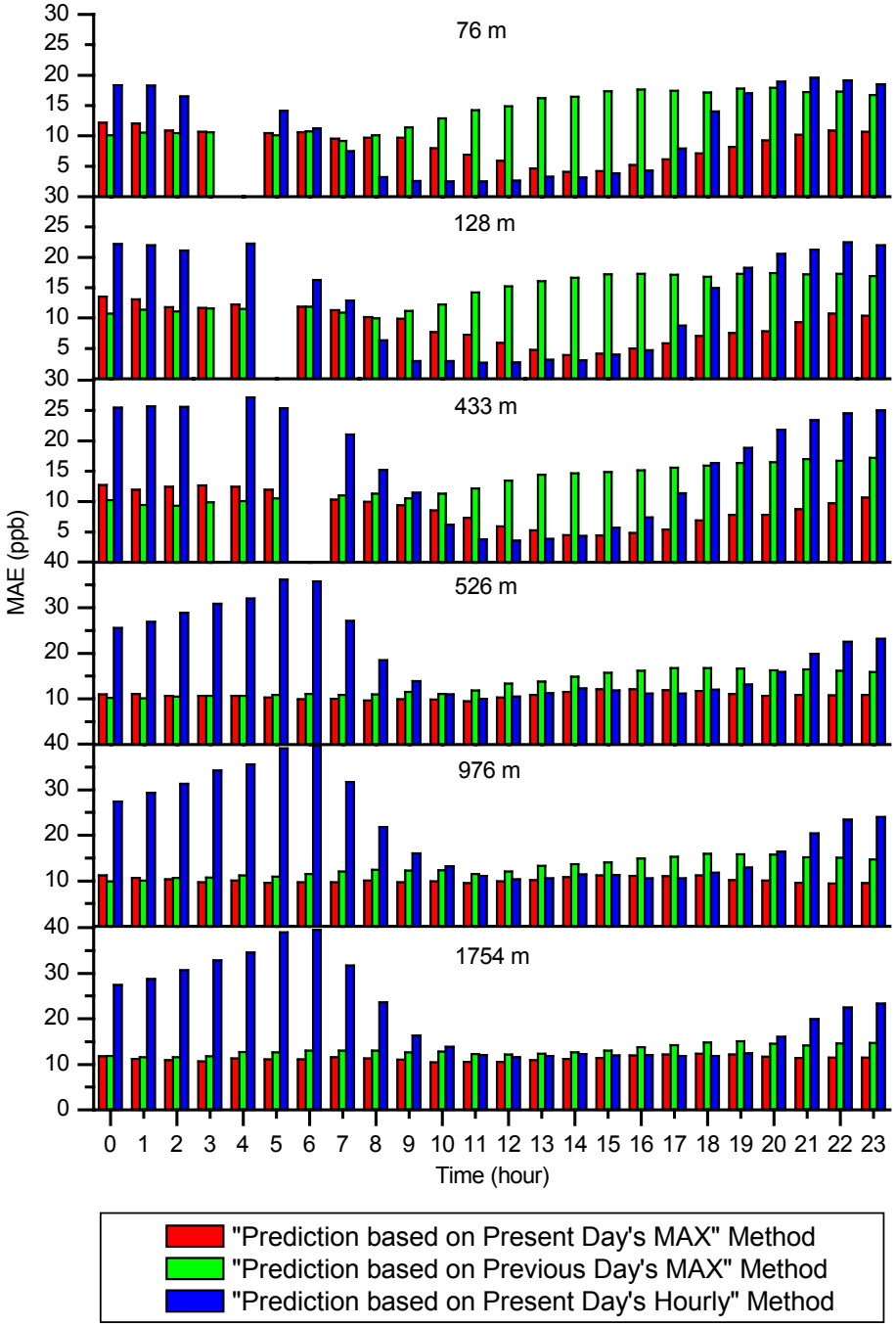

Figure 4-13. Relative Performance in Terms of Mean Absolute Error for High Elevations (76 m, 128 m, 433 m, 526 m, 976 m, and 1754 m), Using "Prediction based on Present Day's Maximum," "Prediction based on Previous Day's Maximum," and "Prediction based on Present Day's Hourly" Methods Full ozone season data (April – October) of 1998 were used.

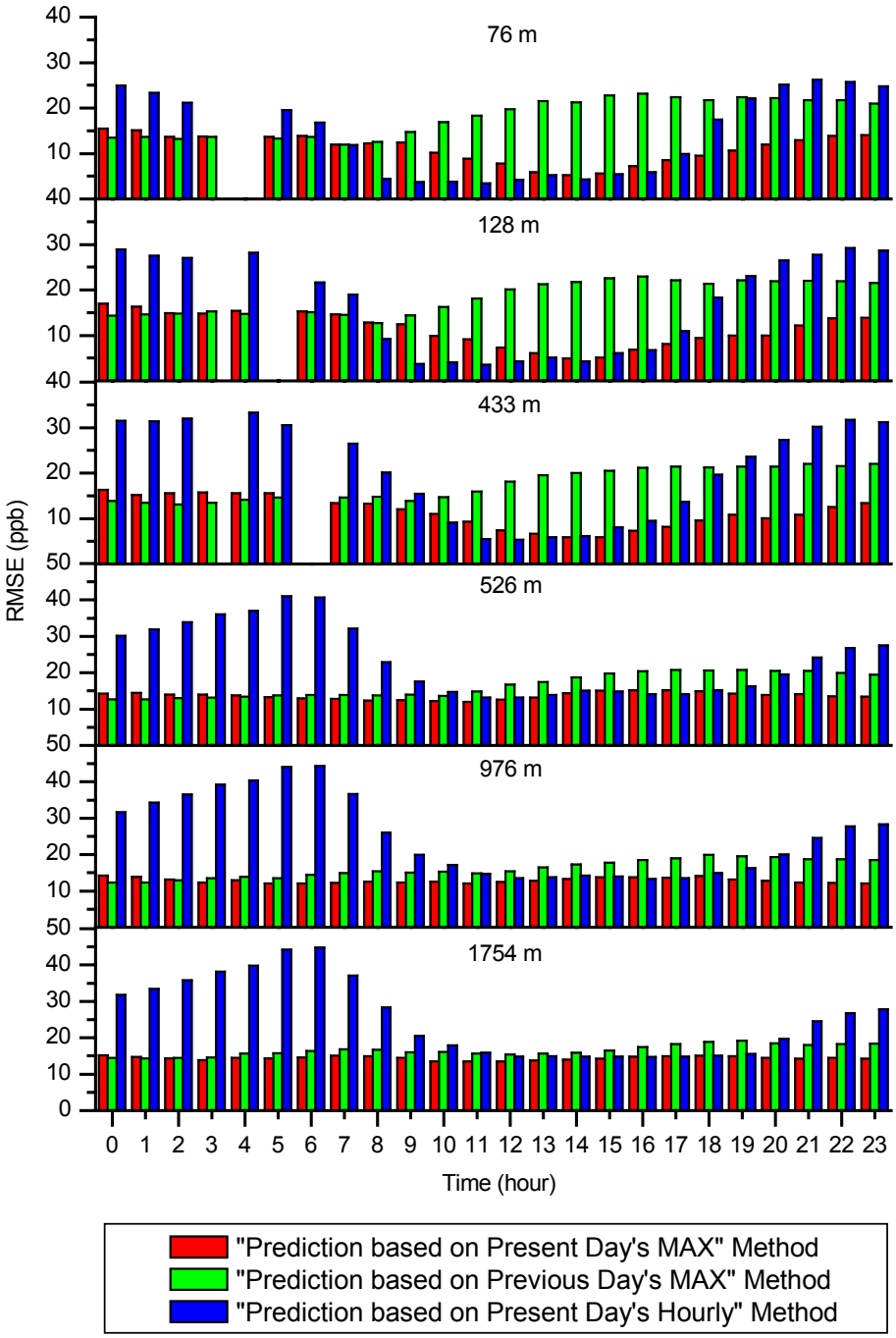

Figure 4-14. Relative Performance in Terms of Root Mean Square Error for High Elevations (76 m, 128 m, 433 m, 526 m, 976 m, and 1754 m), Using "Prediction based on Present Day's Maximum," "Prediction based on Previous Day's Maximum," and "Prediction based on Present Day's Hourly" Methods Full ozone season data (April – October) of 1998 were used.

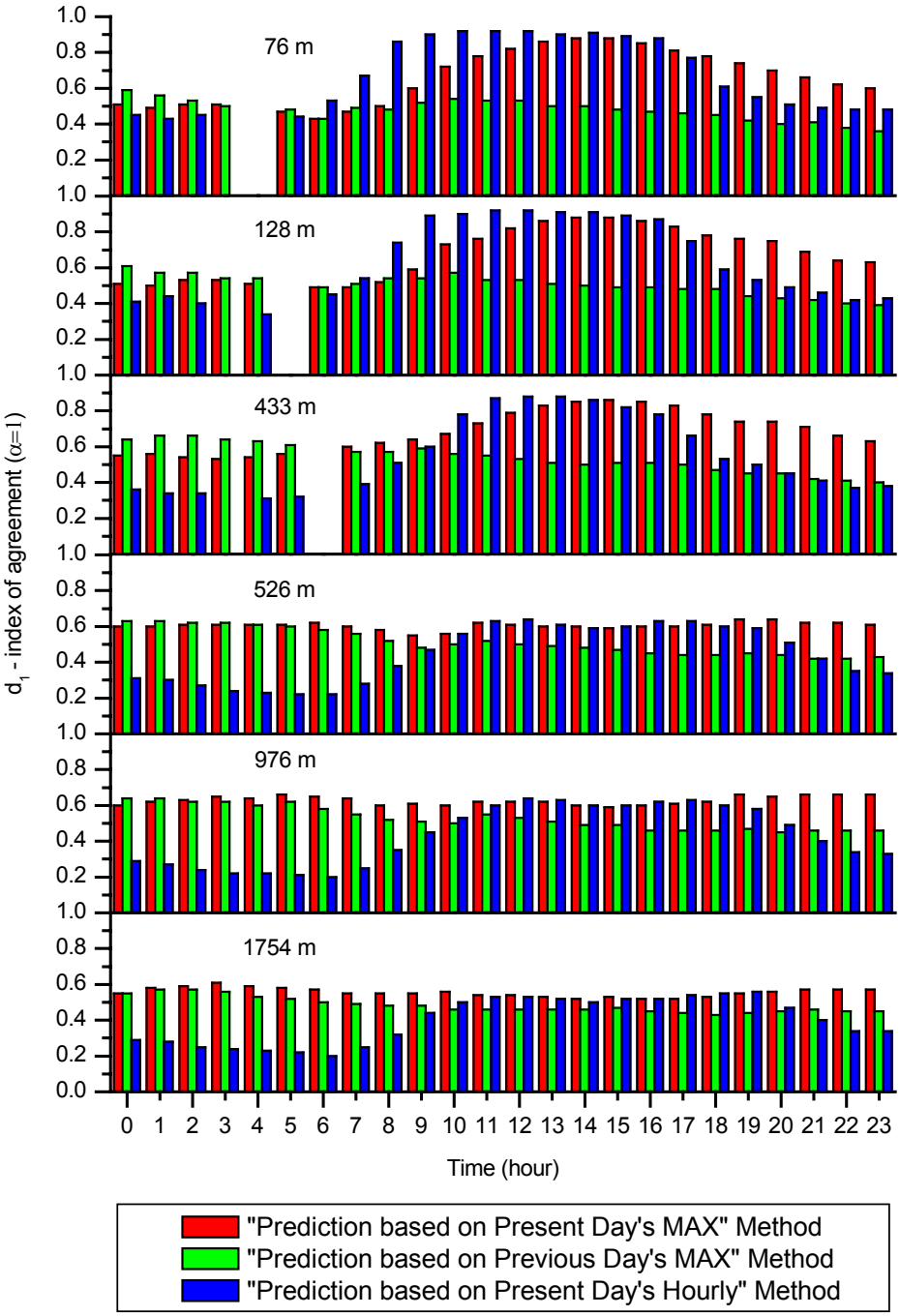

Figure 4-15. Relative Performance in Terms of d_1 (Index of Agreement, α=1) for High Elevations (76 m, 128 m, 433 m, 526 m, 976 m, and 1754 m), Using "Prediction based on Present Day's Maximum," "Prediction based on Previous Day's Maximum," and "Prediction based on Present Day's Hourly" Methods Full ozone season data (April – October) of 1998 were used.

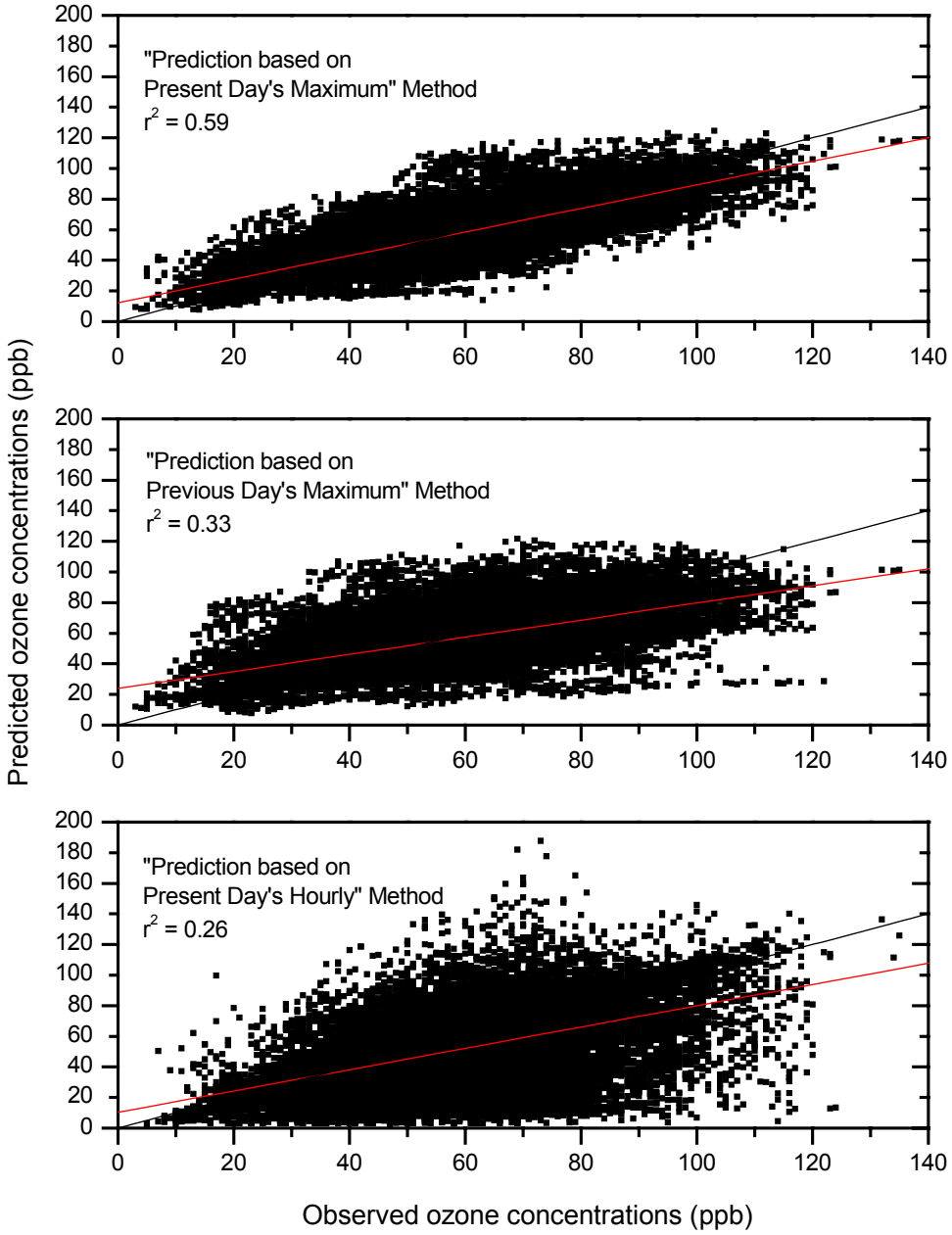

Figure 4-16. Scatter Plot of Ozone Observations (Horizontal Axes) against Predictions (Vertical Axes), Using "Prediction based on Present Day's Maximum," "Prediction based on Previous Day's Maximum," and "Prediction based on Present Day's Hourly" Methods Full ozone season data (April – October) of 1998 were used. The two diagonals in the plot indicate the best-fit regression line through the data and the line of perfect correspondence between observations and predictions.

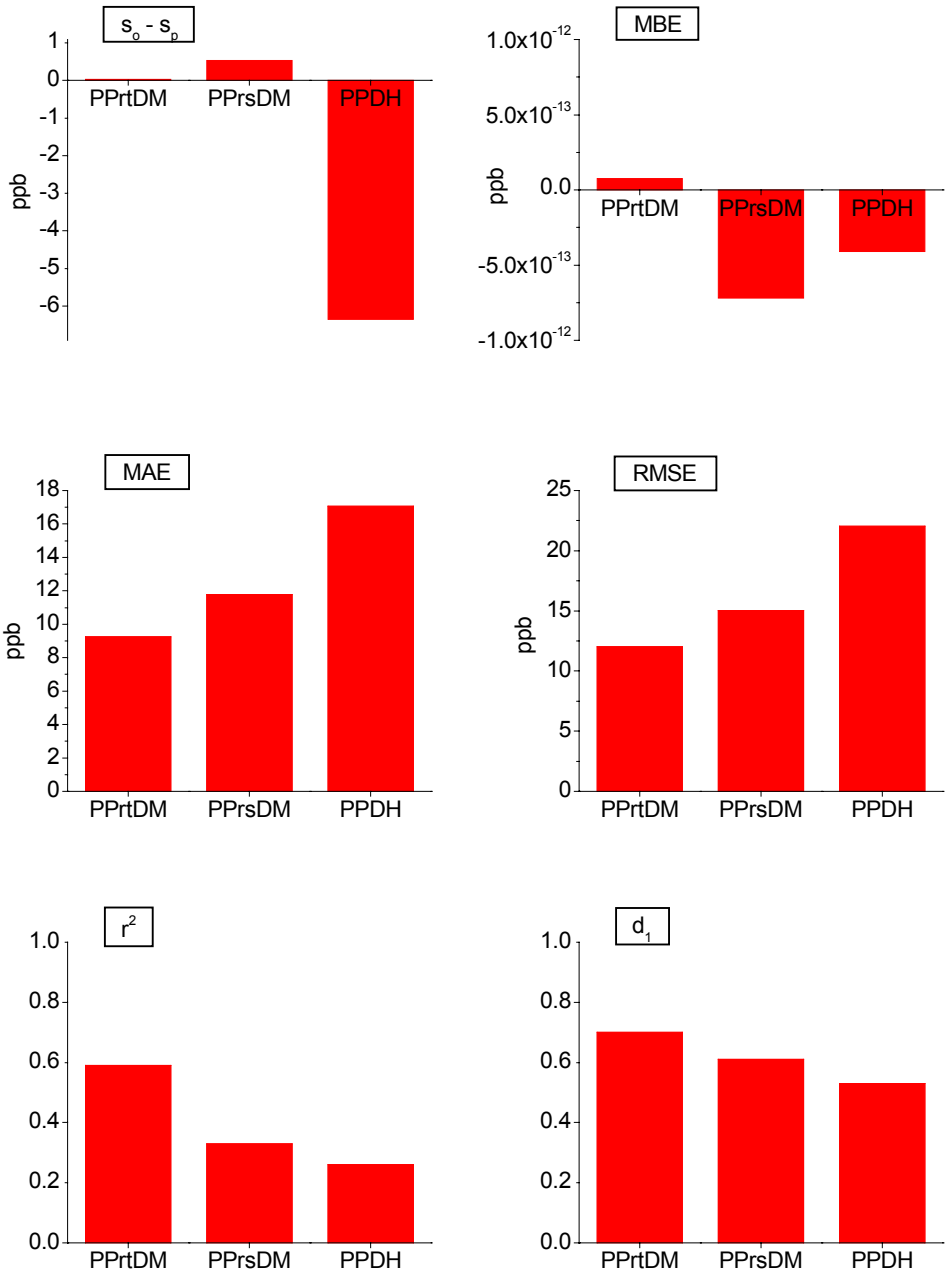

Figure 4-17. Comparison of Relative Performance in Terms of the Statistical Results Produced by "Prediction based on Present Day's Maximum (PPrtDM)," "Prediction based on Previous Day's Maximum (PPrsDM)," and "Prediction based on Present Day's Hourly (PPDH)" Methods Full ozone season data (April – October) of 1998 were used.

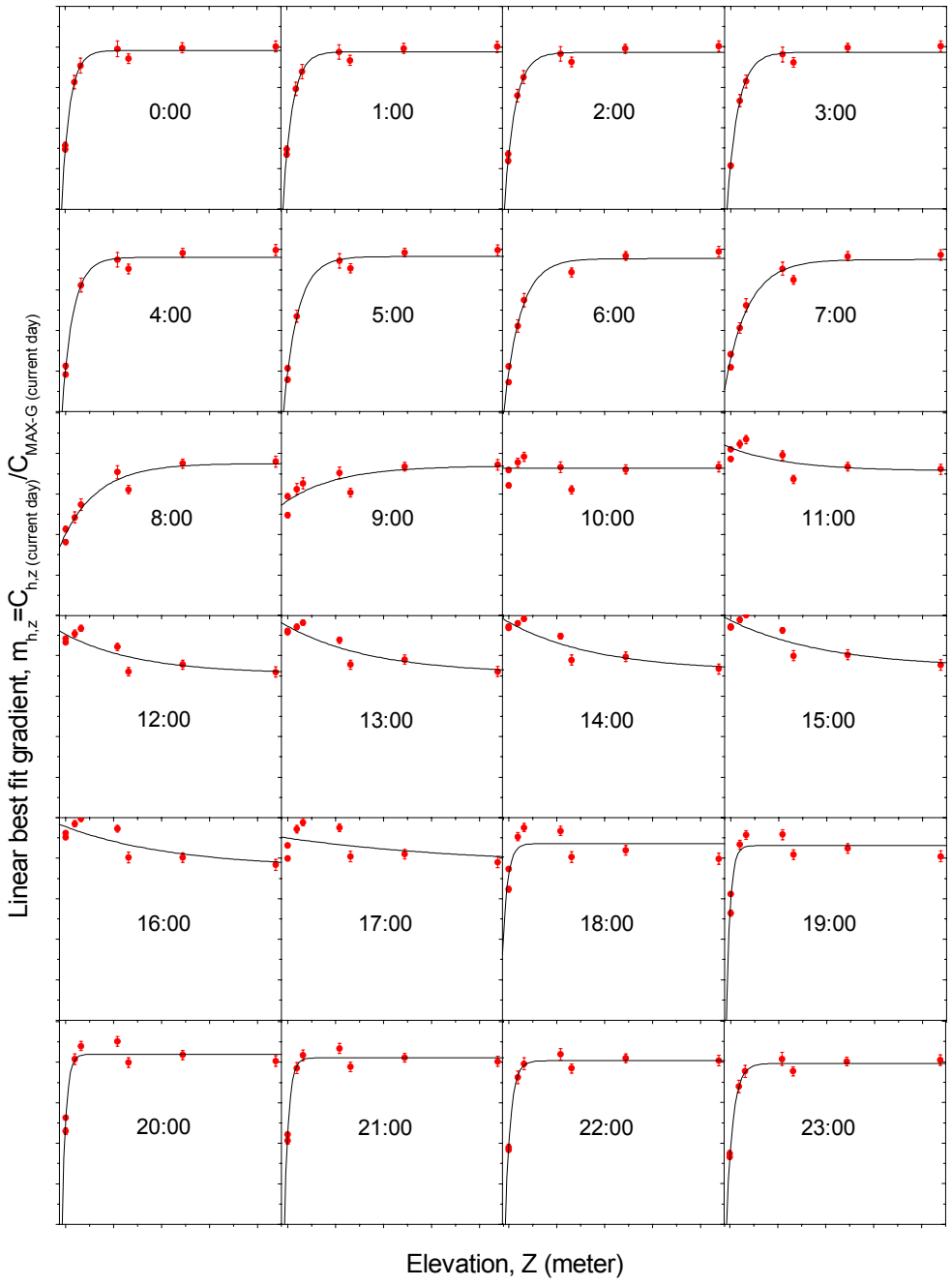

Figure 4-18. Non-Linear Curve Fit of Linear Best-Fit Gradient (Vertical Axes) against Elevation (Horizontal Axes) to Develop the Overall Regression Model as a Function of Elevation for a Particular Time of Day Full ozone season data (April – October) of 1998 were used. The scale on X axes is from 0 to 1800 meter in 200-meter increments. The scale on Y axes is from 0 to 1 in 0.1 increment. Error bars indicate standard error in gradient at 95% confidence level.

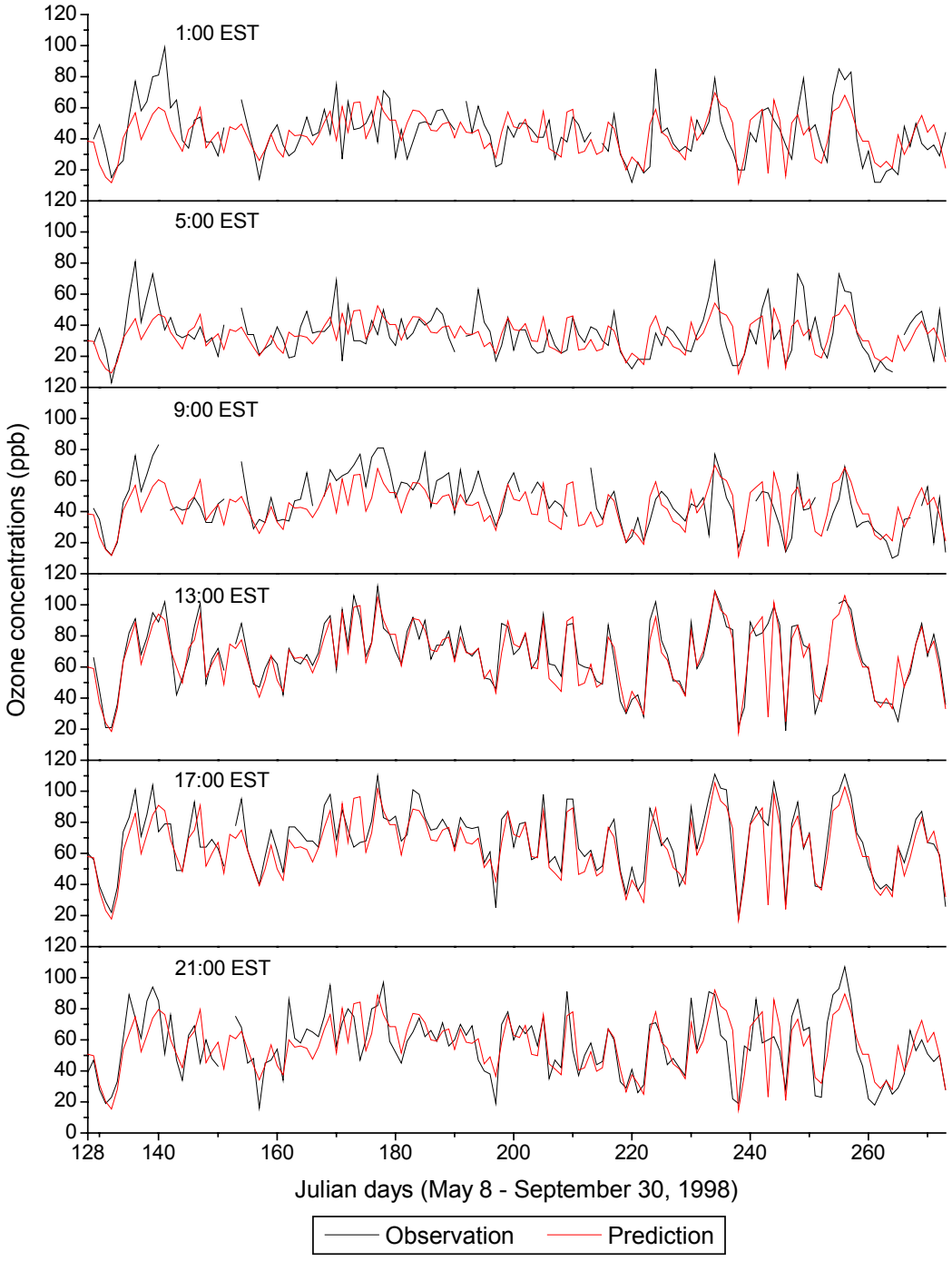

Figure 4-19. Comparison of Ozone Observations and Predictions Predicted by the Overall Regression Model for 76 m High Elevation Site

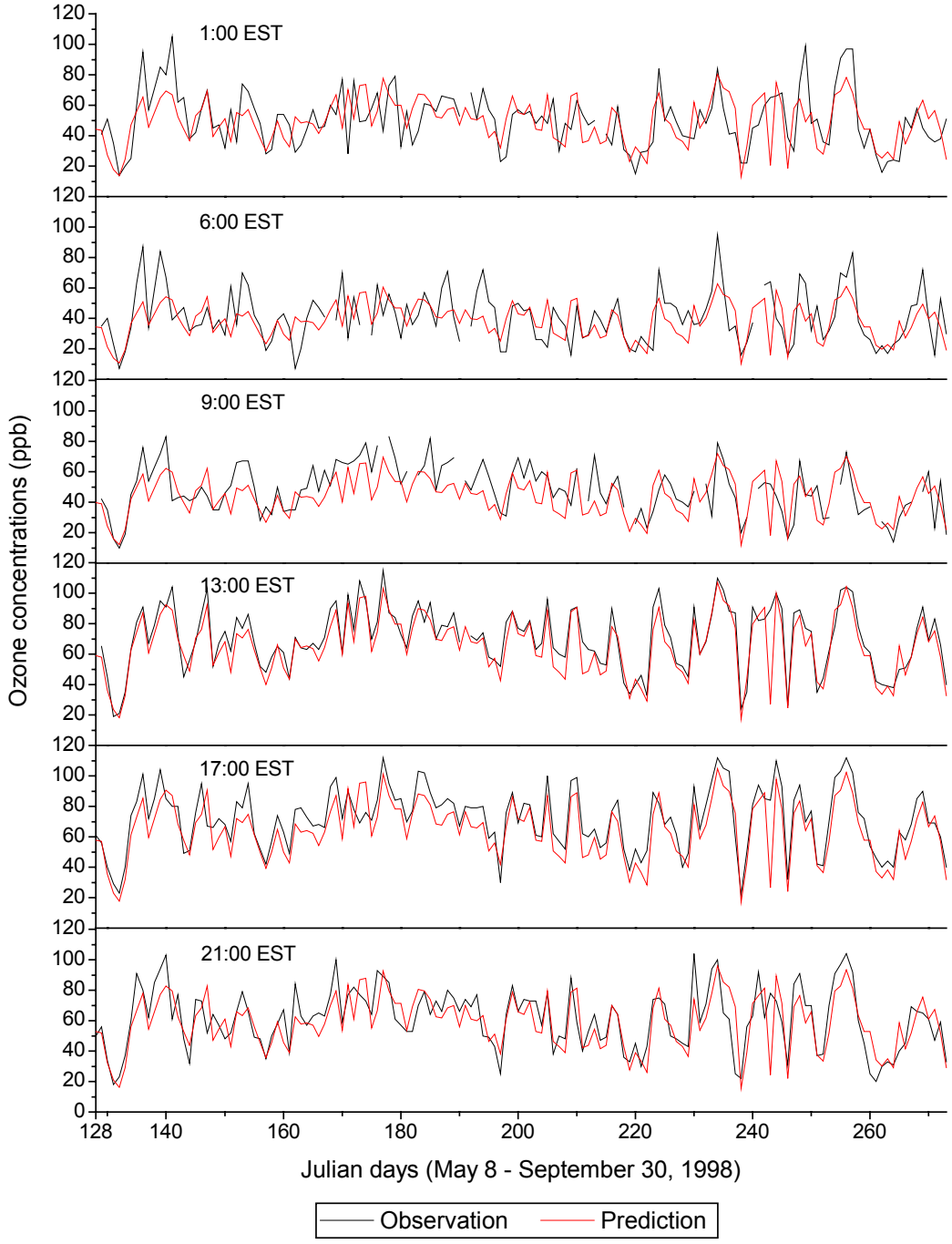

Figure 4-20. Comparison of Ozone Observations and Predictions Predicted by the Overall Regression Model for 128 m High Elevation Site

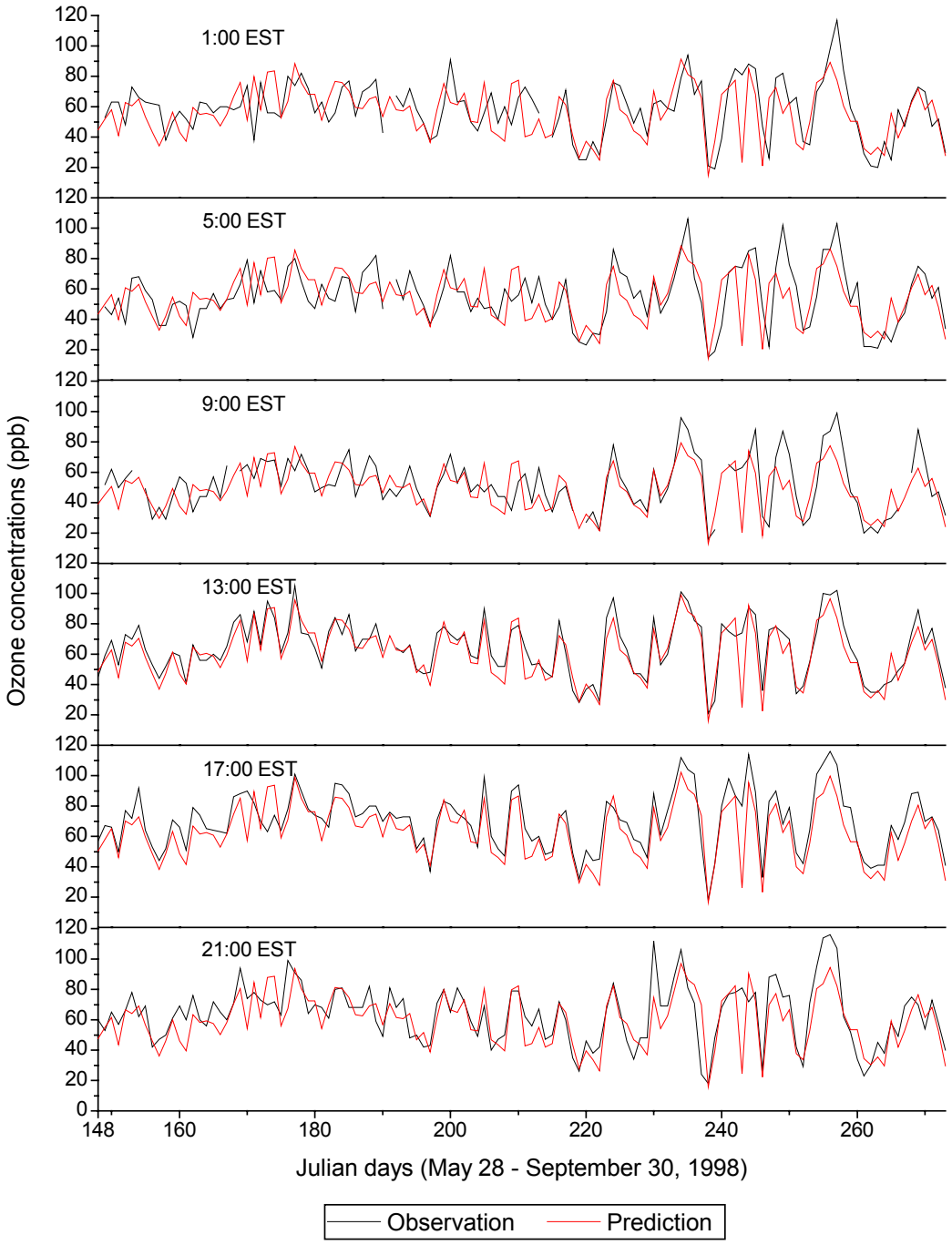

Figure 4-21. Comparison of Ozone Observations and Predictions Predicted by the Overall Regression Model for 433 m High Elevation Site

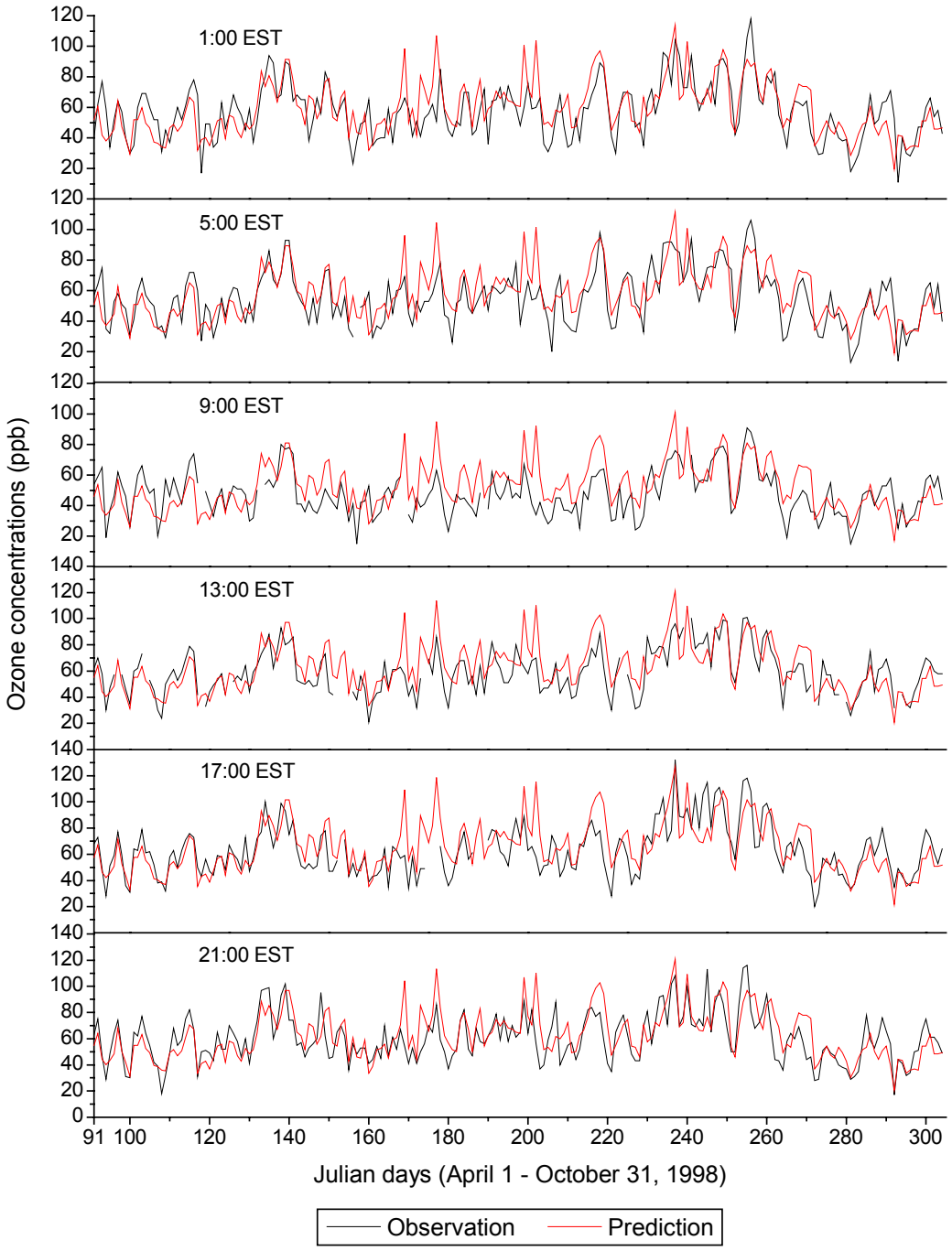

Figure 4-22. Comparison of Ozone Observations and Predictions Predicted by the Overall Regression Model for 526 m High Elevation Site

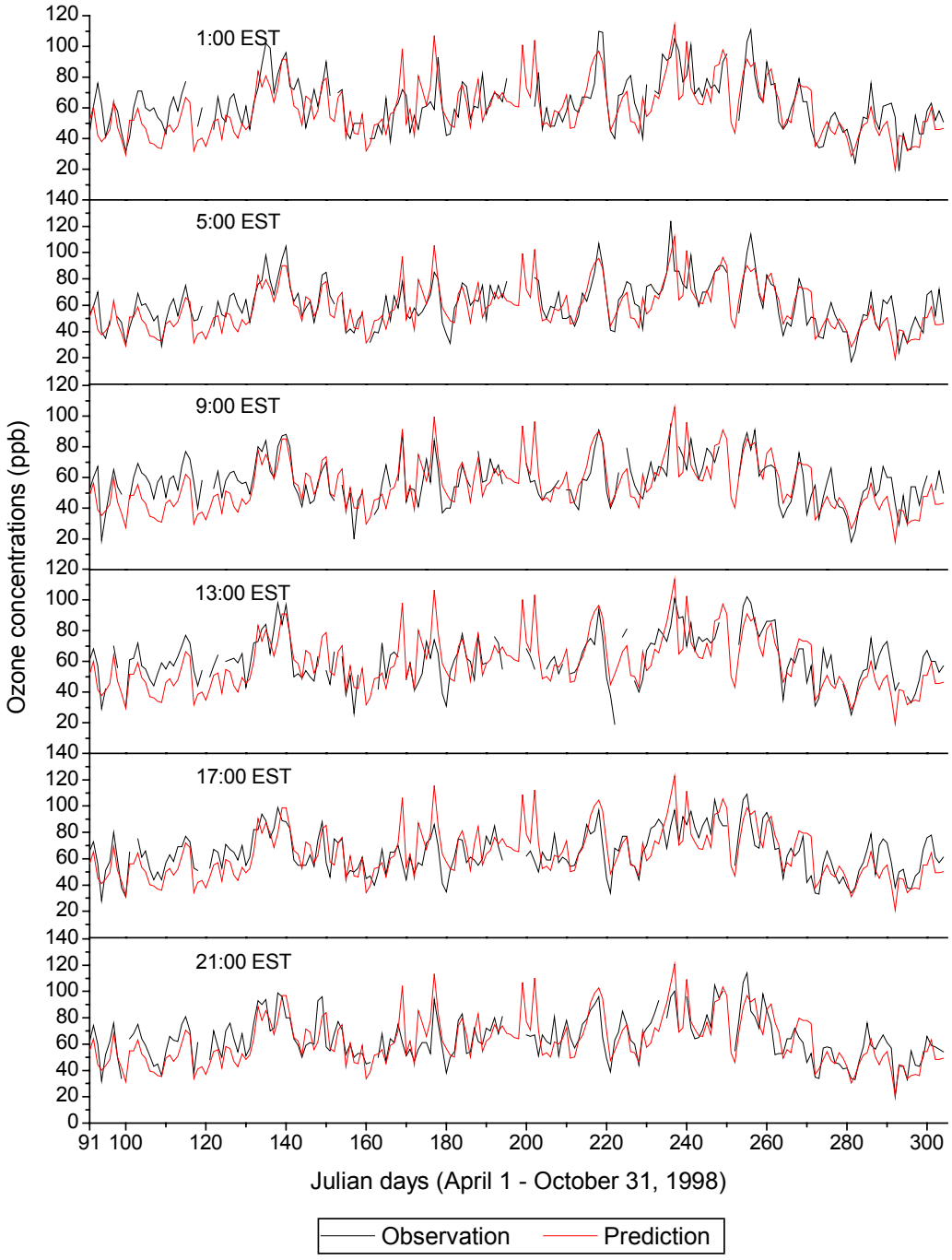

Figure 4-23. Comparison of Ozone Observations and Predictions Predicted by the Overall Regression Model for 976 m High Elevation Site

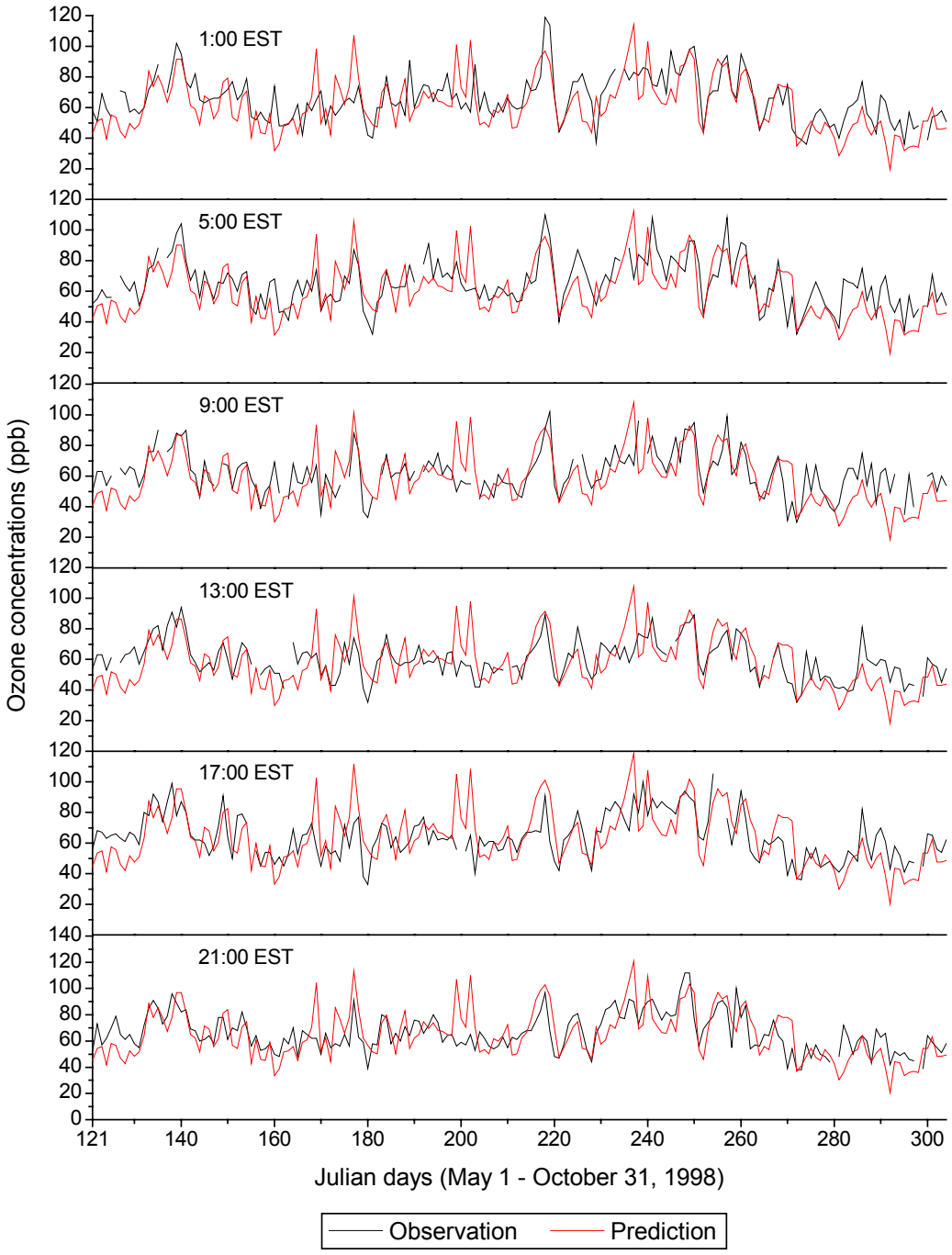

Figure 4-24. Comparison of Ozone Observations and Predictions Predicted by the Overall Regression Model for 1754 m High Elevation Site

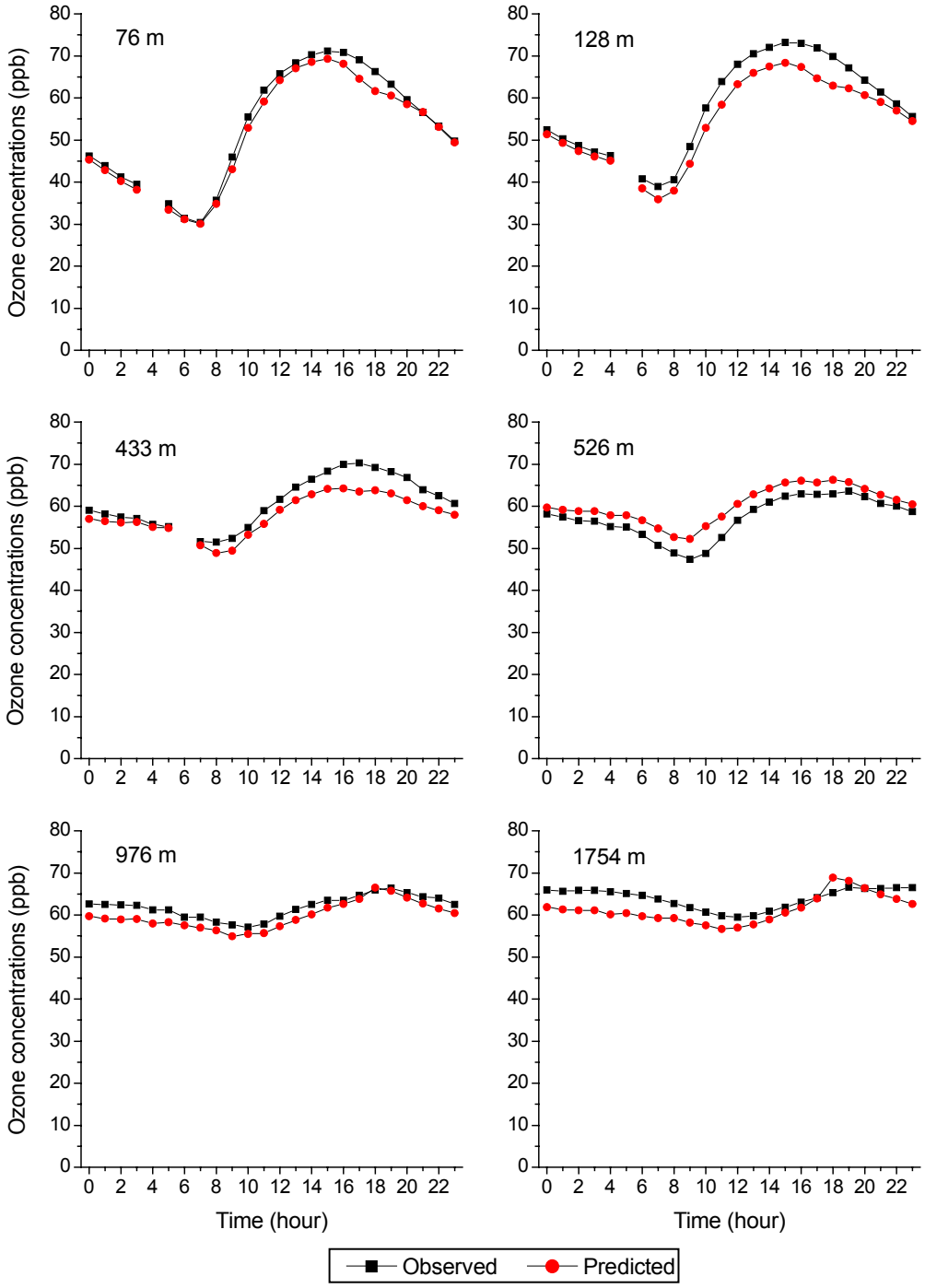

Figure 4-25. Comparison of Mean Diurnal Variations of Observations and Predictions Predicted by the Overall Regression Model Full ozone season data (April – October) of 1998 were used.

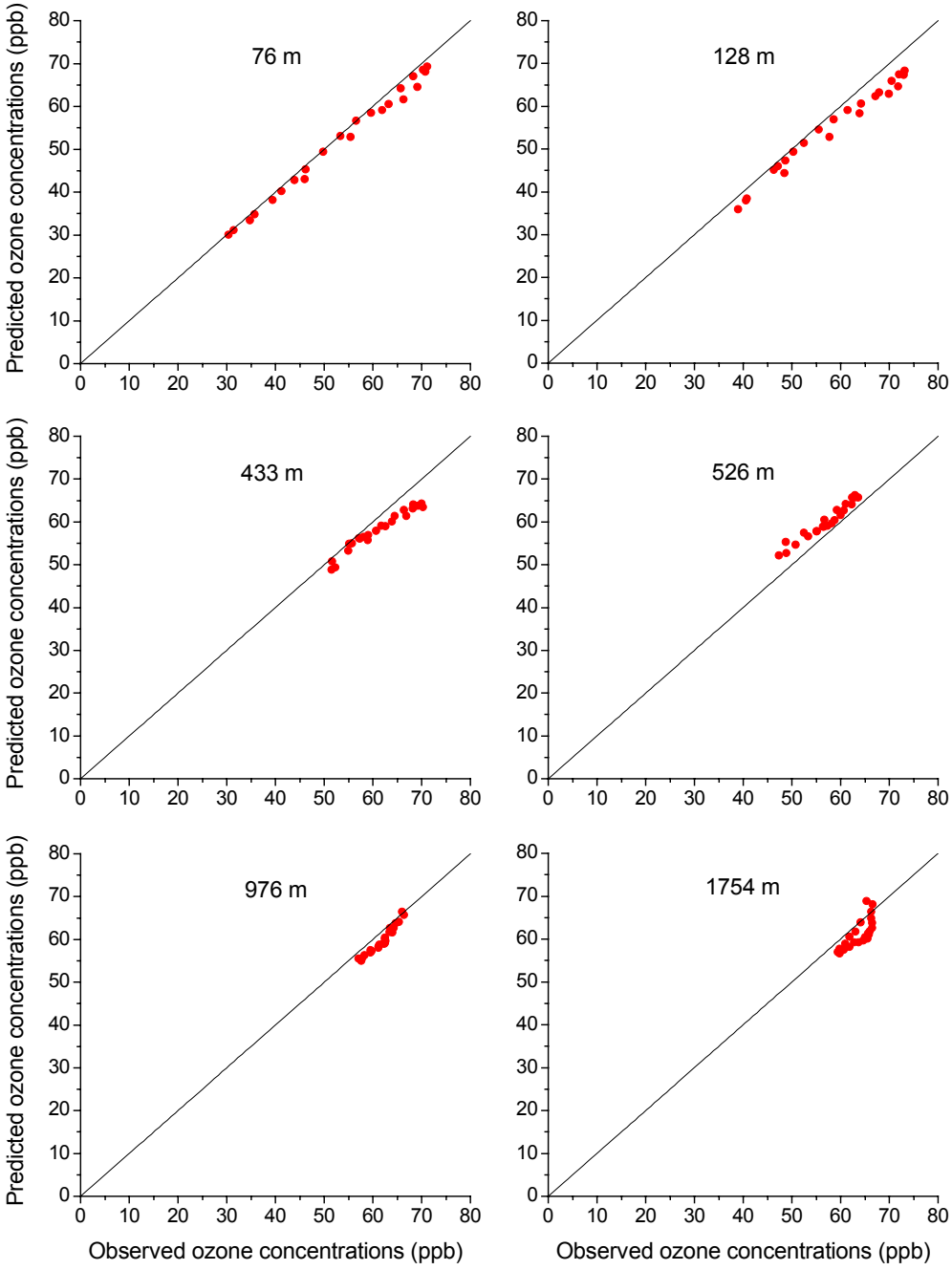

Figure 4-26. Observed versus Predicted Hourly Mean Ozone Concentrations of the Overall Regression Model Full ozone season data (April – October) of 1998 were used. The diagonal in each plot indicates a perfect correspondence between observations and predictions.

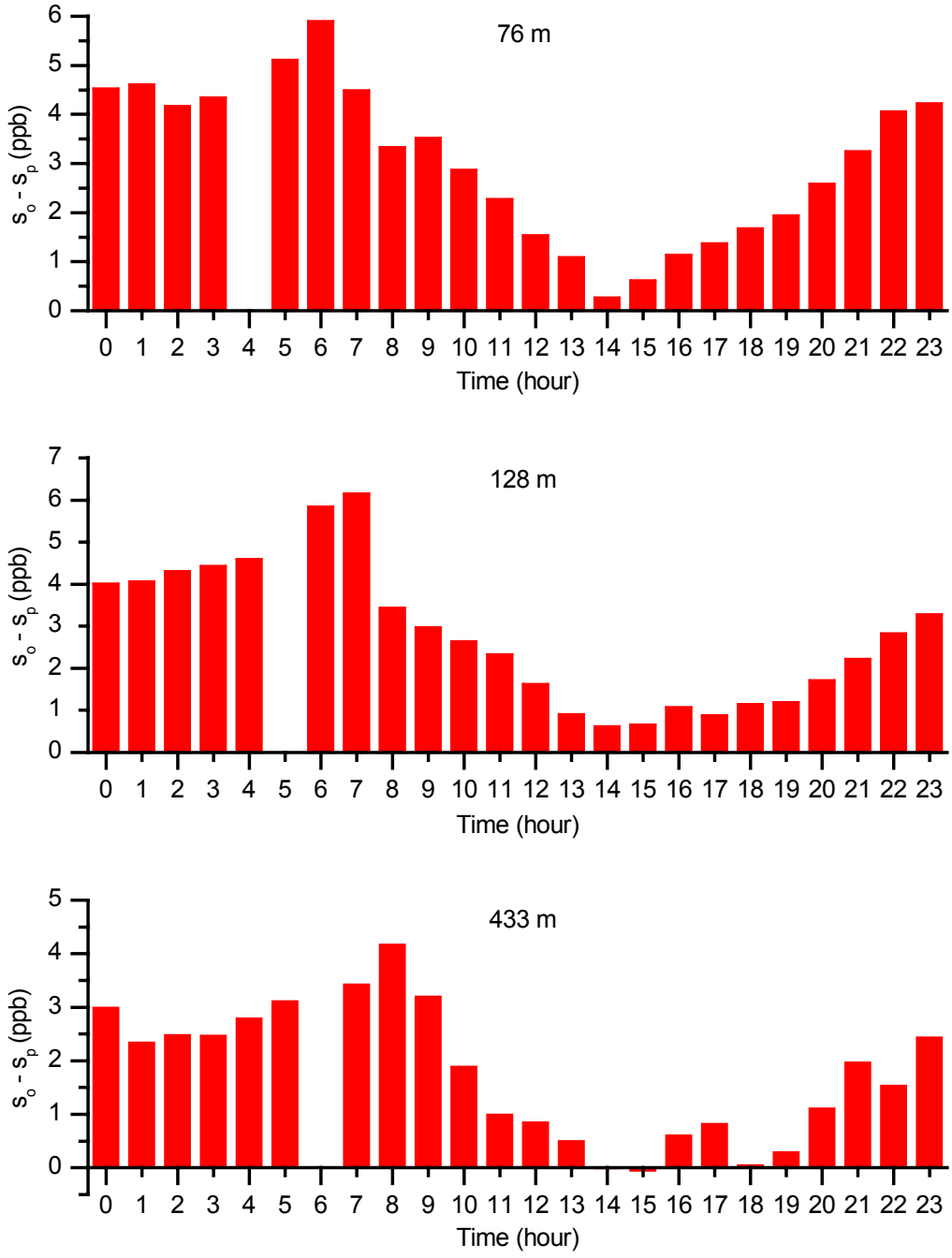

Figure 4-27. Residuals between the Standard Deviations of Ozone Observations and the Overall Regression Model Predictions for High Elevations (76 m, 128 m, and 433 m) Full ozone season data (April – October) of 1998 were used.

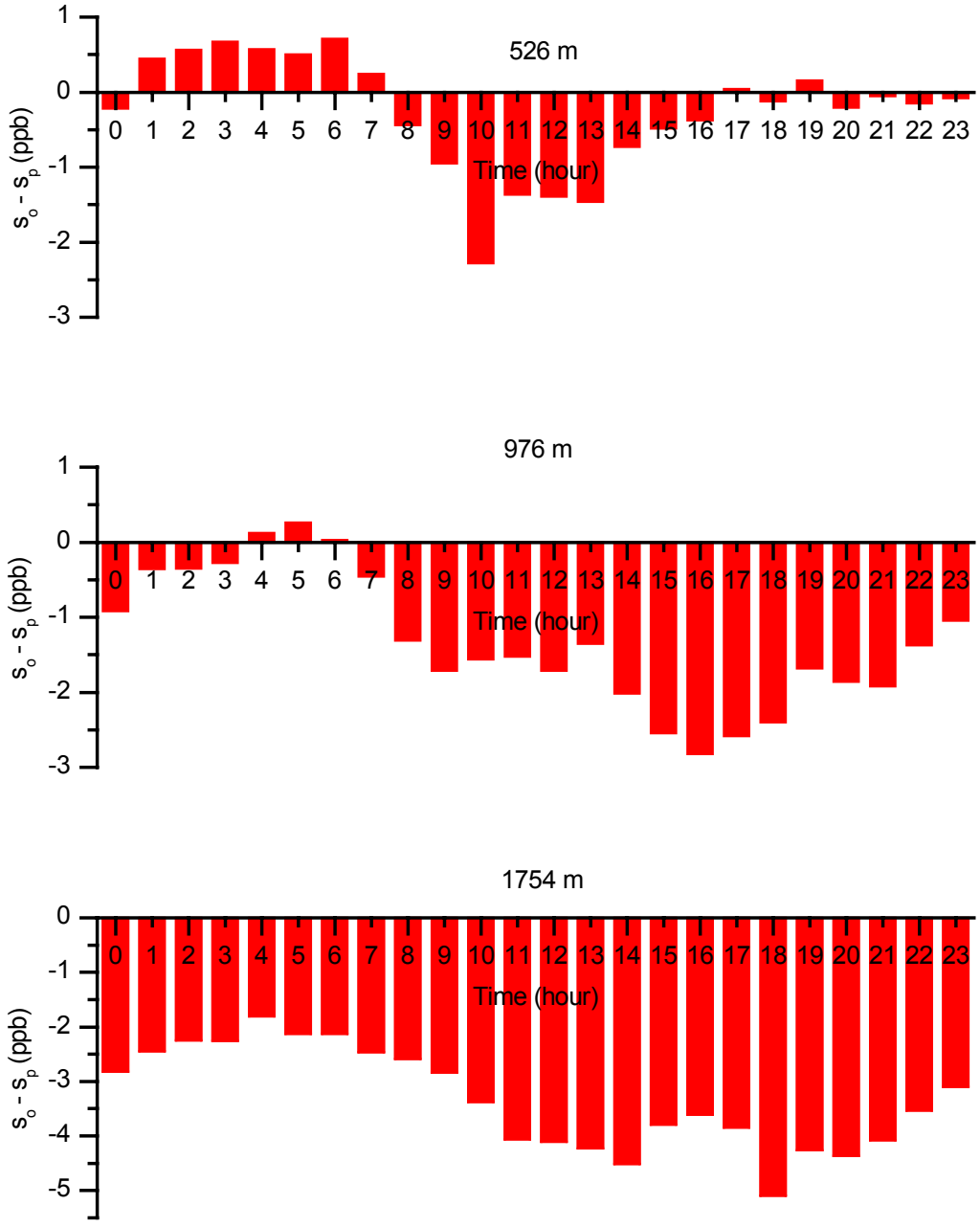

Figure 4-28. Residuals between the Standard Deviations of Ozone Observations and the Overall Regression Model Predictions for High Elevations (526 m, 976 m, and 1754 m) Full ozone season data (April – October) of 1998 were used.

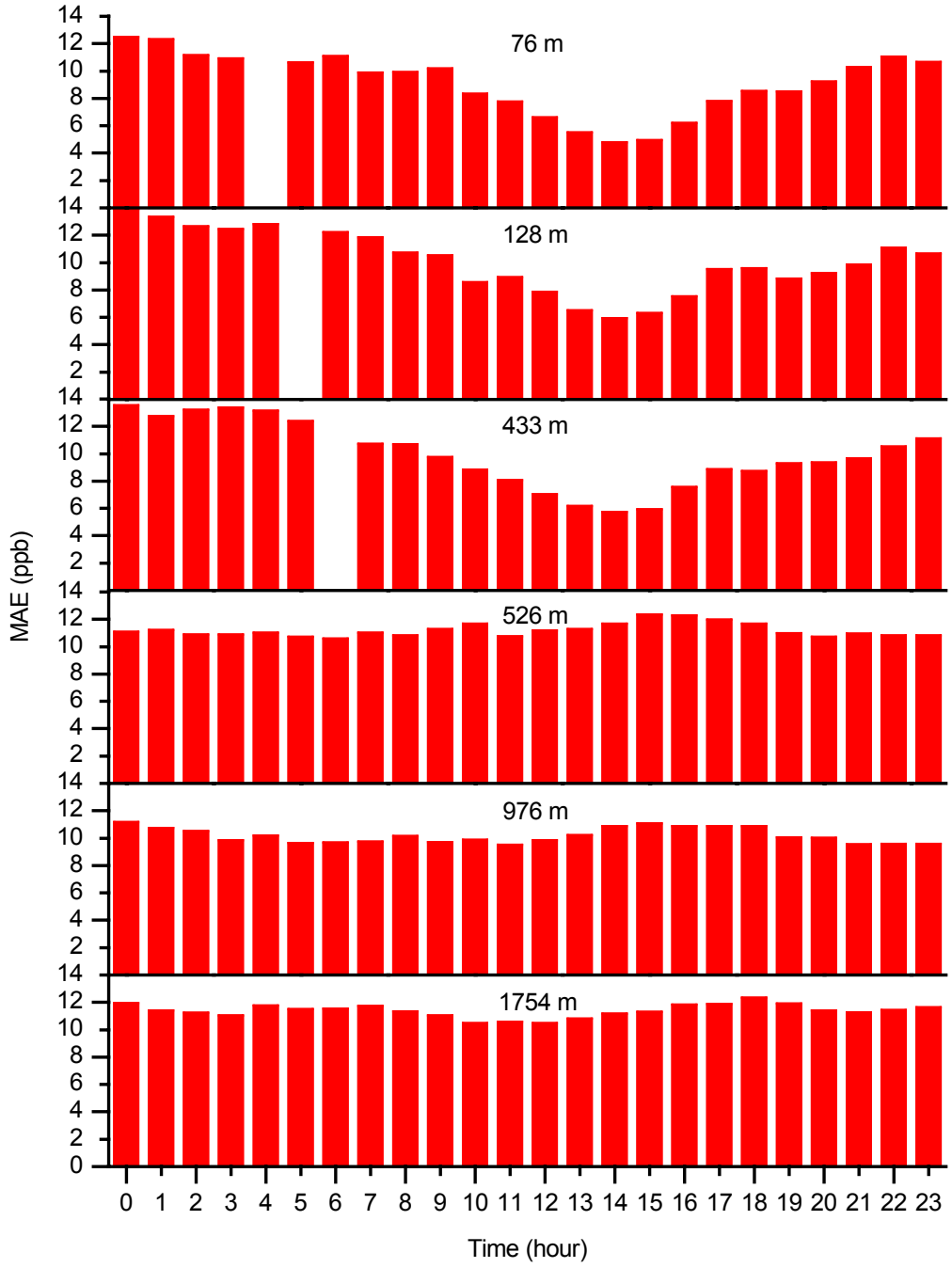

Figure 4-29. Mean Absolute Error Yielded by the Overall Regression Model for High Elevations (76 m, 128 m, 433 m, 526 m, 976 m, and 1754 m) Full ozone season data (April – October) of 1998 were used.

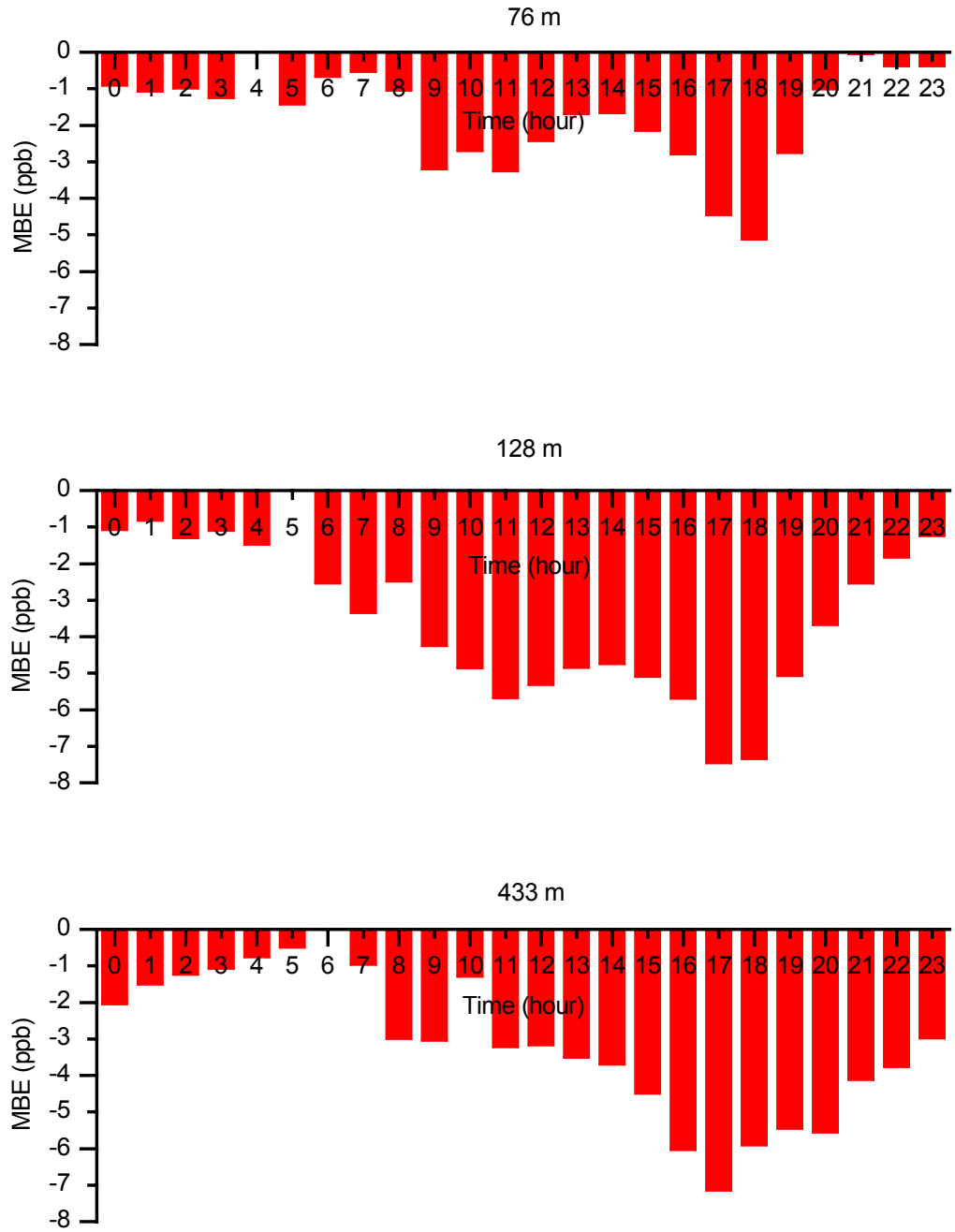

Figure 4-30. Mean Bias Error Yielded by the Overall Regression Model for High Elevations (76 m, 128 m, and 433 m) Full ozone season data (April – October) of 1998 were used.

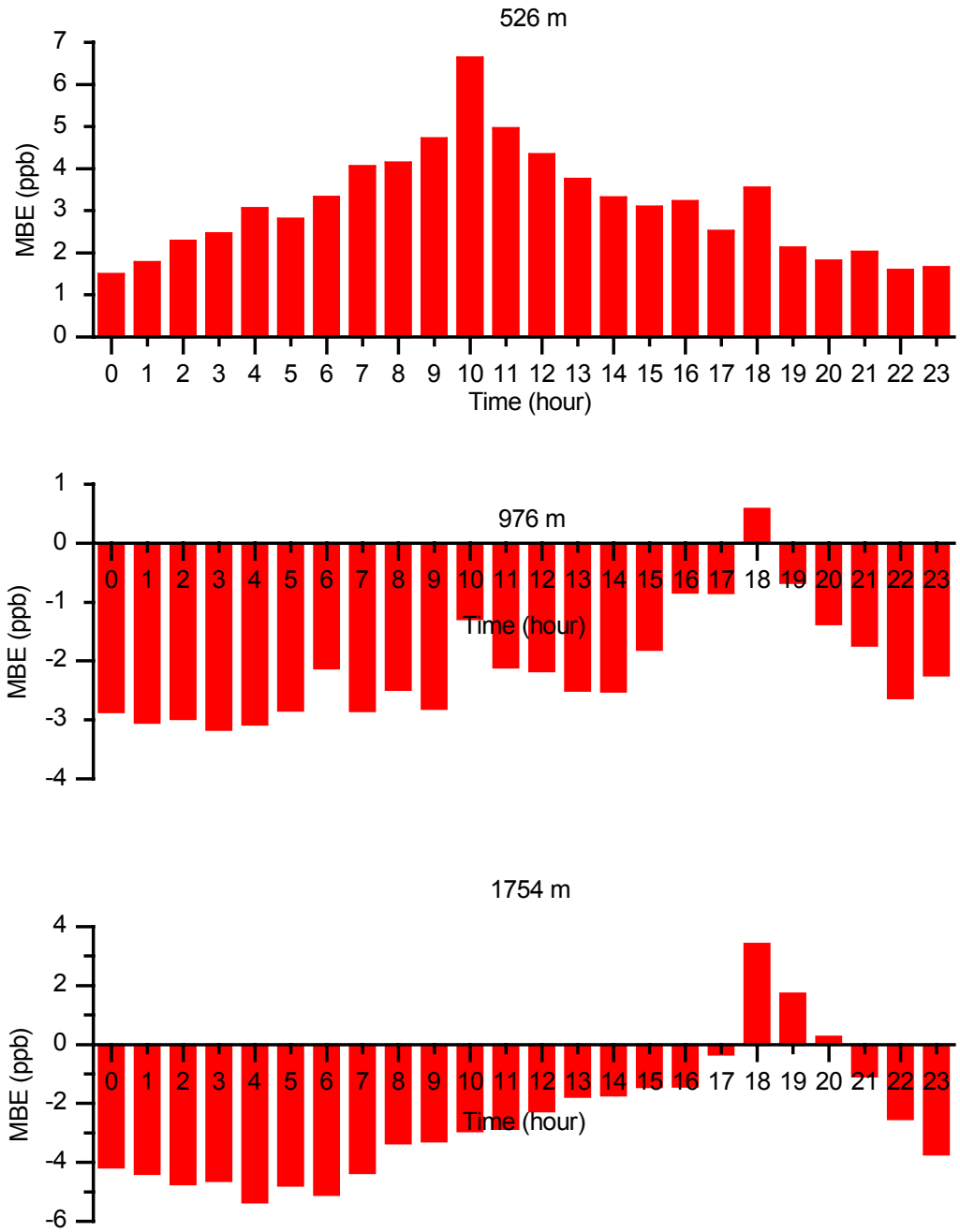

Figure 4-31. Mean Bias Error Yielded by the Overall Regression Model for High Elevations (526 m, 976 m, and 1754 m) Full ozone season data (April – October) of 1998 were used.

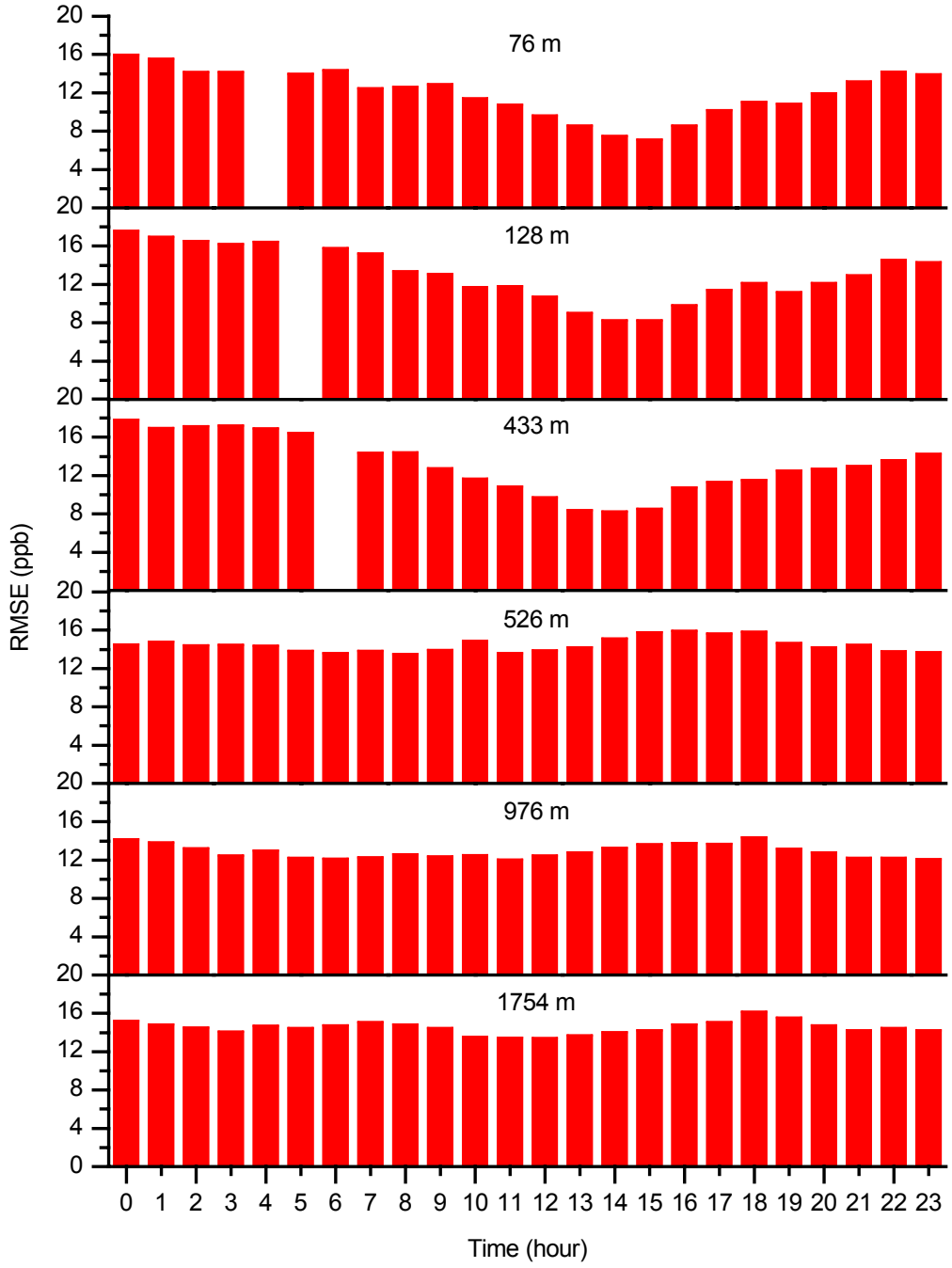

Figure 4-32. Root Mean Square Error Yielded by the Overall Regression Model for High Elevations (76 m, 128 m, 433 m, 526 m, 976 m, and 1754 m) Full ozone season data (April – October) of 1998 were used.

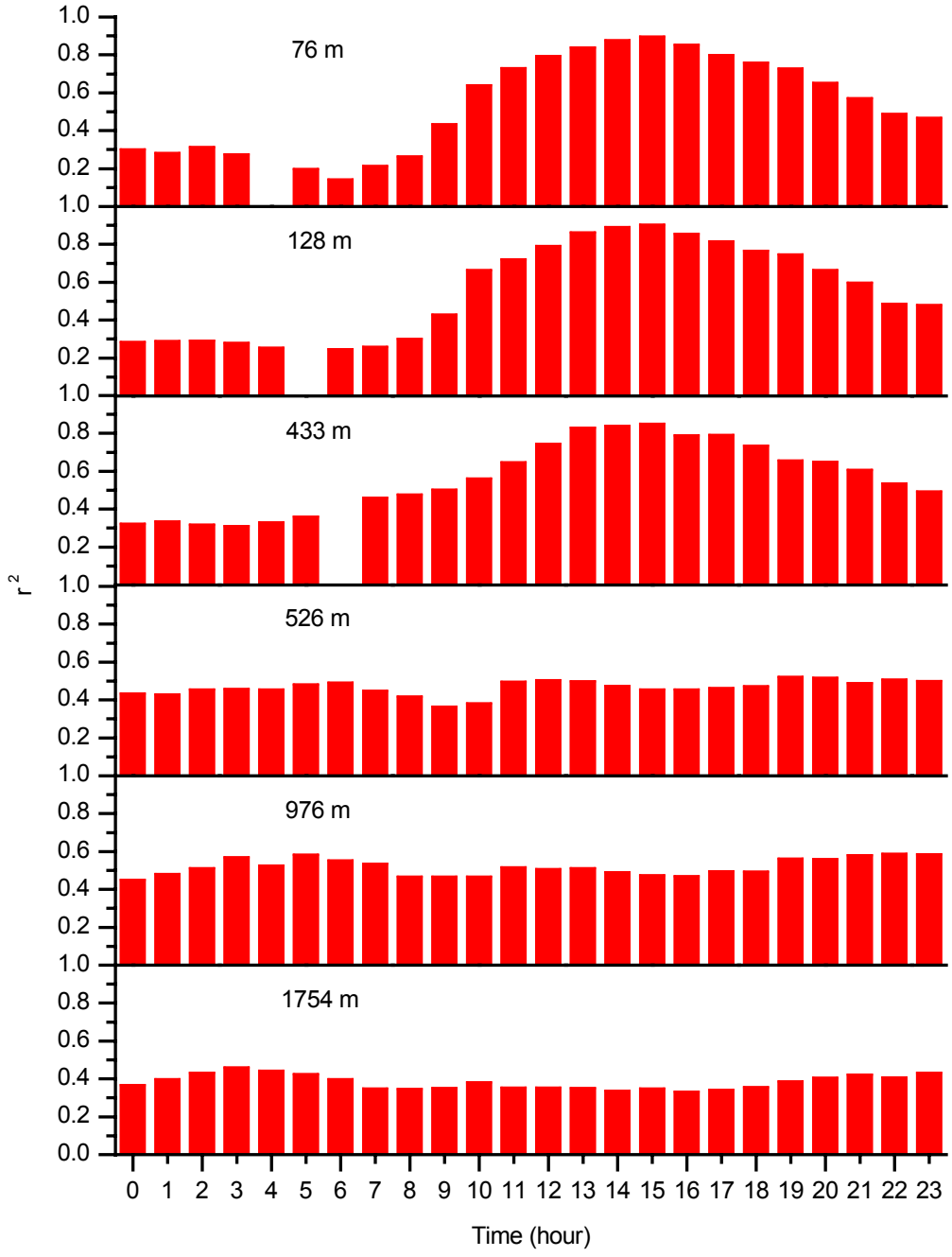

Figure 4-33. Coefficient of Determination (r^2) Calculated to Evaluate the Performance of the Overall Regression Model for High Elevations (76 m, 128 m, 433 m, 526 m, 976 m, and 1754 m) Full ozone season data (April – October) of 1998 were used.

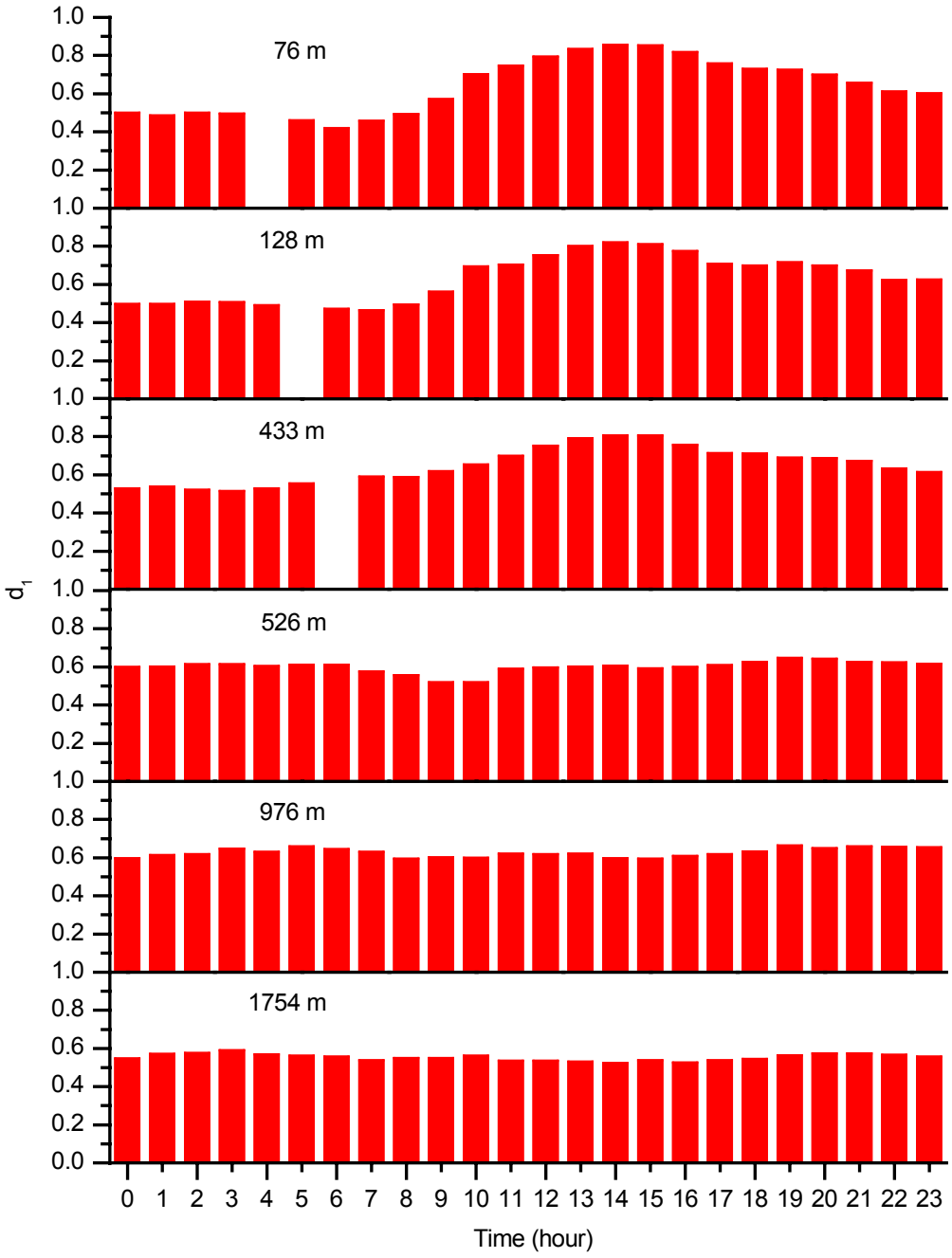

Figure 4-34. Index of Agreement (d_1) Calculated to Evaluate the Performance of the Overall Regression Model for High Elevations (76 m, 128 m, 433 m, 526 m, 976 m, and 1754 m) Full ozone season data (April – October) of 1998 were used.

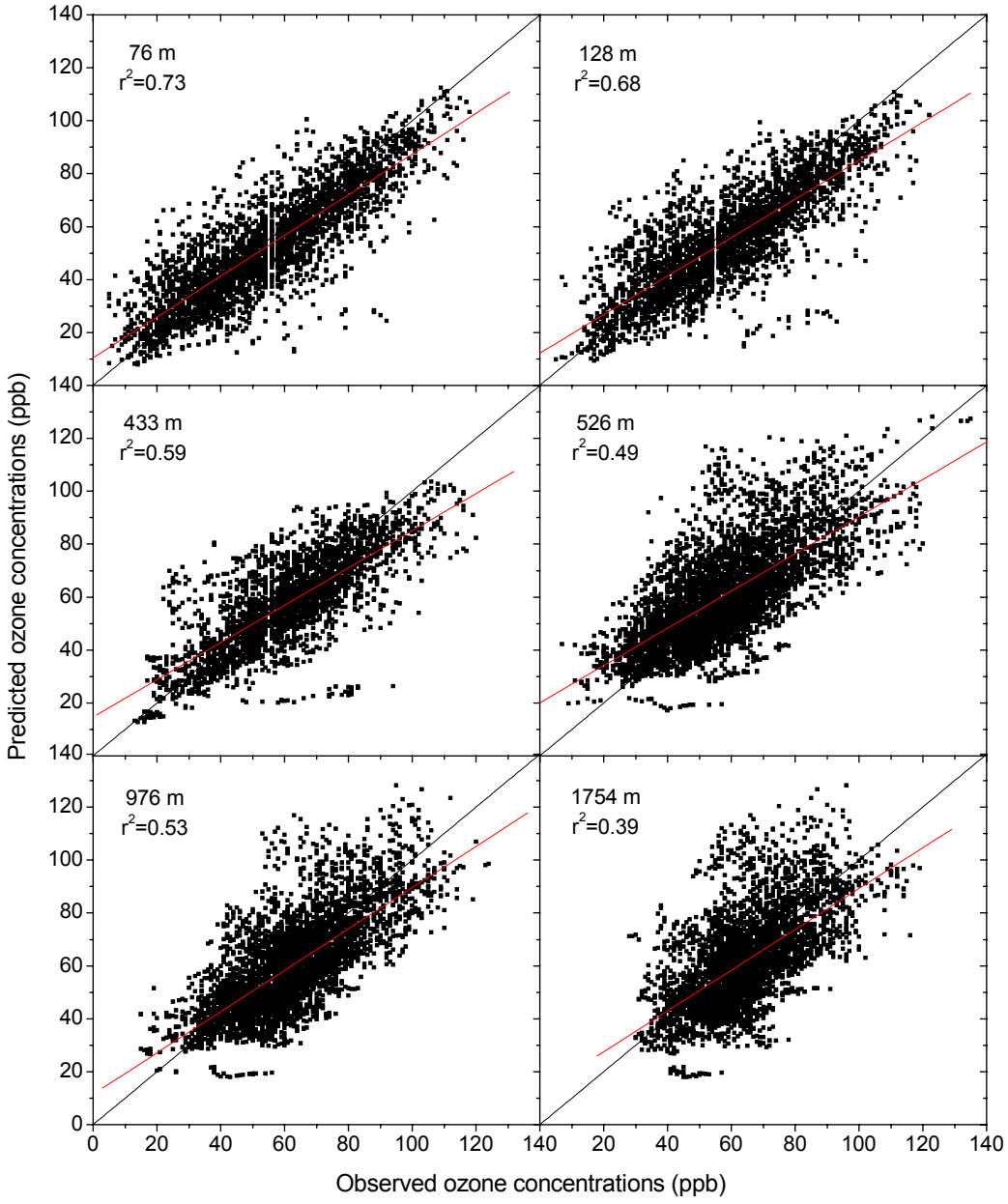

Figure 4-35. Correlation of All Hours Ozone Concentrations between Observations and the Overall Regression Model Predictions for High Elevations (76 m, 128 m, 433 m, 526 m, 976 m, and 1754 m) Full ozone season data (April – October) of 1998 were used. The two diagonals in the plots indicate the best-fit regression line through the data and the line of perfect correspondence between observations and predictions.

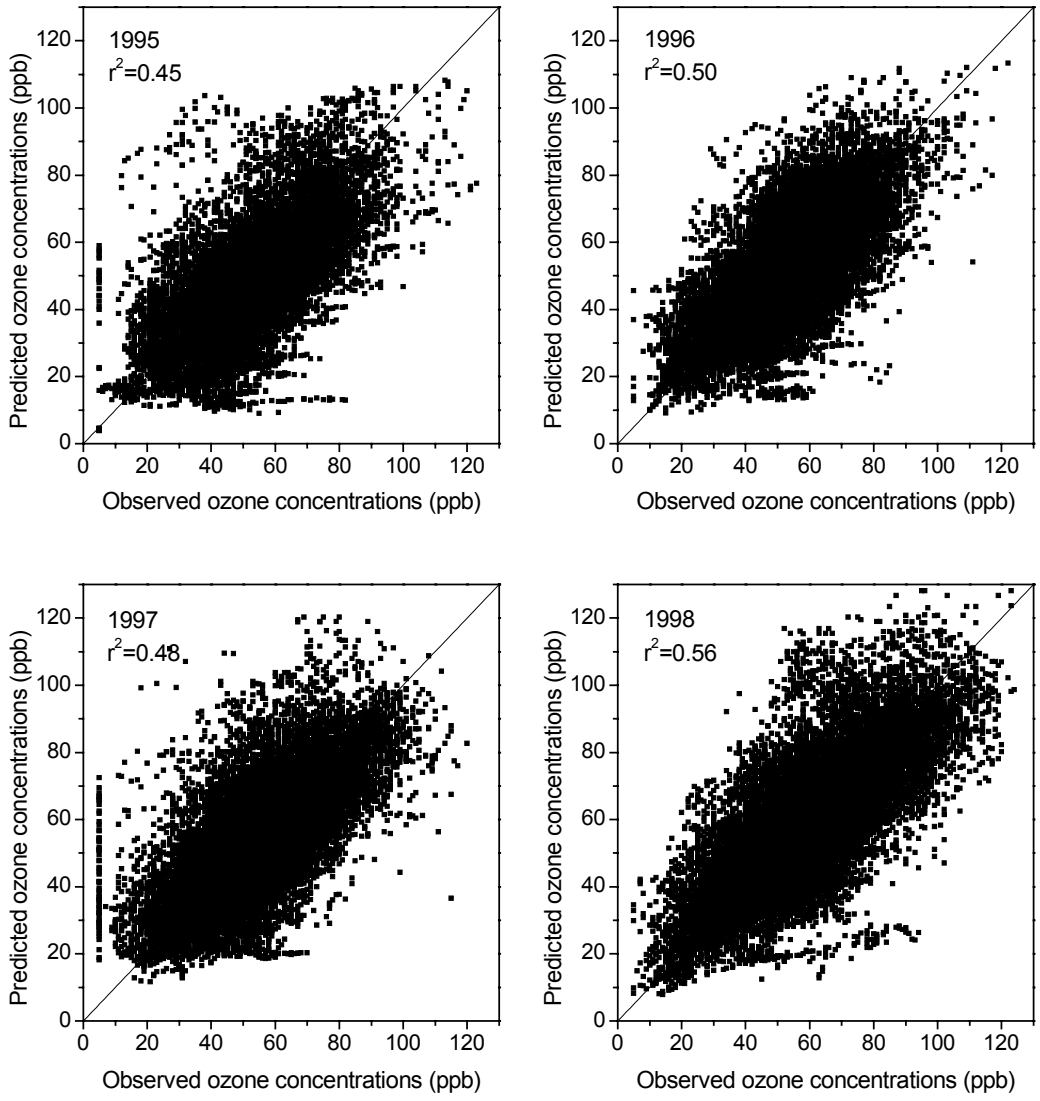

Figure 4-36. Scatter Plot of Ozone Observations (Horizontal Axes) against the Overall Regression Model Predictions (Vertical Axes) for Four-Year Ozone Data (1995-1998) The algorithm developed with 1998 ozone data is applied for four-year ozone data from 1995 to 1998. The scale on all axes is from 0 to 130 ppb in 10 ppb increment. The two diagonals in the plot indicate the best-fit regression line through the data and the line of perfect correspondence between observations and predictions.

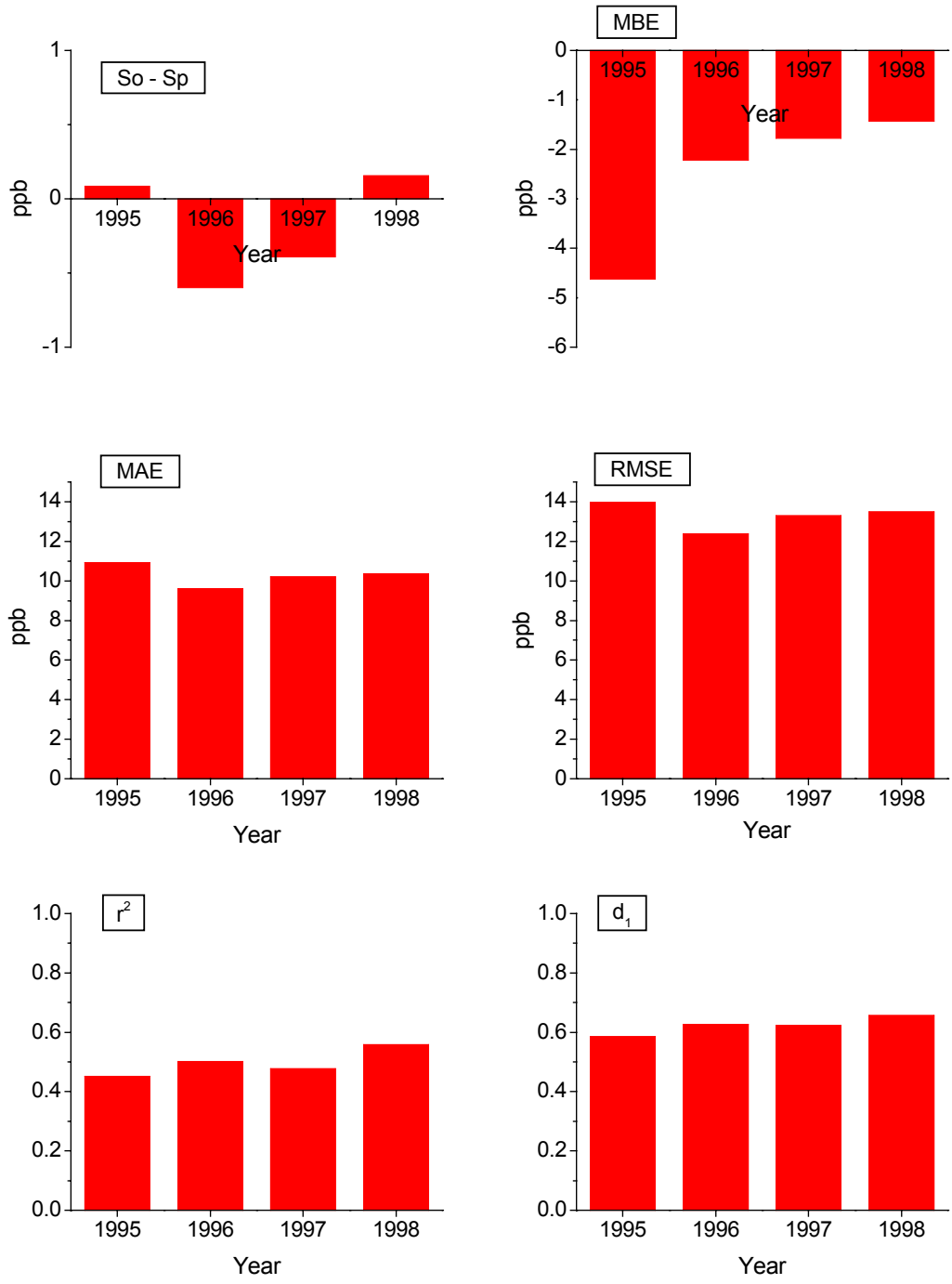

Figure 4-37. Comparison of Relative Performance in Terms of the Statistical Results Produced by the Overall Regression Model When the Model Developed with 1998 Ozone Data Was Applied to Four-Year Ozone Data (1995 - 1998)

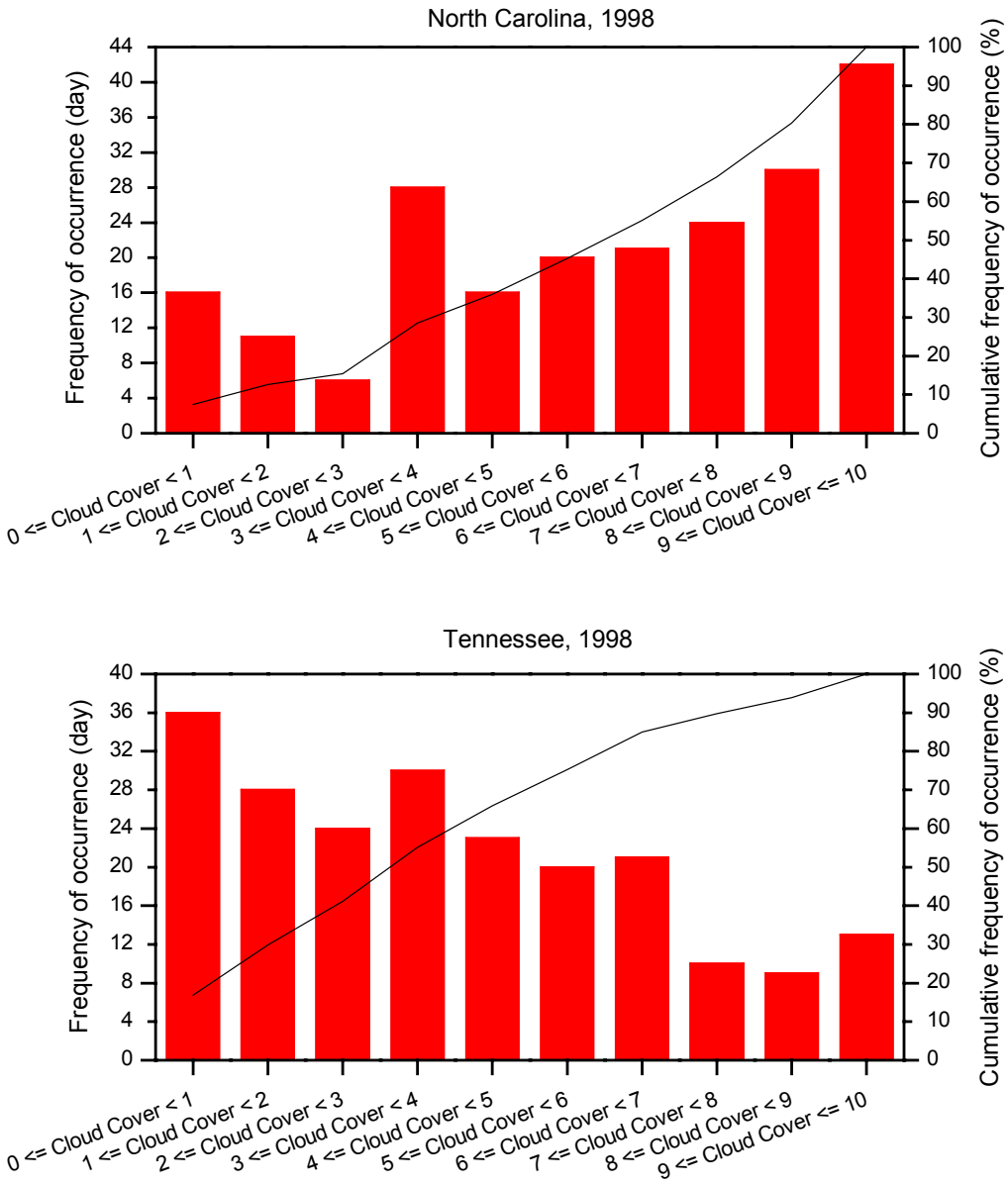

Figure 4-38. Frequency of Cloud Cover Occurred in North Carolina and Tennessee State during Ozone Season (April – October) of 1998

The indexes are calculated 24-hour cloud cover average values of each day. The cloud cover data in TD3240 surface meteorological data format were used and obtained from National Climatic Data Center. The value indicates the degree of cloud cover. Zero means a perfect clear and ten means overcast.

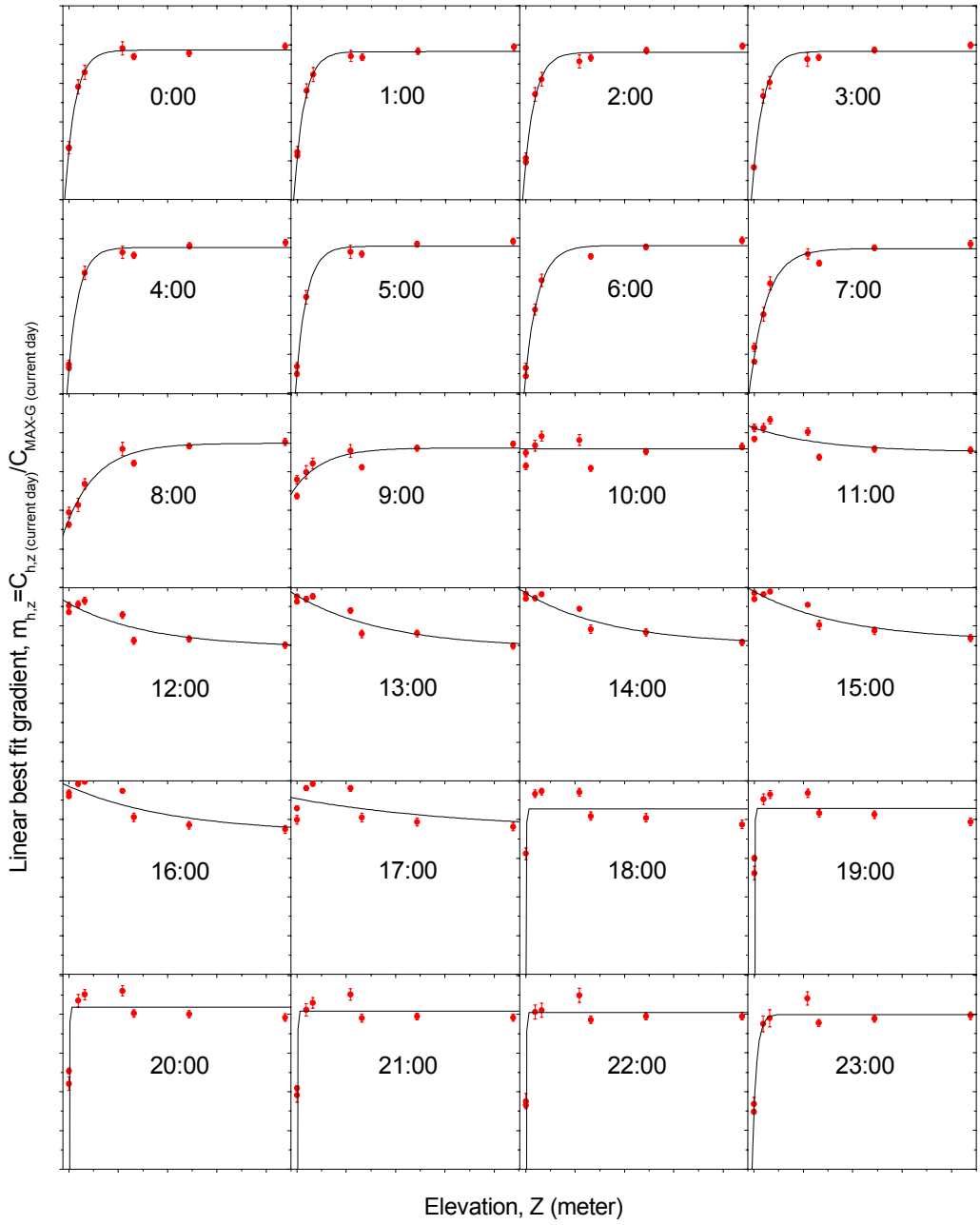

Figure 4-39. Non-Linear Curve Fit of Linear Best Fit Gradient (Vertical Axes) against Elevation (Horizontal Axes) to Develop the "Clear" Component Regression Model as a Function of Elevation for a Particular Time of Day Full ozone season data (April – October) of 1998 were used. The scale on X axes is from 0 to 1800 meter in 200-meter increments. The scale on Y axes is from 0 to 1 in 0.1 increment. Error bars indicate standard error in gradient at 95% confidence level.

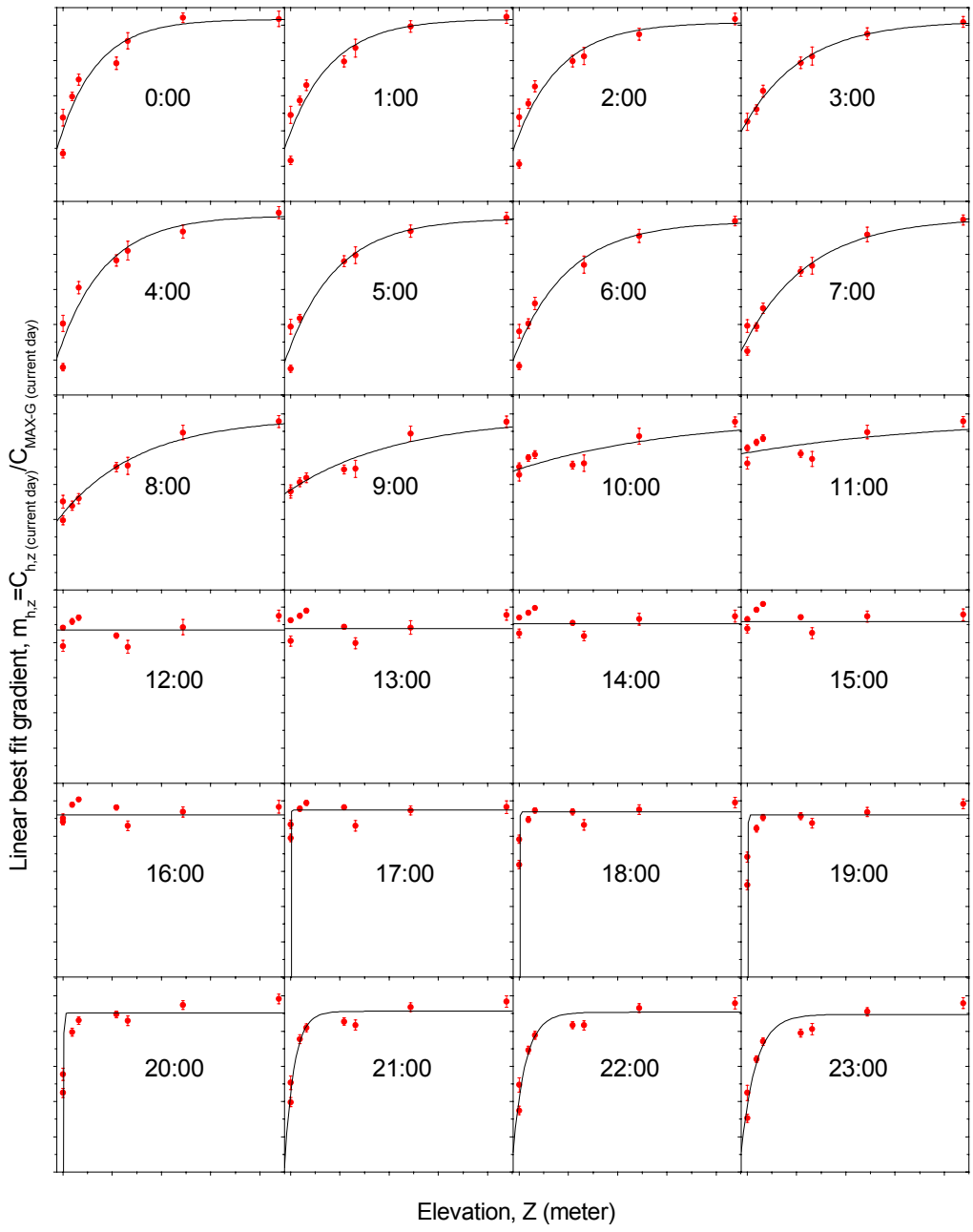

Figure 4-40. Non-Linear Curve Fit of Linear Best Fit Gradient (Vertical Axes) against Elevation (Horizontal Axes) to Develop the "Cloudy" Component Regression Model as a Function of Elevation for a Particular Time of Day Full ozone season data (April – October) of 1998 were used. The scale on X axes is from 0 to 1800 meter in 200-meter increments. The scale on Y axes is from 0 to 1 in 0.1 increment. Error bars indicate standard error in gradient at 95% confidence level.

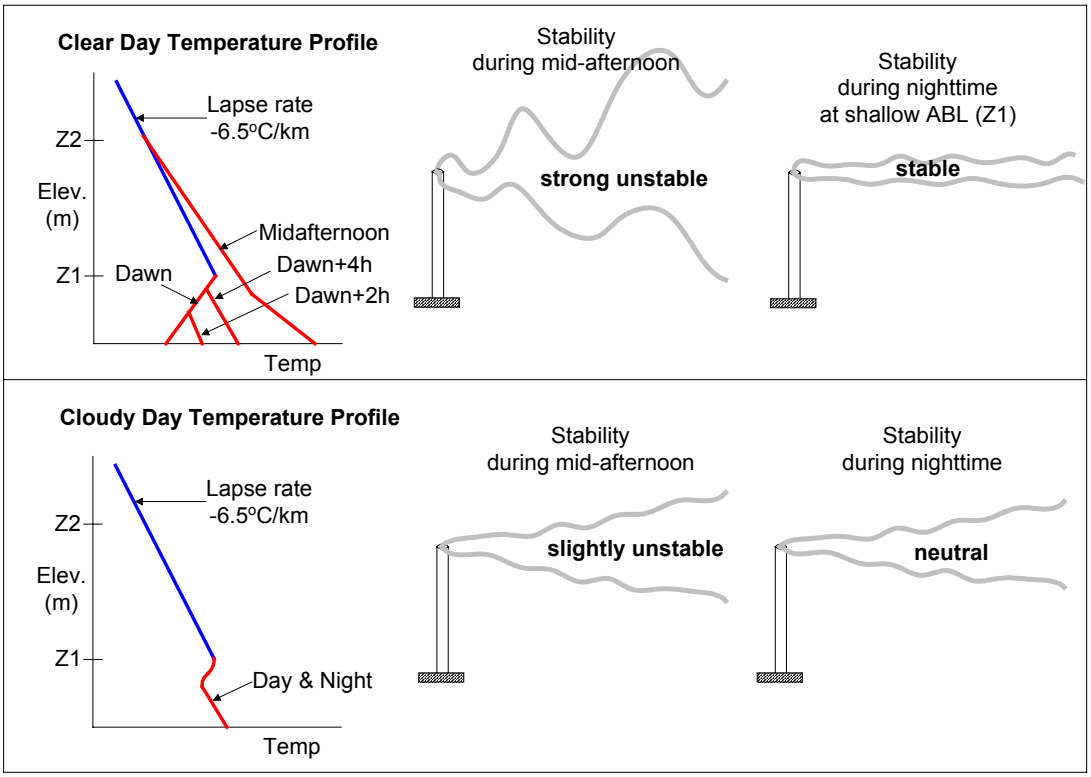

Figure 4-41. Comparison of Vertical Temperature Profile and Atmospheric Stability in "Clear Day" Case and "Cloudy Day" Case
Adapted from Nevers, 1995

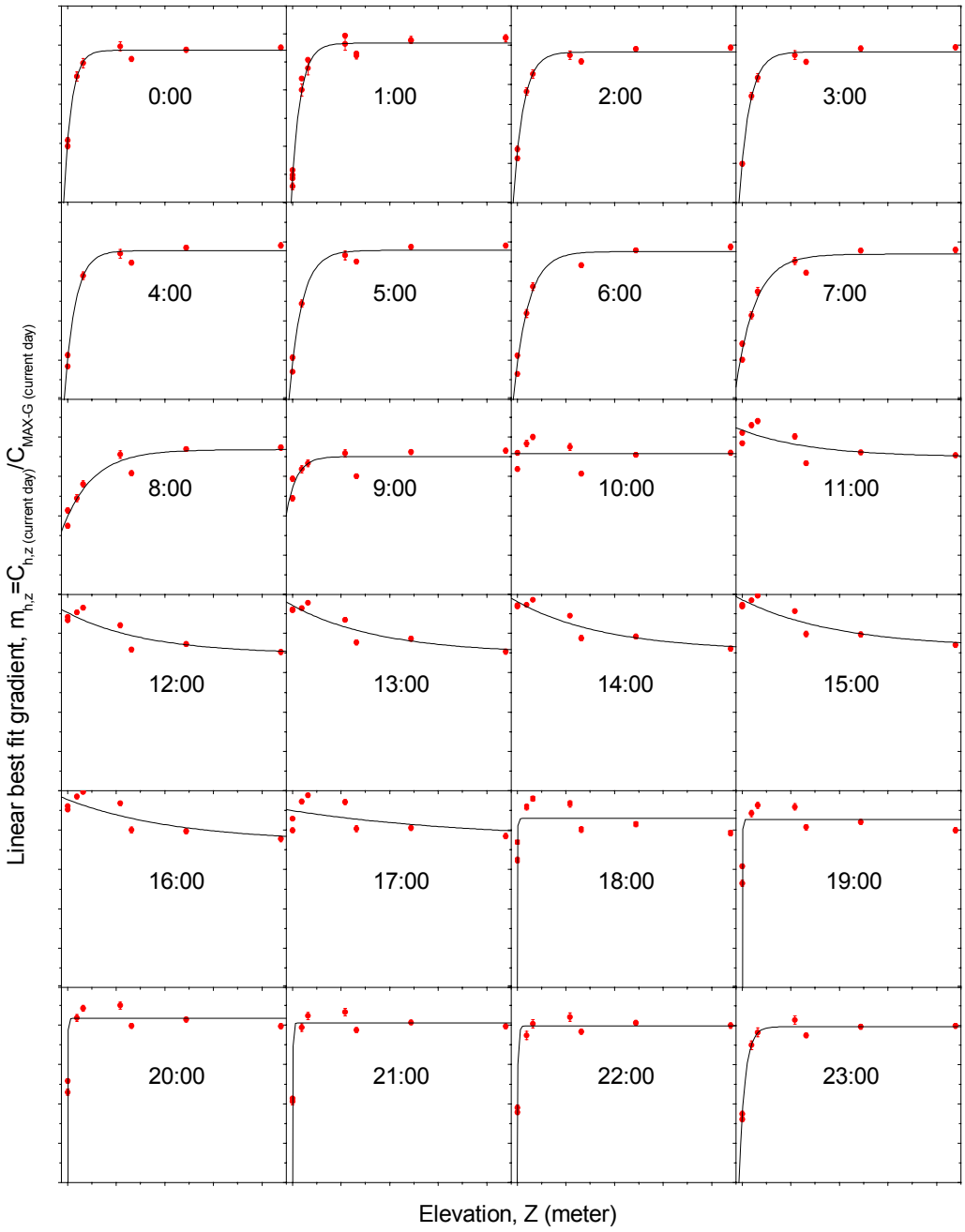

Figure 4-42. Non-Linear Curve Fit of Linear Best Fit Gradient (Vertical Axes) against Elevation (Horizontal Axes) to Develop the "Clear to Partly Cloudy" Component Regression Model as a Function of Elevation for a Particular Time of Day Full ozone season data (April – October) of 1998 were used. The scale on X axes is from 0 to 1800 meter in 200-meter increments. The scale on Y axes is from 0 to 1 in 0.1 increment. Error bars indicate standard error in gradient at 95% confidence level.

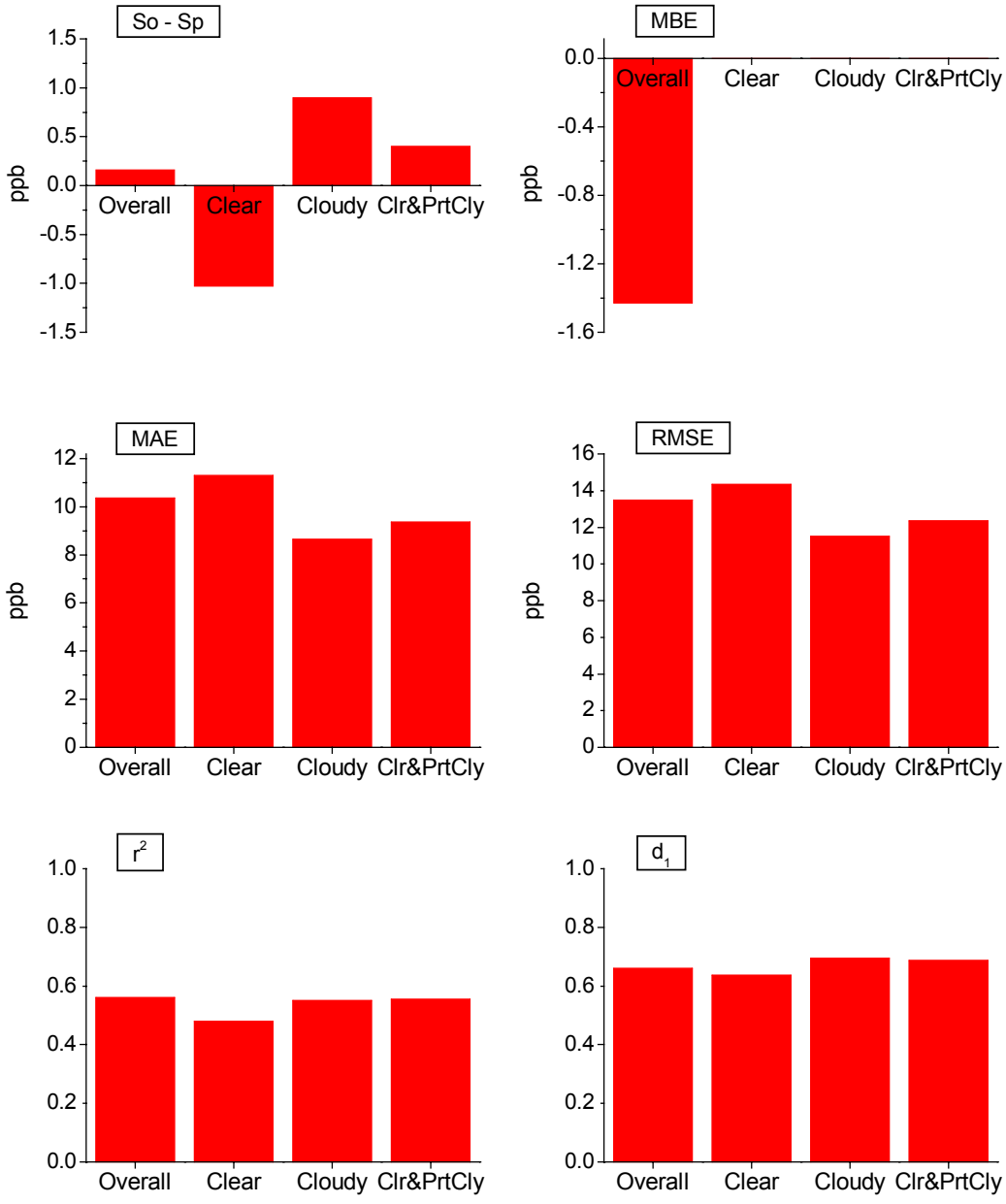

Figure 4-43. Comparison of Relative Performance in Terms of Statistical Results Produced by the "Overall," "Clear," "Cloudy," and "Clear to Partly Cloudy" Component Regression Models Full ozone season data (April – October) of 1998 were used.

Appendix C

Results Produced by the Linear Regression Analysis for "Prediction based on Present Day's Maximum," "Prediction based on Previous Day's Maximum," and "Prediction based on Present Day's Hourly" Methods

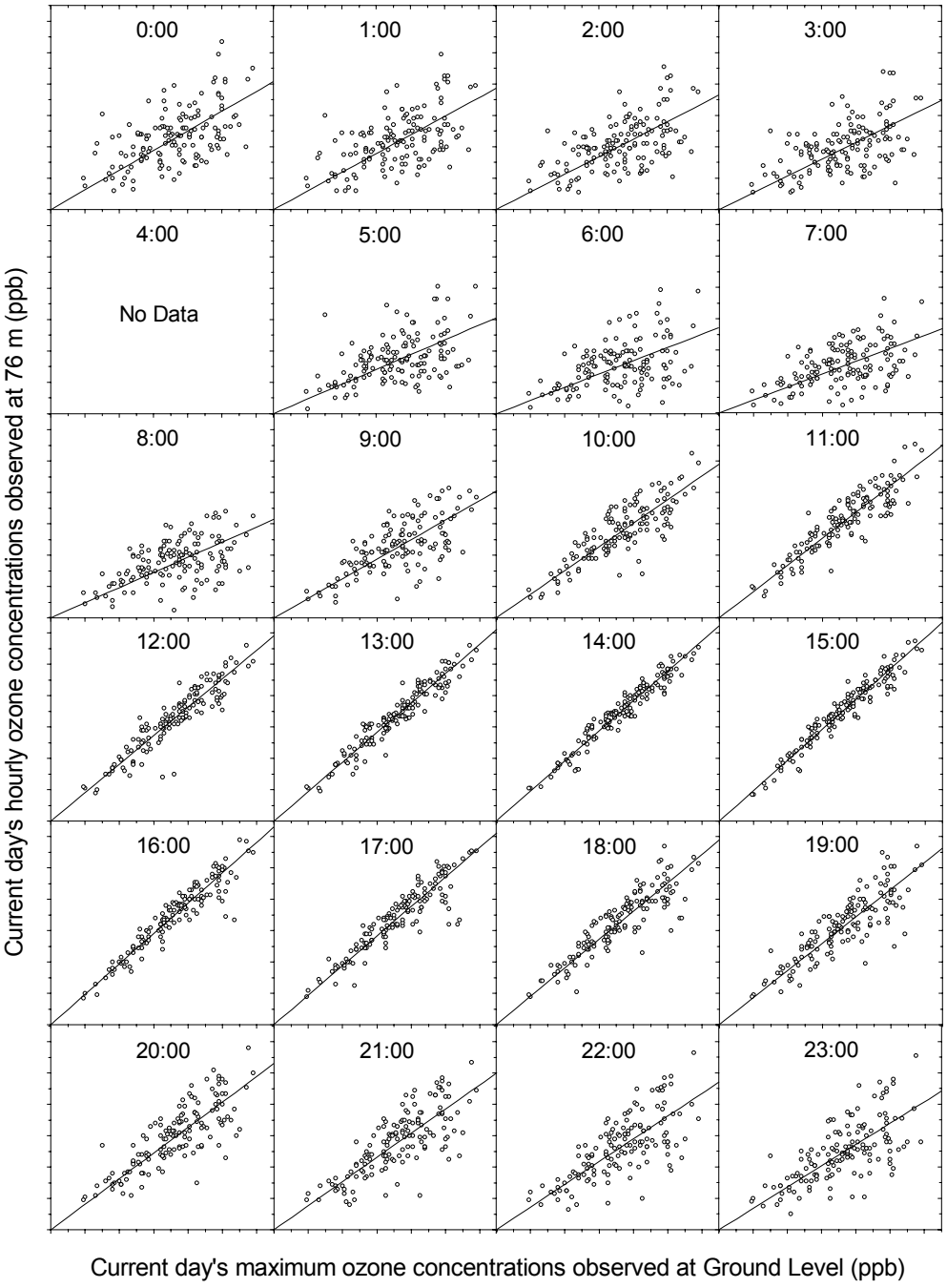

Figure C-1. Scatter Plots of Current Day's Maximum Ozone Concentrations Observed at Ground Level (Horizontal Axes) against Current Day's Hourly Ozone Concentrations Observed at 76 m (Vertical Axes), Using 1998 Data The scale on all axes is from 0 to 130 ppb in 10 ppb increment. The diagonal in each plot indicates the best-fit regression line through the origin.

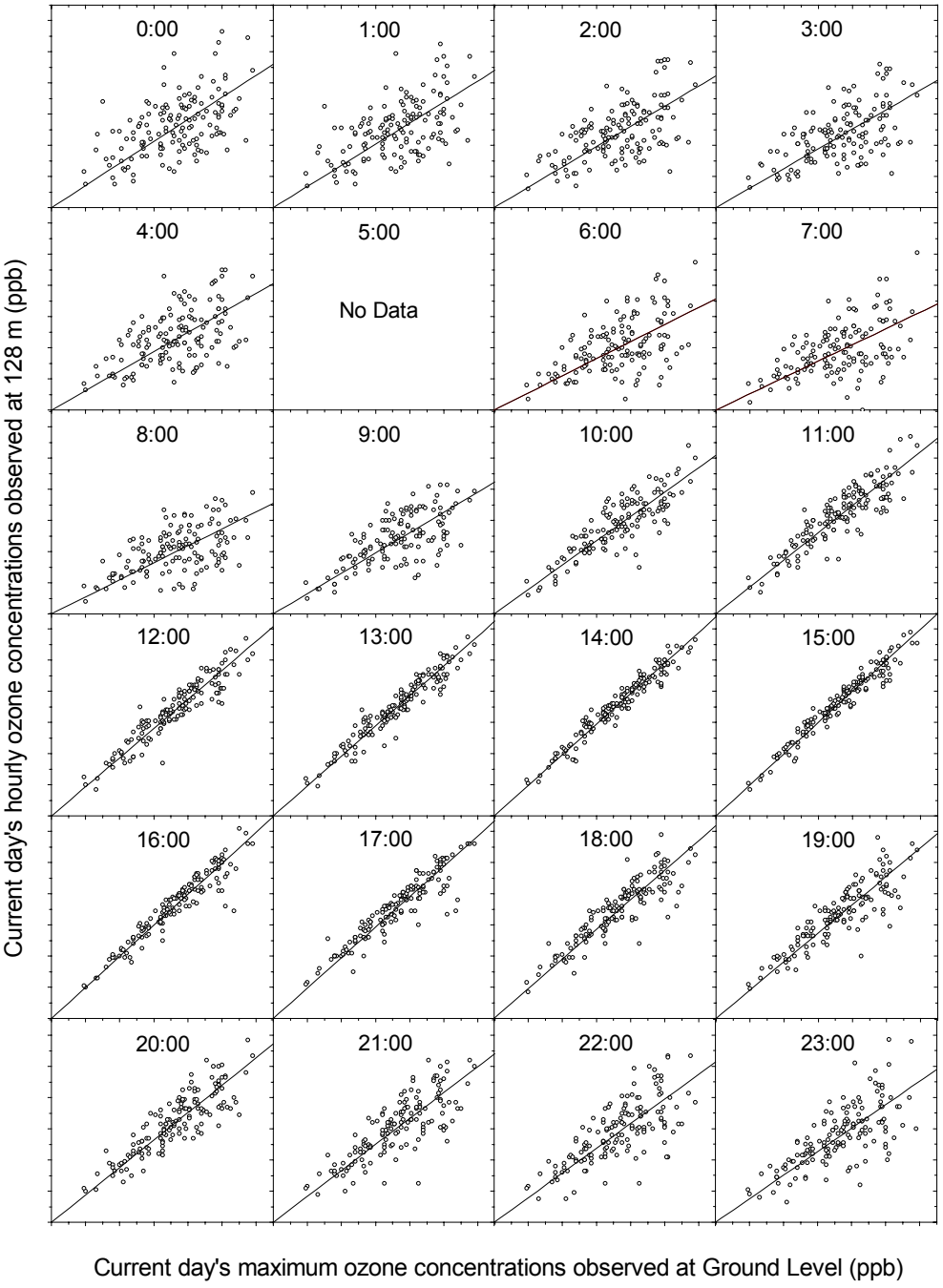

Figure C-2. Scatter Plots of Current Day's Maximum Ozone Concentrations Observed at Ground Level (Horizontal Axes) against Current Day's Hourly Ozone Concentrations Observed at 128 m (Vertical Axes), Using 1998 Data The scale on all axes is from 0 to 130 ppb in 10 ppb increment. The diagonal in each plot indicates the best-fit regression line through the origin.

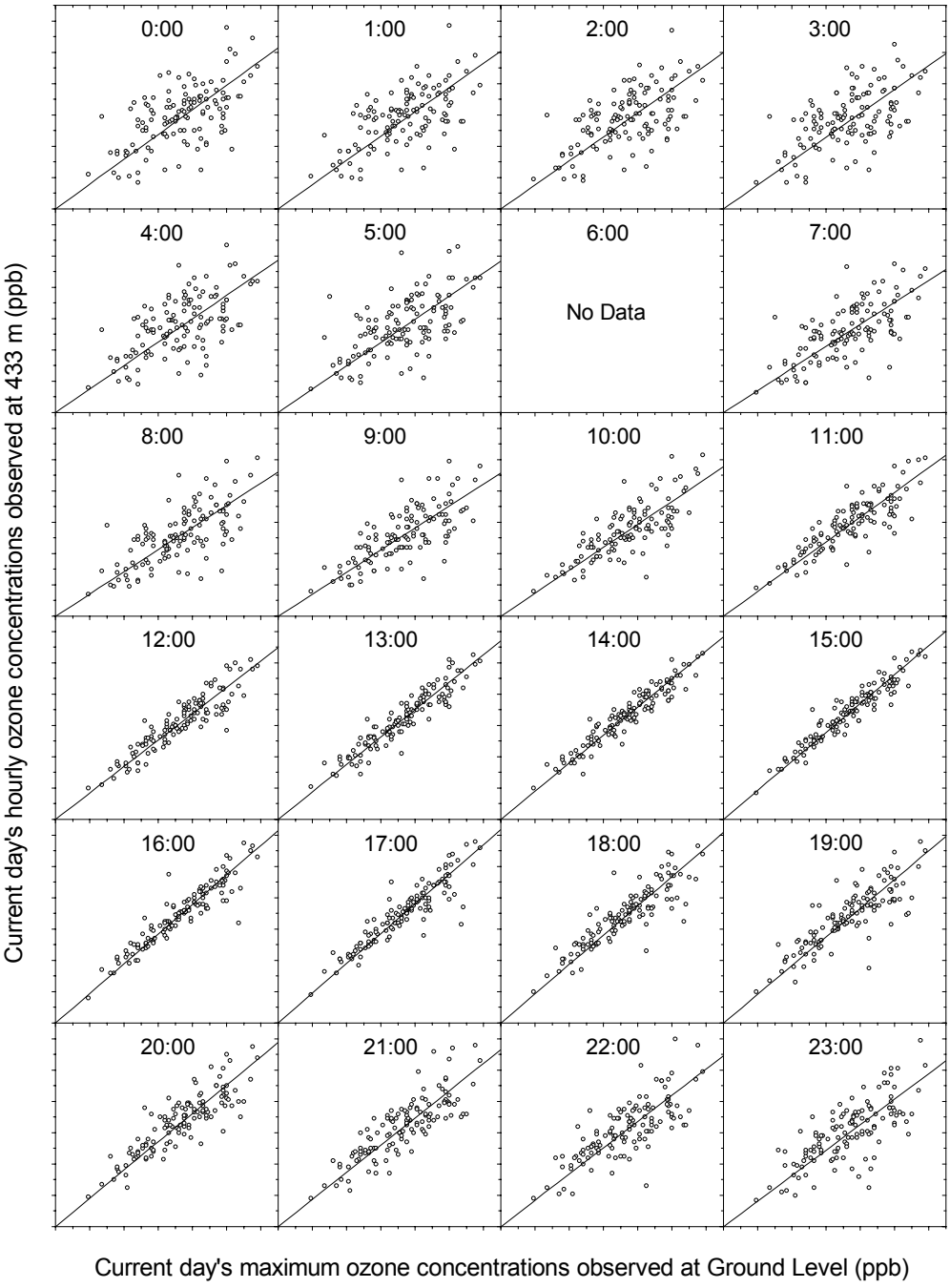

Figure C-3. Scatter Plots of Current Day's Maximum Ozone Concentrations Observed at Ground Level (Horizontal Axes) against Current Day's Hourly Ozone Concentrations Observed at 433 m (Vertical Axes), Using 1998 Data The scale on all axes is from 0 to 130 ppb in 10 ppb increment. The diagonal in each plot indicates the best-fit regression line through the origin.

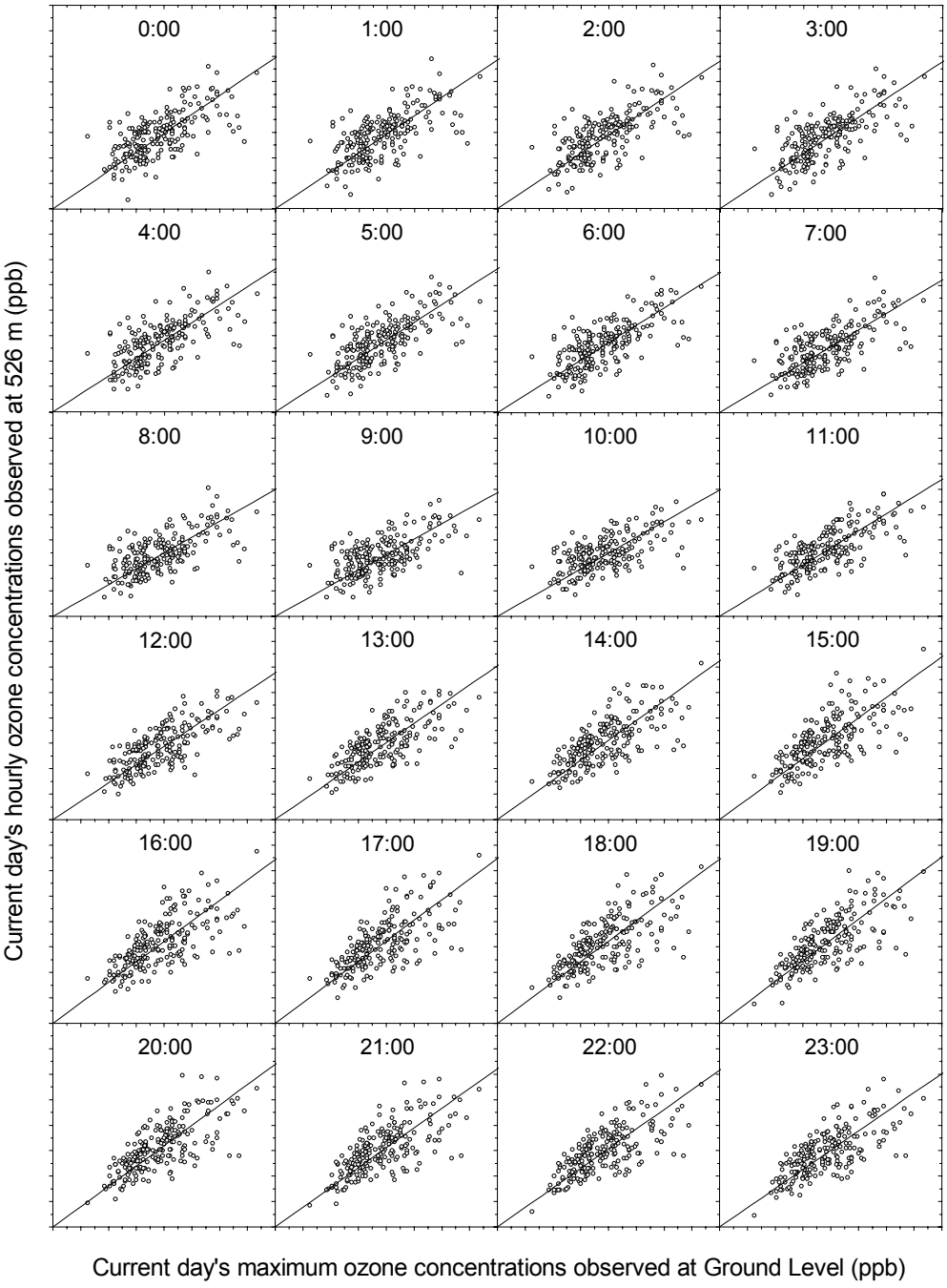

Figure C-4. Scatter Plots of Current Day's Maximum Ozone Concentrations Observed at Ground Level (Horizontal Axes) against Current Day's Hourly Ozone Concentrations Observed at 526 m (Vertical Axes), Using 1998 Data The scale on all axes is from 0 to 160 ppb in 10 ppb increment. The diagonal in each plot indicates the best-fit regression line through the origin.

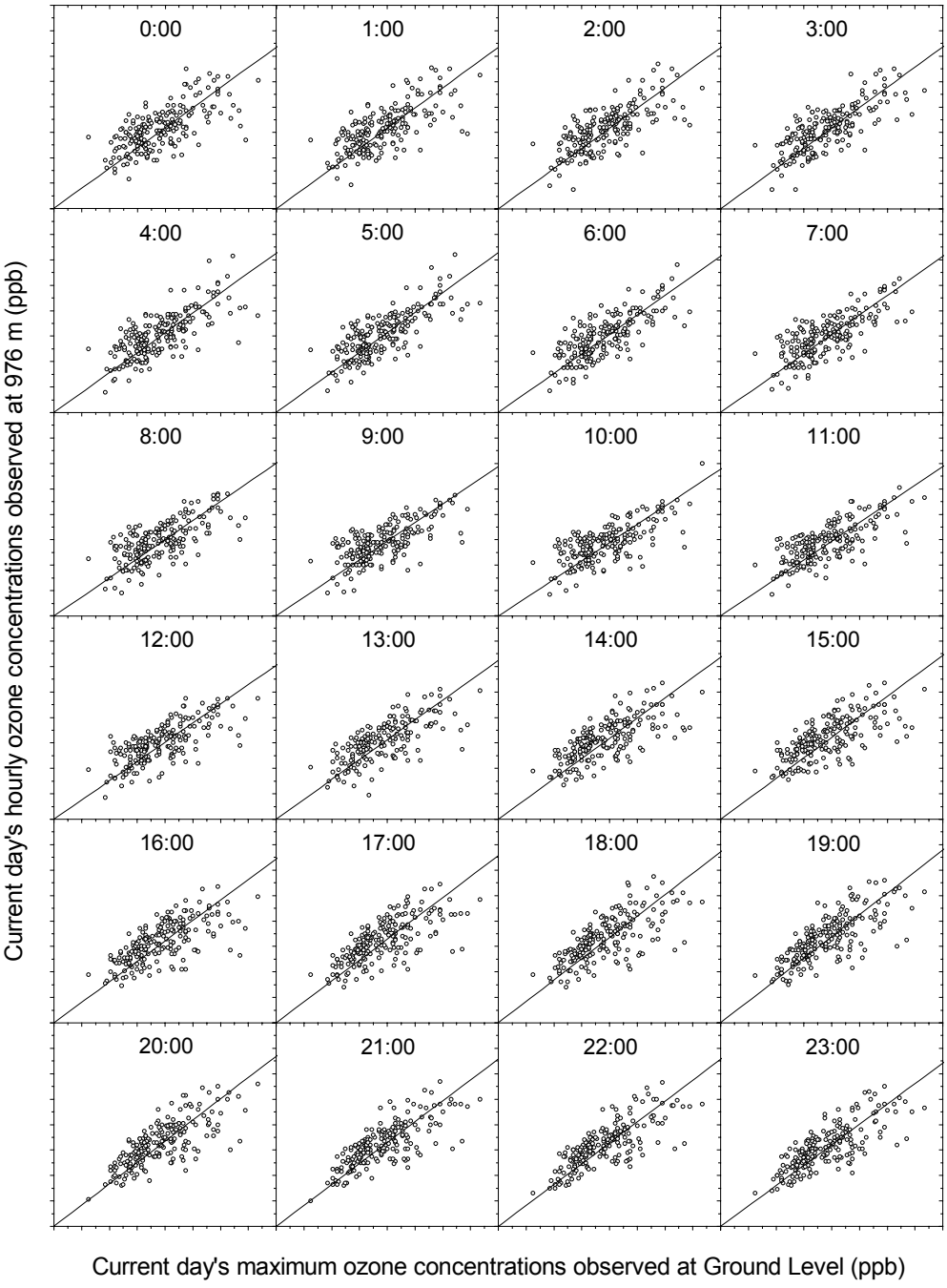

Figure C-5. Scatter Plots of Current Day's Maximum Ozone Concentrations Observed at Ground Level (Horizontal Axes) against Current Day's Hourly Ozone Concentrations Observed at 976 m (Vertical Axes), Using 1998 Data The scale on all axes is from 0 to 160 ppb in 10 ppb increment. The diagonal in each plot indicates the best-fit regression line through the origin.

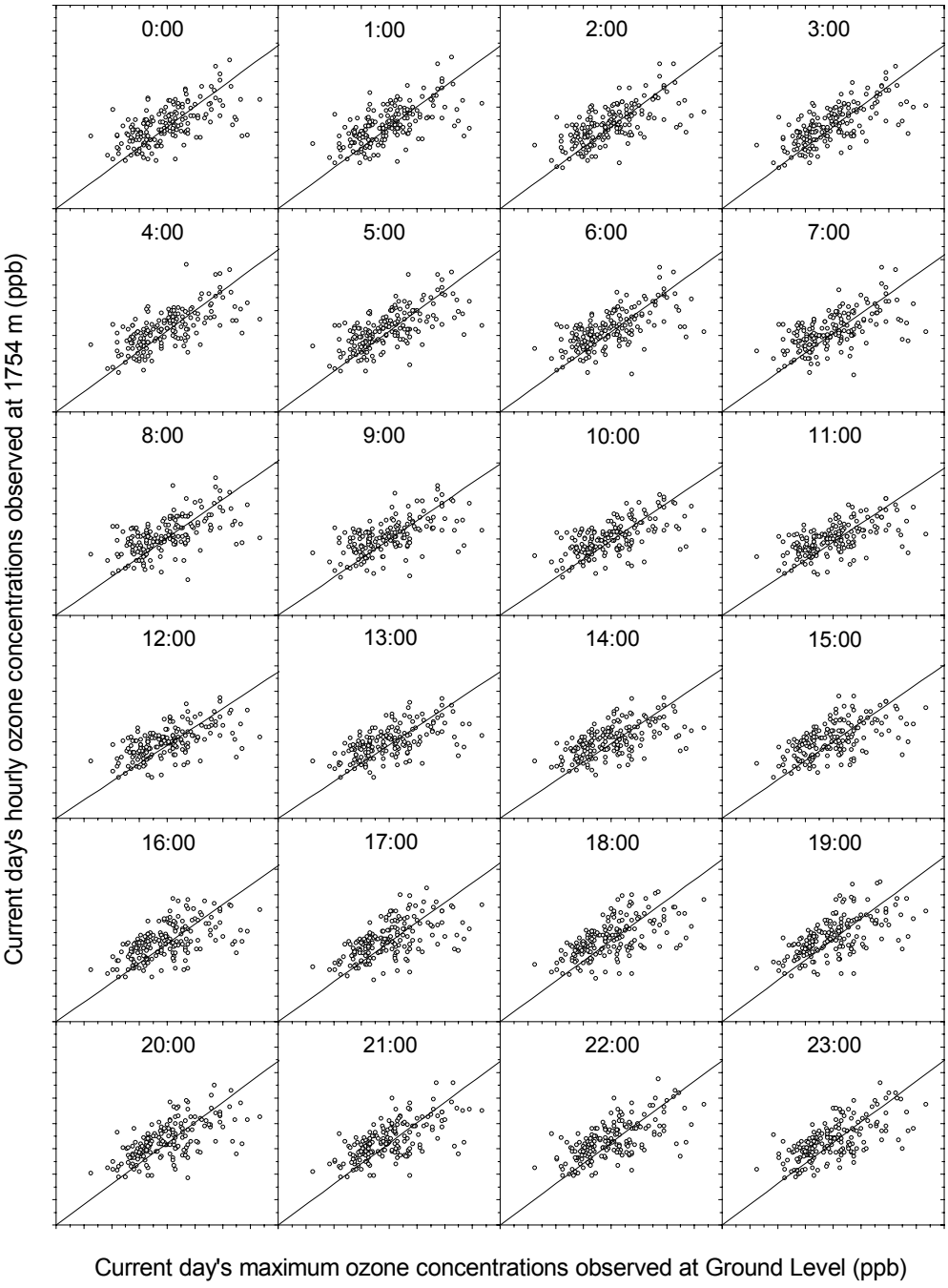

Figure C-6. Scatter Plots of Current Day's Maximum Ozone Concentrations Observed at Ground Level (Horizontal Axes) against Current Day's Hourly Ozone Concentrations Observed at 1754 m (Vertical Axes), Using 1998 Data The scale on all axes is from 0 to 160 ppb in 10 ppb increment. The diagonal in each plot indicates the best-fit regression line through the origin.

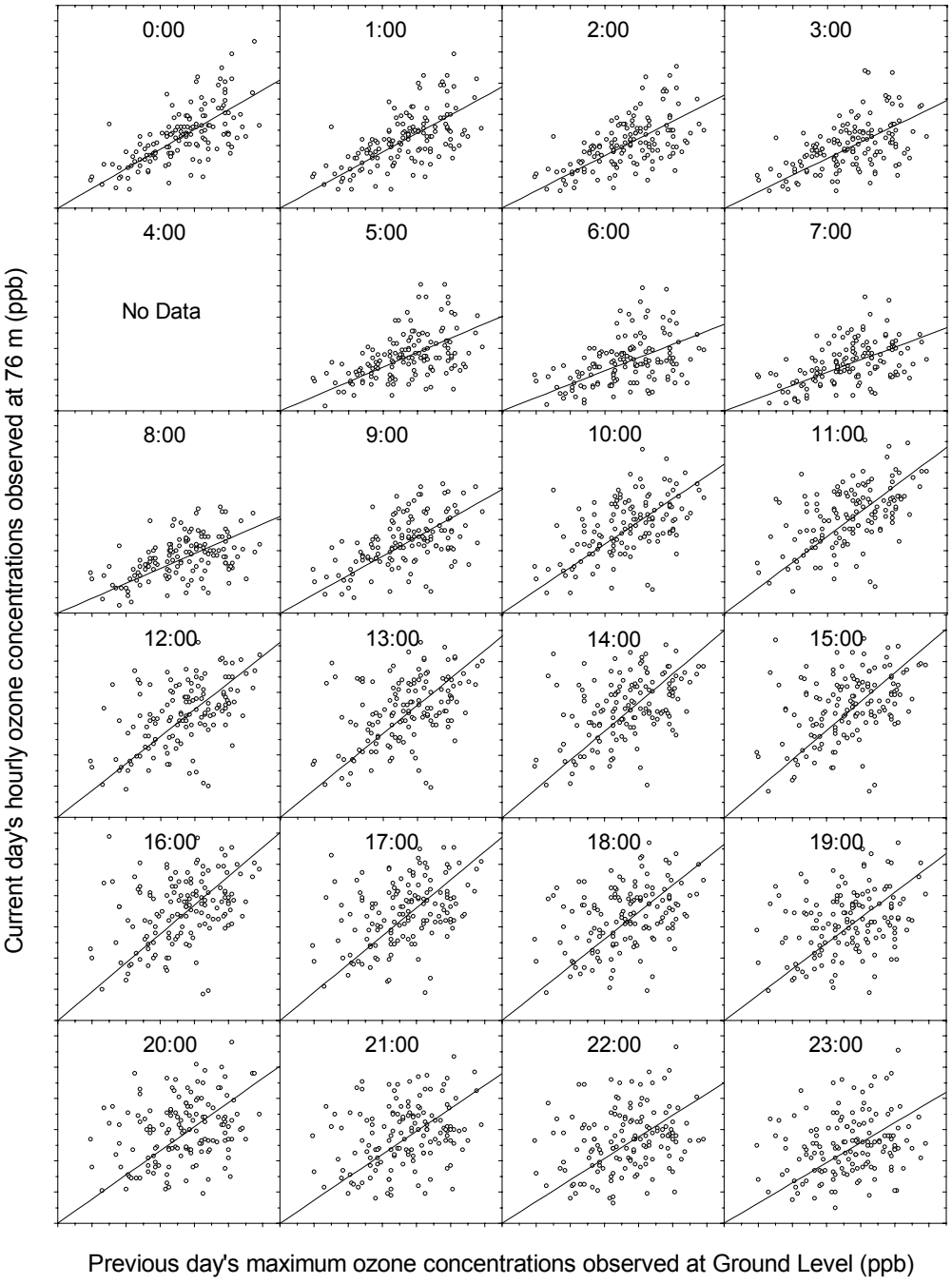

Figure C-7. Scatter Plots of Previous Day's Maximum Ozone Concentrations Observed at Ground Level (Horizontal Axes) against Current Day's Hourly Ozone Concentrations Observed at 76 m (Vertical Axes), Using 1998 Data The scale on all axes is from 0 to 130 ppb in 10 ppb increment. The diagonal in each plot indicates the best-fit regression line through the origin.

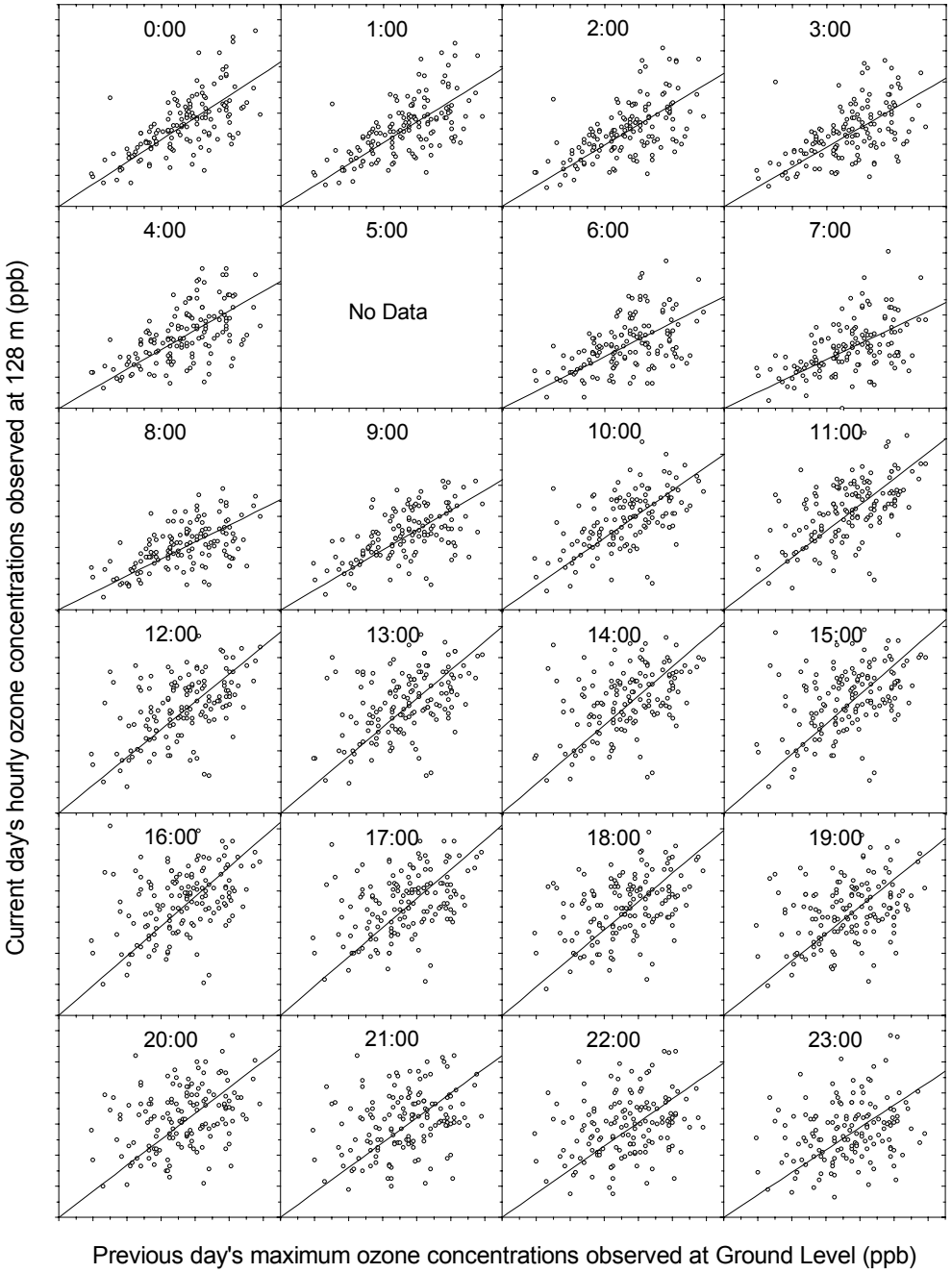

Figure C-8. Scatter Plots of Previous Day's Maximum Ozone Concentrations Observed at Ground Level (Horizontal Axes) against Current Day's Hourly Ozone Concentrations Observed at 128 m (Vertical Axes), Using 1998 Data The scale on all axes is from 0 to 130 ppb in 10 ppb increment. The diagonal in each plot indicates the best-fit regression line through the origin.

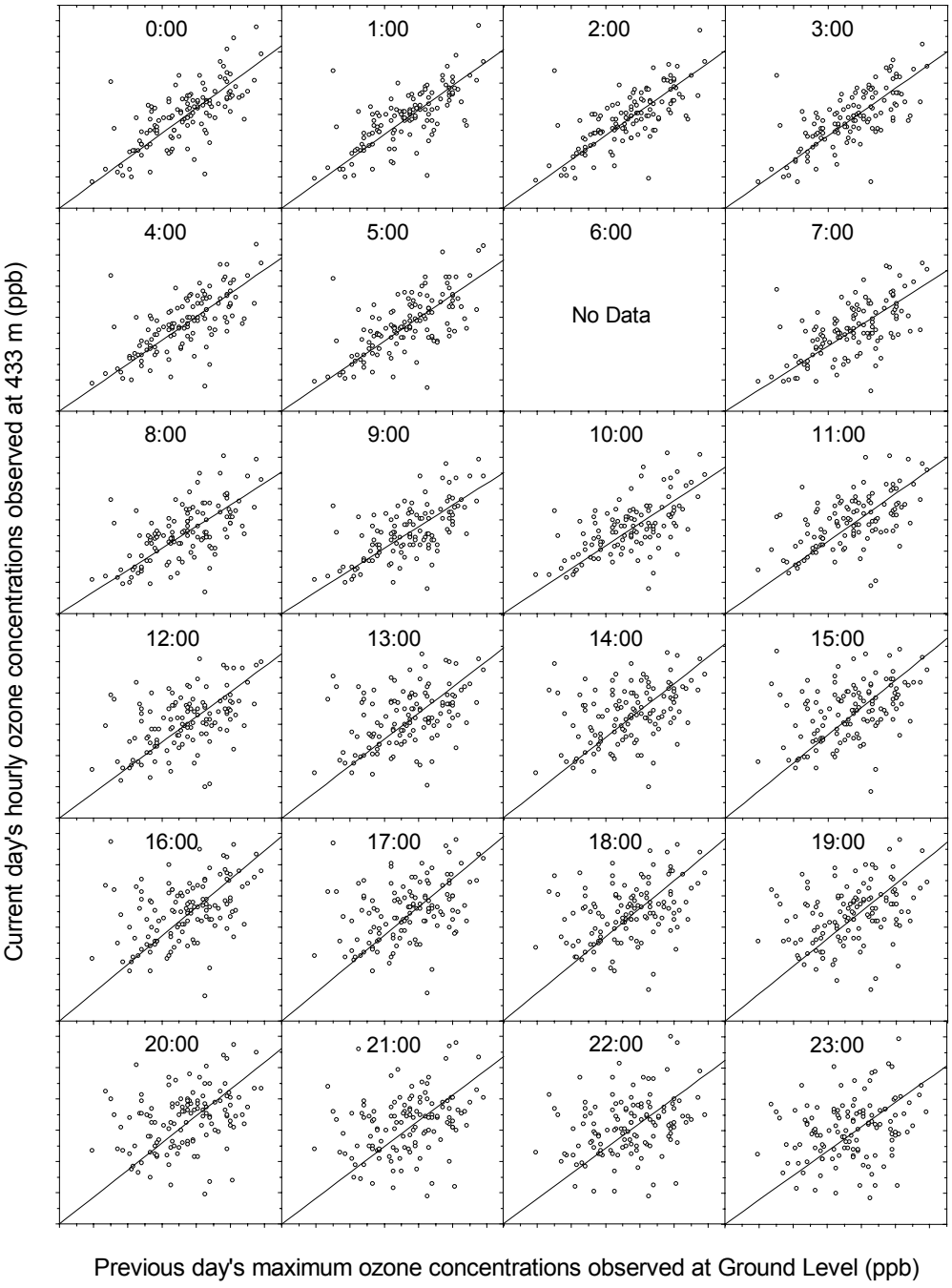

Figure C-9. Scatter Plots of Previous Day's Maximum Ozone Concentrations Observed at Ground Level (Horizontal Axes) against Current Day's Hourly Ozone Concentrations Observed at 433 m (Vertical Axes), Using 1998 Data The scale on all axes is from 0 to 130 ppb in 10 ppb increment. The diagonal in each plot indicates the best-fit regression line through the origin.

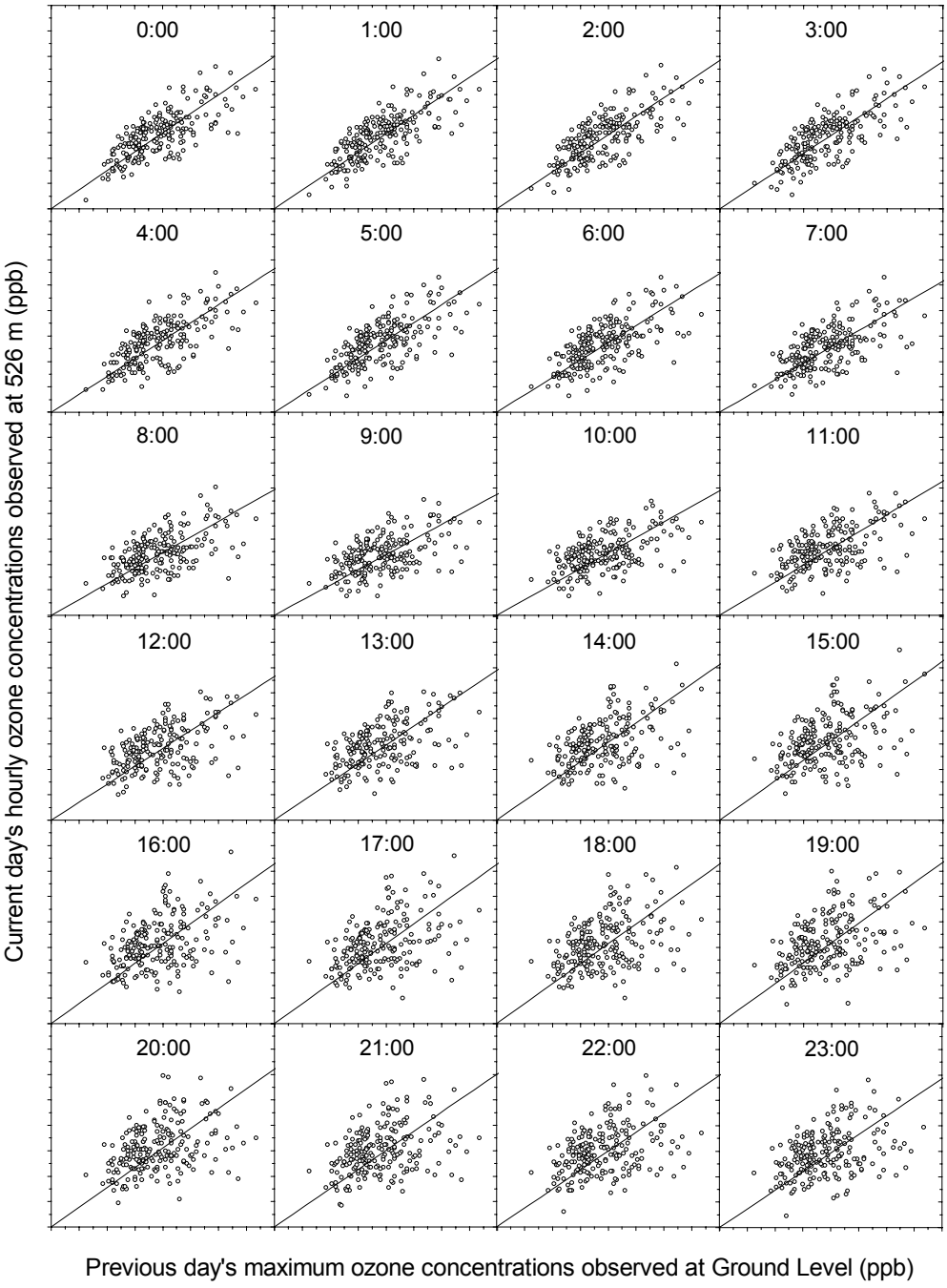

Figure C-10. Scatter Plots of Previous Day's Maximum Ozone Concentrations Observed at Ground Level (Horizontal Axes) against Current Day's Hourly Ozone Concentrations Observed at 526 m (Vertical Axes), Using 1998 Data The scale on all axes is from 0 to 160 ppb in 10 ppb increment. The diagonal in each plot indicates the best-fit regression line through the origin.

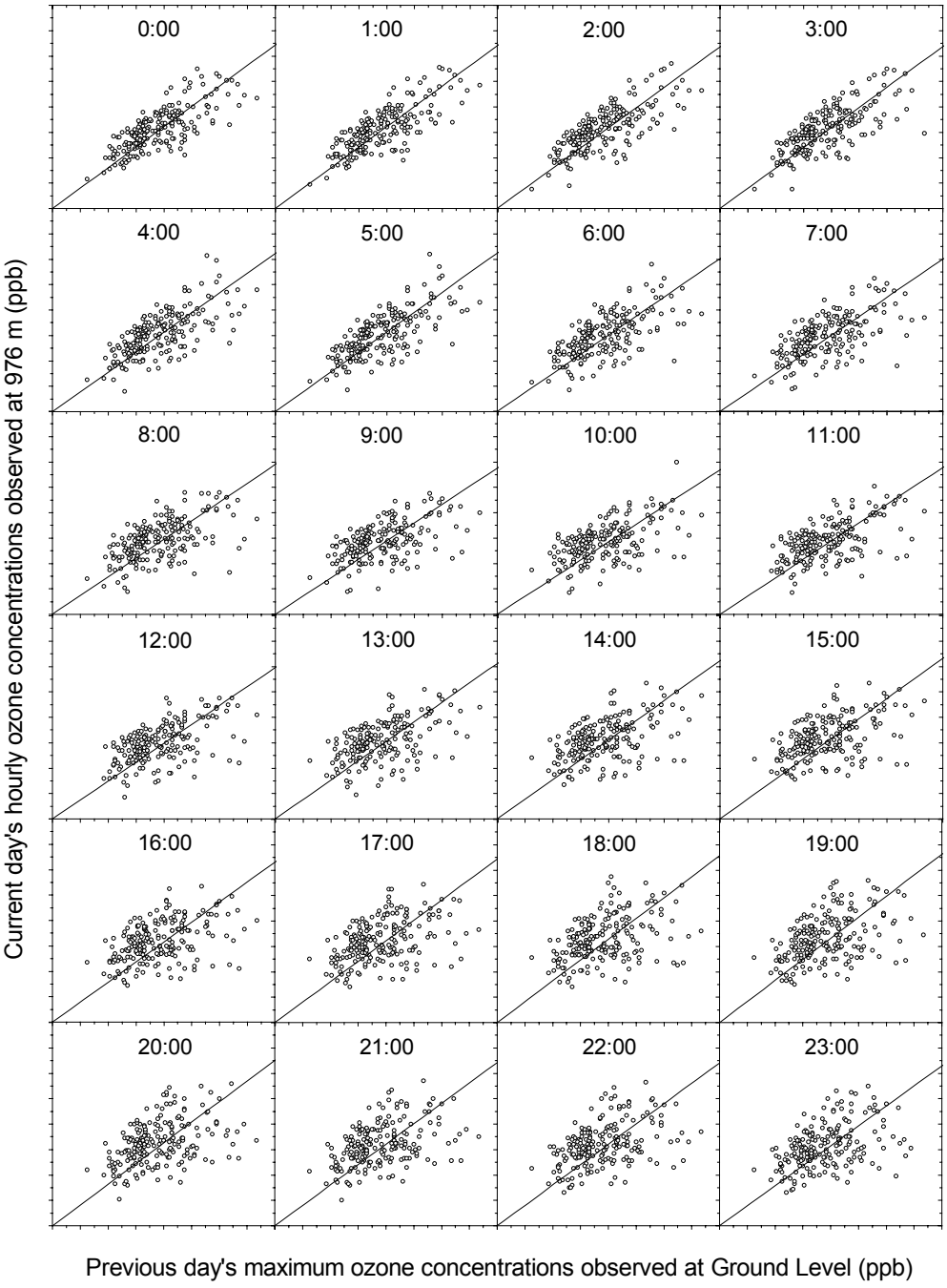

Figure C-11. Scatter Plots of Previous Day's Maximum Ozone Concentrations Observed at Ground Level (Horizontal Axes) against Current Day's Hourly Ozone Concentrations Observed at 976 m (Vertical Axes), Using 1998 Data The scale on all axes is from 0 to 160 ppb in 10 ppb increment. The diagonal in each plot indicates the best-fit regression line through the origin.

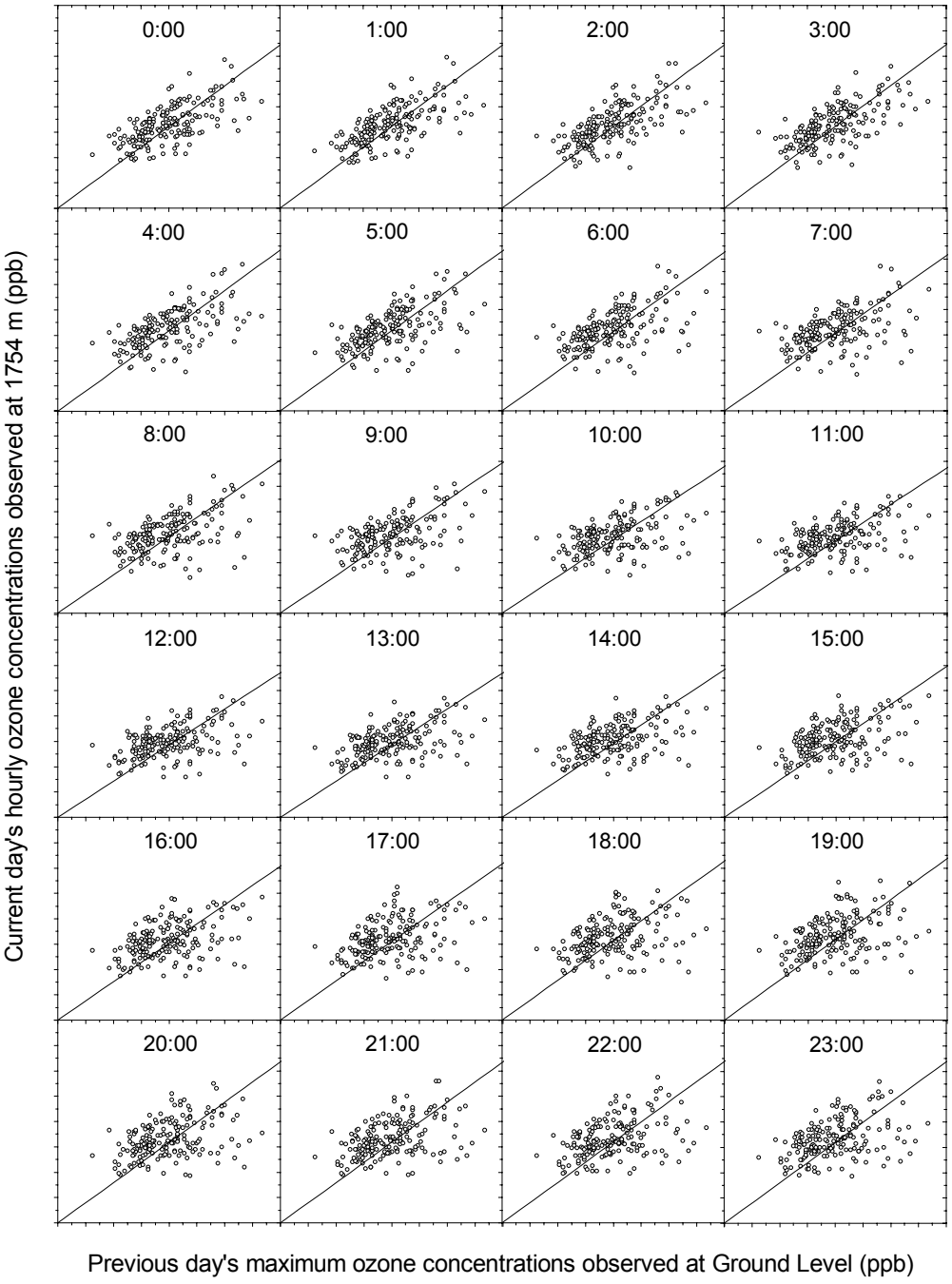

Figure C-12. Scatter Plots of Previous Day's Maximum Ozone Concentrations Observed at Ground Level (Horizontal Axes) against Current Day's Hourly Ozone Concentrations Observed at 1754 m (Vertical Axes), Using 1998 Data The scale on all axes is from 0 to 160 ppb in 10 ppb increment. The diagonal in each plot indicates the best-fit regression line through the origin.

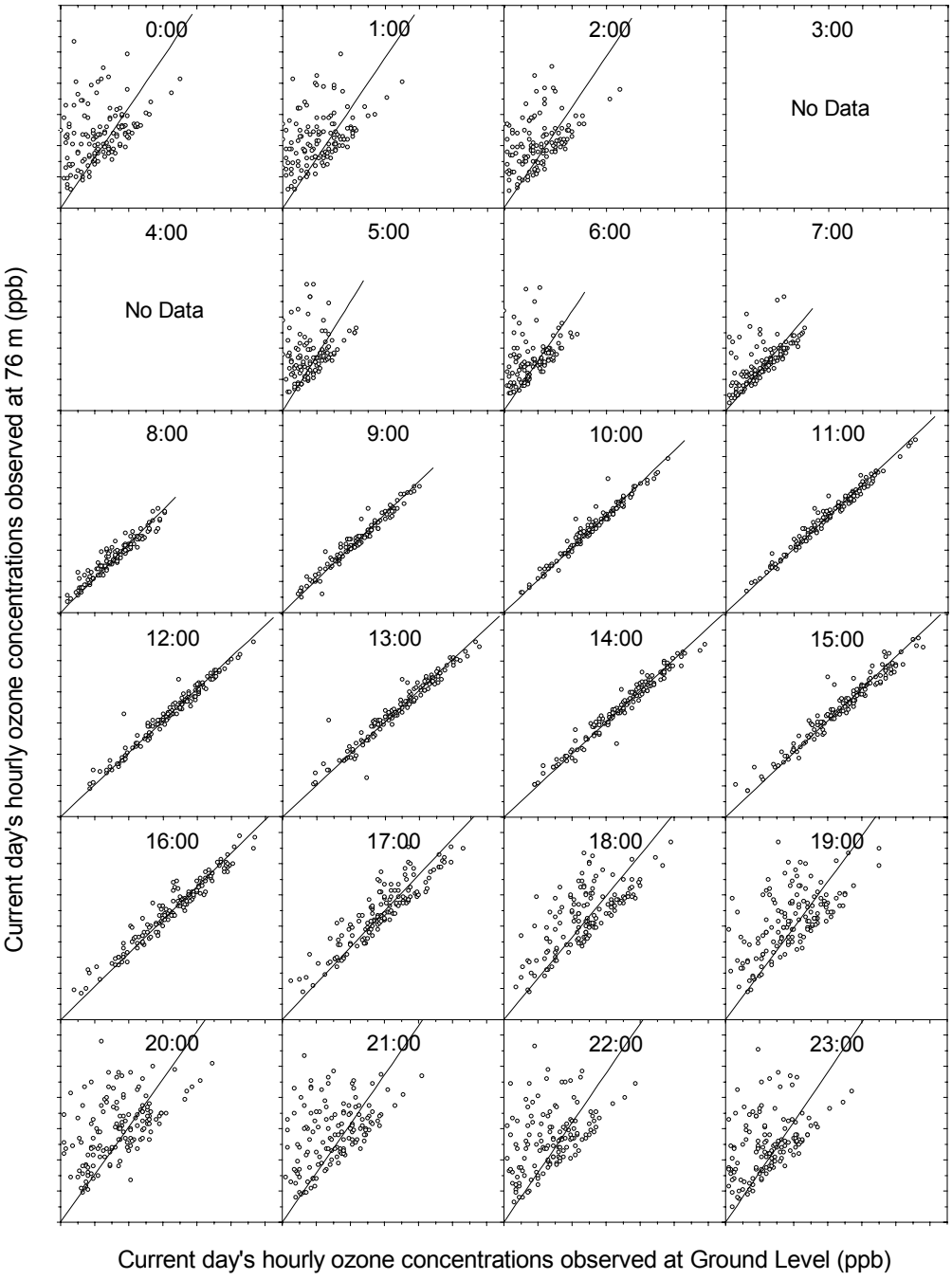

Figure C-13. Scatter Plots of Current Day's Hourly Ozone Concentrations Observed at Ground Level (Horizontal Axes) against Current Day's Hourly Ozone Concentrations Observed at 76 m (Vertical Axes), Using 1998 Data The scale on all axes is from 0 to 130 ppb in 10 ppb increment. The diagonal in each plot indicates the best-fit regression line through the origin.

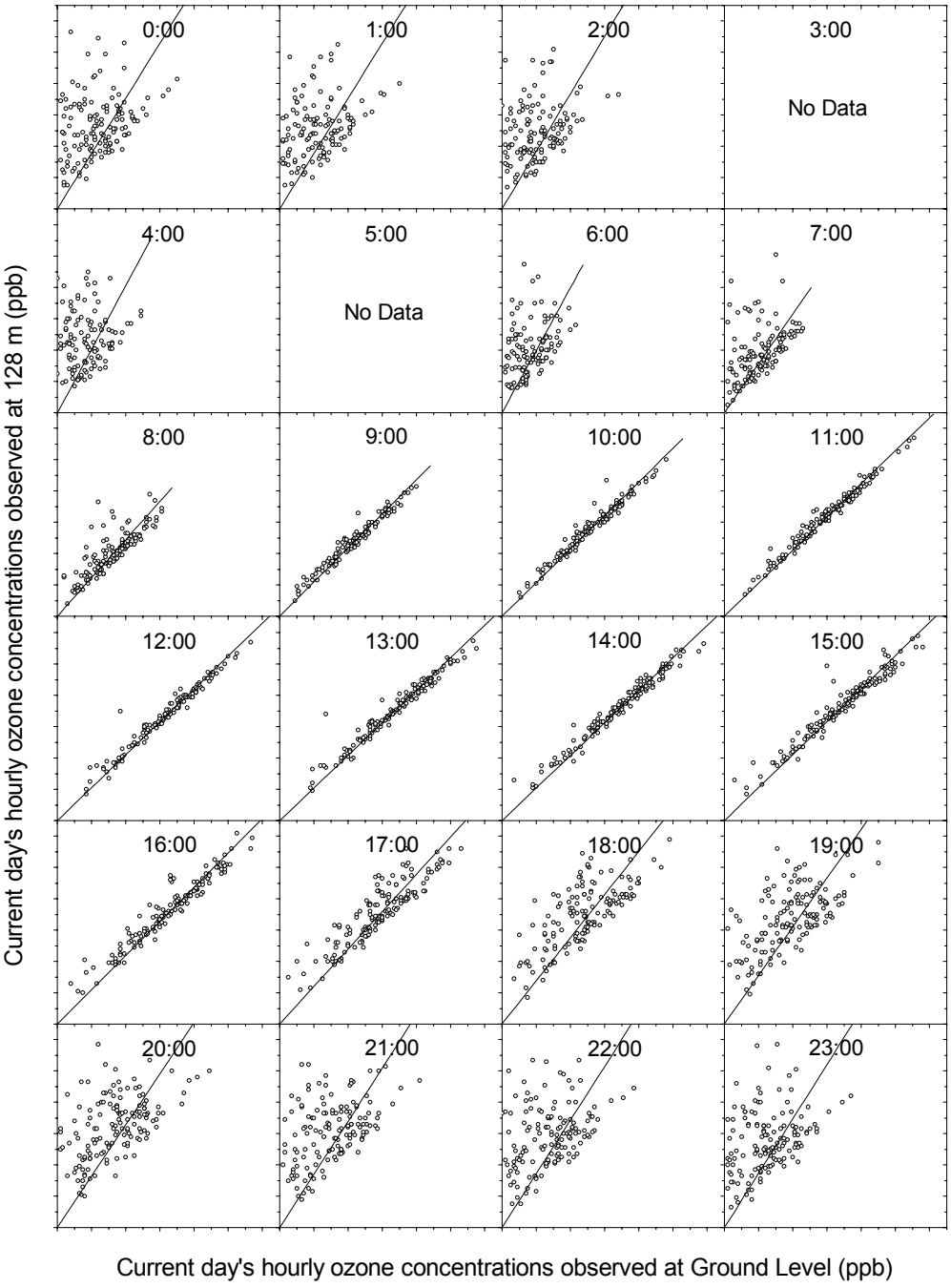

Figure C-14. Scatter Plots of Current Day's Hourly Ozone Concentrations Observed at Ground Level (Horizontal Axes) against Current Day's Hourly Ozone Concentrations Observed at 128 m (Vertical Axes), Using 1998 Data The scale on all axes is from 0 to 130 ppb in 10 ppb increment. The diagonal in each plot indicates the best-fit regression line through the origin.

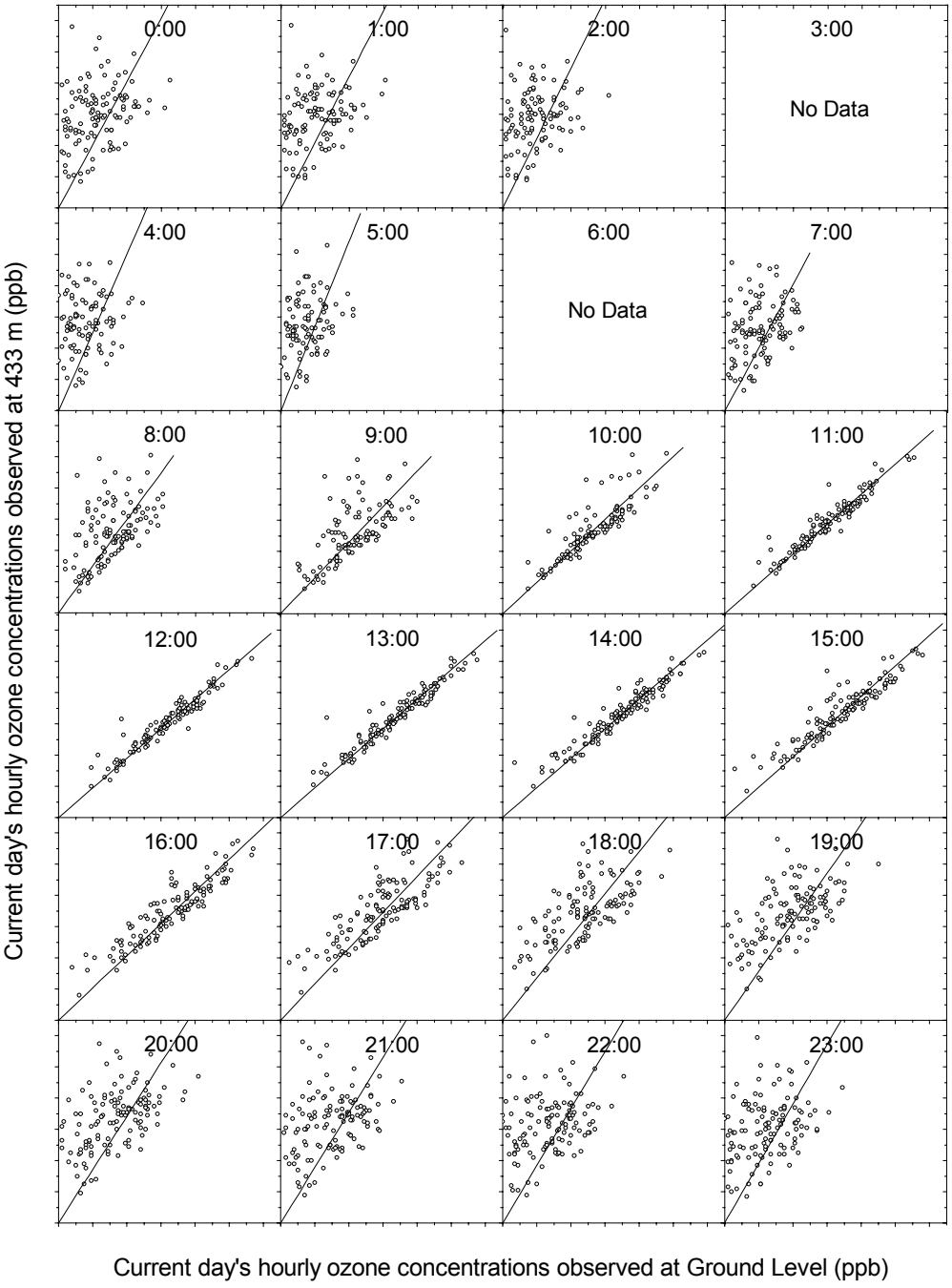

Figure C-15. Scatter Plots of Current Day's Hourly Ozone Concentrations Observed at Ground Level (Horizontal Axes) against Current Day's Hourly Ozone Concentrations Observed at 433 m (Vertical Axes), Using 1998 Data The scale on all axes is from 0 to 130 ppb in 10 ppb increment. The diagonal in each plot indicates the best-fit regression line through the origin.

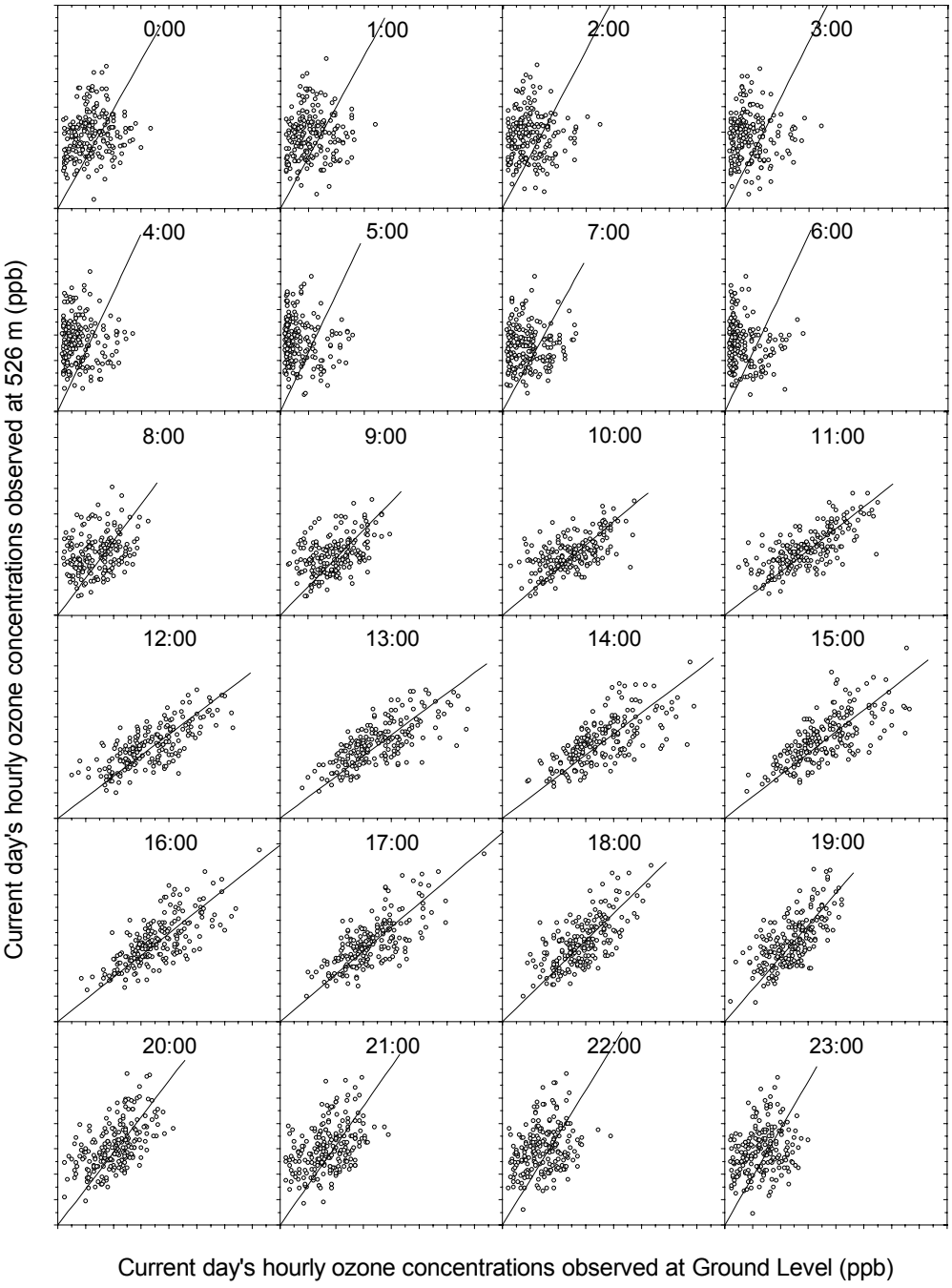

Figure C-16. Scatter Plots of Current Day's Hourly Ozone Concentrations Observed at Ground Level (Horizontal Axes) against Current Day's Hourly Ozone Concentrations Observed at 526 m (Vertical Axes), Using 1998 Data The scale on all axes is from 0 to 160 ppb in 10 ppb increment. The diagonal in each plot indicates the best-fit regression line through the origin.

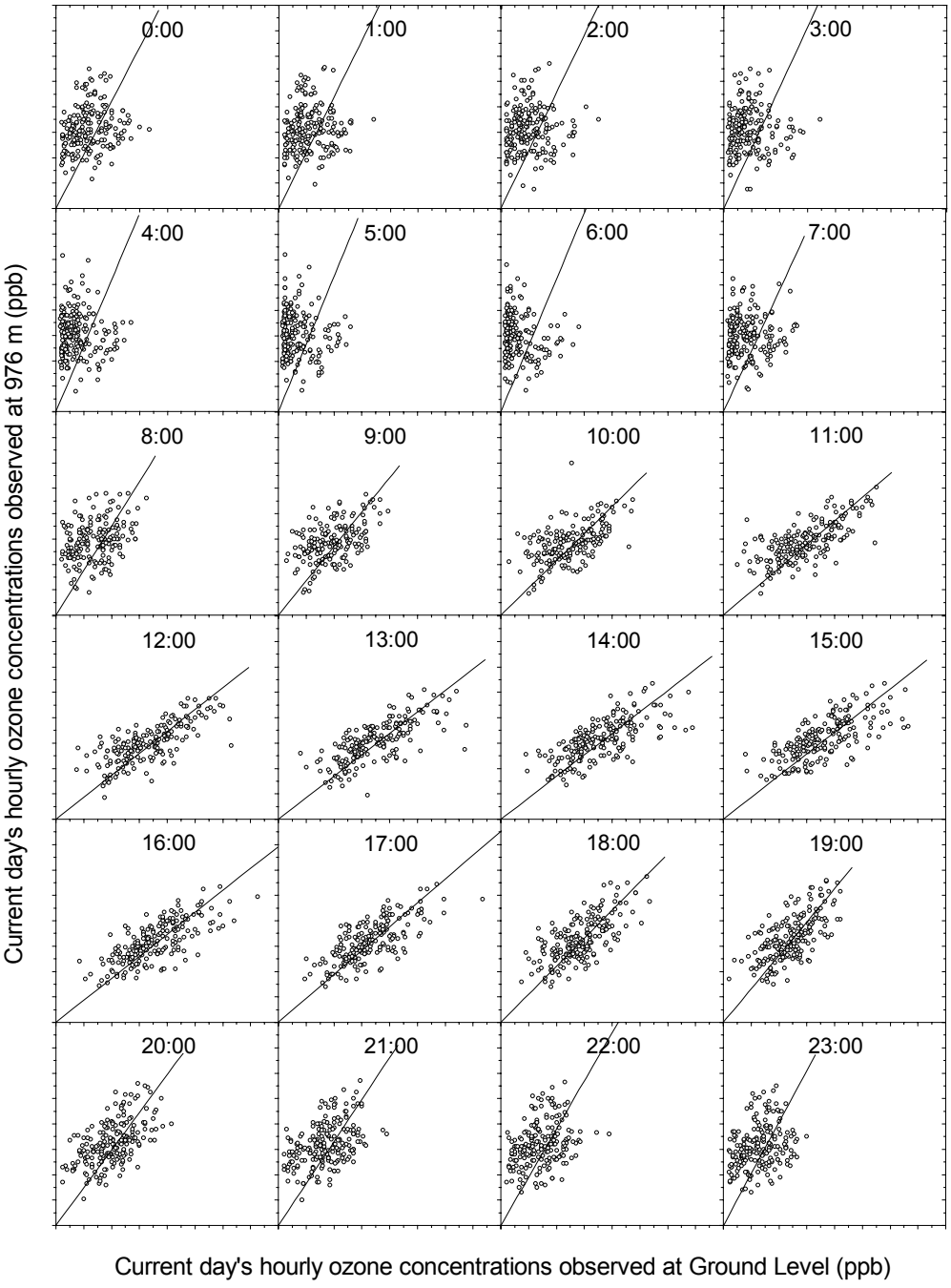

Figure C-17. Scatter Plots of Current Day's Hourly Ozone Concentrations Observed at Ground Level (Horizontal Axes) against Current Day's Hourly Ozone Concentrations Observed at 976 m (Vertical Axes), Using 1998 Data The scale on all axes is from 0 to 160 ppb in 10 ppb increment. The diagonal in each plot indicates the best-fit regression line through the origin.

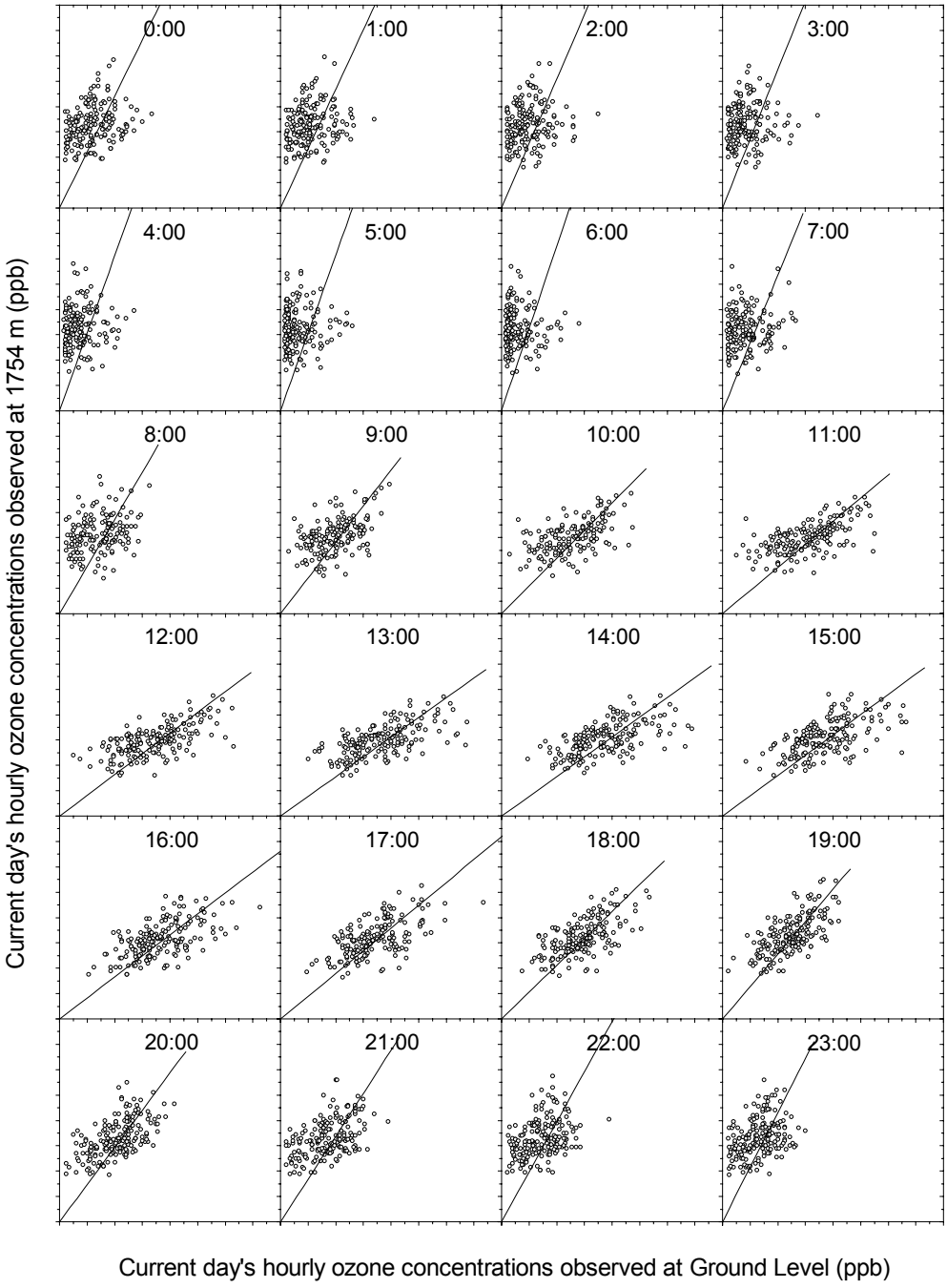

Figure C-18. Scatter Plots of Current Day's Hourly Ozone Concentrations Observed at Ground Level (Horizontal Axes) against Current Day's Hourly Ozone Concentrations Observed at 1754 m (Vertical Axes), Using 1998 Data The scale on all axes is from 0 to 160 ppb in 10 ppb increment. The diagonal in each plot indicates the best-fit regression line through the origin.

VITA

Gi-Dong Kim was born in Daegu, Korea on March 28, 1964. He graduated from Shimin High school in February, 1982. The following March he entered YeungNam University and in February, 1989 received the degree of Bachelor of Science in Architecture Engineering. In August, 1992 he came to the United States and entered The University of North Carolina, Charlotte and in December, 1995 received a Master of Science degree in Civil Engineering focusing on groundwater. Immediately after receiving his Master of Science focusing on Air Quality Study from the University of Tennessee, Knoxville in 1998, he continued his doctoral program. He graduated as a Doctor of Philosophy in Civil Engineering in December 2001.